Synthesis and Photophysical Studies of Fluorescent Probes for Nitric Oxide and Nitroxyl with Bio-imaging Applications

THESIS SUBMITTED FOR THE DEGREE OF

DOCTOR OF PHILOSOPHY (SCIENCE)

OF

JADAVPUR UNIVERSITY

NOVEMBER, 2022

By

DEBJANI MAITI

DEPARTMENT OF CHEMISTRY

JADAVPUR UNIVERSITY

JADAVPUR

K0LKATA-700032

INDIA

2022

Dr. Mahammad Ali, Professor
Department of Chemistry
Jadavpur University
Kolkata 700 032

CERTIFICATE FROM THE SUPERVISOR

This is to certify that the thesis entitled "**Synthesis and Photophysical Studies of Fluorescent Probes for Nitric Oxide and Nitroxyl with Bio-imaging Applications**" Submitted by **Miss Debjani Maiti** who got her name registered on **25.04.2017 (Index No. 09/17/Chem./25)** for the award of **Ph. D. (Science) degree** of **Jadavpur University**, is absolutely based upon her own work under my direct supervision and that neither this thesis nor any part of it has been submitted for either any degree / diploma or any other academic award anywhere before.
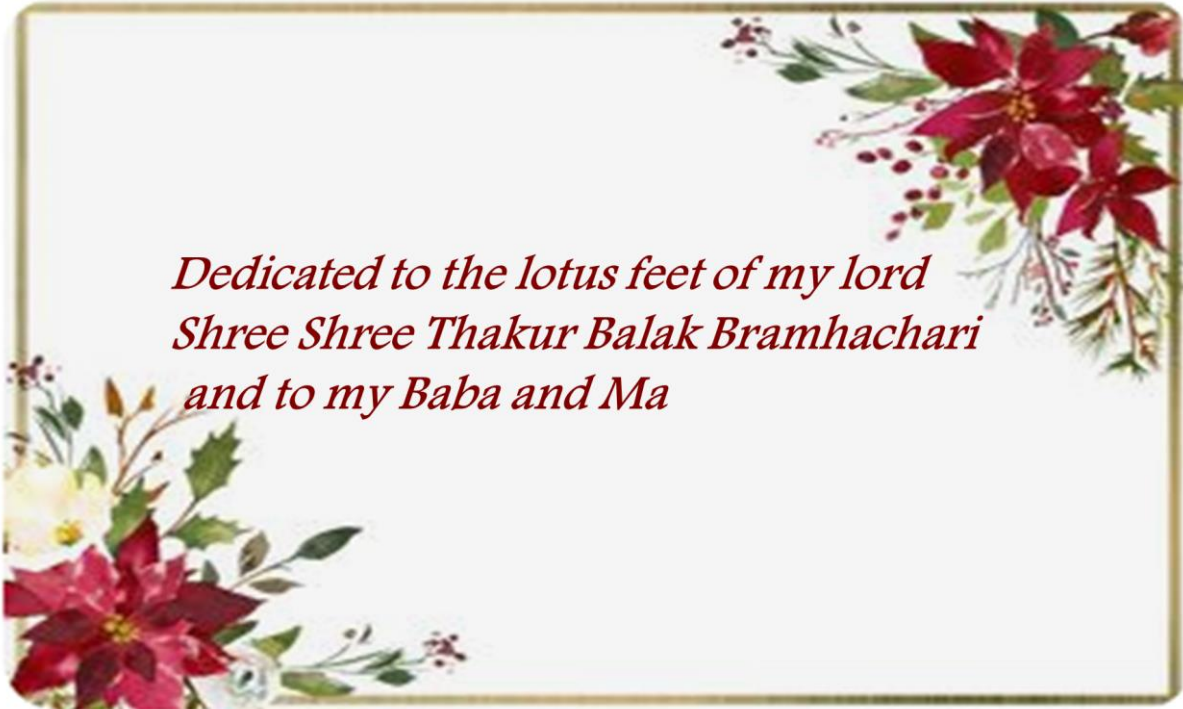
Date: 10/11/2022

Mahammad Ali

(Mahammad Ali)

Signature of the Supervisor & date with seal

Dr. Mahammad Ali
Professor
Department of Chemistry
Jadavpur University
Kolkata-700 032

Dedicated to the lotus feet of my lord
Shree Shree Thakur Balak Bramhachari
and to my Baba and Ma

Acknowledgements

Sasmal, Miss. Ananya Dutta, Miss Rousunara Khatun and Miss Dolan Moni. In every hard and tough situations, they were with me providing their important discussions and friendship which makes my journey into the beautiful memories which I will never forget.

I am thankful to my Collaborators Mr. Chandrodaya Prodhan and Dr. Atul Katarkar, (former research scholar at CSIR-Indian Institute of Chemical Biology, Kolkata-700032, India) for their help in my work.

I am fortunate enough to gratefully acknowledge the assistance of my beloved friends, Rituparna, Subhadeep, Nandita, Madhushree, Arindam, Susmita, subrata, Debashish, Sayan, Poulomi, Tanmoy for their care to me in this journey. In all the hard moments they were always with me to push and motivate me. Without their support this journey would not be easy and plesurable.

I am highly honoured to have such supporting roommates and PG-mates like Wahida di, Amrita, Aditi, Rijia di, Pameli, Sunanda, Priyanka and all others for their nice co-operation. No words can be sufficient to greet their kind supports.

I am highly thankful to my joyful cousins mini, disha, arko, titu, aneek, mintu, mampi, durga di, chandan da for their love and respect to me.

Finally, thanks can not be enough to acknowledge the people who are a lot to me, my parent, didi, vai, dada, adrija and archisa for giving love and affection to me and delivering their significant talk which worked on me as fuel in this challenging journey. They have provided me both the moral and emotional support in my life and prayers on my behalf. I would never be able to compensate their doings which they have done for me.

Also I convey my gratitude to each who had promising insight to this thesis, as well as expresses my apology for not addressing personally one by one.

I gratefully acknowledge DST-INSPIRE for financial support to enjoy and carry out the research work.

Department of Chemistry   Debjani Maiti

Jadavpur University

Kolkata– 700032, India.

Preface

The work presented in this thesis entitled **"Synthesis and Photophysical Studies of Fluorescent Probes for Nitric Oxide and Nitroxyl with Bio-imaging Applications"** was started in june, 2016 and has been carried out in the Department of Chemistry, Jadavpur University.

This thesis is comprised of five chapters which are condensed below:

Chapter 1 consists a short introduction of small bio-molecule NO (Nitric Oxide)/HNO(nitroxyl) along with the brief review of selective detection of NO and HNO by fluorometric method.

Chapter 2 describes about the probe PQPY which was designed and synthesized through the convenient and efficient way. It is a phenanthroquinone–pyridoxal based fluorogenic probe , highly suitable for the selective and sensitive detection of nitric oxide in an aerated aqueous (7 : 3 / H_2O: MeCN) medium at pH 7.0 (10 mM HEPES buffer). Upon addition of nitric oxide, this probe exhibits emission in the green region (λ_{em} = 505 nm) which is ascribed to ICT (intramolecular charge transfer) from the phenanthroquinone moiety to the imidazole –N–N=O fragment. The apparent formation constant, K_f, of the NO product of the ligand is $(1.00 \pm 0.2) \times 10^5$ M^{-1} and the LOD is 78 nM. The substantial enhancement of the life-time of the ligand (τ_0 = 2.68 ns) occurs due to binding with nitric oxide (τ_0 = 3.96 ns). This probe is low cytotoxicity, cell permeable and suitable for living cell imaging application.

Chapter 3 introduces about a highly selective and sensitive nitric oxide fluorescence probe BCM. It is a benzo-coumarin embedded smart molecular probe, employed for NO sensing through detailed fluorescence studies in purely aqueous medium. All the spectroscopic analysis and literature reports clearly validate the mechanistic insight of this sensing strategy *i.e.*, the initial formation of 1,2,3,4-oxatriazole on treatment of the probe with NO which finally converted to its carboxylic acid derivative. This oxatriazole formation results in a drastic enhancement in fluorescence intensity due to the photoinduced electron transfer (PET) effect. The kinetic investigation unveils the second and first-order dependency on [NO] and [BCM] respectively. The very low detection limit (16 nM), high fluorescence enhancement (123 fold) in aqueous medium and good formation constant ($K_f = (4.33 \pm 0.48) \times 10^4$ M^{-1})

along with pH invariability, non-cytotoxicity, biocompatibility and cell permeability make this probe a very effective one for tracking intracellular NO.

Chapter 4 delineates about a novel copper complex based fluorescent probe $[Cu^{II}(DQ_{468})Cl]^+$ that exhibits a significant fluorescence turn-on response towards nitroxyl (HNO) with high selectivity over other biological reactive oxygen, nitrogen and sulfur species, including nitric oxide (NO). A smart strategy, involving HNO-induced reduction of paramagnetic $[Cu^{II}(DQ_{468})Cl]^+$ to diamagnetic $[Cu^{I}(DQ_{468})]^+$ with concomitant fluorescence enhancement via a PET mechanism is focused here. This reduction-based strategy was also supported by X-band EPR response and mass spectroscopy. The metal free probe (DQ_{468}) showed high affinity towards Cu^{2+} to form $[Cu^{II}(DQ_{468})Cl]^+$ with a 0.091 μM detection limit, which subsequently enabled the detection of HNO in an organo-aqueous medium at biological pH (7.4) in the green wavelength region ($\lambda_{em} = 543$ nm) with a LOD of 0.41 μM. The ground-state geometries of DQ_{468}, $[Cu^{II}(DQ_{468})Cl]^+$ and $[Cu^{I}(DQ_{468})]^+$ were optimized by DFT calculations, which revealed that the central metal ion in $[Cu^{II}(DQ_{468})Cl]^+$ is in a distorted tetrahedral geometry with the C1 point group. Additionally, the negligible cytotoxicity and good biocompatibility make the developed probe useful for the in vitro detection of HNO.

Chapter 5 represents the highlights of the thesis.

List of Abbreviations

EDRF	Endothelium-derived Relaxation Factor
NOS	Nitric Oxide Synthase
NADPH	Nicotinamide Adenine Dinucleotide Phosphate
FAD	Flavin Adenine Dinucleotide
FMN	Flavin Mononucleotide
BH_4	(6R-)5,6,7,8-tetrahydro-L-biopterin
GTP	Guanosine triphosphate
cGMP	Guanosine 3',5'-cyclic monophosphate
Hb	Haemoglobin
τ	Fluorescence Lifetime
$\Delta\bar{v}$	Stokes shift
Φ	Quantum yield
OPD	*o*-phenylenediamine
BODIPY	Boron dipyrromethene
RNS	Reactive nitrogen species
ROS	Reactive oxygen species
RCS	Reactive carbon species
LOD	Limit of detection
TP	Two-photon
PA	Photoacoustic
CHEQ	Chelation Enhancement of Quenching
CHEF	Chelation Enhancement of Fluorescence
MLCT	Metal–Ligand Charge Transfer
ILCT	Intra–Ligand Charge Transfer
PET	Photo-induced Electron Transfer
ICT	Intramolecular Charge Transfer
D-A-D	donor–acceptor–donor
FRET	Fluorescence Resonance Energy Transfer
AIEE	Aggregation-Induced Enhanced Emission
ESIPT	Excited-State Intramolecular Proton Transfer
LRET	Luminescence resonance energy transfer
DLS	Dynamic light scattering
SEM	Scanning electron microscope
TEM	Transmission Electron Microscopy
UV-Vis	Ultraviolet-visible
EPR	Electron paramagnetic resonance
HOMO	Highest Occupied Molecular Orbital
LUMO	Lowest Unoccupied Molecular Orbital
AA	Ascorbic Acid
DHA	Dehydroascorbic Acid

MGO	Methylglyoxal
SNP	Sodium nitroprusside
AS	Angeli's salt
SDS	Sodium dodecyl sulfate
L-NMMA Acetate	N(omega)-Monomethyl-L-Arginine
NBD	Nitrobenzoxadiazole
ER	Endoplasmic reticulum
HEPES	4-(2-Hydroxyethyl)piperazine-1-ethanesulfonic acid
DFT	Density functional theory
TDDFT	Time-dependent density functional theory
CPCM	Conductor-like Polarizable Continuum Model
MeCN	Acetonitrile
MeOH	Methanol
NaOH	Sodium hydroxide
HOCl	Hypochlorus acid
NaCl	Sodium chloride
DCM	Dichloromethane
DMF/dmf	Dimethyl formamide
H_2O	Water
DMSO/dmso	Di-methyl sulfoxide
mL	Milliliter
μM	Micro molar
μL	Micro liter
nM	Nano molar
mM	Mili Molar
K_a	Binding constant/Association constant
K_{ass}	Association constant
K_d	Dissociation constant
K_f	Formations constant
ex	Excitation
em	Emission
λ	Wavelength
HUVECs	Human umbilical vein endothelial cells
HeLa	Human epithelial carcinoma cell
HepG2	Human hepatocellular liver carcinoma cells
PBS	Phosphate-buffered saline
DMEM	Dulbecco's Modified Eagle's Medium
MTT	3-(4,5-di methylthiazol-2-yl)-2,5 diphenyltetrazolium bromide
IFN-γ	interferon-γ
LPS	lipopolysaccharide
L-Arg	L-arginine
%T	Percentage of Transmittance

FBS	Fetal Bovine Serum
LOD	Limit of detection
MS	Mass spectroscopy
NMR	Nuclear magnetic resonance
FT-IR	Fourier transform Infrared
LC-MS	Liquid chromatography mass spectrometry
SMMC-7721	Hepatocellular carcinoma cell
FI /F.I	Fluorescence Intensity
GSH	Glutathione
Cys	Cysteine
Raw 264.7	Abelson leukemia virus transformed cell
hMSCs	Human mesenchymal stem cells
BINOL	1,1'-Bi-2-naphthol
NIR	Near-infrared
MCF7	Acronym of Michigan Cancer Foundation-7 cell
FE	Fluorescence Enhancement
EJ	Lung cancer cell
Tris–HCl	Tris (hydroxymethyl) aminomethane hydrochloride
UV	Ultraviolet
Vis	Visible
h	Hours
HPLC	High-performance liquid chromatography
TMS	Tetramethylsilane
KBr	Potassium bromide
K_2CO_3	Potassium carbonate
ESI-MS$^+$	Electrospray ionization mass spectrometry
HRMS	High-resolution mass spectrometry
CH_2Cl_2	dichloromethane
$SOCl_2$	Thionyl chloride
$CDCl_3$	Chloroform-d
DMSO-d_6	Deuterated Dimethyl sulfoxide
LiCl	Lithium chloride
ATP	Adenosine triphosphate
Pi	Phosphate - Wikipedia
PPi	Pyrophosphate
CD_3OD	Methanol-d4
Et_3N	Triethylamine
MHz	Megahertz
f	Oscillator strength
°	Degree
Å	Angstrom
eV	Electron volt

Contents

Chapter 2	Page

Selective sensing of nitric oxide by a 9,10 phenanthroquinone–pyridoxal based fluorophore

Chapter 3	Page

A coumarin embedded highly sensitive nitric oxide fluorescent sensor: kinetic assay and bio-imaging applications

Chapter 4	**Page**

Dansyl-appended CuII-complex-based nitroxyl (HNO) sensing with living cell imaging application and DFT studies

Chapter 5	

Appendix	

CHAPTER 1

Fluorescent Molecular Probes for Sensing of Nitric Oxide and Nitroxyl

CHAPTER-1

1. Introduction

Nitric oxide (NO) is a colorless, hetero-diatomic, paramagnetic and highly reactive gaseous biomolecule which has drawn the heightened interest of chemists and biologists for last few decades because of its unmatched roles in human biology. In spite of its toxicity at higher concentration, NO acts as a prime signaling species in animals. It functions like a messenger molecule which transmits signals to cells in the important biological systems i.e. cardiovascular, nervous, and immune systems. NO exhibits more reactivity than other popular signaling molecule due to its free radical nature. Moreover, due to its small size it can easily penetrate in the cell membranes and walls which makes it one of the leading members of reactive nitrogen species (RNS) associated in a plenty of pathological and biological process during cell signaling.[1] For instance, production in low concentration regulates vasodilatation, defense against pathogens and long-lasting enhancement in signal transmission, whereas production in micromolar concentration causes carcinogenesis and neurodegenerative disorders.[2-7] In other way of consideration, NO is toxic and poisonous, being exhausted from the industrial incomplete combustion of nitrogen containing fossil fuels and automotive engines, imparting a huge impact on environment.[8] However, catalytic converter shows the way to reduce the release of NO in atmosphere. It is also well established that atmospheric NO is responsible for ozone layer depletion, photochemical smog in urban areas and has been implicated in acid rain. The human body enzymatically synthesizes NO from L-arginine in presence of nitric oxide synthase which plays a pivotal role in smooth muscle relaxation, including platelet inhibition, respiration, neurotransmission, immune response and apoptosis.[9,10] Historically, almost 40 years ago nitric oxide was recognized as an endothelial derived relaxing factor (EDRF). The Nobel prize was awarded to Robert F. Furchgott, Ferid Murad, and Louis J. Ignarro for this outstanding findings about nitric oxide in the field of medicine or physiology in 1998.[11] The research dealing with the importance of NO in biology build-up in past 20 years exploring its important roles in cardiovascular system, immune system, gastrointestinal tract, central nervous system and the renal system.[12–16] So, this versatile impact of NO in biology has forced modern scientists to develop some convenient strategies for selective and sensitive detection and quantitative

estimation of NO levels in biological organisms to well-understood the biological roles of it in human body.

Nitroxyl (HNO; also named as nitrosyl hydride, hydrogen oxonitrate (IUPAC)) is an evasive protonated redox cousin of nitric oxide (•NO).[17-19] Postulation has been made about the formation of HNO as an intermediate reactive species generated in the different thermal and photochemical processes.[20,21] The gradual investigation also says that HNO is an intermediate formed in de-nitrification of bacteria, in combustion of fuels which are mainly composed with nitrogen as well as in atmospheric and celestial chemistry. Owing to the near structural resemblance of HNO with NO, it is firstly considered as a probable constituent formed as intermediate in the biosynthesis NO as well as in the time of NO's bio-signaling.[19,22-25] In spite of the structural alikeness with NO, it behaves differently with respect to basic chemical and biological properties.[26-29] The Chemists and biologists become very much curious to unveil the chemical dynamics, structure and spectroscopy of this triatomic signaling biomolecule through experimental and theoretical research.[30-33]

1.1 Mechanisms of Nitric Oxide Syntheses and it's Biological Plea

In biological system NO concentration in different organs was maintained by the enzyme nitric oxide synthases (NOS). In 1989, it was first established that there are three isoforms of nitric oxide synthase (NOS) in mammals. These are named after the site where they are originally found.[34-36] These isoforms are mentioned as neuronal n-NOS, inducible i-NOS, and endothelial e-NOS. All these homologues of NOS deploy L-arginine as the substrate, taking molecular oxygen and reduced NADPH as co-substrates. Flavin adenine dinucleotide (FAD), flavin mononucleotide (FMN), and (6R-)5,6,7,8-tetrahydro-L-biopterin (BH_4) acts as cofactors of all NOS. All these NOS isoenzymes have similar structures containing both an oxygenase domain and a reductase domain that are connected through a binding site for calmodulin.[37,38] All NOS proteins consists of a zinc–thiolate cluster produced by a zinc ion which is tetrahedrally attached to two CysXXXXCys motifs (one contributed by each monomer) at the NOS dimer interface.[39-41] A functional NOS shifts electrons from NADPH, through FAD and FMN in the carboxy-terminal reductase domain to the heam present in the amino-terminal oxygenase domain. There

is a binding of cofactor BH_4, molecular oxygen and L-arginine in oxygenase domain.[38,42] To generate NO, the NOS enzyme proceeds through two steps reactions. The first step comprises of hydroxylation of L-arginine by NOS to generate N^ω-hydroxy-L-arginine which gets highly bounded to that enzyme. The second step carries oxidation of N-hydroxy-L-arginine by NOS to synthesize L-citrulline and NO.[43-44] This NOS mediated NO can work on the plenty of targeted enzymes and proteins. The activation of soluble guanylyl cyclase (sGC) and the formation of cyclic GMP are the prime signaling pathway which are induced by NO.[45-49] **Figure 1.1** demonstrates the process by which NO is bio-synthesized.
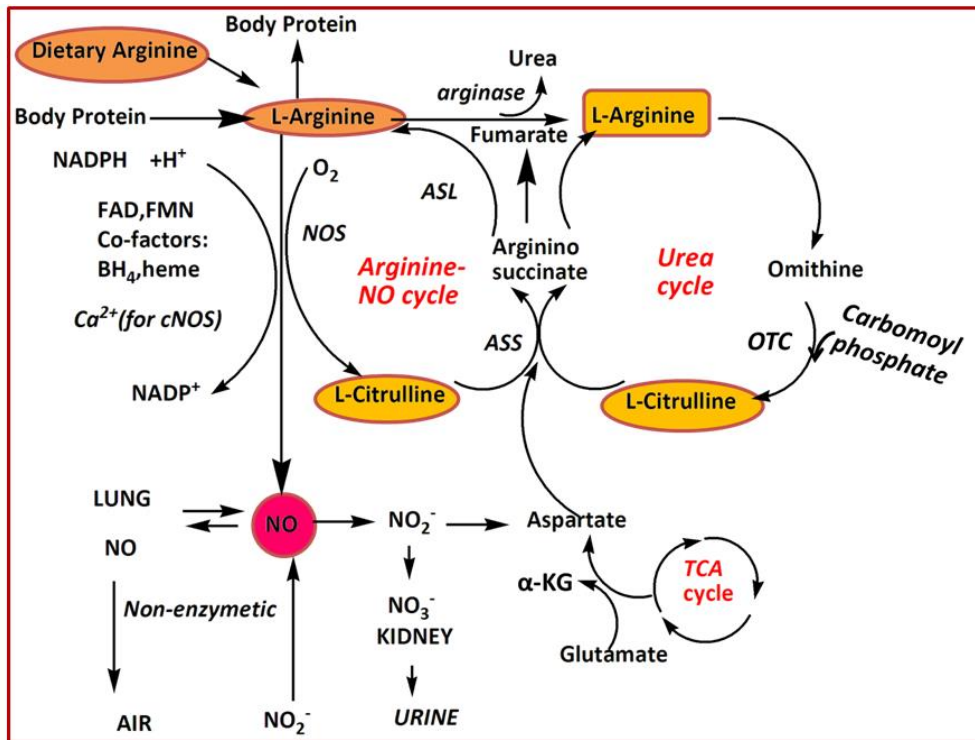
Figure 1.1 Pathway for NO synthesis.

In biological point of view Nitric Oxide has immense contribution in physiological processes where, most of it is revealed regarding its salient behaviors, but much is still unexplored. It is the signaling molecule which is associated with the control of vasodilatation, neuromodulation, smooth muscle relaxation, hormone production, blood pressure control and the immune signaling towards infections due to bacteria.[12,15,50-52] The misregulation of NO in bio-organisms will

resulted in different kind of diseases, like neurodegenerative disorders, arteriosclerosis, cancer and endothelial dysfunction.[53-56]

In gastrointestinal tract, NO shields the stomach epithelium by inducing mucosal and bicarbonate productions.[14,57,58] It regulates gene transcription[59,60] and m-RNA translation by interacting with iron responsive elements[61,62] and produce post-translational moderations of proteins by adensosine-5′-diphosphate ribosylation.[63,64] With the day by day progress in NO research, it is revealed that some biologically reactive nitrogen species, formed by NO oxidation (NO_2, N_2O_3, $ONOO^-$, NO_2^-, NO_3^-, HNO) also play important roles in both physio- and pathological processes.[2-4,15, 65-68]

Therefore, it is highly important to develop some advantageous pathways for selective and sensitive tracking of NO concentration in biological systems to well-understand the biological features of NO in human health which are described below.

1.2 Popular Methods for Monitoring Nitric Oxide

1.2.1. Griess test

Colorimetric Griess method is one of the commonest approaches which estimates nitrite level, as it is the steady by-product of NO. This method is used to calculate the NO concentration in a sample before degradation. Nitrite is formed due to the areal oxidation of NO using following reactions.

$$2NO + O_2 \rightarrow 2NO_2 \qquad (1)$$

$$NO + NO_2 \rightarrow N_2O_3 \qquad (2)$$

$$N_2O_3 + H_2O \rightarrow 2NO_2^- + 2H^+ \qquad (3)$$
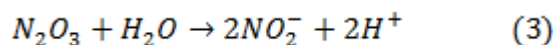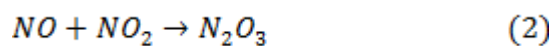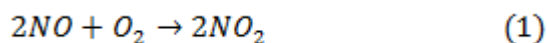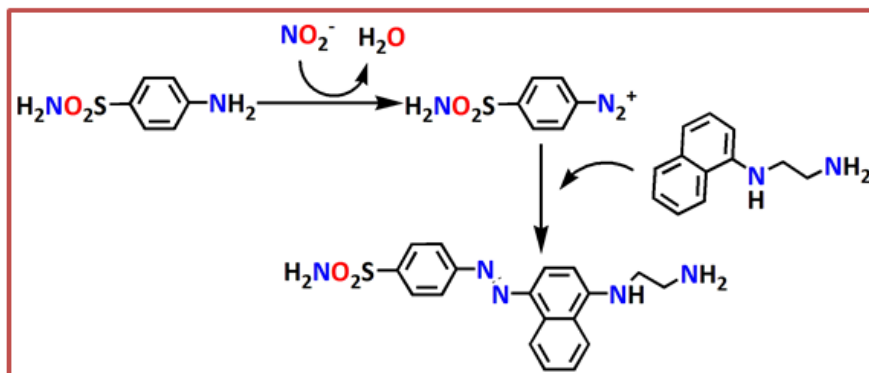
Figure 1.2 The commonly known diazotization reaction by Griess.

After publishing the test by Peter Griess, variety of modifications has been carried out to get it easily available. However, still the Griess's original methods are widely adopted for this purpose.[69] Here, sulfanilamide in phosphoric acid and N-1-napthylethylenediamine di-hydrochloride are added to the experimented sample as described in **Figure 1.2**.

There is a change in colour because of the formation of azo-derivative. Then the absorbance measured for the nitrite ion in the sample is compared with a standard to get the concentration of NO in the sample of interest. But these assays provide an approximate NO levels in a solution leading to approximate results.

1.2.2 Electrochemical detection

An electrochemical method is efficient for continuous monitoring of NO concentration in real-time. Not only that, *in vivo* monitoring of NO, even in human beings, is possible without any interference from common species present in biological systems. Malinski and Taha developed an electrochemical probe where, carbon fibers are covered with polymeric porphyrin and then with Nafion coating to track NO which is generated from a single cell.[70] Shortly thereafter, Malinski's laboratory established that an electrochemical probe can be suitably utilized to monitor nitric oxide within the blood vessels of a living body.[71]

However, there are two serious limitations of these electrochemical sensors as stated below:

a) This electrochemical probe has not been exploited to get information about NO levels throughout a cell.

b)   Also this probe is not suitable to track NO for a prolonged time intervals.

These are of prime requirements to be satisfied to follow the natural activities of NO in physiological processes.

1.2.3 Chemiluminescent probes

Chemiluminescent probes are useful to sense nitric oxide specifically in fluid samples by the stimulation of guanylyl cyclase, converting guanosine triphosphate (GTP) to guanosine 3',5'-cyclic monophosphate (cGMP) with simultaneous formation of pyrophosphate. There is a sequential interaction with adenosine triphosphate sulfurylase to form ATP.[72,73] This formed ATP interacts with a luciferin-luciferase system resulting an emission of light at 560 nm.[72-73] The shortcomings of this proceedure are the inefficiency to track cellular nitric oxide, as here, only the supernatant fluid of the cell is investigated. Additionally, this assay is unable to provide real-time response and also this method cannot be utilzed in presence of Hb (haemoglobin).[74]

1.2.4 Fluorescent probes

For a past few decades some different techniques like fluorescence, amperometry, colorimetry, electrochemical method, chemiluminescent method and electron paramagnetic resonance spectroscopy (epr) etc. has been evolved to analyze the NO diffusion sensitively and selectively in bio-organisms.[75-78] But among these strategies fluorescence spectroscopy is of gold standard due to its efficiency to detect NO both in extra-cellular and intracellular conditions providing spatio-temporal distribution.[79] Now to be a useful and efficient fluorescent probe to track NO in cellular system, it should be:

    a. Highly specific as well as sensitive towards NO without interfering other biologically reactive species

    b. Excitation wavelength (λ_{ex}) of the probe should exceed 340 nm to encounter cell destruction induced by UV and emission wavelength should be $\lambda_{em} \geq 500$ nm to ignore auto-fluorescence which occurs due to the local species present in the cell.

   c. The probe should have high level of water solubility so that the sensor can penetrate to the cell membrane.

   d.   The quantum yield should be high enough to permit the glass microscope objectives.

Till date, there are so many useful fluorescent NO sensors which have been reported with their variety of positive and negative features.

This chapter delineates about the recent development of molecular probes utilizing fluorescence spectroscopy (by our and other research groups) for NO sensing with different possible reaction mechanism.

1.3 Designing Strategies and General Consideration for the Detection of NO Based on Molecular Fluorescent probes

There are two main types of fluorescent probe for NO detection which are associated with two popular approaches.

- **Organic probes**
- **Metal complex based probes**

Organic probes:

Organic probes for nitric oxide sensing using fluorescence, generally contain two typical parts namely (i) an NO receptor moiety and (ii) a fluorophoric moiety. The useful NO recognizing moieties are:

   (i) *o*-phenylenediamine (OPD),

   (ii) aromatic secondary amines,

   (iii) dihydropyridine (Hantzsch ester),

   (iv) aromatic amines leading to diazotization or oxidative deamination on reaction with NO,

   (v) acylhydrazide and

   (vi) some others which lead to turn-on fluorescence response.

In some cases, these probes have been made organelle targeting by equipping with some delivery vehicles which are generally positively charged quaternary pyridinium or triphenyl phosphonium

groups with mitochondria targeting properties. Again, there are some probes embedded with morpholine as lysosome tracker.

The metal based fluorescent probes has been used in NO detection by two strategies one is trapping of NO by the metal–ligand complexes and another one is NO trapping with simultaneous removal of metal and restoration of fluorescence. This strategy is described latter.

Most of the NO probes shows turn-on fluorescence owing to blocking of photo-induced electron transfer (PET) process.

1.3.1 Organic Probes for NO Detection

1.3.1.1 NO sensing through triazole formation on reaction of *o*-phenylenediamine

Here, NO sensing strategy is constructed on the generation of electron deficient triazole from *o*-phenylenediamine (OPD) moiety attached to a fluorophore. The absence of NO allows PET process facilitating charge transfer from electron populated OPD moiety to fluorophore making the probe non-fluorescent (turn-off). On reaction with NO the diamine is converted to its corresponding electron deficient triazole that blocks the PET process thereby making turn-on fluorescence response.

Taking advantage of this strategy, Nagano et al. has pioneered a series of fluorescein based NO sensors **1-8 (Figure 1.3),** where, *o*- phenylenediamine group is attached with fluorescein moiety in the ring-closed spirolactam form. Here, increment in fluorescence emission peak (>100 fold) was noticed because of triazole ring formation with simultaneous opening of spirolactam ring, providing a very low LOD value (5 nM).[80] Probe **7** and **8** were slightly modified to avoid pH dependency of the probe and making it more biocompatible.[81]
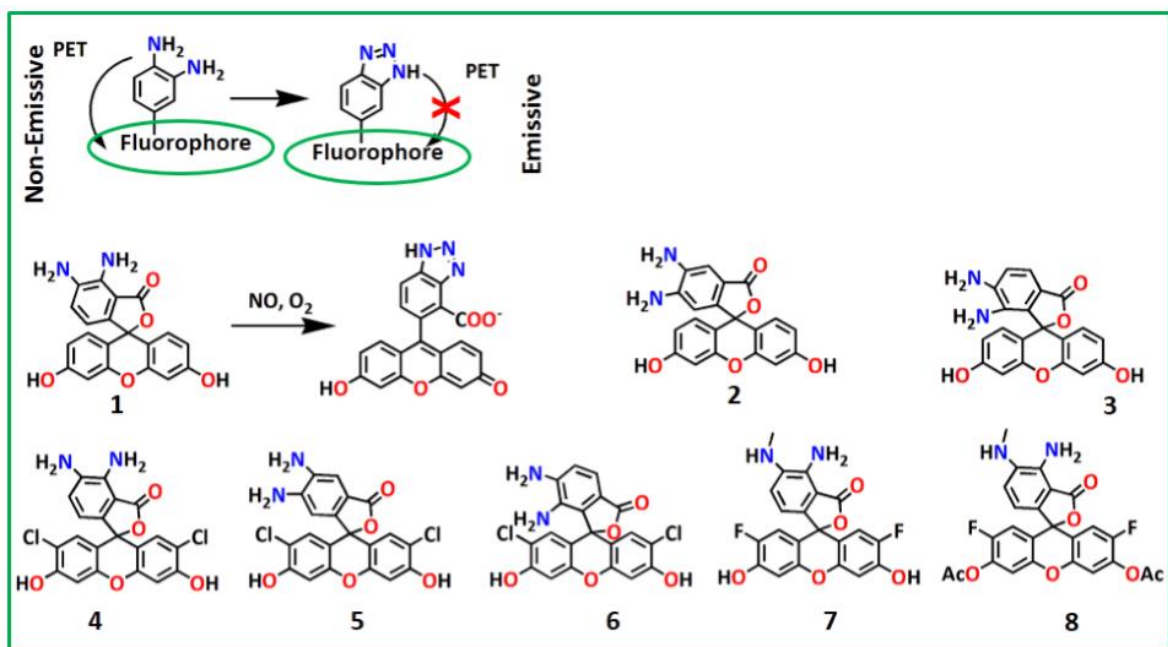
Figure 1.3 Fluorescein based NO probes.

In 2016, Wang group published a NO fluorescent sensor **9 (Figure 1.4)** by exploiting this strategy using boron dipyrromethene (BODIPY) as a fluorophore showing amphiphilic property and with a possibility to be anchored on the cell membrane making it suitable for imaging NO released from cells.[82] The probe exhibits huge enhancement of fluorescence emission ($\lambda_{em} = 529$ nm) on addition of NO within a minute with substantially low LOD which is calculated to be 0.83 nM. Liang and coworkers reported an OPD based probe **10 (Figure 1.5)** in 2016, where, diamine moiety is connected with phenylalanine (amino acid) through amide bond making it highly water soluble and biocompatible. The weak fluorescence emission of **10** at 440 nm, shifted to blue region 367 nm after NO treatment due to ICT mechanism with LOD 6 nM.[83]
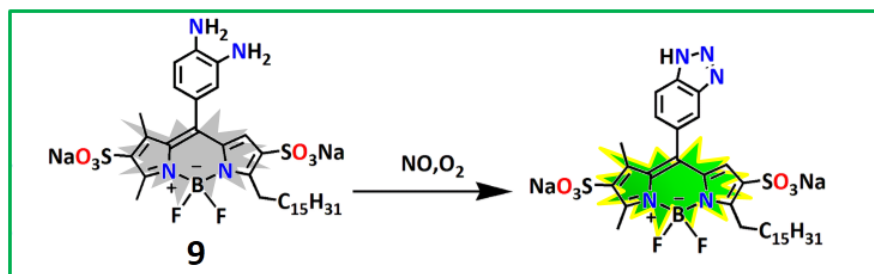
Figure 1.4 A BODIPY based OPD probe for NO sensing.

Zheng group disclosed an innovative NO probe **11 (Figure 1.5)** where a Nile Red[84] fluorophore moiety was embedded with OPD through an ether bond.[85] Treatment with NO, **11** shows a strong red fluorescence at longer wavelength (658 nm, 28 fold) due to inhibition of PET between Nile Red core and OPD moiety. The LOD was reported to be 9 nM. The emission at 658 nm helps to avoid interference from auto-fluorescence which occurs due to intracellular native species like folic acid, retinol and riboflavin. Interestingly, this probe shows one and two photon excitation after NO treatment revealing its *in-vitro* and *in-vivo* applicability. This kind of NO sensor can be excited by NIR wavelength delineating high efficiency to monitor endogenously generated NO in animal samples, due to the red emissive fluorescence and good tissue penetrating ability.

Another OPD appended Nile red conjugate **12 (Figure 1.5)** was developed by Liu's group[86] which facilitates both *in vitro* as well as *in vivo* imaging of NO, though OPD was at a distance from the Nile red moiety attached through an ethylenedioxy (–OCH$_2$CH$_2$O–) chain. This design was to avoid the fluorescence quenching by PET, as caused by short distance between donor and accepter moieties. They developed this two photon excitation and red-emissive (650 nm) fluorescent probe with LOD 46 nM. The probe **12** exhibited very fast response towards NO (180 s) enabling the detection of exo-and endogenous NO.
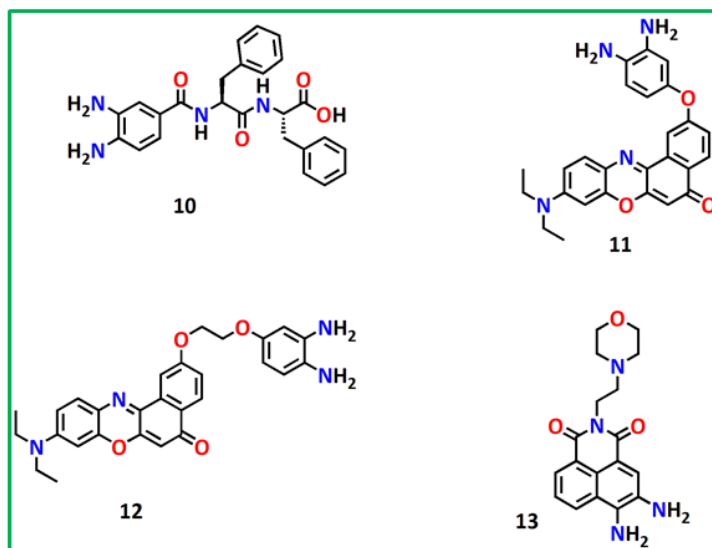
Figure 1.5 Structure of some probes with different fluorophore for NO sensing.

In 2016 Xu and coworkers[87] published an article, where they described the NO sensing behavior of a morpholine equipped lysosome targeting fluorescent probe **13 (Figure 1.5)** which was found

to emit blue fluorescence at 460 nm upon interaction with NO. The probe **13** exhibits pH stability in the range 4-12. They also reported the LOD of **13** for NO as 4.57 μM. The lysosome targeting property of **13** was established in CHO cells where co-localization study using a lysosome tracker (Neutral Red) showed an overlap between the two images. This experiment clearly indicates the specific accumulation of the probe in lysosome.

Another OPD embedded lysosome targeting NO sensing probe **14 (Figure 1.6)** with novel donor–acceptor–donor (D-A-D) system undergoes a Far-Red fluorescence emission.[88] The benzothiadiazole-diamine acts as electron accepting moiety and alkyoxyl groups behaves like electron donating one. The probe **14** displays negligible fluorescence at 625 nm on excitation at λ_{ex} = 488 nm, because of mild ICT mechanism influenced by TOPD (thiadiazolefused OPD). But NO treatment converted the di-amine in benzotriazole system which acts as stronger electron acceptor making prominent ICT effect and concomitant fluorescence emission has been noticed (446 fold). More importantly, this probe is efficient enough to identify the difference of lysosomal NO concentration in acute liver injury mouse model *ex vivo*.

There is another D-A-D based photoacoustic nitric oxide probe **15**[89] **(Figure 1.6)** where di-phenylamine moieties were connected to benzothiadiazole-1,2-diamine moiety. To improve its amphipathic and cell-penetrating capacity an oligo-ether tail was incorporated to each diphenylamine group.
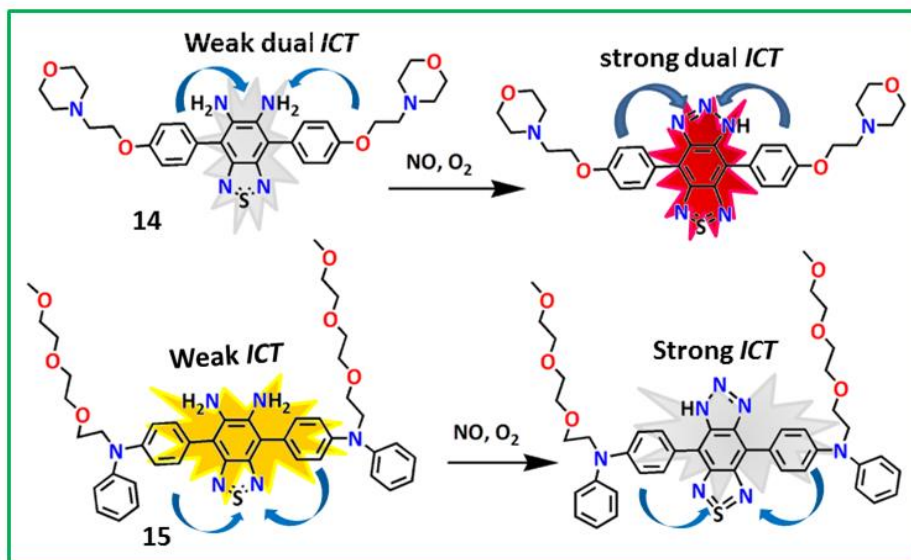
Figure 1.6 Benzothiadiazolediamine (D-A-D) based NO sensors.

In this system, yellow fluorescence of the probe gets quenched on NO treatment, probably due to dipole–dipole interactions between solvent–solute i.e. between PBS buffer and NO product which inhibit the ICT effect. The LOD value was calculated to be 0.261 μM. Probe **15** also showed promising photoacoustic emission, in inflamed mice model at 532 nm in the presence of NO and remains silent towards other reactive species**.**

In solid tumor, Hypoxia is a common and significant feature indicating the necessity for cancer chemotherapy.[90,91] Hypoxia is also associated with the excessive production of nitric oxide in tumor cells leading to metastasis and proliferation.[92,93] Singh and coworkers developed a new strategy where chlorambucil, an anticancer drug was embedded with a coumarin based fluorophore equipped with nitro and amino groups in adjacent positions of **16 (Figure 1.7)** [94], This probe has performed wisely to detect hypoxia and NO which finally releases the drug in cancer cells. Thus this probe can function efficiently as a dual-analyte sensing tool as well as a prodrug. This nitro group in coumarin gets reduced to amine in hypoxia environment generating *o*-diamine moiety which shows green fluorescence. On subsequent reaction with NO, *ortho-* di-amine is converted to triazole which shows blue fluorescence. Additionally, this probe in triazole state wonderfully releases the cancer drug, chlorambucil, on photo irradiation at ≥410 nm causing cell death.
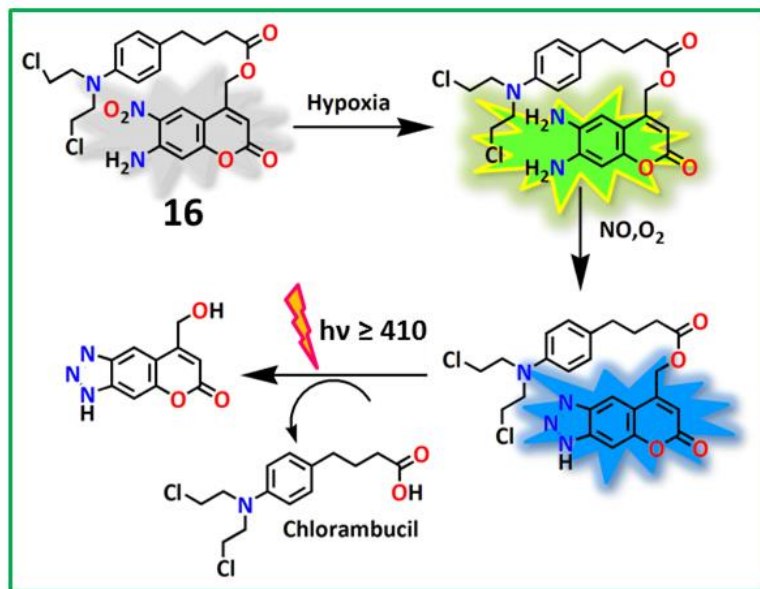
Figure 1.7 A drug based NO sensor in hypoxia environment.

Though there are significant developments and modifications in OPD based fluorescent NO probes but still there exists some serious short-comings due to interference by certain biological species like dehydroascorbic acid (DHA), ascorbic acid (AA) and methylglyoxal (MGO). AA is easily oxidized to DHA. DHA and MGO react easily with OPD to form quinoxaline derivatives which are highly fluorescent and interfere in the detection of NO which may provide false positive response.[95] These problems have been sorted out by reducing the reactivity of OPD by converting it into secondary amine, which acts as a good NO trapping agent thereby judiciously avoiding the interference from the above mentioned reactive species.

So keeping this strategy in mind, Wang et al. has prepared an OPD based amphiphilic probe **17 (Figure 1.8)** through multistep reactions. Here, 1,8-naphthalimide acts as a fluorophore; one secondary amine group equipped with quaternary ammonium ion as hydrophilic recognition unit and a long chain hydrocarbon ($C_{17}H_{35}$) as hydrophobic lipid chain. The latter is useful to anchor the probe on to the cell membrane.[96] This plasma membrane targeting probe is almost non-fluorescent and resulted in 16.7 fold increase in fluorescence intensity after NO treatment. It also exhibits low LOD value of 74 nM at 538 nm. Additionally, this probe reveals a strong two-photon excitation fluorescence emission. The authors established that the probe is suitable to image exogenous NO in neurons and endogenous NO in HUVECs cell line. Thereby they proposed that this probe has a potency to monitor endogenous NO in mouse brain tissues.

Here, another OPD based a near-infrared (NIR) fluorescent sensor, **18 (Figure 1.8)** with protection of one amine group by linking with fluorophore (silicon-substituted xanthene, SiR) was reported by Guo et al. in 2017.[97] This probe was found to be fast and selective for real-time tracking of mitochondrial NO in living cells with Pearson's co-localization coefficient of 0.98. It displays a fluorescence enlargement centered at 710 nm upon NO treatment owing to controlled PET effect.
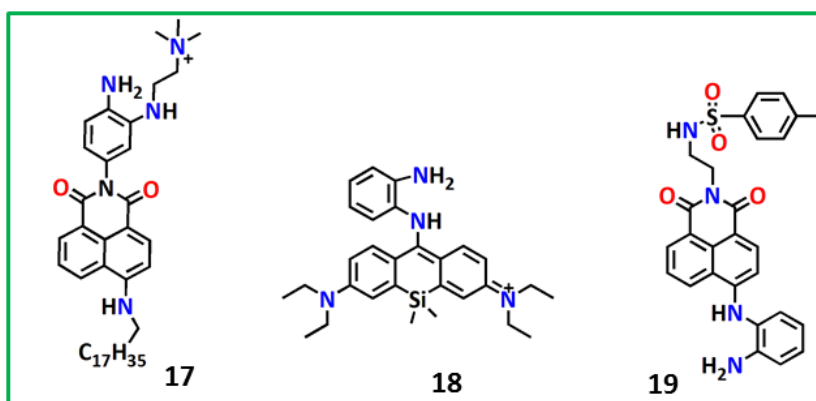
Figure 1.8 OPD based NO sensors utilizing one secondary amine.

Endoplasmic reticulum (ER) displays a title role in protein synthesis which can be perturbed by NO leading to the ER stress and cell apoptosis.[98] This NO influenced stress is associated with the pathogenesis of most of the vascular disorders.[99,100] So the ER targeting NO fluorescent probe **19** **(Figure 1.8)** is of great importance and reported by Li et al. where methyl sulfonamide moiety was attached to target endoplasmic reticulum. On reaction with NO **19** depicts a 22 fold fluorescence increment (λ_{em} = 538 nm) due to triazole formation that inhibits the PET process of transferring electron from OPD to napthalimide moiety. A very low LOD (3.3 nM) implies that it is highly sensitive towards monitoring NO.

In 2019, a dual-channel analyzing probe **20 (Figure 1.9)** based on BODIPY system was first reported by Yang et al. for the recognition of NO and GSH.[101] Here, 4-amino-3-(methylamino)-phenol group reacts with NO to form corresponding benzo-triazole resulting the generation of highly florescent entity which on excitation at 505 nm emits at 528 nm in the green region. On parallel reaction with glutathione (GSH) it replaces the 4-amino-3-(methylamino)-phenol moiety to form the corresponding glutathione substituted BODIPY which on excitation at 538 nm portrayed an 1800-fold enhanced red fluorescence (λ_{em} = 558 nm). This probe was promisingly employed to monitor the exo- and endogenously produced NO and GSH in macrophage cells. Interestingly, endogenous formation of NO stimulated by interferon-γ (IFN-γ), lipopolysaccharide (LPS), and L-arginine (L-Arg) could also induce the enlargement of intracellular GSH. The authors were enthusiastic to claim that the probe might be useful to investigate the redox equilibrium in biological processes.
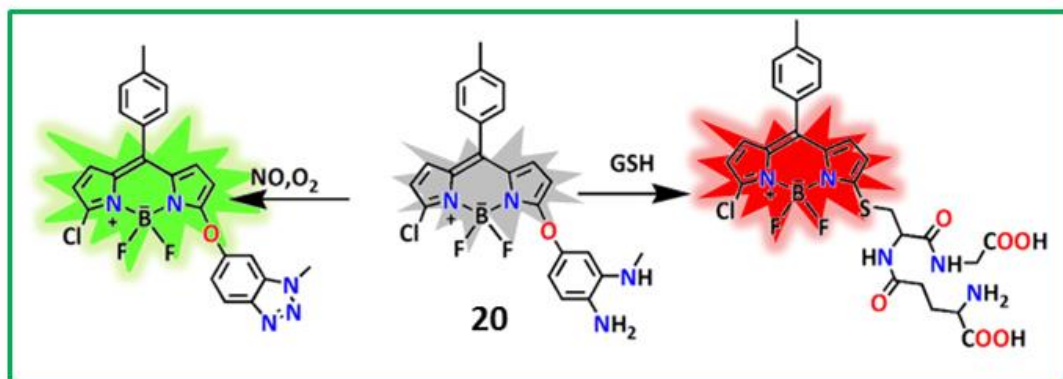
Figure 1.9 Another N-protected dual analyzing OPD based NO probe.

Here a Si-rhodamine based probe **21 (Figure 1.10)**, an OPD bounded Si-rhodamine deoxylactam was reported by Guo et al. for NO imaging. It was non-florescent in its ring closed form. However, on treatment with NO it exhibited 6300 fold enhancement in fluorescence at 680 nm in the NIR region on excitation at 645 nm due to triazole formation. This NIR activity makes the probe tissue penetrable and can be successfully applied for detecting endogenously produced NO in RAW 264.7 macrophages, pancreatic β-cells, and endothelial EA.hy926 cells along with in inflamed and diabatic mouse model. It also exhibited very low LOD of 0.12 nM.[102]

Likewise, the Li group[103] also reported a rhodamine-B embeded (OPD)-locked deoxylactam based NO sensor **22 (Figure 1.10)**, derived from the lactam form of rhodamine-OPD conjugate by reduction with LiAlH₄ in THF. The NO treatment of the probe leads to a drastic fluorescence enhancement (170-fold) at 590 nm (λ_{ex} =550 nm) under physiological conditions within 40 s devoiding of the serious interference from cysteine. This probe was efficiently employed in bioimaging of NO in HepG2 and RAW 264.7 cell without any interference from biomolecules like DHA, AA, and MGO.
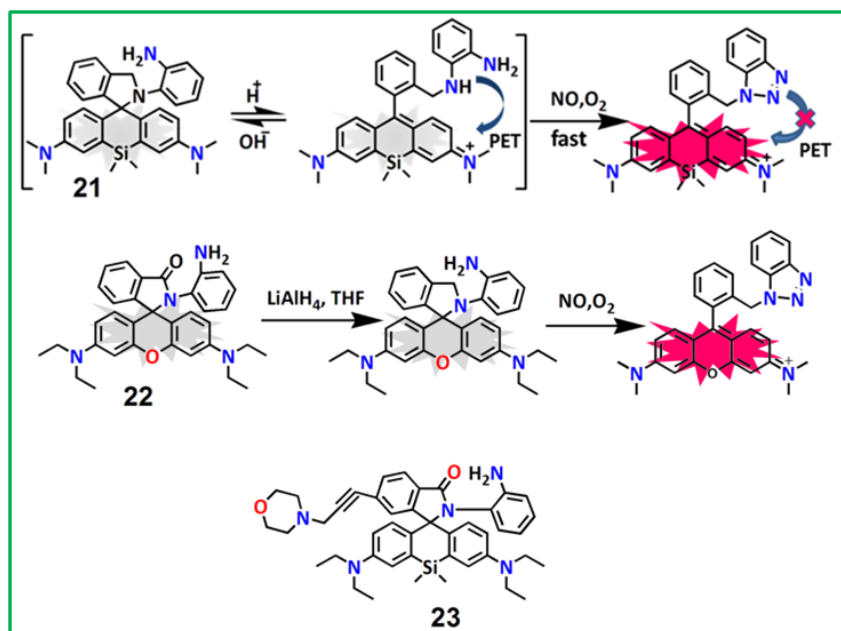
Figure 1.10 Si-rhodamine based NO probe utilizing spirolactam ring opening.

Another Si-rhodamine based fluorescent probe **23 (Figure 1.10)** bearing morpholine side arm to target lysosome was reported by Wang group.[104] It exhibits fluorescence emission at 680 nm upon NO treatment. Most importantly, Si-rhodamine in its spirolactam form displays superior tolerance to H^+, showing immensely low background emission both in physiological domain as well as under acidic circumstances. Additionally, the stability of fluorescent product in acidic solution for longer time furnishes opportunity to carry out imaging experiments analyzing the level and localization of NO products in lysosomes *in vivo* in RAW 264.7 macrophages. The Pearson's co-localization coefficients has been shown as 0.86.

Zhang group reported a probe **24 (Figure 1.11)** where rhodamine-B acts as a fluorophore, galactose as hepatocyte-targeting moiety and OPD as NO receptor to understand the role of NO in liver diseases. This high water solubility along with high selectivity and sensitivity towards NO (LOD 1.62 nM) manifests its application towards diagnosing liver disease. The probe emits fluorescence at 580 nm (λ_{ex} = 550) upon NO treatment and exhibits good biocompatibility for hepatocellular-specific imaging of nitric oxide in HepG2 cells and in zebra fish (*in vivo*).[105]
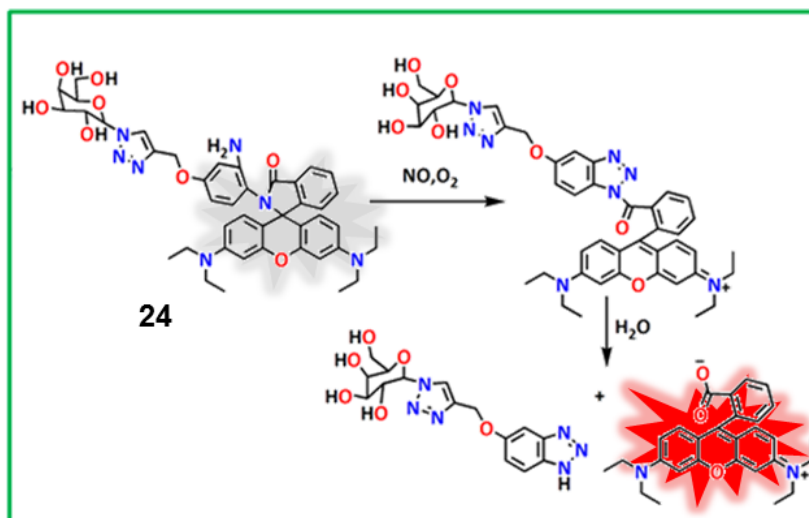
Figure 1.11 Galactose conjugated rhodamine based NO probe: generation of free rhodamine.

1.3.1.2 NO fluorescence probe utilizing N-nitrosation at secondary aromatic amine

In terms of specificity/selectivity N-nitrosation at aromatic secondary amine has been found to be more selective precluding the interference from one or more biological reactive species (RNS, ROS and RCS), thereby exhibiting its superiority to OPD based NO sensing probes. Moreover, aromatic secondary amines having poor coordination ability towards metal ions in biological milieu enhances its specificity towards NO.[106]

Taking 4-hydroxylaniline group as NO trapping unit Guo group[106] designed an N-nitrosation-based fluorescent probe **25 (Figure 1.12)** exploiting BODIPY as fluorescence reporter. This probe shows 92-fold fluorescence increment towards NO (λ_{em} = 518 nm, λ_{ex} = 490 nm) having LOD 4.8 nM which can be successfully applied for NO detection in mitochondria. Here, the basal and stimulated nitric oxide in RAW264.7 murine macrophages was nicely analyzed by the author and they also depicted about the endogenous nitric oxide release in endothelial cells ocurring after oxygen-glucose distress. The same group further reported another NO probe **26 (Figure 1.12)** by changing hydroxyl group to methoxy group[107] which is more efficient than their 1st work providing lower LOD value (0.4 nM). Here, the author has showed that the probe **26** is useful to discriminate M1 (proinflammatory) and M2 (anti-inflammatory and prohealing) macrophages, to evaluate repolarization of TAMs (Tumor-associated macrophages)

from pro-tumoral M2 phenotype to anti-tumoral M1 phenotype, as well as to visualize NO transmission in the course of immune-mediated phagocytosis of cancer cells due to M1 macrophages.
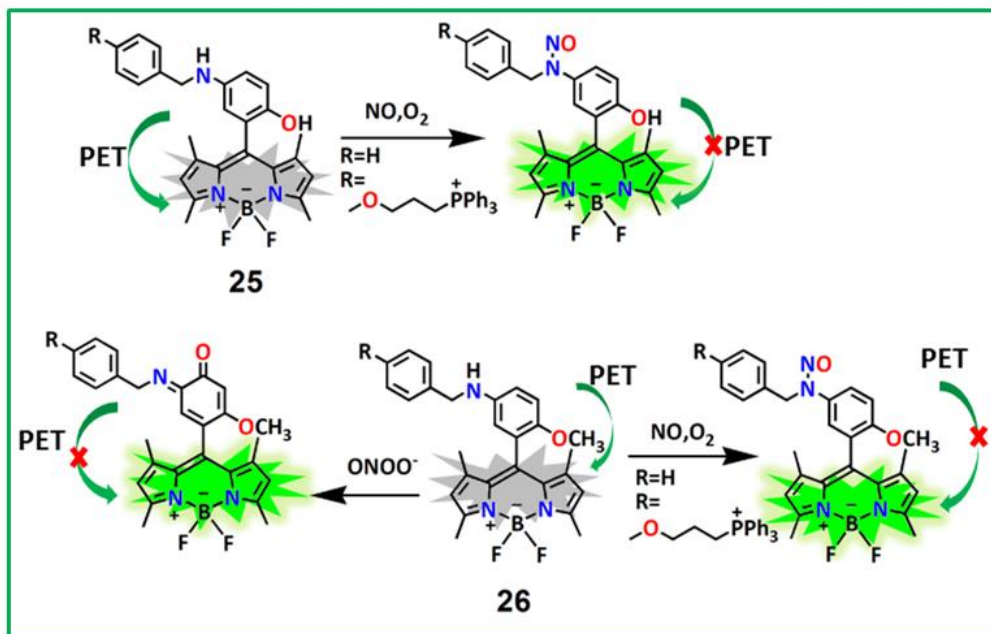
Figure 1.12 4-hydroxy aniline derivative as NO tracking moiety in probe **25,26.**

Chen and coworkers[108] published another BODIPY based NO probes **27 (Figure 1.13)** taking N-propynyl-4-methoxylaniline as NO tracker with sufficient pH tolerence and little toxicity. These probes are suitable to track nitric oxide exogenously in HeLa cells in presence of DEANO with significant fluorescence enhancement located at 515 nm. They have developed these probes by introducing triphenyl phosphonium ion as mitochondria targeting agent through hydrophilic triazole/phenoxo linkers, demonstrating the overlap co-efficient 0.94. Other derivative with morpholino-ethyl moiety exhibits lysosome targeting property with overlap co-efficient 0.83. So these organelle-targeted sensors can be of feasible tool to provide information regarding NO associated physiological and pathological process in cellular level. Taking 4-hydroxylaniline derivative as good NO tracker Liu group[109] has synthesized a two-photon(TP) NIR fluorescent probe **28 (Figure 1.13)** using Si-rhodamine dye as fluorophore. This probe shows remarkable fluorescence enhancement (81 fold) upon NO addition at 672 nm showing the promising LOD value (14 nM)**.** Because of NIR excitation and emission ("NIR-to-NIR"), the probe is capable

enough to study NO in the xenograft tumor mouse model *in situ*. This work described that **28** may be a classical system for the emerging of NIR emissive two-photon NO sensor as well as it can assist the development of NIR imaging**.**
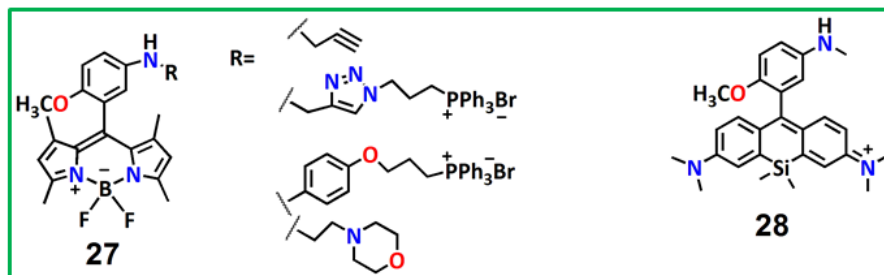
Figure 1.13 Two more 4-methoxylaniline derivative as NO tracking moiety.

They also developed another two-photon NIR fluorescent probe **29 (Figure 1.14)** exploiting *p*-phenylenediamine as NO tracking moiety and coumarin as fluorophore. It features a fast reaction showing a linear relationship towards NO level between the concentration values 1–11 µM showing 37 nM detection limit (emission at 613 nm).
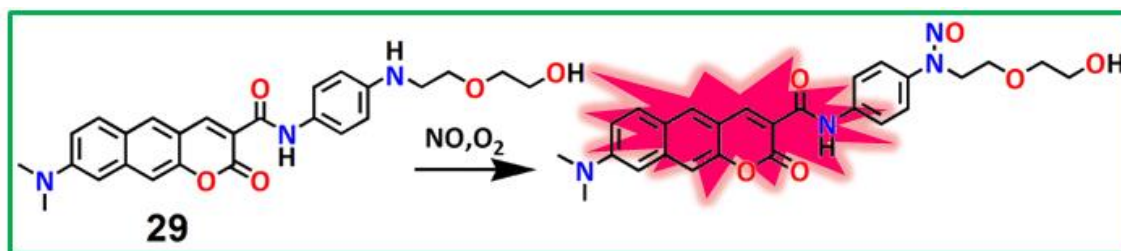
Figure 1.14 Benzocoumarin based probe using p-phenylenediamine as NO tracker.

This probe successfully monitors endogenously produced NO in RAW 264.7 macrophages induced by L-Arg, IFN-γ and LPS. However, fluorescence could be declined by incubating the cells with potassium salt of (2-(4-carboxyphenyl)-4,4,5,5-tetramethyl-imidazoline1-oxyl-3-oxide (carboxyl-PTIO), an NO scavenger, before loading NO. It has also been employed for the first time to image NO in mouse kidney bearing ischemia reperfusion injury results in obvious inflammatory responses.[110] Overall, this red-emissive NO sensor may be utilized as an efficient chemical agent to analyze NO-mediated biological processes *in situ*.

A BODIPY based photoacoustic (PA) NO Probe **30 (Figure 1.15)** with *o*-methoxy methylaniline moiety as NO tracker moiety displayed better sensitivity, fast reaction kinetics and possibility of

deep tissue imaging in live animals. A PEGylated tetraalkylammonium group has been attached to this system to increase the water solubility, thereby increasing its cellular uptake.[111] Moreover, the probe exhibits the essential photophysical traits for *in vivo* PA imaging as well as good biocompatibility, stability, good sensitivity (91 nm hypsochromic shift) towards NO over a plenty of reactive analytes. The probe was efficiently utilized to detect endogenously produced NO in a murine lipopolysaccharide-induced inflammation model resulting an enhancement of 1.9-fold photoacoustic signal at 680 nm and 1.3 fold ratiometric response.
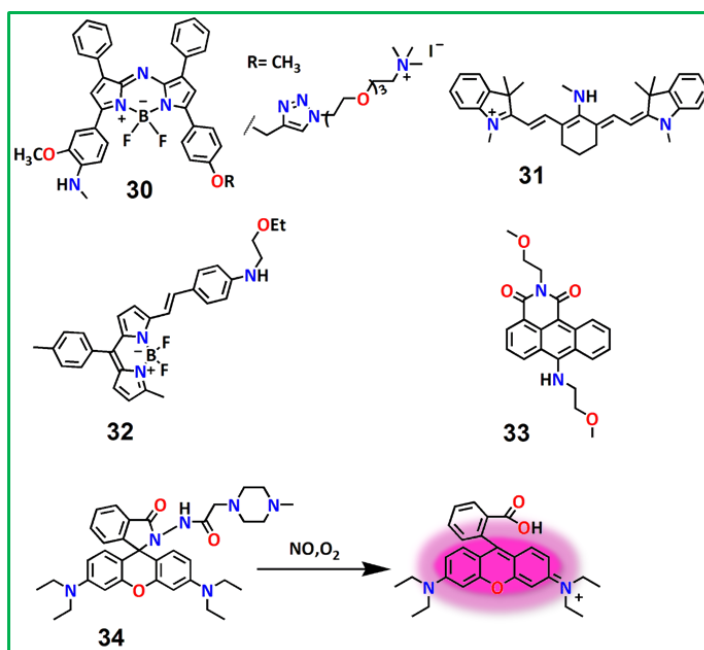
Figure 1.15 Some more N-nitrosation based NO probes using BODIPY, Cyanine, rodamine and anthracene carboximide fluorophore.

A cyanine-based NIR fluorescent Probe **31(Figure 1.15)** [112] displayed a 30 fold magnification in fluorescence intensity at 800 nm (λ_{ex} = 760 nm) through N-nitrosation at aromatic secondary amine by ICT mechanism with the response time 5 min. It also exhibited a very good selectivity with respect to the widely used OPD based NO fluorescent probes. The LOD was determined to be 11.3 nM. Additionally, this probe displays good performances in *in vitro* cell imaging study (HeLa cells,) as well as in inflamed mouse model *in vivo*.

A nitric oxide fluorescent probe **32 (Figure 1.15)** formed with BODIPY (fluorophoric moiety) and an aromatic secondary amine (NO receptor) has disclosed very fast (10 s) response towards

NO. The fluorescence enhancement occurs through PET process where electron drifting occurs from amine group to the BODIPY moiety. This probe exhibits high selectivity towards NO (LOD value 10 nM at 585 nm) over other reactive bio-analytes excluding biothiols where a distinctive interference has been observed in the presence of GSH.[113]

A novel anthracene carboximide based ratiometric NO sensor **33 (Figure 1.15)** was developed where, N-nitrosation chemistry was exploited to monitor NO. The probe itself is red fluorescent (λ_{em} = 625 nm). However, on N-nitrosation to the amine at 6th position, it exhibits green fluorescence (λ_{em} = 525 nm) which is ascribed to the intramolecular charge transfer (ICT) mechanism. It also shows high sensitivity (LOD= 4.05 nM) towards NO being employed for monitoring endogenously produced NO in Raw264.7 cell line and in zebrafish.[114]
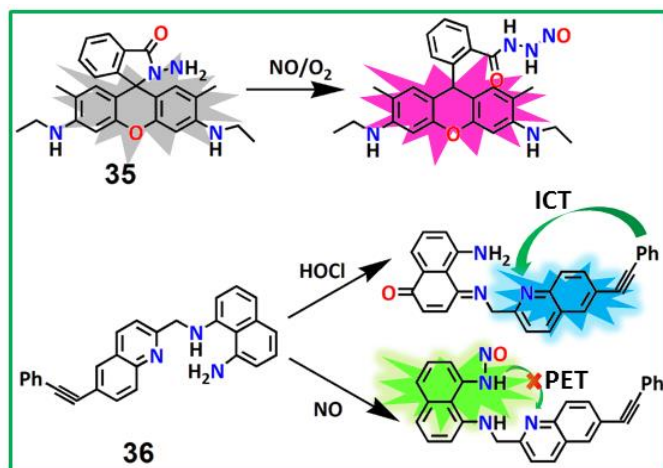
Figure 1.16 N-nitrosation in primary amine.

The N-nitrosation mechanism is also prevailing in a rhodamine based fluorescent NO sensor **34 (Figure 1.15)**. It shows 24 fold fluorescence enhancement due to N-nitrosation induced spirolactam ring opening with LOD 36.8 nM. It is also potent enough to track NO in live cells. [115] Another such rhodamine 6G based fluorescent NO sensor **35 (Figure 1.16)** has displayed fluorescence enhancement due to N-nitrosation with concomitant spirolactam ring opening. This probe shows detection limit 0.06 uM and ability to detect NO in inflammatory model of zebrafish.[116]

A dual channel NO probe **36 (Figure 1.16)** was developed using 1,8 naphthalene diamine moiety as NO receptor showing a turn-on fluorescence enhancement within 20s, at λ_{em} = 512 nm upon treatment with NO due to N-nitrosation that inhibits PET process. The LOD was evaluated to be (25.7 ± 3.4) nM. Moreover, a rapid (10 s) turn-on fluorescence responses was observed due to ICT mechanism when the probe was treated with HOCl (λ_{em} = 464 nm). This probe is highly eligible to detect these two analytes both exo- and endogenously in live cells.[117]

1.3.1.3 NO probes based on oxidization of dihydropyridine (DHP)

The dihydropyridine can easily undergo quantitative oxidative aromatization by NO[118-120] making the probe suitable for selective sensing of NO *in vitro* and *in vivo* under anaerobic environment.

A dihydropyridine embedded 7-methoxy coumarin conjugate **37 (Figure 1.17)**[121] has displayed very strong turn-on fluorescence towards nitric oxide which can successfully be utilized for endogeneously produced NO imaging. It exhibits 80 fold fluorescence enhancement within 0.31 min at 392 nm through PET block mechanism. The probe is stable within a wide pH range 4–9 and showed outstanding selectivity towards NO being inert to different reactive reductants. The LOD of the probe for NO detection was 17nM. Incorporation of hydrophilic quaternary ammonium units in **37** leads to probe **38 (Figure 1.17)** which displayed good water solubility making it suitable for endogenous imaging application for NO. The detection limit was evaluated as 18 nM.[122] This probe also displays its ample efficiency in cell imaging study to detect endogeneous NO. It exhibits almost 17 fold emission enhancement at 450 nm upon NO treatment showing stability at the pH range 4–9.

A mitochondria targeting dihydropyridine based NO probe **39 (Figure 1.17)**[123] was constructed with BODIPY as fluorescence reporter exhibiting 63 fold fluorescence enhancement at λ_{em} 525 nm (λ_{ex} 470 nm) upon treatment with NO. The good sensitivity of the probe towards NO was established with low LOD of 25 nM. This probe also can effectively monitor endo- and exogenously generated NO in RAW 264.7 cells and HepG2 cells respectively**.** This organelle specific probe mainly accumulated at mitochondria which was established through co-localization experiment with high Pearson's coefficient 0.93.
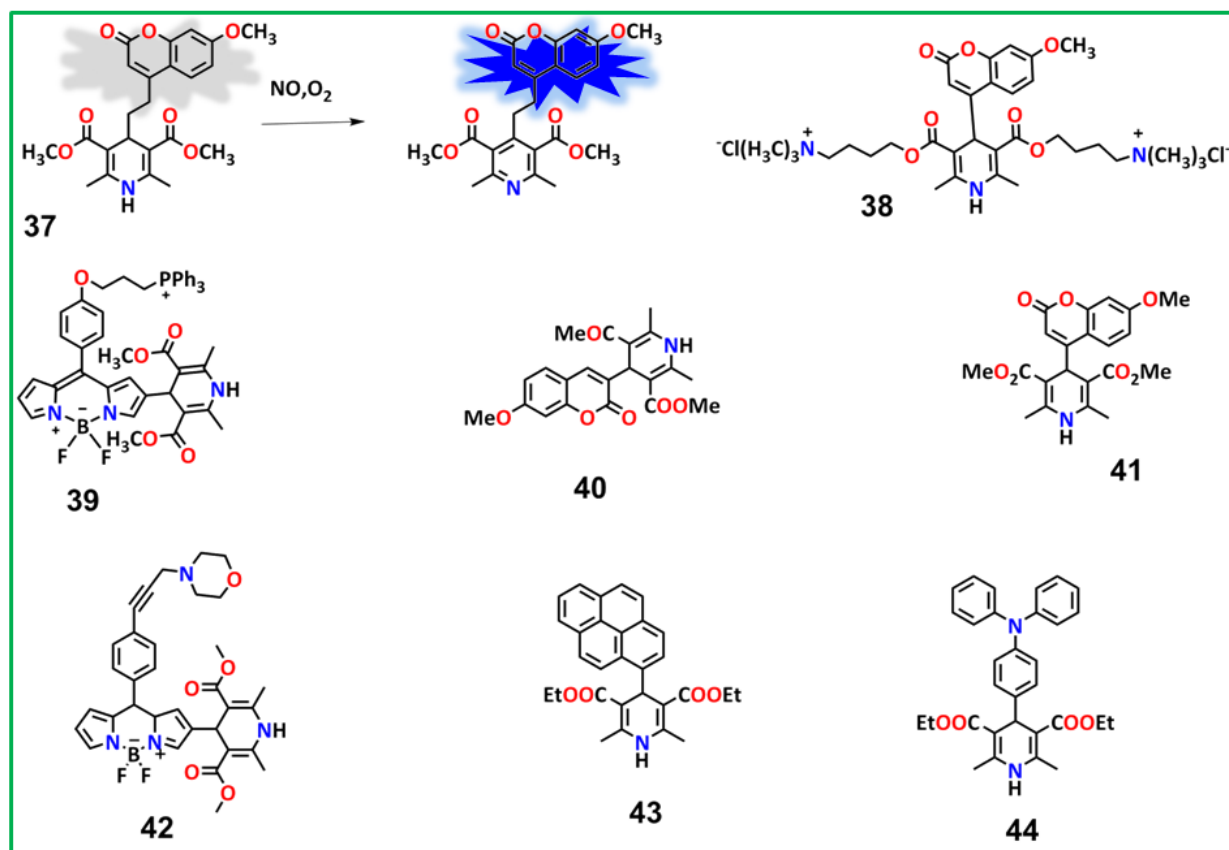
Figure 1.17 Dihydropyridine Based NO Sensors.

Two NO probes **40, 41 (Figure 1.17)** were structured from the coumarin and dihydropyridine moiety**.** Probe **40** displays high selectivity and sensitivity with turn-on fluorescence signal towards NO at λ_{em} 423 nm on excitation at 365 nm. The probe **40** displays fluorescence stability in the pH range 3-10 and very little cytotoxicity, indicating its suitability to detect *in vivo* NO.[124] The Probe **41** differs from **40** only with respect to the position of DHP which is located at position 4 of coumarin in the former instead of position 3 in the latter.[125] Photophysical studies revealed that the probe **41** displays linear relationship towards the change in NO concentration up to one equivalent. It reveals specific affinity to NO only, among biological reactive analytes in a wide array of pH and found as an appropriate candidate for intracellular as well as extracellular NO detection.

Probe **42 (Figure 1.17)** is the modified form of **39** where, lysosome attacking morpholine group was introduced in BODIPY fluorophore. This system has displayed an ultrahigh fluorescence

response (140 fold, at λ_{ex}=475 nm and λ_{em}=535 nm) and ultralow detection limit (47nM). Lysosome targeting ability of this probe has been experimented in HEPG2 cell which shows almost full overlap of fluorescence response of the probe with that from the LysoTracker Blue with a Pearson coefficient value as high as 0.96. Additionally, probe and its aromatized pyridine product are cytocompatible having the potential application to image exo- and endogenous NO with high precision and brightness.[126]

Mahapatra et al. has designed two NO sensors where pyrene **(43)** and pyrenyl **(44) (Figure 1.17)** systems were exploited as fluorophore and DHP as the NO receptor. The probe **44** exhibits fluorescence growth at 502 nm (λ_{ex} = 308 nm) bearing LOD 0.08 μM, whereas probe **43** shows fluorescence quenching with LOD 2.6 μM upon NO interaction. Theses probes were structurally established by XRD, DFT and TDDFT studies.[127] Moreover, probe **44** has the potential ability for cell imaging to endogenous NO in thin epithelium Vero cells.
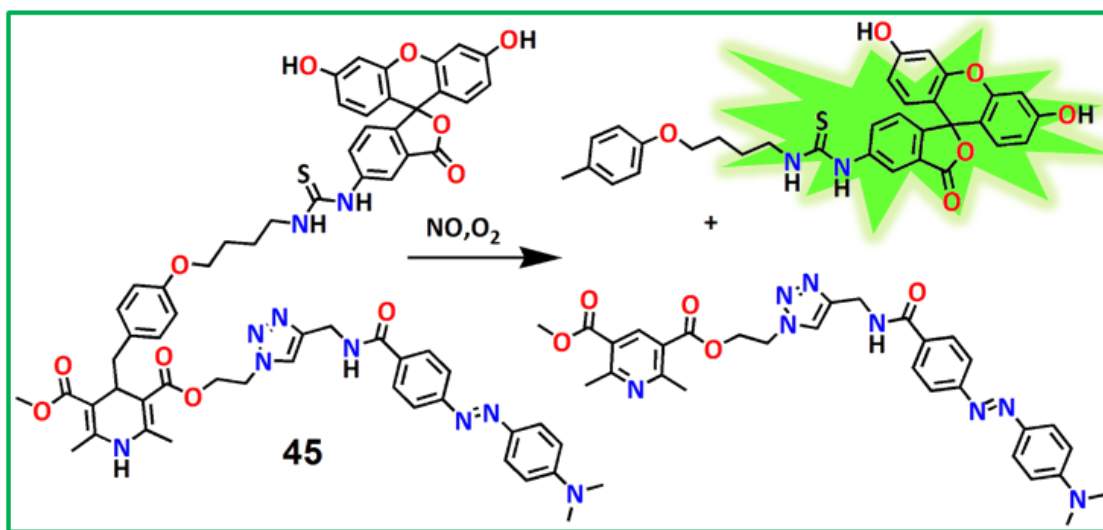
Figure 1.18 Dihydropyridine based NO sensors upon C-C cleavage.

Probe **45 (Figure 1.18)** is uniquely featured by Li group where C-C bond breaking is induced by FRET mechanism towards NO interaction. Here, *in vitro* experiments have resulted a ratiometric response at 525 nm (λ_{ex}= 490 nm) to NO avoiding variety of reactive species. After giving intravenous injection to the mice, *in vivo* study revealed that there is 8-fold contrast between Freund's adjuvant stimulated feet and normal feet. It is the pioneering work for semi quantitative fluorescence imaging of NO in mammals.[128]

1.3.1.4 NO probes based on cyclization of *o*-amino-3'-dimethylaminophenyl aromatics

In this type of NO fluorescent probe the fluorophore is attached with *o*-amino-3′-dimethylaminophenyl moiety which acts like a NO recognition unit to preclude interference from the biologically reactive species like DHA, AA, MGO etc.[129] In the presence of NO, aromatic –NH$_2$ undergoes diazotization reaction which subsequently undergoes cyclization leading to an extended conjugation which facilitates an enhancement in fluorescence intensity.

Song and coworker unveiled a NO probe **46 (Figure 1.19)** where 6-Bromo-2-methylquinolin-5-amine undergoes Suzuki coupling with 3-dimethylaminophenyl boronic acid which plays roles as pre-fluorophore and the active site to detect NO. The probe **46** has negligible fluorescence in water but upon reaction with NO, the electron defficient diazo ring is generated which displayed robust green fluorescence (λ_{em} = 540 nm) upon one photon excitation (λ_{ex} = 430 nm) with LOD 15 nM.[130] Mechanistically, upon reaction with NO, the non-fluorescent probe rapidly forms a diazonium intermediate which finally converted to two azoic regioisomers. Between these two isomers one displays its high fluorescence intensity owing to the ICT process. Furthermore, it acts as a specific imaging tool, described by achievement of exo- and endogenous imaging of NO in living organisms upon one- and two-photon excitation.

Another mitochondria signalling two-photon ratiometric NO probe **47 (Figure 1.19)** was reported by Zhang and coworkers[131] where *o*-amino-3′-dimethylaminophenyl unit acts like a NO recognizing moiety. After addition of 10 equivalent of NO, the fluorescence intensity at 595 nm (yellow region) was appeared along with the simultaneous vanishing of fluorescence peak at 540 nm (green region) within 20 min which has shown LOD value 21 μM. This probe has potency enough to detect mitochondrial NO levels in presence of exo- or endogenously produced NO in live cells with Pearson's co-efficient 0.9503 as well as the probe has shown LPS-induced inflammatory response in mice model.

Another ratiometric *o*-amino-3′-dimethylaminophenyl based NO probe **48 (Figure 1.19)** was reported by Yoon group[132] where a simultaneous development of yellow fluorescence at 560 nm with gradual disappearance of blue fluorescence at 470 nm (λ_{ex} = 420 nm) was encountered. This ratiometric NO sensing occurs through the ESIPT mechanism. In addition, the probe can be useful to image NO in living organism also**.**
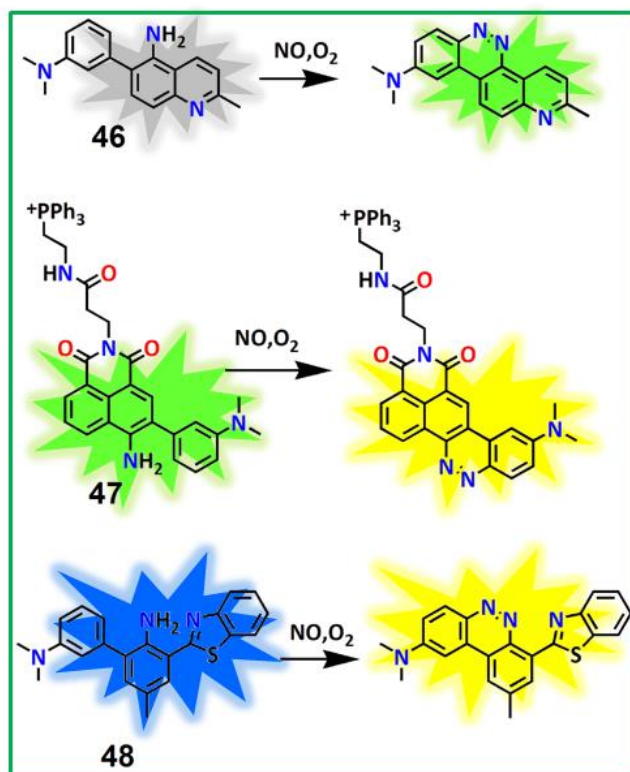
Figure 1.19 *o*-amino-3'-dimethylaminophenyl based NO sensors.

1.3.1.5 Nitric Oxide probes based on deamination of aromatic primary amines

To avoid the shortcomings associated with the interference by AA, DHA, MGO etc. in sensing of nitric oxide which leads to the misinterpretation of data, attempts were taken to design probes which exclusively react through NO specific novel mechanism. One of such mechanism is the oxidative deamination of aromatic primary amines induced by NO.

Wang group published a flourescein based NO sensor **49 (Figure 1.20)** which shows a high fluorescence generation at 524 nm (λ_{ex} = 460 nm) upon reaction with NO. This probe has sufficient selectivity to NO with no interference from biological oxygen (ROS) & nitrogen (RNS) species. Here after NO treatment, the probe shows fluorescence enhancement due to oxidative deamination of primary amino group thereby blocking the PET process.[133] The LPS pretreated Raw 264.7 murine macrophages showed high fluorescence caused by the reaction of endogenously generated NO.

Two related NO probes **50, 51**[134] **(Figure 1.20)** were reported recently which contains electron-rich methoxyl group at 4th position of aromatic moiety to improve the reactivity of aromatic amine towards NO. In case of probe **50** BODIPY was used as the fluorophore whereas, cyanine in the probe **51**. The probe **50** exhibits a huge enhancement in fluorescence intensity at $\lambda_{em} = 519$ nm on excitation at ($\lambda_{ex} = 475$ nm) upon NO treatment at pH range of 6– 9. The LOD was determined as19 nM. Similarly, **51** exhibits fluorescence enhancement at $\lambda_{em} = 794$ nm ($\lambda_{ex} = 750$ nm) showing the best fluorescence off-on response for NO at pH = 7.4. These probes has shown high selectivity and fast response towards NO and successfully exhibits its potency to detect endogenously generated NO in RAW 264.7 cells as well as in mouse model with deep tissue penetrating ability**.**
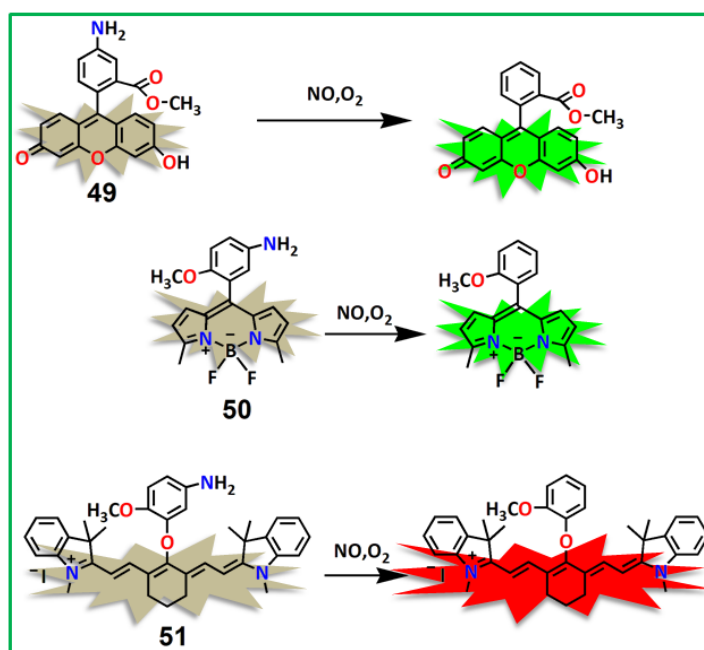
Figure 1.20 Deamination based NO probes.

Luis, Galindo and coworkers published another probe **52 (Figure 1.21)** based on *ortho*-hydroxyamino-triarylpyrylium.[135] Among the four derivatives (R = H, CH₃, OCH₃ and Ph) the probe **52-c** shows highest NO response (83 fold) at $\lambda_{em}=550$ nm ($\lambda_{ex}= 470$ nm) with LOD 2.1 μM.
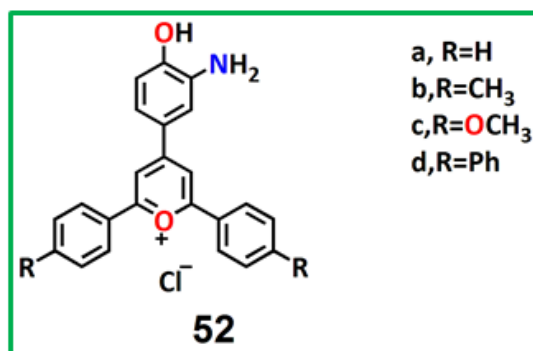
Figure 1.21 Structure of pyrylium based NO sensor.

The mechanism was well established by common spectroscopic studies as well as by XRD study which has shown oxidative de-amination of the probe upon NO treatment. This mechanism is well functioning due to the presence of adjacent –OH group. This pyrylium based NO sensor can detect NO in live macrophages (RAW264.7, activated by LPS and IFN-γ) by enhancement of fluorescence which is not occurs in the presence of NOS inhibitor L-NMMA.
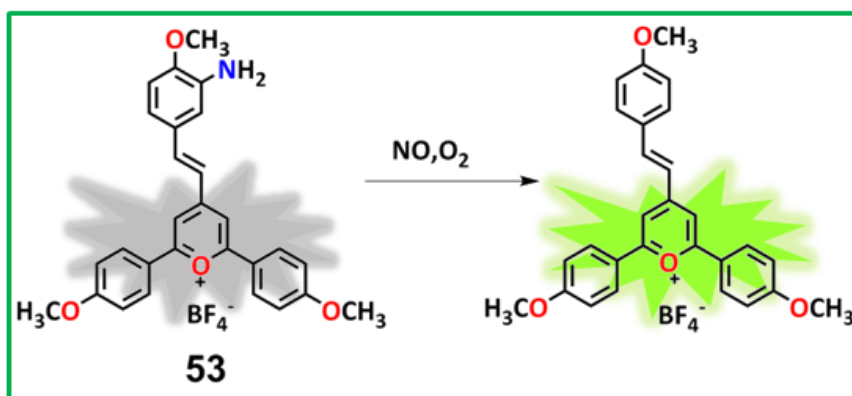
Figure 1.22 Pyrylium based mitochondria targeting NO sensor.

Very recently, a mitochondria targeting pyrylium based probe **53** (**Figure 1.22**) has been demonstrated by Galindo et al. which selectively detects NO in aerated aqueous medium over other reactive species with LOD 88 nM at emission wavelength 585 nm (λ_{ex} = 480 nm). They claimed this as a novel probe due to its simple architecture with mitochondrio-tropic behavior without any normal mitochondria tracking groups, with Pearson's co-efficient 0.94. This probe also responses towards both exogenous and endogenous NO stimuli in human colon carcinoma

cells HT-29 and mouse macrophage RAW 264.7 cells with the ability to discriminate NO-generating phagocytes from other leukocytes.[136]

1.3.1.6 NO probes based on some special reaction mechanism

In addition to the above mentioned probes there are reports of few probes which can monitor nitric oxide through some novel mechanisms thereby minimizing the interference from other biological species. These are enumerated below.

A dehydrazination-based fluorescent probe **54**[137] **(Figure 1.23)** where hydrazine moiety is at 8th position of BODIPY has been reported recently. Upon bubbling with NO gas the probe converted to BODYPY and 8-azido BODYPY with 65% and 15% yields respectively. The former was found to be highly fluorescent (λ_{ex} = 480 nm and λ_{em} = 512 nm) with 50 fold enlargement of fluorescence emission whereas the latter was obtained as non-fluorescent. This probe was found to be suitable for monitoring endogenously produced NO in RAW 264.7 cells.
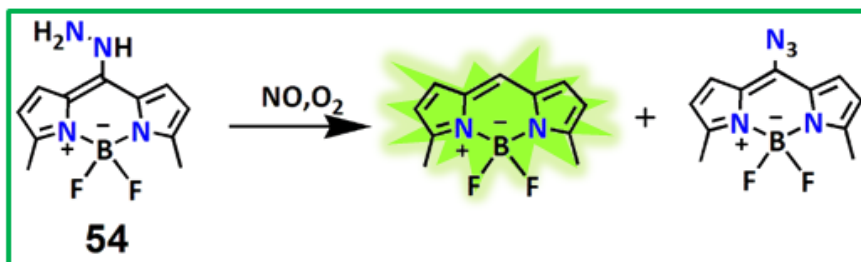
Figure 1.23 Dehydrazination-based fluorescent probe for NO.

Li and Co-workers[138] has reported two-photon fluorogenic Schiff base based probes **55**, **56** **(Figure 1.24)**. The probe **55** exhibits very quick reaction with NO (<50s) at pH range 5-9 with LOD 97.81 nM and 7.5-fold fluorescence increment at 590 nm. The probe **56** displays only 2.8 fold fluorescence enhancement. Furthermore, **55** has lysosome-targeting property with a potency to detect exo- and endogenous NO in live cells and zebra fishes having the Pearson's coefficient value 0.83.
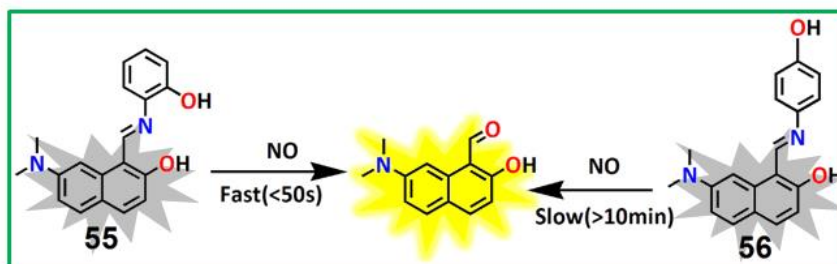
Figure 1.24 Schiff base for NO detection.

Majority of the organic probes discussed so far have one or more shortcomings like: electron-riched aromatic diamine normally proceeds self-oxidation or may interact with biological reactive analyte which may generate fluorescence intensity. Additionally, maximum studies were performed in organo-aqueous medium and gets interfered by AA, DHA, MGO resulting false elucidation in biological application. Ali and coworkers have taken attempts to overcome the aforementioned limitations where NO reacts with the designed probes through a novel chemical reaction which removes the chances of interferences due to the intracellular native reactive species thereby providing exclusivity of NO sensing.

Ali and co-workers[139] has designed a novel probe **57a (Figure 1.25)** containing thiosemicarbazide as NO receptor and quinoline as fluorophore which uniquely reacts with NO transforming into 1,3,4-oxadiazole and there is a simultaneous release of an important biomolecule thionitrous acid (HSNO) in quantitative yield. This specific class of probe furnishes some important outlook about the reaction between NO and H_2S. The probe exhibits strong fluorescence emission at 490nm (~8 fold λ_{ex} = 400) and 58 nM LOD upon NO treatment. This NO sensor can be employed to image exogeneous NO in HeLa cells and endogenously produced NO in Raw 264.7 cells. By this group another structurally modified NO sensor **57b (Figure 1.25)** has been reported where acylhydrazide moiety converted to 1,2,3,4-oxatriazole, accompanied with PET inhibition, leading to 23-fold fluorescence enhancement at 490 nm (λ_{ex} = 380 nm) showing 45.4 nM LOD.
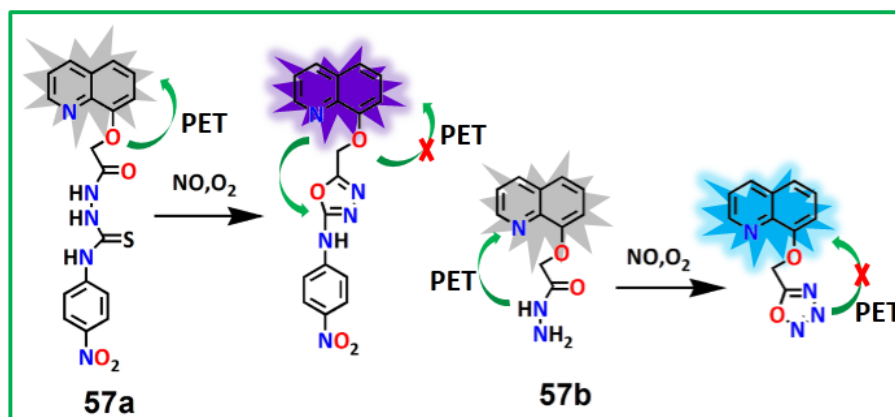
Figure 1.25 NO sensing by oxadiazole and oxatriazole formation.

Added advantages are (i) good solubility in aqueous medium, (ii) little toxicity, (iii) photo stability in wide pH range (4.0–8.0). All these makes the probe efficient to monitor endogenously generated NO in RAW 264.7 cells stimulated by LPS and IFN-γ.[140] In these works, the authors have clearly delineated the mechanism of reactions of NO with the probes through detailed kinetics studies where the rate of the reaction has shown first-order and 2nd-order dependences on probe and NO concentrations, respectively.

Ali et al. has reported another two differently designed N-nitrosation-based fluorescent probes **58[141], 59[142] (Figure 1.26)** utilizing pyrene and quinolone scaffold as fluorophore, respectively with good photostability. The dual emission pyrene probe emits green fluorescence (66 fold, 523nm) for nitric oxide sensing by ICT process, while it exhibits blue emission (833 fold at 467 nm) upon increase in water quantity through AIEE process. The AIEE behavior has been well-established by fluorescence, photoluminescence, DLS, SEM, TEM, X-ray diffraction and fluorescence microscope studies. Interestingly, the LOD value of the probe for NO sensing was sufficiently low (2.13 pM) making it suitable for bio-imaging of NO in living system. In probe **59** NO reacts here at the secondary NH of amide leading to fluorescence enhancement (7 fold) at 480 nm (λ_{ex} = 390 nm) through PET block process within a wide pH range (5.0-8.0). Indeed, the probe is successful for exogeneous NO imaging in living HeLa cells[142] with 53 nM LOD value.
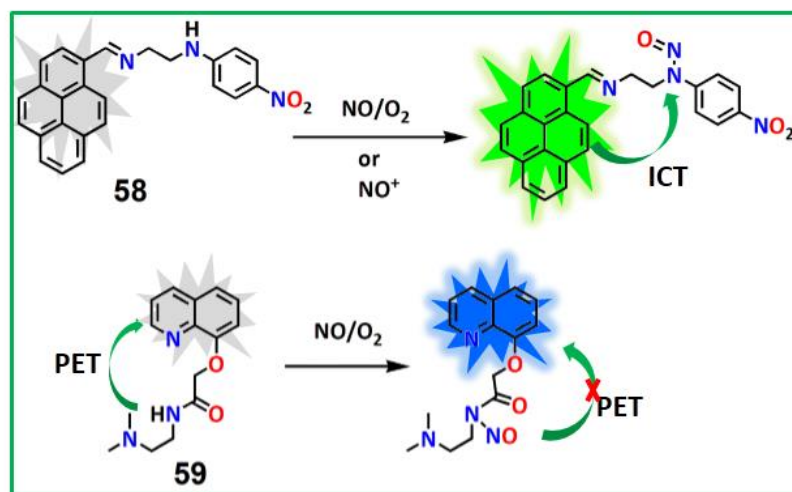
Figure 1.26 Structures and NO sensing mechanism of probe **58, 59.**

Another thiosemicarbazide based NO sensor **60 (Figure 1.27)** has been reported by Zhang group using coumarin as fluorophore and thiosemicarbazide as NO recognition unit. The N-N bond rotation has made the probe non-fluorescent but oxadiazole formation upon NO treatment restricted the rotation which consequences the ~5 fold fluorescence enhancement at 475nm (λ_{ex} = 436 nm) showing limit of detection 47.6 nM. It is a biocompatible probe having low cytotoxicity which can detect exo- and endogenous NO as well as in zebra fish.[143]
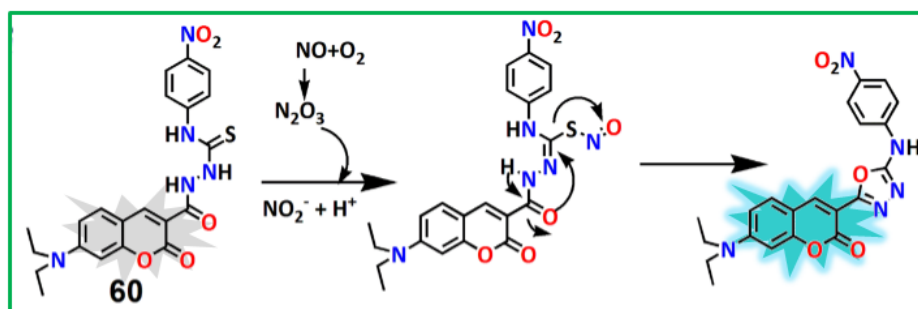
Figure 1.27 Coumarin based thiosemicarbazide probe for NO sensing.

Here also naphthalimide-thiosemicarbazide based NO sensor **61 (Figure 1.28)** was denoted as an efficient probe for simultaneous measurement of cellular viscosity and nitric oxide concentration in cells. This probe exhibits no fluorescence due to N-N bond rotation which gets restricted due

to increase in viscosity by water-glycerol mixture with concomitant fluorescence enhancement at 470 nm (λ_{ex} = 405 nm). It is interesting to note that NO induces the N—C bond cleavage at Ar—NH—CO leading to the formation of Ar-NH$_2$ resulting the fluorescence enhancement at 550 nm (λ_{ex} = 450 nm) showing LOD value 0.17μM.[144]
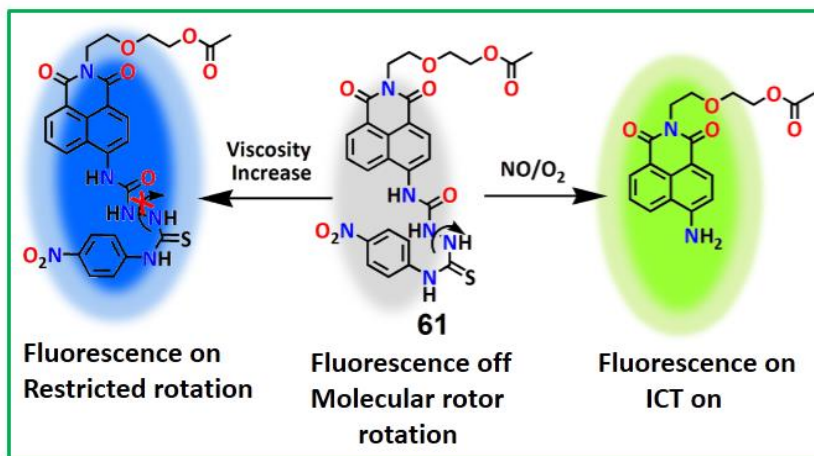
Figure 1.28 Napthalimide based thiosemicarbazide as NO sensor.

This probe is useful for monitoring exo- and endogenously produced NO in HeLa cells using LPS as NO stimulator. The well-known NOS inhibitor, aminoguanidine diminishes the fluorescence intensity of LPS pretreated cells confirming NO induced fluorescence enhancement of the probe.
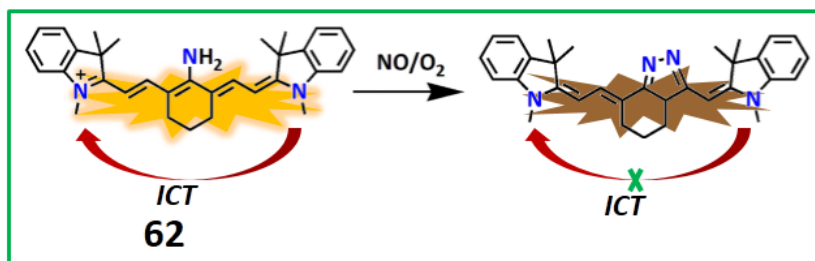
Figure 1.29 Cyanine based probe for N-nitrosation followed by cyclization.

A differently dual channel mitochondria-targeted NO fluorescent sensor **62 (Figure 1.29)** has been unveiled for NO detection, based on cyanine7 fluorophore.[145] The emission intensity gets diminuated upon NO treatment at two wavelengths (460 nm and 581nm, λ_{ex} = 400 nm) due to the

formation of electron deficient 4H-pyrazole ring which weakens the ICT process between the two indolium groups. This NO sensor can be employed to image NO in HeLa cells and zebrafish with high colocalization coefficient 0.92 which proves its precise mitochondria targeting ability.

1.3.2 NO detection method by using metal-complex probe

The NO probes based on organic compounds discussed so far have faced some shortcomings like: (i) shows NO detection with the interference of other biomolecules in biological milieu (ii) sometime organic probes faces pH effect resulting its limited application in different type of cells (iii) they are prone to aerial oxidation (iv) this probe interacts with NO in irreversible manner where reversibility is very important to explore temporal– spatial kinetics regarding NO generation in live cells (v) most of the organic probe shows NO detection by the reaction between probe and oxidized product of NO which interrupts in real time NO detection.
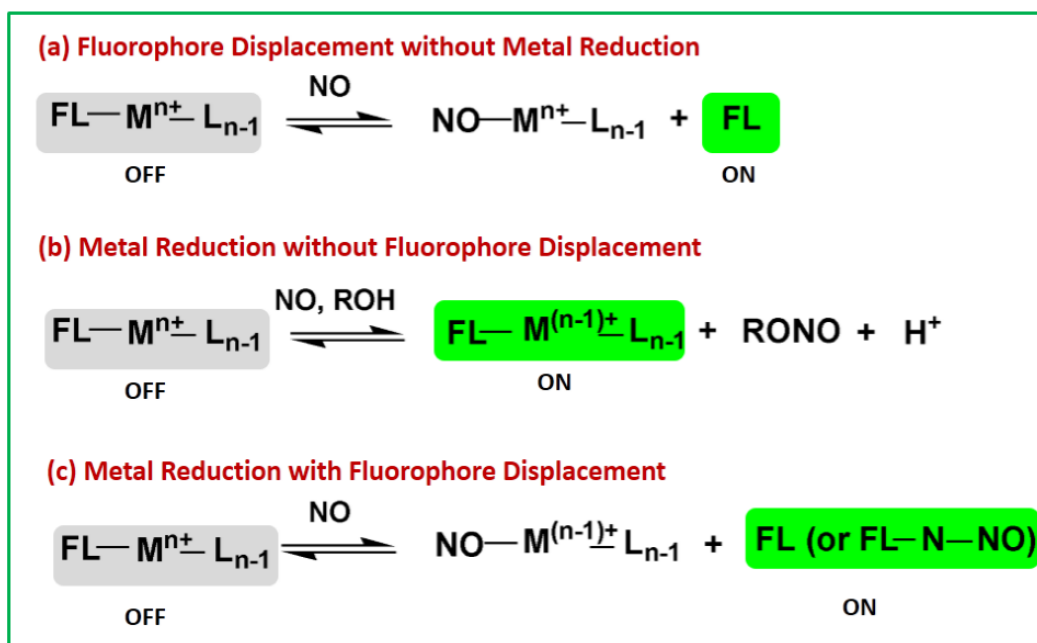
Figure 1.30 Different operative mechanisms for metal based NO sensors.

To beat these limitations, many researchers have focused on NO detection using metal complexes as probes. These type of probes bear a fluorophore moiety with a receptor site either

on the ligand fragment or on the metal center (transition and heavy metal ions) which exhibits excellent photo-stabilities, large Stokes shifts along with intense and long-lived fluorescence emissions **(Figure 1.30)**.

❖ **Fluorophore displacement without metal reduction:**

In this type of mechanism the probe itself is highly fluorescent, which gets quenched on coordination to a metal ion with partially filled d orbitals (paramagnetic in nature). But upon treatment with NO the metal-nitrosyl adduct is formed with the simultaneous release of the fluorophore/detachment of one of the chelating arms of the fluorophore to a sufficient distance from the metal centre may occur resulting a turn-on fluorescence event **(Figure 1.30a).**[146-150]

❖ **Metal reduction without fluorophore displacement:**

In this category the paramagnetic metal centre is converted to the diamagnetic one due to reduction by NO resulting the regeneration of fluorescence. Many copper based probes fall in this category **(Figure 1.30b).**[151]

❖ **Metal reduction with fluorophore displacement:**

This type of mechanism is particularly observed in many copper complexes where paramagnetic metal centre (Cu(II), d^9 system) is reduced to diamagnetic one (Cu(I), d^{10}) by nitric oxide results into release of probe which is fluorescent in free state but non-fluorescent when coordinated to a paramagnetic metal centre. This mechanism shows that nitric oxide may be either attached to metal centre or nitrosate the metal free probe **(Figure 1.30c).**[152-159]

1.3.2.1 Metal-based fluorescent probes for NO detection

The stable iridium(III) complex **63 (Figure 1.31)** coordinated by phenanthroline ligand with diamino substituents at 5,6–positions can act as a NO responsive probe exhibiting 48 fold phosphorescence enhancement [160] being suitable for endogenous NO detection in Zebra fish model along with imaging of mitochondrial NO levels in live cells and 3D multicellular spheroids.

Another very similar iridium(III) complex **64 (Figure 1.31)** was reported by Ma and coworkers[161] which induces 15-fold of luminescence enhancement at 580 nm on reaction with NO leading to the generation of electron withdrawing 1,2,3-triazole. The LOD of NO detection was evaluated to be 0.18 μM and this probe could be utilized to image exogenous NO using sodium nitro-prusside as NO donor in HeLa cells.
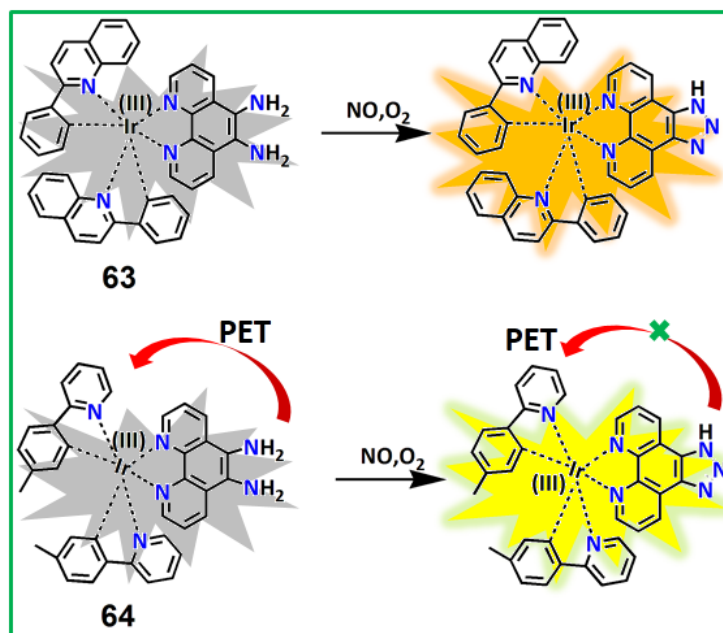
Figure 1.31 Iridium based OPD probe for NO sensing.

Though there are reports on various type of lysosomal targeted fluorescent probes for NO detection in recent times, some of them were found to suffer from various limitations including (i) photo-bleaching (ii) auto-fluorescence and (iii) background signals from biological systems.[162-163] The Yuan group[164] has developed a multifunctional luminescent Tb^{3+} complex (LTC) **65 (Figure 1.32)** conjugated with rhodamine (5-carboxytetramethylrhodamine, CTMR) system which is linked by piperazine moiety. This spirolactam ring closed CTMR unit in the probe has displayed least fluorescence due to inhibition of LRET (luminescence resonance energy transfer) process. Therefore, it exhibits a strong luminescence only due to LTC group. However, treatment with NO induces opening of that spirolactam ring in the CTMR fragment, resulting the decrease in luminescence intensity of LTC with the simultaneous remarkable increase in emission intensity of CTMR moiety stimulated by LRET process (28.8-fold). The

LOD for the detection of NO by this probe was found to be 1.8 µM. This probe is also suitable to monitor lysosomal NO in HepG2 cells and Daphnia magna devoiding of any interference from biological reactive species.
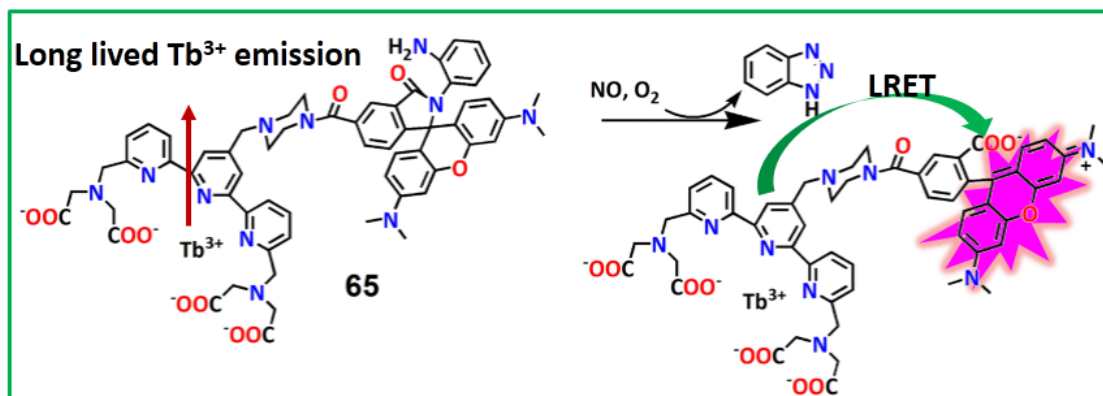
Figure 1.32 Tb^{3+} based OPD probe for NO sensing.

Among the metal complex embeded fluorescent probes for sensing NO, the Cu(II)-based complexes are found to be best for monitoring NO. In these cases the probes are fluorescent; however on coordination to paramagnetic copper(II) ion it becomes non-fluorescent. On further treatment with NO it reduces Cu(II) to diamagnetic Cu(I), restoring fluorescence of the probes.[165]
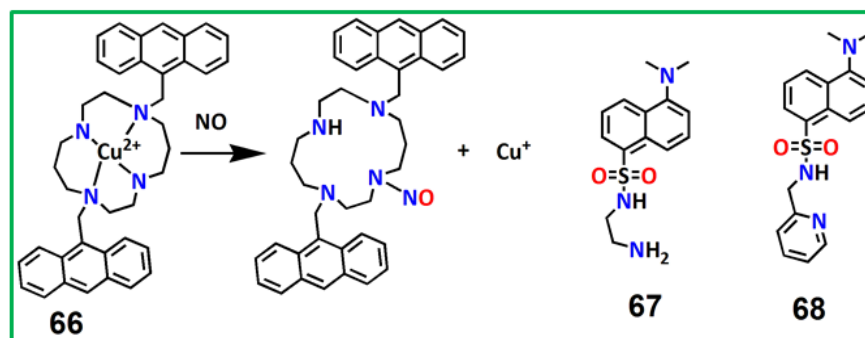
Figure 1.33 Anthracene-cyclam based Cu(II) complex for NO sensing.

An anthracene-tetraamine cyclam based Cu(II) complex **66 (Figure 1.33)** [158] was synthesized by Ford et al. which reacts with NO resulting reductive elimination of Cu(I) with simultaneous nitrosylation at N atom of a secondary amine group,. Additionally, two water soluble probes **67,**

68 (**Figure 1.33**) were reported by Lippard et al. which detect NO by the reduction of Cu(II) ion with the enhancement of fluorescence intensity by almost 6 and 8 fold respectively.[165]

The same group also reported the NO sensing by seminaphtho-fluorescein based probes **69** (**Figure 1.34**).[166] Here, Cu(II) → Cu(I) reduction followed by demetallation and simultaneous N-nitrosation of secondary aromatic amine occur with restoration of fluorescence emission (20-45 fold) in the range 550 nm to 625 nm.
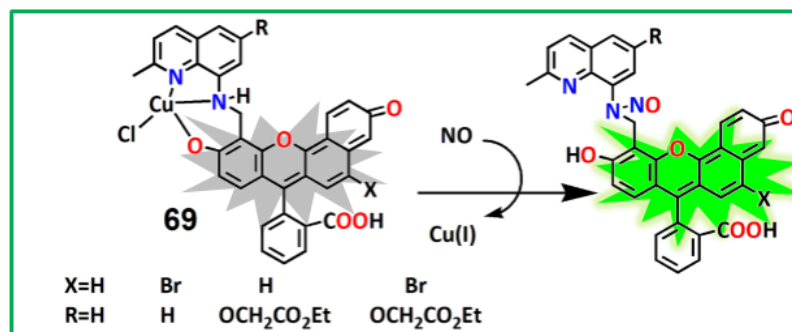
Figure 1.34 N-nitrosation of a copper complex.

These probes were found to be suitable to image endogenously produced NO in live RAW264.7 cells. Additionally, they display strong selectivity to NO devoiding the interaction of biological reactive species which includes NO_3^-, NO_2^-, HNO, $ONOO^-$, OCl^- and H_2O_2.

Vilar et al.[167] published a copper (II) based NO sensor **70 (Figure 1.35)** prepared by the reaction between 4-N-octyl-N-methylaminosulfonyl-7-chloro-2,1,3-benzoxadiazole and N^1-(Pyridyl-2-ylmethyl)ethane1,2-diamine. The probe itself is highly fluorescent, however on reaction with Cu(II) it becomes non-fluorescent due to paramagnetic quenching by Cu(II). Further reaction with NO the regeneration of fluorescence at 580 nm was observed due to the release of free ligand. This probe also shows good cellular uptake due to the hydrophobic lipid chain (octyl group) and can be used for endogenous NO detection in living MCF-7 cells exploiting hormone 17β estradiol as the NO stimulator.

James et al.[168] also reported a highly water soluble probe **71 (Figure 1.35)** using 1,8-naphthalimide as fluorophore and 8-aminoquinoline as Cu(II) receptor. The introduction of a hydroxyethoxy side arm increases its solubility in aqueous medium as well as furnishes a potential tool in the improvement of polymer-bound receptors. The probe itself is fluorescent but becomes non-fluorescent on complexation with Cu(II). However, NO treatment converted Cu(II)

to Cu(I). Due to little stability, this Cu(I) complex eliminates Cu(I), making the ligand free, with simultaneous N-nitrosation on secondary amine group close to the quinoline moiety. This probe also can detect HNO following the same mechanism at 534 nm (λ_{ex} = 450nm). After NO and HNO treatment almost 18 fold and 32 fold fluorescence enhancement were observed. This dual analyte probe also can be taken to image exogenously and endogenously produced NO in live cells.
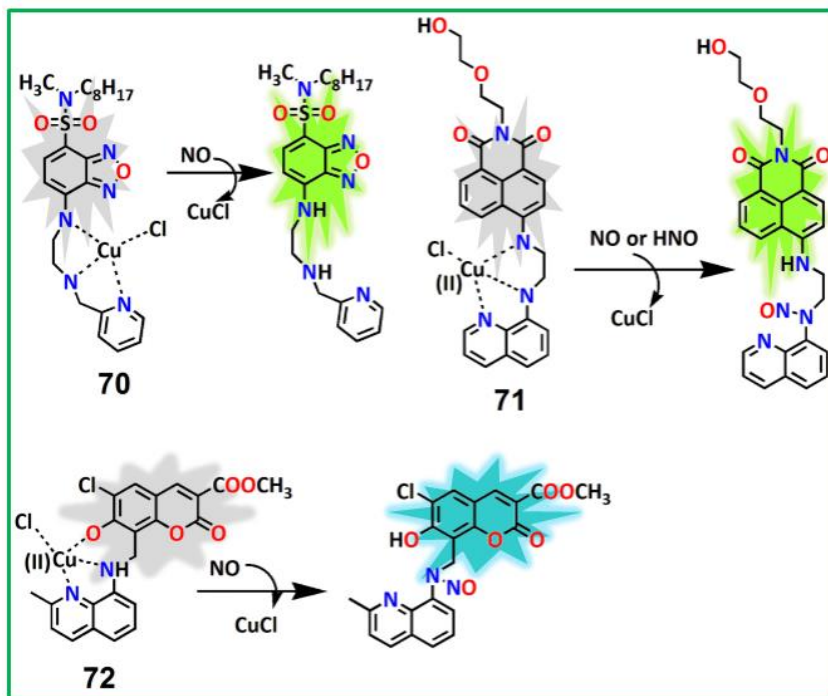
Figure 1.35 Copper complex based NO probes.

Norton group[169,170] also published a NO sensor **72 (Figure 1.35)** using same strategy taking coumarin as fluorophore. This probe generates strong blue fluorescence at 445 nm (λ_{ex} = 405 nm) upon reaction with NO and can be suitably utilized for endogenous NO tracking. It delineates very strong selectivity and sensitivity towards NO being little interfered by other reactive species and permits the NO visualization inside a biofilm. The co-localization experiments by digital image studies has expressed that NO production and conditions of oxidative stress take place primarily in living organisms in the time of normal biofilm growth.

A ratiometric Cu(II) complex based NO probe **73 (Figure 1.36)** was reported by Lippard and coworkers where hydroxycoumarin and fluorescein are linked by a piperazine spacer which

allows Förster resonance energy transfer (FRET) process. It could directly detect NO by N-nitrosation (11-fold fluorescence intensity, within 2 minutes) with improving the emission intensity ratio of two fluorophores and showing LOD of 21 nM. This piperazine scaffold improves resistance to the biological reductants and exhibits the enhanced cellular permeability with subcellular localization.[171]
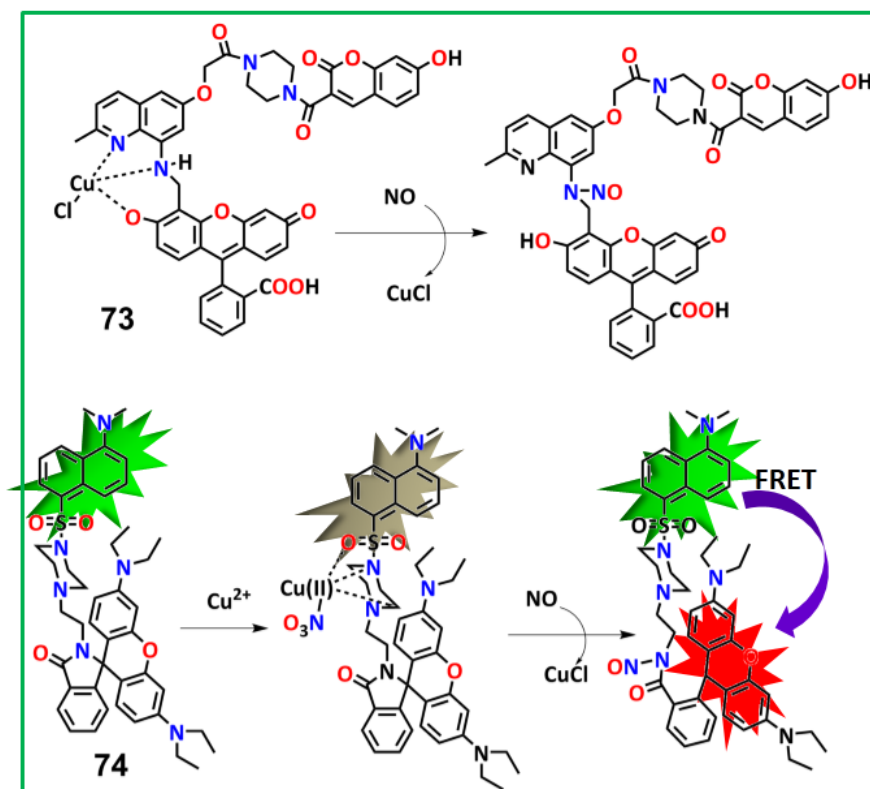
Figure 1.36 Two FRET based Cu complexes for NO sensing.

Another FRET-based Cu(II) complex was designated as NO sensor **74 (Figure 1.36)** by Patra group[172] using rhodamine B and dansyl platform linked by a piperazine moiety. The probe itself shows green fluorescence for dansyl group where addition of Cu(II) facilitates the quenching of fluorescence of dansyl fluorophore. Upon reaction of the probe with NO, Cu(II) gets reduced to Cu(I), making the complex unstable. This facilitates the release of Cu(I) which in turn simultaneously induces nitrosylation on N-atom of the spirolactum ring, resulting a red fluorescence (λ_{em} = 580 nm, 750 fold) with LOD value 1 nM. This probe also displays the

negligible emission of metal bound probe as well as outstanding NO imaging capability in HeLa cells with least cytotoxicity.

Lippard et al.[173] also synthesized a series of benzoresorufin-based copper complexes **75**, **76**, **77** **(Figure 1.37)** which display 1.5−4.8 fold emission increment at 625nm (λ_{ex} = 563 nm) in response to NO and HNO. These probes can be employed for endogenous NO detection in HeLa cells and RAW 264.7 macrophages. Mechanistically, here fluorescence magnification upon reaction with NO occurs, due to the release of metal in its reduced state. The simultaneous N-nitrosation to the metal free probe also occurs here. Whereas, HNO also reduces Cu(II) to Cu(I) with subsequent demetallation but N-nitrosation does not occurs here. Authors assume that the lower regeneration of fluorescence upon treatment with HNO and NO may be due to tighter binding of the probes with Cu(II) which precludes 100% reduction and release of the probe. These sensors show ample efficiency to detect NO and HNO in cuvette and living cells too.
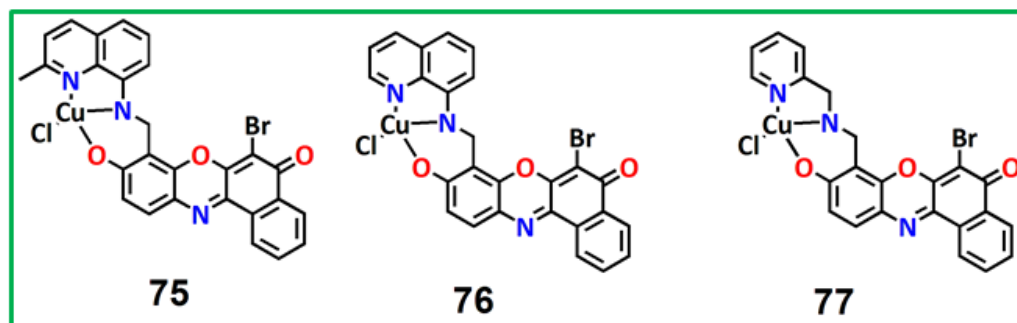
Figure 1.37 Benzoresorufin derivatives as NO sensors.

Duan et al.[174] has published a rhodamine–triethylene tetraamine Cu(II) complex **78 (Figure1.38)** which on treatment with NO reduces Cu(II) and follows N-nitrosation with opening of spirolactam ring. This probe has attributed in 700-fold fluorescence magnification upon reaction with NO as well as exhibited 1 nM detection limit in water with suitable application for monitoring intracellular NO in MCF-7 cell. Mondal's group[175] has published a Cu(II) complex **79 (Figure 1.38)** attached with tridentate N-donor ligand for NO detection which exhibits 8.3 fold fluorescence enhancement at ~555 nm in aqueous medium due to the reduction of the metal centre with 10 nM LOD.
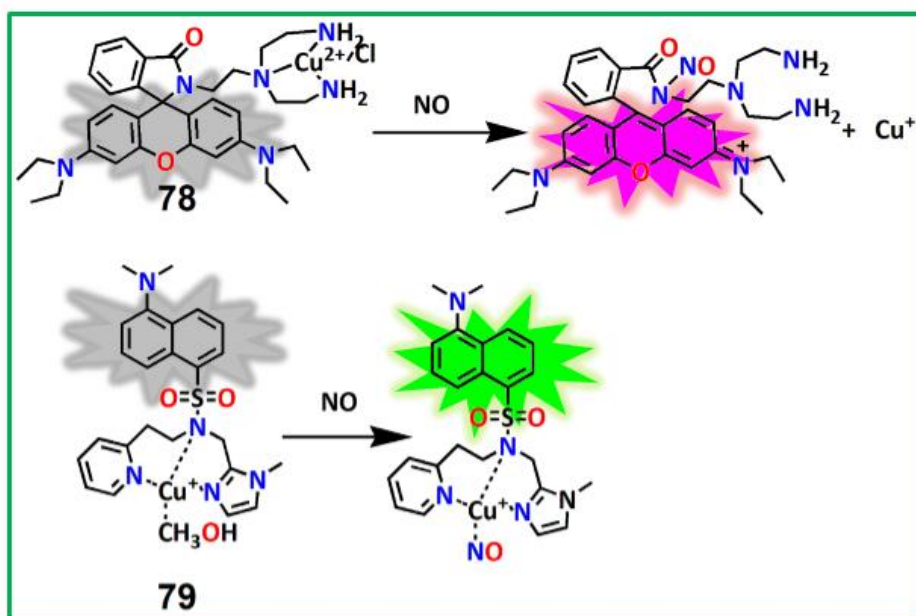
Figure 1.38 Structure of another two Cu complexes for NO detection.

Another well-designed copper complex based NO probe **80 (Figure 1.39)** is consists of napthalimide moiety which shows N-nitrosation upon treatment with NO having 8-fold fluorescence generation at 530 nm (λ_{ex} = 466 nm). It has provided 1 nM LOD value in water medium.[176] This probe also specifically detects NO being unaffected by biological reactive species like ClO^-, NO_2^-, NO_3^-, H_2O_2, $ONOO^-$, and $^1O_2$. Moreover, intracellular NO imaging is also done by this probe.

Ali et al. has unveiled a dansyl-embeded turn-on NO sensor **81 (Figure 1.39)**. The probe itself is highly fluorescent but on treatment with Cu(II) it undergoes complexation and it's fluorescence intensity gets quenched dramatically (60 fold). The quenching of fluorescence intensity of this Cu(II) bound probe may occur due to PET process as well as paramagnetic effect of Cu(II) ion. However, on further treatment with NO the turn-on fluorescence occurs at 532 nm (λ_{ex} = 345 nm) with 15 fold enhancement which might be due to PET blocking as well as the diamagnetic nature of Cu(I) being coordinated to the probe [177]. The LOD value of NO detection was determined to be 1.6 nM. This system also can be efficient enough to image exogeneous NO in HeLa cells.

This group also reported another copper complex based NO probe **82 (Figure 1.39)** using phenazine fluorophore which upon reaction with NO and HNO, gets reduced and fluorescence

was regenerated at 560 nm (67 and 84% respectively, λ_{ex} = 400 nm). Here metal is still remain bound to the ligand as proven by EPR study. This probe is found to be efficient to detect exo- and endogenously generated NO and HNO in A549 and RAW 264.7 cells which can be quantified by flow cytometry application.[178]
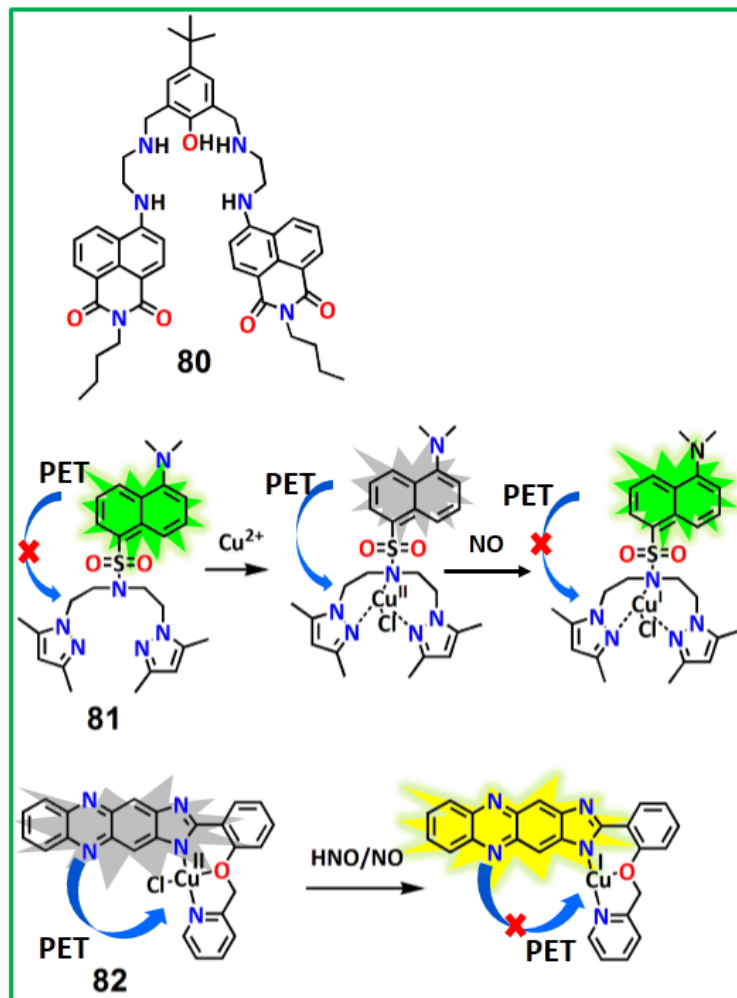
Figure 1.39 Structure and reaction mechanism of probe **80**, **81**, **82.**

1.4 Chemical and Biological Aspects of NITROXYL (HNO)

Nitroxyl is the simplest nitroso compounds (R-N=O, R=H) which undergoes dimerization (k = 8 $\times$ 10^6 $M^{-1}s^{-1}$) like other C-nitroso derivatives and ultimately produces nitric oxide (**reaction 4, 5**).[179]

$$2Ar-NO \rightleftharpoons \overset{\bar{O}}{\underset{Ar}{N}}\overset{+}{=}\overset{+}{\underset{Ar}{N}}\overset{\bar{O}}{} + \overset{\bar{O}}{\underset{Ar}{N}}\overset{+}{=}\overset{+}{\underset{\bar{O}}{N}}\overset{Ar}{} \qquad (4)$$

$$HNO + HNO \longrightarrow HON=NOH \longrightarrow N_2O + H_2O \qquad (5)$$
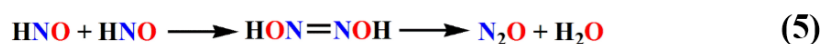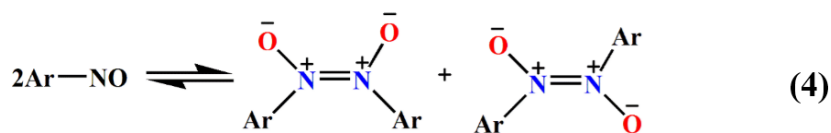
So like nitric oxide, nitroxyl is also an important biomolecules and exerts immense effect on chemistry and biology. Though, its chemical activities are well understood, its physiological and pathological impact has not been well uncharted. So a rapid and reliable method to monitor HNO in living organism is highly demanding and attracting immense attentions of chemists and biologists.

1.4.1 Nitroxyl in Chemistry

HNO may induce the following biological consequences in chemistry:

1. This very fast self-reactivity of HNO makes a very difficult task to identify and detect HNO in any endogenously generating systems.
2. The pK_a value of HNO is reported to be 11.4 and is in well agreement between experimental and theoretical values which indicates that the predominant species present at physiological pH is HNO rather NO⁻.[180,179]
3. For normal acids, the protonation–deprotonation rates fall in the diffusion control limit ($\sim 10^{10}$ s^{-1}). However, for HNO the proton transfer rate constant is slower than other acid-base reactions. Thus, it may be said that, the formed anion (NO⁻) may have a sufficient lifetime.
4. Because of the strong reactivity of HNO towards thiols it readily reacts with biological thiol containing proteins and enzymes leading to the formation of disulfides. However,

the reversiblity or irreversibility of this reactions depends upon the reaction conditions.[181-183]

5. Both the oxidant and reductant behavior of HNO forces to consider the detailed biological implication of HNO.[184-187]

6. Endogenous production of HNO is not well established, though formation of HNO from NO through one electron reduction is difficult but possible.[67]

1.4.2 Nitroxyl in Biology

1. HNO exhibits its specific ability in increasing cardiac signal and decreasing venous resistance simultaneously. HNO becomes an ideal drug for the treatment of heart failure for these pharmacological traits.[28,188]

2. Tissue pretreatment with HNO defends against the ischemia-reperfusion toxicity.[27]

3. HNO is efficient enough to interact with peptides and thiol proteins which leads to the blocking of their functions.

4. HNO reacts with metalloproteins, either at the metal center or with ligands.

5. The high concentration of HNO leads to toxicity due to the oxidation of biomolecules.[67]

6. Previously reported information indicated that HNO could activate sGC, resulting to increase in cGMP which finally causes vasorelaxation.

7. The impressive and significant therapeutic activity of HNO, is its role in failing hearts. HNO also enhances Ca^{2+} cycling, Ca^{2+} sensitivity of myofilament, obtaining a combined arterial and venous dilation without affecting the heart rate[189]

8. HNO interacts quickly towards cysteine proteases as well as different cysteine derived proteins, modifying their activities.

9. The highly reactive nature of HNO towards thiols of proteins and enzymes to generate corresponding disulfides or sulfinamides inhibits their activity.[190,191]

10. In addition, HNO induced signalling process is distinct and different from the NO mediated signalling in case of thiol modification. NO-mediated thiol moderation generally consequences in the production of S-nitrosothiol[192] requiring a one-electron oxidant to transform NO to nitrosonium (NO^+) derivative. Whereas, HNO interacts with

thiol derivatives without any "pre-activation" leading to the formation of disulfide or sulfinamide (via N-hydroxysulfenamide intermediacy). Thus, it is getting more clear that HNO signalling is totally different from NO signalling.

11. HNO activates cardiac sarcoplasmic ryanodine receptors affording important strategies for the therapy of cardiovascular disorders.[193]

12. HNO also functions as an efficient vasodilator inducing positive inotropic/lusitropic consequences as well as inhibiting platelet aggregation.[23,194]
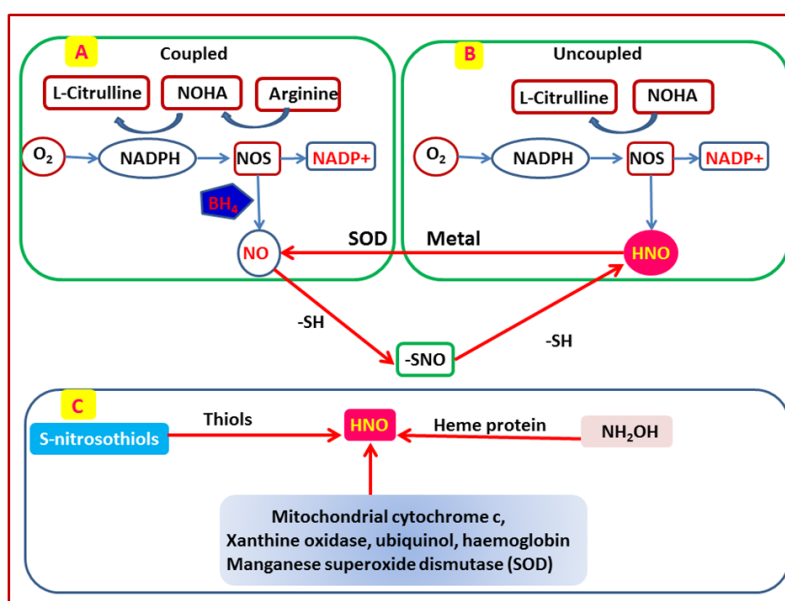
Figure 1.40 *In vitro* formation of HNO.

1.4.3 HNO Donors

Self-dimerization of HNO subsequently generates N_2O and water which prevents the storage of HNO. So there was a need to generate some stable donors of HNO for chemical and biological studies. Fortunately, chemists have synthesized some manageable stable donors of HNO which are enumerated below.

1.4.3.1 Angeli's salt

Angeli's salt (AS) is one of the well-studied and most utilized HNO donors named as sodium trioxodinitrate (Na$_2$N$_2$O$_3$).[195,196,21] Due to its easy synthetic procedure and stability for longer period at low temperature and instant release of HNO in aqueous solution the scientists have utilized it for most of the biological and pharmacological studies. It decomposes spontaneously to produce equivalent amount of HNO and NO$_2^-$ at pH>4 (**reaction 6**) and rate of thermal decomposition remains almost indifferent in the pH range 4-8 however rate decreases at pH higher than 8.0. At pH<4 Angeli's salt releases NO[195], so studies at acidic condition must be carefully interpreted.

$$N_2O_3^{2-} + H^+ \rightarrow HNO + NO_2^- \qquad (6)$$
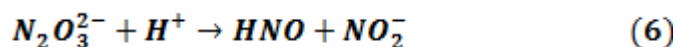
1.4.3.2 Piloty's acid and derivatives

N-hydroxysulfinamides, also named as Piloty's acid was found to be stable at lower pH and it releases HNO on elevation of pH (**reaction 7**).[197]

$$(7)$$
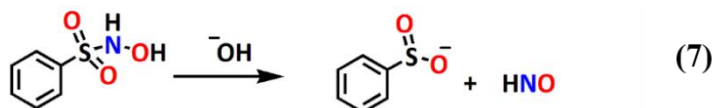
So, it liberates HNO at pH beyond the biological conditions. Additionally, at biological pH it gets oxidized to release NO rather HNO.[198] So this pH parameter limits the use of these compounds as HNO donor.

1.4.3.3 HNO-generating diazeniumdiolates

A Diazeniumdiolate [($^-$XN(O)=NO$^-$) may act as a source of HNO or NO based on the nature of X as nucleophile. It is observed that when X= O, it is Angeli's Salt, a source of HNO; When X=R$_1$R$_2$N, (secondary amine) it acts as a source of NO. [199] However, the primary amine makes it HNO releaser at biological pH similar to Angeli's salt[200] (**reaction 8,9,10**) [201, 202]

$$(8)$$

$$[RNH-N(O)=NO]^- \rightleftharpoons [RN=N(O)-NHO]^- \longrightarrow HNO + RNNO^- \qquad (9)$$

$$(10)$$

$$[RNH - N(O) = NO]^- \rightleftharpoons [RN = N(O) - NHO]^- \rightarrow HNO + RNNO^-$$

$$RNHNO \rightarrow RNN^+ + HO^- \rightarrow ROH + N_2 \qquad (11)$$
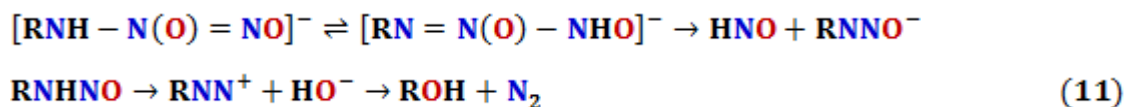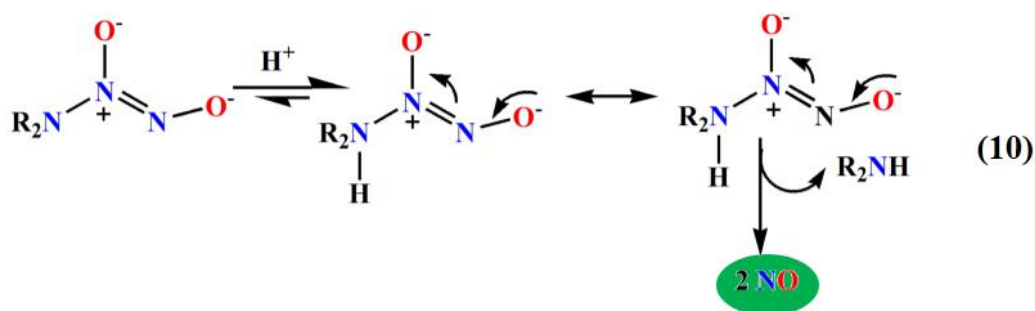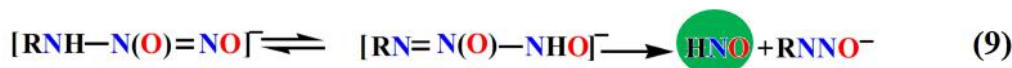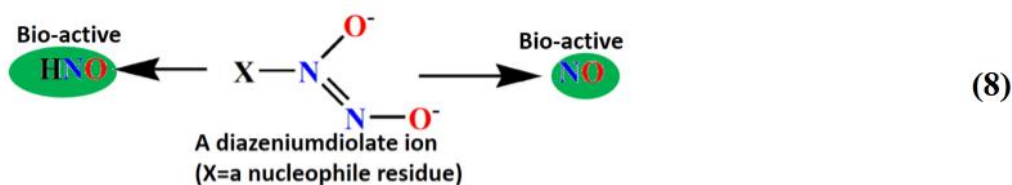
N-nitrosated primary aliphatic amine ($RNNO^-$) (**Reaction 11)** is unstable than corresponding secondary aliphatic amine as first one finally converted to N_2 and alcohol as final product. So, NONOates exploited primary amines can be more precisely used for application of HNO *in vivo*.

1.4.3.4 Nitrosocarbonyls

Nitrosocarbonyl compound is also denoted as another class of HNO donor which are spontaneously hydrolases in aqueous solution to produce HNO and corresponding carboxylic acid **(Reaction 12)**. However, this type of in situ HNO precursors has not been well-studied for biological information.

$$(12)$$
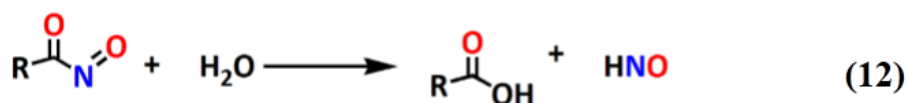
1.4.3.5 Hydroxylamine

Considering oxidation state, NO is converted to HNO, N_2 and then NH_2OH. So 2-electron oxidation can make NH_2OH to HNO.[203] Till date, the NH_2OH can't be used as HNO source in biological sample analysis. Donzelli group[204] has illustrated indirectly the oxidation of NH_2OH by HRP (horseradish peroxidase) which releases HNO getting trapped by GSH **(Reaction 13)**.

$$\mathbf{RSH + HNO \rightarrow RSNHOH \rightarrow RS(O)NH_2} \qquad (13)$$
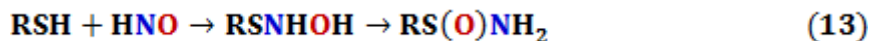
1.4.3.6 Cyanamide

Cyanamide is an anti-alcoholism drug which may be applied as HNO releasing agent in the treatment of cardiovascular problems. Due to oxidation by the enzyme catalase, cyanamide is activated which leads to the formation of N-hydroxycyanamide intermediate. This gets decomposed to produce cyanide and HNO **(Reaction 14).**[181]

$$\text{NH}_2\text{CN} \xrightarrow{\text{catalase/H}_2\text{O}_2} \underset{\text{H}}{\overset{\text{HO}}{\text{N}}}\text{-C≡N} \longrightarrow \text{HNO} + {}^-\text{CN} + \text{H}^+ \qquad (14)$$
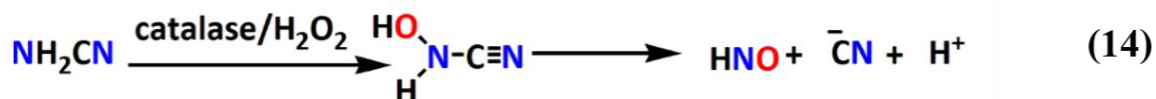
Though this cyanide formation has limited the use of cyanamides still cyanamide accomplishes both the practicability of clinical application of HNO donating agent and shows the efficiency to selectively attack protein thiols.

1.4.3.7 Acyloxy nitroso compounds

To perceive the deeper knowledge about the pharmacological applicability of HNO it is necessary to develop a variety of HNO donors, complimentary of Angeli's salt.[205] This newly derived HNO donor will confirm about the biochemistry of only HNO not its decomposed species. Following this theory a new HNO donor alpha-acyloxy-C-nitroso compound has been prepared by King laboratory **(Reaction 15)**. [206]

$$(15)$$
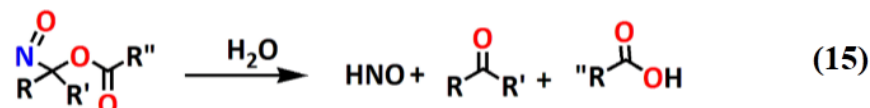
These compounds can be easily prepared by the oxidation of oximes and releases HNO at physiological conditions. The HNO release is envisaged through the hydrolysis of ester or by the activity of esterase and the release rate may be controlled by the rational choice of organic moieties. Due to the constructional adjustability, this type of releaser may take an significant role in drug discovery with exact pharmaco-kinetics and distribution profiles.

1.4.4 Different Type of Fluorescent Sensor for HNO Detection

The development or establishment of the biological and chemical profile of HNO is very crucial and requires sophisticated HNO detection methods. Previously this includes (i) recognition of sulfinamides arising from biological thiols trapped with HNO by high pressure LC-MS, (ii) identification of the nitrosyl mediated product found from ferric heme proteins by UV-Vis or (iii) by EPR spectroscopy. The lower selectivity and sensitivity[19,22-24] of these methods has led to the development of fluorescent probes following different strategies:

   A. Fluorescent probe on complexation with Cu(II) becomes non-fluorescent which on subsequent treatment with HNO fluorescence is regenerated.
   B. Triphenylphosphine-based probes which after reaction of HNO liberate the fluorescent dye (Staudinger ligation).
   C. Nitroxide-based pro-fluorescent (turn-off) probes on reaction with HNO is reduced to hydroxylamine with the generation of fluorescence.
   D. A non-fluorescent species generated through the attachment of 2-mercapto-2-methylpropionic acid and a fluorophore. This probe upon HNO treatment forms an N-hydroxysulfenamide species. Finally this species is converted to the intramolecular cyclized product and the fluorophore resulting the regeneration of fluorescence intensity.
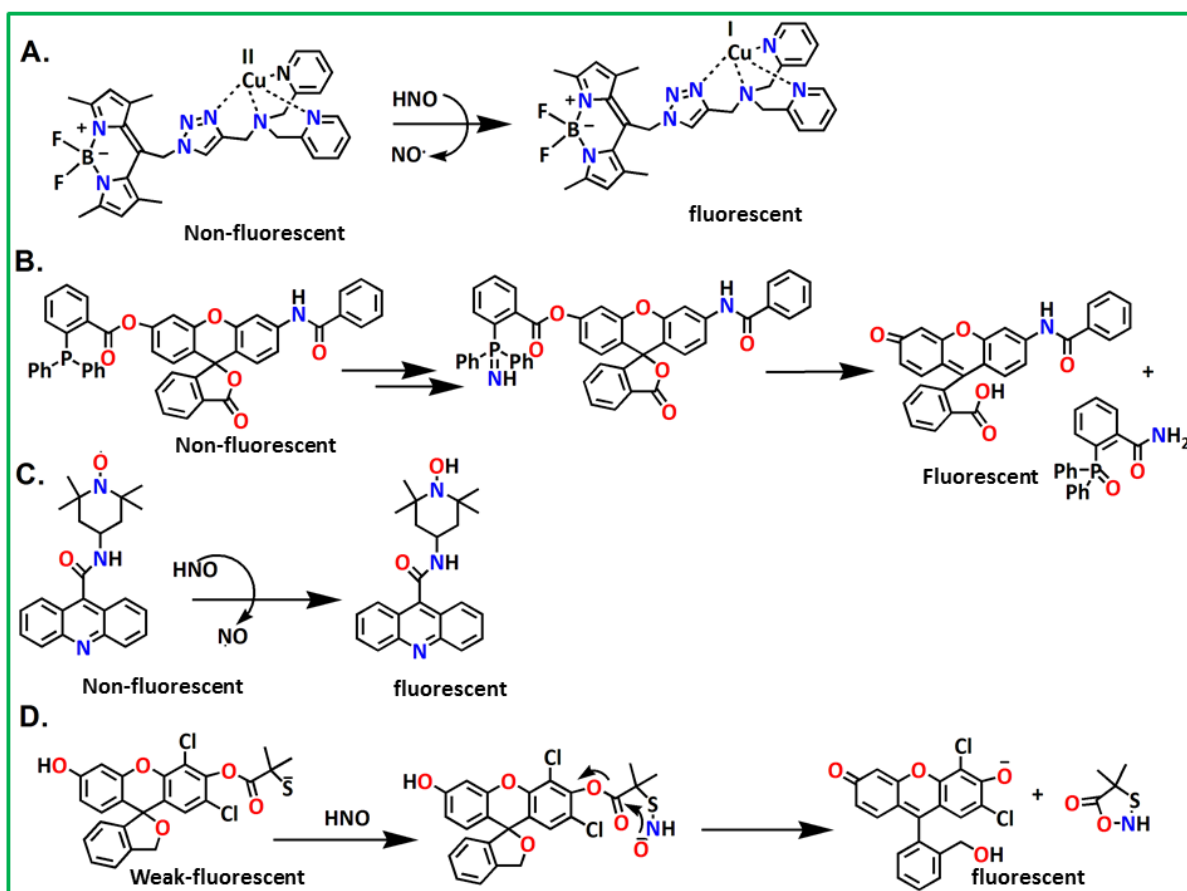
Figure 1.41 The established strategies of HNO recognition by various types of fluorogenic probes like **A**. reduction of copper complex, **B**. Staudinger ligation of triphenylphosphine, **C**. proton abstraction by nitroxide radical, **D**. fluorophore regeneration from 2-mercapto-2-methylpropionic acid.

These fluorescent based HNO probes reveals many advantages over some previously used methods in terms of selectivity and specificity for HNO detection with distinct mechanism **(Figure 1.41)**. These methods also show their capability to track HNO in living organisms also.

1.4.4.1 Cu(II) complex appended HNO Probes

Nitroxyl displays interaction mainly towards heme proteins which go through the reductive nitrosylation. Another example of colorimetric HNO detection occurs by Mn^{III} porphyrins system through reductive nitrosylation which easily differentiate HNO and NO. Mn^{III} porphyrins

system reacts with HNO through very quick and specific way that concomitantly forms the {MnNO}^{7} complex ($k_{(HNO)} \approx 10^5$ M^{-1} s^{-1}), showing least reactivity towards NO donors.[207] This reactivity of HNO towards metal complexes was extended largely to the Cu^{II} complex appended HNO probe. This mechanism was first pioneered by Lippard group by reporting a probe **83 (Figure 1.42)** where, a tripodal dipicolylamine unit is attached with BODIPY fluorophore through a triazole bridge. Here, emission of the probe gets quenched upon addition of the Cu^{II} ion due to PET mechanism which further restored at 526 nm (4.3 fold enhancement, $\lambda_{ex} = 450$ nm) by the treatment with Angeli's salt without interference by other biological reactive species. Here, Cu^{II} is reduced to Cu^I and PET process is inhibited. This probe is eligible to detect exogeneous HNO in HeLa cell. They also studied the reduction power of Cu^{II} ion in presence of biological reductive species like cysteine which also shows the fluorescence enhancement due to Cu^I formation but the cell imaging study clearly indicates that the normal intracellular cysteine concentration can't reduce the Cu^{II} to Cu^I.[208]

After this primary report using such novel strategy, researchers get impetus to generate different type of more improved Cu^{II} complex based HNO sensors.[173,209-212] Yao et al. has developed Cu(II)-based HNO probe **84 (Figure 1.42)** using coumarin fluorophore keeping fixed the coordination site like Lippard's pioneering work where, HNO sensing has been studied by both fluorescence and EPR spectroscopy.[209] In this probe the attributing PET mechanism between fluorophore to chelating Cu(II) gets inhibited due to conversion of Cu(II) to Cu(I) which consequences 17.3 fold fluorescence restoration at 499 nm. This probe also can detect exogeneous HNO in A375 cell with ample efficiency. Yao group has further developed an analogous HNO probe **85 (Figure 1.42)** by a simple improvement in the coordination site by changing one of the pyridine group by an ester group[210] which makes the probe more cell permeable and monitors HNO in living cells as well as in vertebrate *in vivo*. In this work the probe is interfered by cysteine which can also be avoided by the use of masking agent N-ethylmaleimide (NEM). In spite of these important modifications these probes contains some shortcomings like high energy demanding absorption as well as emission with comperatively short Stokes shifts.
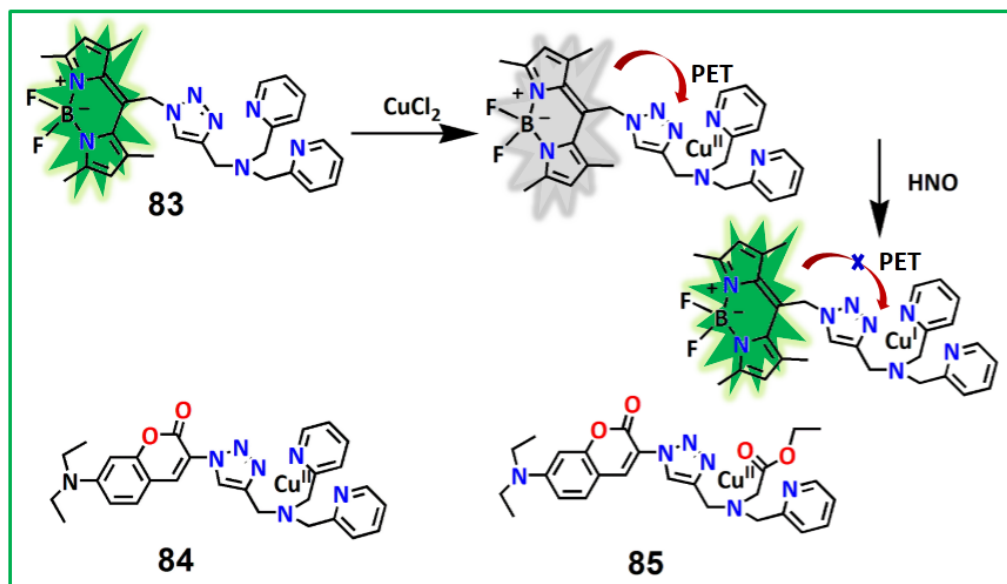
Figure 1.42 Structure and HNO reaction mechanism of copper complex **83**,**84**,**85.**

To overcome these limitations, Lippard group has also developed a novel benzoresorufin embedded Cu(II) complex based HNO sensor **86**, **87**, **88 (Figure 1.43)** where they employed aminoquinoline and methyl pyridine as Cu binding site. Mechanistically HNO has converted Cu(II) to Cu(I) with removal of metal ion and concomitant generation of fluorescence intensity. These probes are also capable for HNO detection in RAW 264.7 macrophages and HeLa cells.[173] Near-infrared (NIR) light is superior one due to its less photo damage, negligible background noise and tissue penetrating ability with respect to the visible light. The NIR Probe **89 (Figure 1.43)** has been reported by Lippard group utilizing a dihydroxanthene fluorophore which exhibits 5-fold emission peak enlargement centered at 715 nm upon reaction with HNO without any interference by H_2S and thiols including NO. Here, multicolor imaging analysis shows the HNO-influenced enhancement of cellular mobile zinc.[211] They have also demonstrated another Cu(II)-complex based HNO sensor **90 (Figure 1.43)** where tetramethyl-rhodamine unit acting as a fluorophoric moiety linked to a copper chelating scaffold cyclam. Upon reaction with HNO, 4-fold increase in fluorescence emission peak (λ_{em} = 580 nm) was noticed. This probe is potent also to monitor HNO in biological environment.[212]
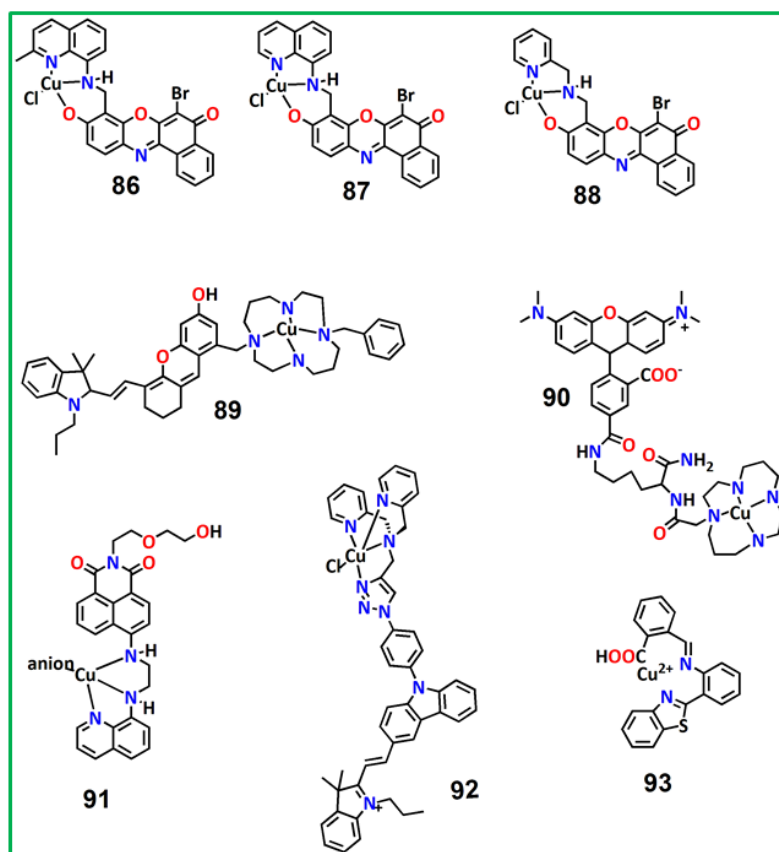
Figure 1.43 Structure of some other copper complexes for HNO sensing.

James group published a highly water soluble copper complex **91 (Figure 1.43)** where napthalimide moiety acts as fluorophore and ethylenediamine–8-aminoquinoline as chelating agent. The probe **91** upon treatment with HNO/NO exhibits a significant increase in fluorescence at 534 nm. This is because of the reduction of Cu(II) to Cu(I) and simultaneous N-nitrosation to the metal free probe followed by release of Cu(I). This probe was found to be useful for biological application. [168]

Xing and coworker reported a HNO sensor **92 (Figure 1.43)** embedding, hemicyanine conjugated carbazole (fluorophoric moiety) and bipyridine-triazole-Cu(II) complex (receptor). They have shown that H_2S abstracts Cu^{2+} as CuS, resulting the recovery of the fluorescence of the probe, while HNO simply reduces Cu^{2+} to Cu^+ resulting an enhancement of the emission intensity. The probe **92** holds separate dispersity and binding capability towards Cu^{2+} resulting in the distinct monitoring of H_2S and HNO in various SDS micellar environment. This probe

upon treatment with Angeli's salt shows an obvious increment in fluorescence emission at 595 nm along with LOD 23.0 μM. Though this probe is interfered by H_2S but shows ample selectivity towards HNO detection in liposomes.[213]

Palanisamy and co-workers developed Cu(II) complex based highly fluorescent material **93 (Figure 1.43)** which could monitor HNO through quenching of fluorescence due to the quantitative HNO induced reduction of paramagnetic Cu(II) at 450 nm (λ_{ex} = 358 nm). The authors claim that the probe **93** has no individual binding sites towards Cu^{2+} and hence in the presence of Cu^{2+} it fluoresces due to PET blocking. However, upon reaction with HNO, Cu^{2+} is reduced to Cu^+ thereby induce the PET process and it becomes non-fluorescent. The LOD value for the detection of HNO was estimated to be 9.05 uM and finds applications in live cells and zebrafish model devoiding of any interaction from biological reactive species in living organism.[214]

1.4.4.2 Triphenylphosphine-based (Staudinger ligation) HNO probes

The extensively used triphenylphosphine embedded nitroxyl probes **(Figure 1.44)** (where R_2 is the fluorophore moiety) are bio-orthogonal, as the phosphine is abiotic in nature and almost unreactive towards native biomolecules present in the living cells.[215,216] With respect to the metal based HNO sensor, this type of probes are quiet *reductant resistant* towards reducing agents present in the bio-system and thus showing highly selective fluorescence response towards HNO. It is reported that the reaction between phosphines and Nitroso compounds, generates equivalent amount of phosphine oxide and azaylide, via hetero three-membered ring intermediate **(Figure 1.44)**.[215,217]

In this strategy, an intramolecular nucleophilic attack of ylide amine (P=NH) to the C=O of the ester group occurs, leading to the formation of transient five membered ring. This is the key step of the reaction after which the intermediate is stabilized by release of alcohol and the remaining species is hydrolyzed to produce ultimate product, benzamide phosphine oxide **(Figure 1.44)**. This specific chemically stable benzamide, formed from this reaction, is represented as the distinct HNO marker.
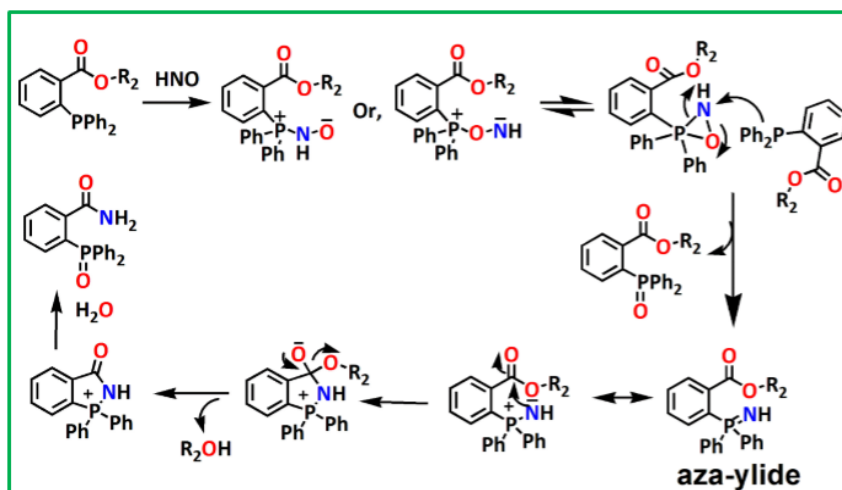
Figure 1.44 Mechanism of Staudinger-ligation based HNO sensing.

Exploiting this strategy, Nakagawa has pioneered the HNO probe **94 (Figure 1.45)** taking triphenylphosphine moiety as the HNO recognition site and rhodol as fluorophore where amino group was acylated with benzoic acid.[218] This upon HNO treatment shows dramatic increment in fluorescence at 526 nm (λ_{ex} = 491 nm) being hardly interfered by biologically reactive molecule like H_2S, GSH, AA, etc. This probe recognizes HNO found from different systems and describes the applicability to detect fluorescence in A549 cells upon addition of HNO.
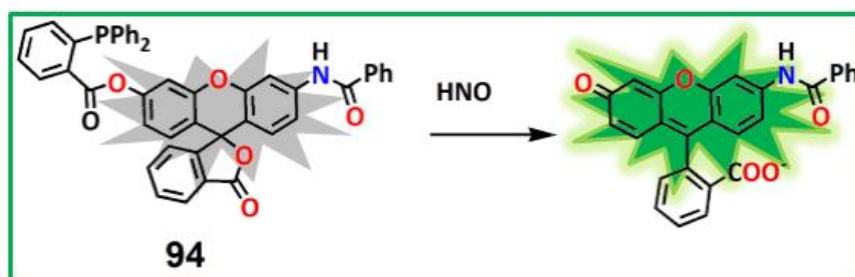
Figure 1.45 First Staudinger-ligation based HNO sensor done by Nakagawa.

By employing the pioneering mechanism, involved in triphenylphosphine embedded nitroxyl probes, a number of Staudinger ligation based HNO probes has been largely emerged. Though they have followed the same mechanistic strategy but can be divided into two types **a) intensity-based probe (turn-on):** this type of probe has shown turn-on fluorescence response upon

treatment with HNO at a fixed wavelength. **b) Ratiometric probes**: These probes have allowed the analysis of photo-physical properties at various wavelengths.

Tan group reported an intensity-based fluorescent probe **95 (Figure 1.46)** using simple 7-substituted coumarin which shows 76 times fluorescence magnification at 450 nm in water. This probe was also found to detect HNO in bovein serum with moderate efficiency; as HNO reacts with thiols present in serum. This probe responses selectively towards HNO without interference by other reactive species and exhibits a 20 nM LOD.[219]

Bhuniya et al. has published a resorufin embedded Staudinger ligation based HNO sensor **96 (Figure 1.46)** which has revealed the 30 fold fluorescence enhancement centered at 590 nm (in naked eye, yellow transformed to pink, λ_{ex}=565 nm) with 20 nM detection limit.[220] The authors also performed cell (*in vitro*) as well as nematode (*in vivo*) imaging studies implying the efficiency of **96** for monitoring HNO level in the living systems.

Another fluoresceine based HNO probe **97 (Figure 1.46)** has been reported by King et al. which upon incubation with Angeli's salt shows emission intensity at 520 nm with least disturbance from biological reductant species. HNO detection is performed also in HeLa cells by confocal fluorescence microscopy and also by mass spectrometric studies of cell lysates**.**[221]

Thinking about the benefits of NIR light in bio-organisms a NIR probe **98 (Figure 1.46)** was reported by Chen group using BODIPY fluorophore and triphenylphosphine recognition unit. This probe fluoresces at 700 nm with 60 nM LOD value and visualizes lysosomal HNO in RAW 264.7 cells, due to lysosome tracker morpholine unit. Additionally the probe can be successfully applied for the recognition of HNO in mice model.[222] They have further developed the HNO probes **99,100 (Figure 1.46)** on the basis of BODIPY fluorophore with slight modifications. These probes are strongly selective and sensitive (LOD 30 nM) towards HNO having applicability in bioimaging study of HNO in live cells as well as in mice model.[223, 224] Utilizing flow cytometry analysis the authors has highlighted that the probe can potentially detect intracellular HNO qualitatively and quantitatively.

There are another two NIR fluorescence probe **101** and **102 (Figure 1.46)** reported by Sun and Yang group where merocyanine skeleton was used as fluorophore. There is a slight structural difference between **101** and **102** with an ester group was attached to merocyanine N-atom in **101** while a benzyl group in **102.** While probe **101** displayed fluorescence response towards

lysosomal HNO with LOD value 0.043μM (λ_{ex} = 680 nm, λ_{em} = 696nm), **102** specifically detects mitochondrial HNO with LOD value 60 nM (λ_{ex} = 727nm, λ_{ex} = 690 nm).[225,226]

As under the physiological condition, HNO is produced from the interaction between H_2S and NO, it is very difficult to correlate H_2S and HNO precisely by a single fluorescent sensor. However, the bifunctional fluorescence probe **103 (Figure 1.46)** can monitor the generation of endogenously produced HNO and H_2S sequentially which was synthesized using NBD (fluorophore) and 2-(diphenylphosphine) benzoate (reaction site) by Niu et al. carrying detection limit 1.42 uM, and 0.46 uM for HNO and H_2S detection, respectively.[227] The probe was effectively employed for H_2S and HNO detection in MCF-7 cells being a smart and efficient agent for interdependent detection of endogenously produced HNO generated from the reaction of H_2S and NO in living cells.
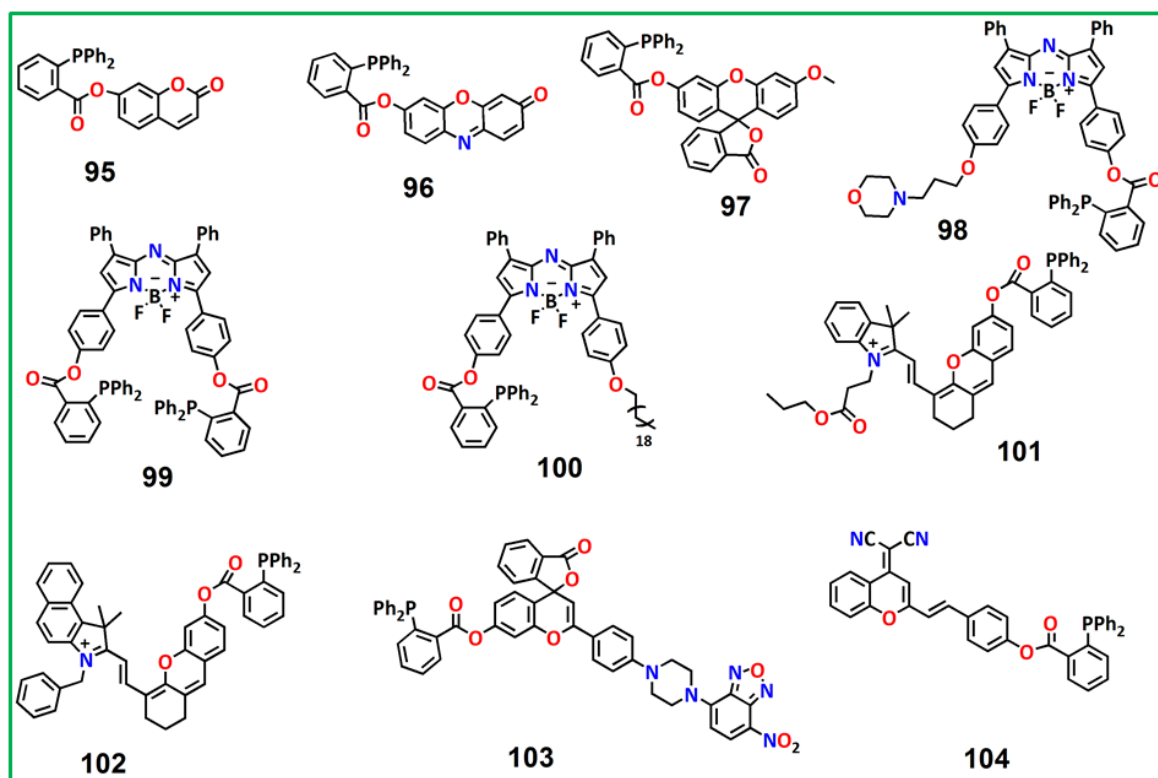
Figure 1.46 Structures of some intensity based HNO probes **95**-**104**.

An NIR based fluorescent HNO sensor **104 (Figure 1.46)** has been reported by Zhang group by employing (2-(4-hydroxystyryl)-4H-chromen-4-ylidene) malononitrile (fluorophore) and 2-

(diphenyl-phosphino) benzoate (recognition moiety). This one displays very fast reaction (within 2 min) with HNO and fluoresces at NIR emission (700 nm) with a large Stokes' shift (150 nm), that are suitable to track dynamic and transient HNO in living organisms.[228]

The recognition of HNO by the probe **105 (Figure 1.47)** involves a slightly different mechanism where HNO induced cascade reaction is prevailing resulting an imino-coumarin as the green fluorescent final product.[229] This probe makes very quick and selective responses towards HNO at 520 nm with LOD 9 nM in presence of some biological redox species and can be efficiently utilized to detect HNO in living HeLa cells and zebrafish larvae.
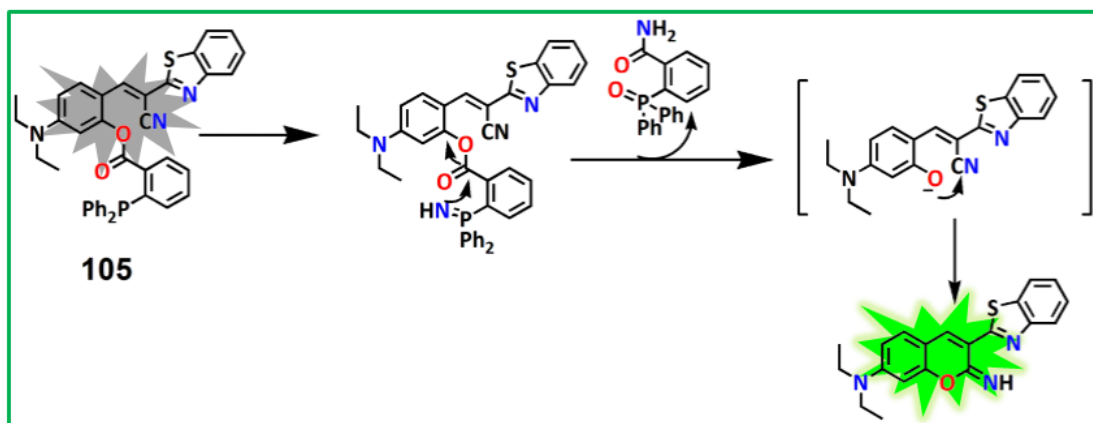
Figure 1.47 Staudinger based cascade reaction by HNO of probe **105**.

Very recently, another NIR based HNO probe **106 (Figure 1.48)** was fabricated which illustrates the brilliant advantages in HNO detection through NO and H_2S cross-talk, associated with very large Stokes shift (303 nm), sharp selectivity, rapid response (15 min) and strong sensitivity (LOD of 59.6 nM). In this probe the dicyanoisophorone moiety is in conjugation with benzothiazole unit resulting NIR emission at 728 nm.[230] Authors have also demonstrated that the probe is capable enough to visualize exogenously generated HNO in mice *in vivo*.

Jiang group has reported a non-emissive HNO sensor **107 (Figure 1.48)** with large stokes shift (160 nm) and emits at NIR region (λ_{em}=740 nm, λ_{ex}=580 nm) with detection limit 0.05 μM. This probe shows fast response (600s) with high selectivity and ample potency to image endogenously secreted HNO in live cells. [231]

Li group has constructed a multichannel fluorescent probe **108 (Figure 1.48)** which provides different emission profiles, towards peroxynitrite and hypochlorite (λ_{em} = 450 nm, blue emission) and HNO (λ_{em} = 540 nm, green emission) in a facile manner. Also this probe delineates real-time response to the peroxynitrite along with nitroxyl in Hela cells.[232]

Zhu et al. fabricated a metal free NIR probe **109 (Figure 1.48)** conjugating dicyanomethylene-4H-pyran and triarylphosphine moieties which upon exposure to HNO gives fluorescence emission at 688 nm with the opportunity for *in vivo* imaging in zebrafish models.[233]

A cyanine appended turn-on red-emissive fluorescent probe **110 (Figure 1.48)** was constructed by Wang group which exhibits emission at 780 nm with 15 nM LOD and able to detect exo- and endogenous HNO without any interference from background fluorescence.[234] Another coumarin-semirhodamine based HNO fluorescent probe **111 (Figure 1.48)** has exhibited synchronous and unhampered fluorescent output in green (λ_{em} = 520 nm) and in NIR (λ_{em} = 673 nm) region both, with LOD value 111.6 nM being able to detect HNO *in vitro* and *in vivo*.[235]
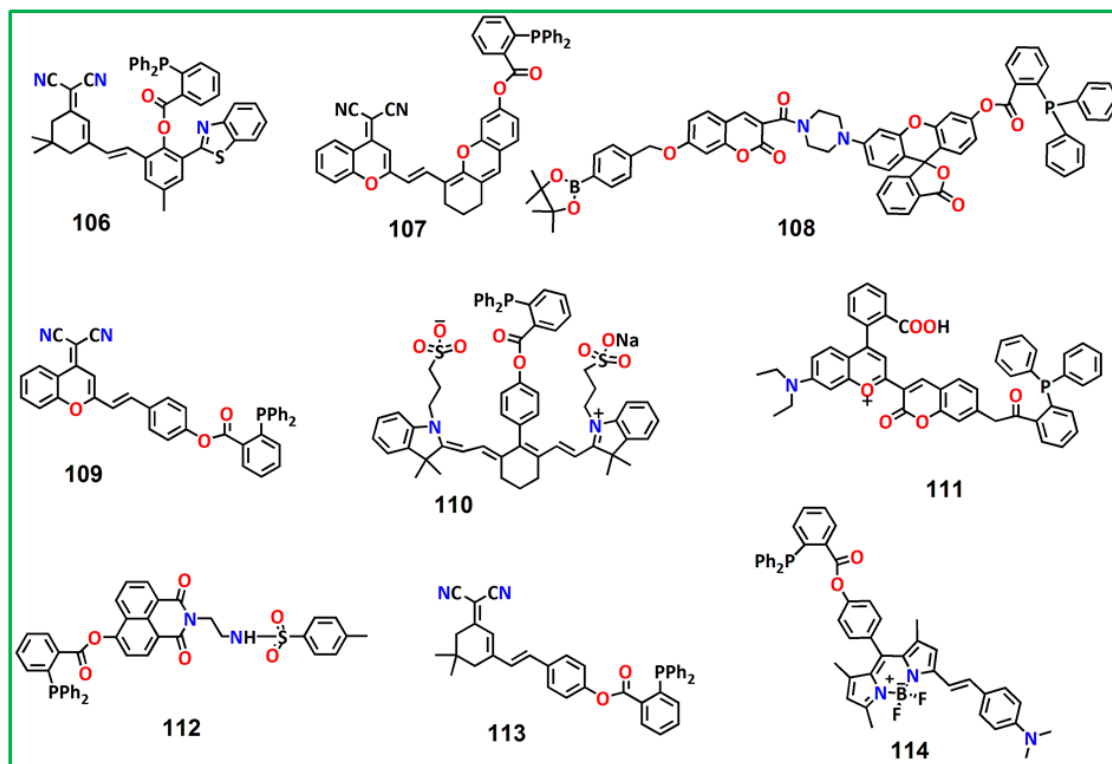
Figure 1.48 Structures of some intensity based HNO probe **106-114.**

Peng and group has designed a two-photon fluorescent sensor **112 (Figure 1.48)**, illustrating the NO–H₂S cross-talk with rapid visualization towards HNO in endoplasmic-reticulum. The weak fluorescence gets enhanced due to reaction of HNO at 555 nm (λ_{ex} = 450 nm) with excellent selectivity, good sensitivity (32 nM), rapid response (2 min.), low cytotoxicity and accurate imaging in endoplasmic-reticulum.[236]

Wei et al. has fabricated an isophorone bounded NIR HNO fluorescent sensor **113 (Figure 1.48)** showing large stokes shift (265 nm), strong sensitivity (LOD 39.6 nM) with efficient detecting capability to endogenously produced HNO in Hela cells and zebra fish.[237]

Liu group has disclosed a BODIPY based NIR HNO probe **114** which emits at 740nm with LOD 12 nM and applicable in HNO tracking in Hela cells **(Figure 1.48)**.[238]

Other than popular Staudinger method, the probe **115 (Figure 1.49)** is fabricated with napthalimide-dansyl fluorophore moiety and benzeneboronic acid pinacol ester as reacting group. This probe upon interaction with HNO undergoes hydrolysis to form aromatic alcohol revealing the increase in emission intensity at 555 nm with a detection limit 0.44uM. This probe exhibits high tolerance as well as least cytotoxicity in the wide array of biological pH. Overall this probe is a promising tool to recognize HNO in live cells and in mice liver.[239]
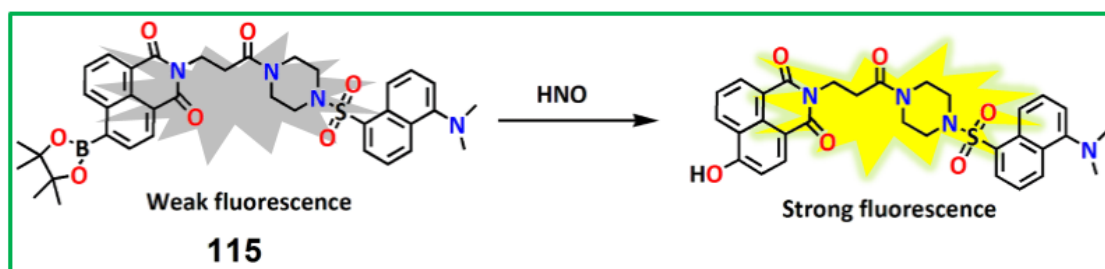
Figure 1.49 A different mechanism for HNO sensor **115.**

Back to the Staudinger-ligation based HNO probe, 6-hydroxyl-quinonline-2-benzothiazole based two photon HNO sensor **116 (Figure 1.50)** with excellent selectivity and sensitivity (LOD = 0.19 uM, λ_{em} =550nm) along with fast response (20 min) has been developed by Li group. Due to strong cell penetrating capability and little bio-toxicity, this probe has been promisingly demonstrated to be useful for monitoring fluctuations of HNO concentration qualitatively, along with bio-imaging application by two-photon confocal microscopy.[240]

Ma group has disclosed a fluorescent probe **117 (Figure 1.50)** for quantitative HNO detection using naphthalene backbone (λ_{ex} = 360 nm, λ_{em} = 500 nm). This probe exhibits a distinct change in fluorescence emission in the large array of pH (1-10) providing a detection limit 43 nM with low cytotoxicity in living HepG2 cells.[241]

Another two-photon HNO probe **118 (Figure 1.50)** using 6-acetyl-2-naphthol system was published by Zhang group which has shown more than 140 fold increment in fluorescence emission at 432 nm and 78 nM LOD value with efficiency in HNO imaging in HeLa cells.[242]

First bioluminescent fluorescent HNO probe **119 (Figure 1.50)** has been reported by Li et al. which reveals a 10 nM detection limit towards HNO and can be a potent candidate to detect HNO in living cells and mice model successfully along with strong signal-to-noise ratio devoiding of auto-fluorescence.[243]

A robust, reductant resistant ICT based NIR fluorescent probe **120 (Figure 1.50)** was designed by Yang group which exhibits rapid HNO sensing at 676 nm (within 5 min) with large stokes shift (131nm). This probe visualizes endogenously produced HNO by NO/H$_2$S crosstalk in cells and tissues of live mice with 0.09 uM detection limit.[244]
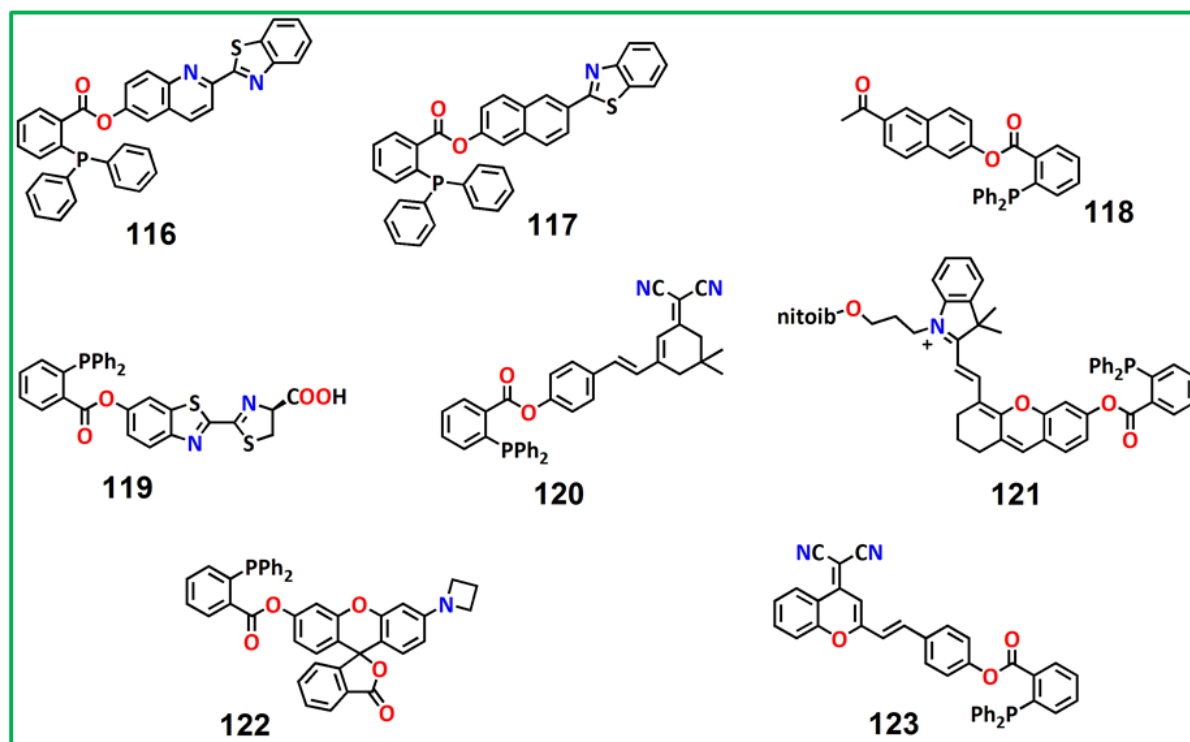
Figure 1.50 Structure of some intensity based HNO sensors **116-123.**

Chai group fabricated a NIR fluorescent probe **121 (Figure 1.50)** having tumor targeting ability *in vivo* which is consisted of hemicyanine moiety as fluorophore and biotin moiety to confer the tumor-targeted delivery. This non-fluorescent probe shows 20 fold fluorescence enhancement upon HNO treatment at 708 nm (λ_{ex} = 670 nm) which also can detect HNO in mice tumor *in vivo*.[245]

Staikopoulos et al. has evaluated, for the first time, the endogenous production of HNO in myocardial like cells. They have derived super bright, non-cytotoxic, highly specific rhodol based HNO fluorescent probe **122 (Figure 1.50)** exhibiting 75 fold fluorescence enhancement (in HBSS buffer) with extensive validation in the application in various biological systems utilizing both spectroscopy and confocal microscopy.[246]

Another mitochondria targeted NIR probe **123 (Figure 1.50)** has been reported by Wang group which demonstrates the rapid (within 4 min) detection of HNO through fluorescence enhancement in the NIR region (700 nm) showing LOD 13 nM. This probe locates HNO mainly in mitochondria with Pearson's colocalization coefficient 0.84 and visualizes exo- and endogenous HNO in HeLa cells produced by the NO and H_2S cross-talk. It also exhibits remarkable imaging performances towards *in vivo* and *ex vivo* HNO in mice.[247]

Very recently some phosphine based ratiometric probes has revealed significant role in HNO detection. Zhang group has demonstrated a napthalimide appended HNO probe **124 (Figure 1.51)** which itself emits blue fluorescence at 418 nm but after HNO addition it emits at 546 nm with excellent selectivity and sensitivity (LOD 0.5 μM)**.**[248] It also probe possess a high resolution bioimaging capability in living RAW 264.7 macrophage cell.

Another ICT based ratiometric and colorimetric probe **125 (Figure 1.51)** was synthesized by the same group which upon HNO treatment has shown a large red-shift (185 nm) in UV spectrum (blue from yellow colour in naked eye) with enhancement in emission peak at 614 nm, displaying 10 nM LOD and application in biological system.[249]

Zheng group has demonstrated a ratiometric HNO detector **126 (Figure 1.51)** structured on BODIPY-coumarin platform. This probe upon AS treatment exhibits a shift in emission wavelength by 129 nm with gradual increase in fluorescence at 463 nm and decrease at 592 nm having LOD 0.27 μM.[250] The ample sensitivity and selectivity, low cytotoxicity and membrane

diffusibility affords this probe suitable for fluorescence ratiometric imaging of HNO in SMMC-7721cells.
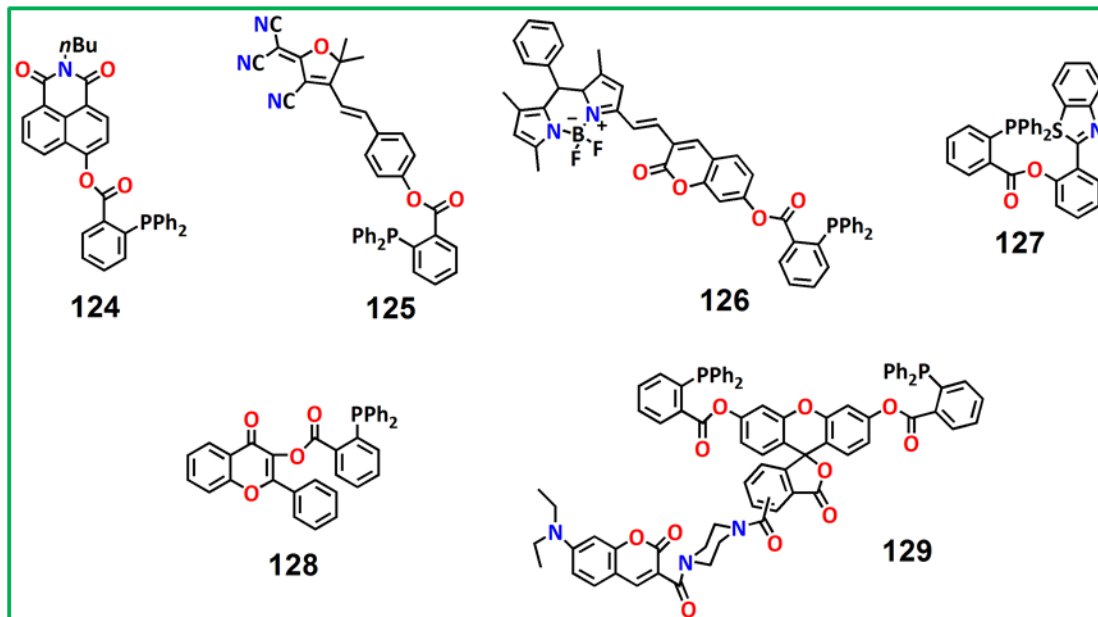
Figure 1.51 Some Staudinger-ligation based ratiometric HNO sensor **124-129.**

An ESIPT based ratiometric probe **127 (Figure 1.51)** containing benzothiazole fluorescence moiety has exhibited a gradual increment in fluorescence intensity at 460 nm with concomitant decrease at 380 nm upon HNO treatment. This probe can be applied for HNO imaging in living organisms also.[251] Another flavone based fluorescent probe **128 (Figure 1.51)** was also reported by Zhu et al. having LOD 0.128 µM which recognizes HNO by development of fluorescence intensity at 520 nm (λ_{ex} =344 nm) and can be employed for HNO monitoring in aqueous solution and in biological fetal bovein serum.[252]

Here another FRET based ratiometric HNO fluorescent sensor **129 (Figure 1.51)** was constructed by Sun group using coumarin-fluorescein conjugate where fluoresceine moiety is attached with HNO receptor phosphine moiety. The fluorescence intensity of the probe was decreased at 470 nm and increased at 517 nm upon addition of AS. This probe has displayed rapid reactivity towards HNO with high sensitivity (LOD 1.4 µM) as well as strong selectivity, among variety of reactive analytes under biological circumstances and can be applied for intracellular HNO imaging in a ratiometric way.[253]

Tan group has designed a ratiometric HNO probe **130 (Figure 1.52)** where, FRET mechanism is operative due to the energy donor naphthalene and energy acceptor rhodol system conjugated with HNO marker phosphine group. Upon addition of angeli's salt the emission of the probe has diminished at 448 nm and simultaneously increased at 541 nm with LOD 0.59 μM. By two photon microscopy, this sensor also can be applied for HNO detection in tissues and living cells.[254]

Another ratiometric HNO probe **131 (Figure 1.52)** was demonstrated by Yang et al. using a benzo-coumarin and rhodol system which also displays FRET mechanism. After treatment with AS the probe has shown the diminishing of fluorescence emission at 470 nm with the obvious enhancement at 540 nm. This differently designed probe can be utilized in endogenous detection of HNO in HUVECs cells and in rat brain tissues, released from NO - H_2S cross-talk through two-photon bioimaging microscopy in ratiometric way.[255]
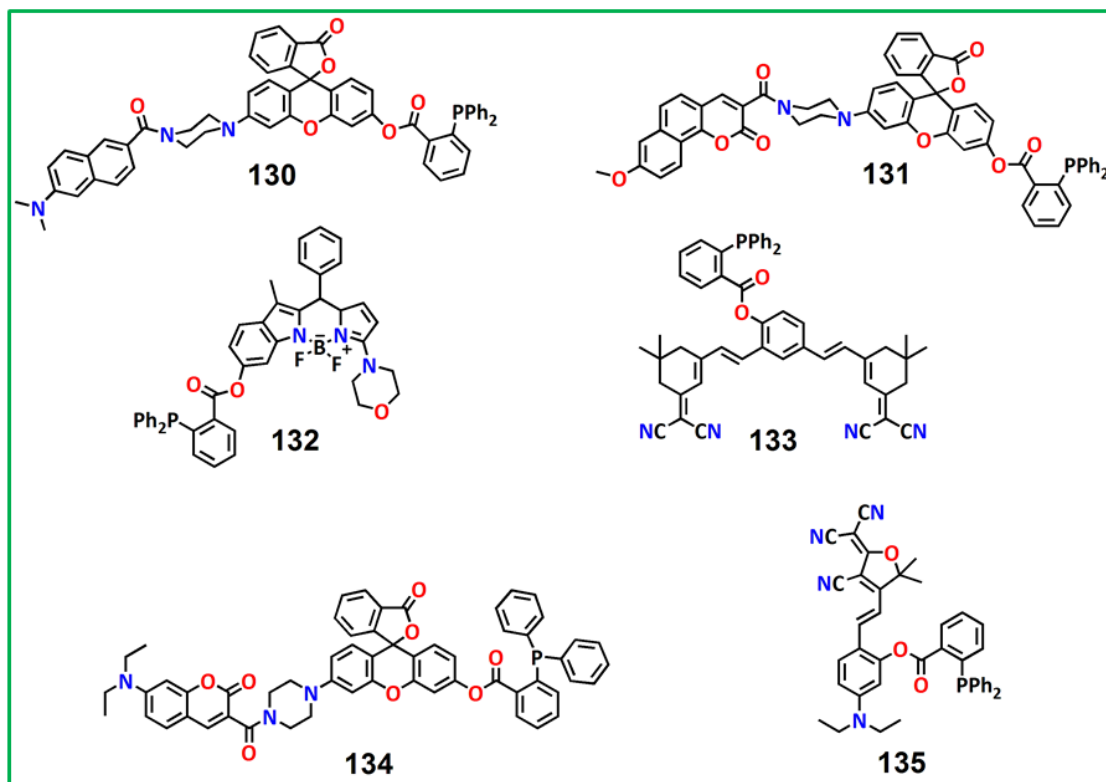
Figure 1.52 Structures of some ratiometric HNO sensor **130-135.**

Yuan et al. for the first time, unveiled the biological evaluation of a ratiometric BODIPY based micellar nanoprobe **132 (Figure 1.52)** to monitor HNO in water both *in vitro* and *in vivo*. It

interacts with HNO resulting the change in fluorescence intensity i.e., increase at 601 nm and decrease at 568 nm (λ_{ex} = 480 nm). It exhibits brilliant stability, selectivity and sensitivity with 8.82 nM LOD, possessing the eligibility to capture HNO endogeneously in zebrafish larvae.[256]

T. D. James group has revealed another ratiometric HNO fluorescent sensor **133** (**Figure 1.52**) based on two isophorone units which delineates the diminishing of fluorescence peak at 552 nm with simultaneous development of the fluorescence at 606 nm containing iso-emissive point at 574 nm (green region to red region emission shift, LOD = 1.01uM) upon HNO treatment. This ratiometric imaging also has been performed in the detection of exo- and endogenously generated HNO in HeLa cells at physiological environment. It has also been used in solid-state fluorescence emission readout in the form of portable test strips.[257]

Xu group has used Rhodol-coumarin conjugates to design a ratiometric HNO probe **134 (Figure 1.52)** which upon HNO addition makes the non-fluorescent spironolactone form to fluorescent xanthene structure. The emission wavelength was shifted from 470 nm to 543 nm due to FRET mechanism where, coumarin derivative acts as an energy donating and rhodol moiety as an energy accepting unit. It also shows ratiometric HNO detection in HEPG2 cells.[258]

For the first time an aggregation induced emission based ratiometric HNO sensor **135 (Figure 1.52)** was published by Li group. AS makes this probe highly fluorescent by 10 fold with the shifting in emission wavelength from 670 nm to 618 nm. Here, the probe has executed 157.6 nM detection limit to HNO. It also facilitates the real time detection of HNO in live sample (MCF-7 cells).[259]

1.4.4.3 Nitroxide-based prefluorescent probes

4-Hydroxy-TEMPO (TEMPOL) interacts with HNO through the hydrogen atom absorption from HNO by the nitroxide radical.[26] With the knowledge of this mechanism, Toscano et al. constructed a nitroxide based prefluorescent probe **136** (TEMPO-9-AC) conjugating TEMPO with acridine at 9 position through the intervening –CONH- bond **(Figure 1.53)**. The probe is weakly fluorescent. However on treatment with HNO, it becomes highly fluorescent (λ_{em} = 430 nm) with great selectivity towards HNO being inert to NO in water medium. There exists the

chance regarding HNO abstraction by the incipient nitric oxide, limiting its use in biological milieu.[260]
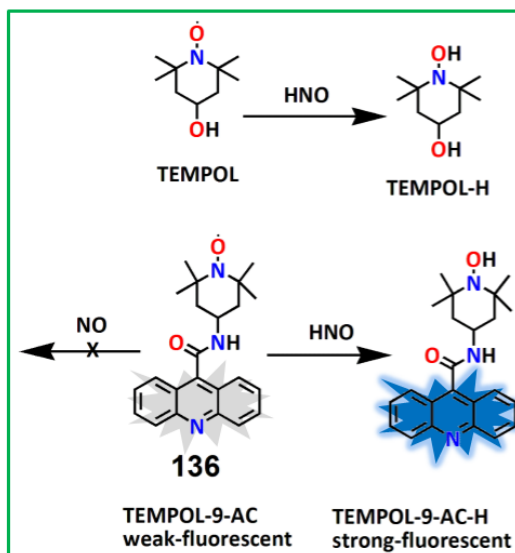
Figure 1.53 Mechanism and structure of radical based HNO sensor **136.**

1.4.4.4 2-Mercapto-2-methylpropionic acid-based fluorescent probes

A newly designed fluoroscent probe for HNO sensing has been demonstrated, in which 2-mercapto-2-methylpropionic acid acts as HNO identifying unit being attached with the fluorescent dyes. The mechanism involves a rapid reaction between 2-mercapto-2-methylpropionate and HNO which results in the generation of analogous N-hydroxysulfenamide species. This intermediate undergoes cyclisation and finally releases the fluorophore **(Figure 1.41 D)**. Here probes **137** and **138 (Figure 1.54)** are synthesized using coumarin and fluoresceine as fluorophore respectively, follow the above mentioned mechanism in HNO detection. The probe **138** is highly selective to HNO even in presence of thiols and provides opportunity to perform live cell imaging of HNO successfully.[261,262]
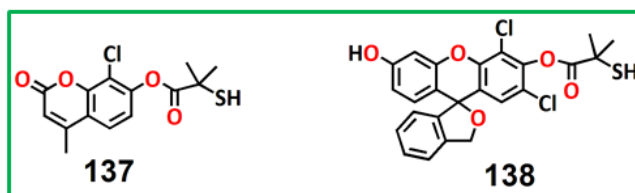
Figure 1.54 2-Mercapto-2-methylpropionic acid based HNO probes **137,138**

1.5 Objective and Aim of the Thesis

Though the biological reactive species are potentially cytotoxic in higher concentration still they play the pivotal role as signal transducers in growth factors and biomechanical forces when they are present in physiologically tolerable level of concentration. [263-264] Nitric oxide (NO) and nitroxyl (HNO) are crucial leading members among these reactive biomolecules for their biological and pathological activities. Like the physiological messenger molecule, NO has very short life time with lipophilicity and strong diffusibility playing a key role in different signaling actions like vascular smooth muscle relaxation, defense against microbial pathogens, immune response, apoptosis etc. It is also related with amyotrophic lateral sclerosis (ALS), Parkinson's and Alzheimer's diseases etc.[265] In mammals, endogenous NO is generated from arginine by a family of three different gene-encoded iso-enzymes which are neuronal (nNOS), inducible (iNOS) and endothelial (eNOS). All these isozymes of NOS enhances the reaction rate to generate NO in presence of calmodulin. NO displays its actions through both cGMP-dependent and independent way which consists of post-translational moderations in cysteine, tyrosine. Also it is associated with gene transcription, genotoxic damage, modification in cell-cycle check points, apoptosis and DNA renovations etc. These numerous functions of NO in the tumor area is connected to heterogeneous cell signalling with specific attention in the controll of the stress response generated by the hypoxia inducible factor-1 and p53 which commonly leads to growth arrest, apoptosis or adaptation.

Nitroxyl (HNO) is another nitrogen species with one electron reduced and protonated analogue of NO that regulates cellular function and acts as important alternative in therapeutic application. Like NO, HNO also exerts its efficacy as a famous signaling molecule in different biological processes. Because of its strong chemical functions, nitroxyl can spontaneously interact with thiols to produce disulfides or sulfinamides diminishing the enzyme's sensitivity. HNO also depicts the distinct capability to stimulate cardiac sarcoplasmic ryanodine receptors and can impart significant strategies for the therapy of cardiovascular disorder. Therefore the bio-chemical field of NO and HNO with rapid and reliable detection strategies using the development of organic probes is an active and exciting area of research field to explore their roles in living biological systems. Considering these important traits and challenging perspective

of these biomolecules we have developed some fluorescent NO and HNO sensors which successfully meet the following salient features:

a) Due to the fast reactivity and connection in physiological process it is very necessary to develop NO and HNO probe which will provide fast response towards these molecules well in the biological system.

b) Classical OPD based NO sensors are facing interference from some other biomolecules like AA, DHA, MGA etc. It may also be affected by pH leading to false positive response. So strategically we have developed some NO/HNO sensors which work differently to avoid these type of problems.

c) NO and HNO detection by the probe should be selective by the fluorescence 'ON' mechanism as the 'OFF' mechanism may lead to the misinterpretation of the data. Quantum yield (θ) and limit of detection also should be determined to know the efficiency of the probe in biological milieu.

d) We will also delineate the kinetics and mechanism of the probe when reacting with the HNO and NO so that a clear picture of the mechanism of interaction could be recognized.

Therefore, taking these key points we have synthesized some smart fluorescent molecules which are highly sensitive and selective to either NO or HNO, other biomolecules being silent towards these probes. These probes show bio-compatibility and least cytotoxicity in organo-aqueous medium. My research works on NO and HNO probes are demonstrated here in detail in this thesis which are enlisted in **Figure 1.55.**
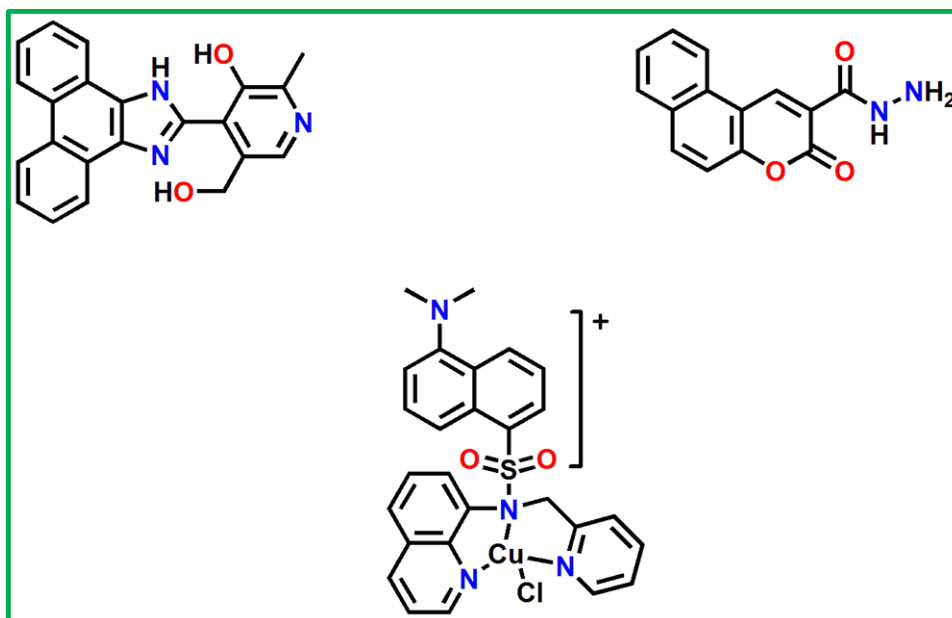
Figure 1.55 Structures of the targeted probes for NO and HNO sensing.

1.6 Physical measurements

(i) **FTIR spectra:** Infrared spectra (400−4000 cm^{-1}) were recorded on a Nickolet Magna IR 750 series-II FTIR spectrometer on solid KBr discs.

(ii) **NMR spectra:** ^{1}H-NMR spectra were recorded in DMSO-d$_6$, CDCl$_3$, CD$_3$CN on a Bruker 300 MHz and 400 MHz NMR spectrometer using tetramethylsilane (δ = 0) as an internal standard.

(iii) **UV-vis spectra:** UV-vis spectra were collected on an Agilent diode-array spectrophotometer (Model, Agilent 8453).

(iv) **Mass spectra**: ESI-MS$^+$ (m/z) of the ligand and complexes were found from Waters' HRMS spectrometer (Model: QTOF Micro YA263).

(v) **Fluorescence spectra:** All the fluorescence studies were performed with a PTI (Model QM-40) spectrofluorometer.

(vi) **Life times measurements:** Lifetimes were calculated in Horiba−Jobin−Yvon on a Hamamatsu MCP photomultiplier (R3809) and surveyed using IBH DAS6 software.

(vii) **DFT calculations:** Ground state electronic structure of the ligand and complexes have been calculated using using Gaussian 09W software package, correlated with the conductor-like polarizable continuum model (CPCM).

(viii) **Cell imaging:** Cell imaging experiments have been carried out using fluorescence microscope. Bright field and fluorescence images of the HepG2 cells, A375cells, Raw 264.7 murine macrophages cells, were obtained utilizing a fluorescence microscope (Leica DM3000, Germany) having the objective lens of 40x, 63x magnification.

(ix) **pH study:** The pH of the solutions was recorded in a Systronics digital pH meter (Model 335, India) in 2–12 pH range.

References

1. P. F. Bove and A. van der Vliet, *Free Radical Biol. Med.,* 2006, **41**, 515–527.

2. R. F. Furchgott, *Angew. Chem. Int. Ed.,* 1999, **38**, 1870-1880.

3. L. J. Ignarro, *Angew. Chem. Int. Ed.,* 1999, **38**, 1882-1892.

4. F. Murad, *Angew. Chem. Int. Ed.,* 1999, **38**, 1856-1868.

5. F. L. Ricciardolo, P.J. Sterk, B. Gaston and G. Folkerts, *Physiol. Rev.*, 2004, **84**, 731-765.

6. D. A. Wink, Y. Vodovotz, J. Laval, F. Laval, M. W. Dewhirst and J. B. Mitchell, *Carcinogenesis*, 1998, **19**, 711-721.

7. V. Calabrese, T. E. Bates and A.M.G. Stella, *Neurochem. Res.*, 2000, *25*, 1315-1341.

8. A. J. Burke, F. J. Sullivan, F. J. Giles and S.A. Glynn, *Carcinogenesis*, 2013, *34*, 503-512.

9. B. C. Smith, E. S. Underbakke, D. W. Kulp, W.R. Schief and M.A. Marletta, *Proc. Natl. Acad. Sci.,* 2013, *110*, E3577-E3586.

10. S. Singh and A. K. Gupta, *Cancer Chemother. Pharmacol.,* 2011, *67*, 1211-1224.

11. G. Yetik-Anacak and J. D. Catravas, *Vasc. Pharmacol.,* 2006, *45*, 268-276.

12. V. Calabrese, C. Mancuso, M. Calvani, E. Rizzarelli, D. A. Butterfield and A. M. Giuffrida Stella, *Nat. Rev. Neurosci.,* 2007, **8**, 766-775

13. J. Loscalzo and G. Welch, *Prog. Cardiovasc. Dis.,* 1995, **38**, 87–104

14. A. Lanas, *Arthritis Res. Ther.,* 2008, **10**, 1-6

15. C. Bogdan, *Nat. Immunol.,* 2001, **2**, 907–916.

16. P. F. Mount, D. A. Power, *Acta Physiol.,* 2006, **187**, 433–446.

17. F. Doctorovich, P. J. Farmer and M. A. Marti, 1st edition. ed., Elsevier, Waltham, MA, 2016.

18. K. M. Miranda, *Coord. Chem. Rev.,* 2005, **249**, 433–455

19. J. M. Fukuto, M. D. Bartberger, A. S. Dutton, N. Paolocci, D. A. Wink and K.N. Houk, *Chem. Res. Toxicol.,* 2005, **18**, 790–801

20. J. M. Fukuto, C. H. Switzer, K. M. Miranda and D. A. Wink, *Annu. Rev. Pharmacol. Toxicol*, 2005, **45**, 335-355.

21. A. Angeli, and F. Angelico, *Gazz. Chim. Ital*, 1903, *33*, 245-252.

22. N. Paolocci, M. I. Jackson, B. E. Lopez, K. Miranda, C. G. Tocchetti, D. A. Wink, A. J. Hobbs and J. M. Fukuto, *Pharmacol. Ther.,* 2007, **113,** 442-458.

23. J. C. Irvine, R. H. Ritchie, J. L. Favaloro, K. L. Andrews, R. E. Widdop and B. K. Kemp-Harper, *Trends Pharmacol. Sci.,* 2008, **29**, 601-608

24. J. M. Fukuto, K. Chiang, R. Hszieh, P. Wong and G. Chaudhuri, *J. Pharmacol. Exp. Ther.* 1992, **263**, 546-551.

25. R. A. Pufahl, J. S. Wishnok and M. A. Marletta, *Biochem.,* 1995, **34**, 1930-1941.

26. K. M. Miranda, N. Paolocci, T. Katori, D. D. Thomas, E. Ford, M. D. Bartberger, M. G. Espey, D. A. Kass, M. Feelisch, J.M. Fukuto and D. A. Wink, *Proc. Natl. Acad. Sci.,* 2003, **100**, 9196−9201.

27. X. L. Ma, F. Gao, G. L. Liu, B. L. Lopez, T. A. Christopher, J. M. Fukuto, D. A. Wink and M. Feelisch, *Proc. Natl. Acad. Sci.,* 1999, **96**, 14617−14622.

28. N. Paolocci, F. W. Saavedra, K. M. Miranda, C. Martignani, T. Isoda, J. M. Hare, M. G. Espey, J. M. Fukuto, M. Feelisch, D. A. Wink and D. A. Kass, *Proc. Natl. Acad. Sci*., 2001, **98**, 10463−10468.

29. S. Donzelli, M. G. Espey, W. Flores-Santana, C. H. Switzer, G. C. Yeh, J. Huang, D. J. Stuehr, S. B. King, K. M. Miranda and D. A. Wink, *Free Radical Biol. Med.,* 2008, **45**, 578−584.

30. F.W. Dalby, *Can. J. Phys.,* 1958, **36**, 1336-1371.

31. H. A. Brown and G. C. Pimentel, *J. Chem. Phys.,* 1958, **29**, 883-888.

32. A. Luna, M. Merchán and B.O. Ross, *Chem. Phys.,* 1995, **196,** 437-445.

33. D. H. Mordaunt, H. Flothmann, M. Stumpf, H. M. Keller, C. Beck, R. Schinke and K. Yamashita, *J. Chem. Phys.,* 1997, **107**, 6603-6615.

34. J. S. Nishimura, P. Martasek, K. McMillan, J. Salerno, Q. Liu, S. S. Gross and B.S. Masters, *Biochem. Biophys. Res. Commun.,* 1995, **210**, 288–294.

35. S. J. Green, S. Mellouk, S. L Hoffman, M. S. Meltzer and C. A. Nacy, *Immunol. Lett.,* 1990, **25**, 15–19.

36. M. W. Radomski, R. M. Palmer and S. Moncada, *Br. J. Pharmacol.* 1987, **92**, 639–646.

37. M. A. Marletta, *J. Biol. Chem.,* 1993, **268**, 12231-12234.

38. W. Alderton, C. Cooper and R. G. Knowles, *J. Biochem.,* 2001, **357**, 593-615.

39. B. Hemmens, W. Goessler, K. Schmidt and B. Mayer, *J. Biol. Chem.,* 2000, **275**, 35786–35791.

40. C. S. Raman, H. Li, P. Martásek, V. Král, B. S. S. Masters and T. L. Poulos, *Cell,* 1998, **95**, 939-950.

41. H. Li, C. S. Raman, C.B. Glaser, E. Blasko, T. A. Young, J. F. Parkinson, M. Whitlow and T. L. Poulos, *J. Biol. Chem.*, 1999, **274**, 21276-21284.

42. B. R. Crane, A. S. Arvai, D. K. Ghosh, C. Wu, E. D. Getzoff, D. J. Stuehr and J. A. Tainer. *Science*, 1998, **279**, 2121-2126.

43. M. A. Noble, A. W .Munro, S. L. Rivers, L. Robledo, S. N. Daff, L. J. Yellowlees, T. Shimizu, I. Sagami, J. G. Guillemette and S. K .Chapman, *Biochemistry,* 1999, *38*, 16413-16418.

44. D. Stuehr, S. Pou, G. M. Rosen. *J. Biol. Chem.,* 2001, **276**, 14533–14536

45. R. M. Rapoport, M. B. Draznin and F.Murad., *Nature,* 1983, **306**, 174–176.

46. U. Fo¨rstermann, A. Mu¨lsch, E. Bo¨hme and R. Busse. *Circ. Res.,* 1986, **58**, 531–538.

47. R. F. Furchgott, P. D. Cherry, J. V. Zawadzki and D. Jothianandan, *J. Cardiovasc. Pharmacol*., 1984, **53**, 557–573

48. R. G. Knowles, M. Palacios, R. M. Palmer and S. Moncada. *Proc. Natl. Acad. Sci*. 1989, **86**, 5159–5162.

49. J. Garthwaite, *Trends Neurosci.,* 1991, **14**, 60–67.

50. A. R. Butler and D. L. H. Williams, *Chem. Soc. Rev.,* 1993, **22**, 233–241.

51. F. C. Fang, *Nat. Rev. Microbiol.,* 2004, **2**, 820–832.

52. M. D. Pluth, E. Tomat and S. J. Lippard, *Annu. Rev. Biochem.,* 2011, **80**, 333–355.

53. C. S. Cobbs, J. E. Brenman, K. D. Aldape, D. S. Bredt and M. A. Israel, *Cancer Res.,* 1995, **55**, 727–730.

54. A. Castegna, V. Thongboonkerd, J. B. Klein, B. Lynn, W. R. Markesbery and D. A. Butterfield, *J. Neurochem.,* 2003, **85**, 1394–1401.

55. R. J. Giedt, C. Yang, J. L. Zweier, A. Matzavinos and B. R. Alevriadou, *Free Radicals Biol. Med.*, 2012, **52**, 348-356.

56. P. Pacher, J. S. Beckman and L. Liaudet, *Physiol. Rev.,* 2007, **87**, 315–424.

57. J. F. Brown, A. C. Keates, P. J. Hanson, B. J. Whittle, *Am. J. Physiol.,* 1993, **265**, G418–G422.

58. J. L. Wallace and A. W. Tigley, *Pharmacol. Ther.,* 1995, **9**, 227–235.

59. B. V. Khan, D. G. Harrison, M. T. Olbrych, R. W. Alexander and R. M. Medford, *Proc. Natl. Acad. Sci. U.S.A.*, 1996, **93**, 9114−9119.

60. T. Gudi, G. K. Hong, A. B. Vaandrager, S. M. Lohmann, R. B. Pilz, *FASEB J.,* 1999, **13**, 2143−2152.

61. K. Pantopoulos and M. W. Hentze, *Proc. Natl. Acad. Sci. U. S. A.,* 1995, **92**, 1267−127

62. X. B. Liu, P. Hill and D. J. Haile, *Blood Cells Mol. Dis.,* 2002, **29**, 315−326.

63. N. Pozdnyakov, A. Lloyd, V. N. Reddy and A. A. Sitaramayya, *Biochem. Biophys. Res. Commun.,* 1993, **192**, 610−615.

64. B. Brune, S. Dimmeler, L. M. y Vedia, E. G. Lapetina, *Life Sci.,* 1994, **54**, 61−70.

65. L. J. Ignarro, *Nitric oxide: biology and pathobiology*. Academic press, ed., 2000.

66. J. Garthwaite, *Eur. J. of Neurosci.,* 2008, **27**, 2783-2802.

67. J. M. Fukuto, A. S. Dutton, K. N. Houk, *ChemBioChem,* 2005, **6**, 612-619.

68. C. Szabó, H. Ischiropoulos, R. Radi, *Nat. Rev. Drug Discov.,* 2007, **6**, 662-680.

69. P. Griess, *Ber. Deutsch. Chem. Ges.,* 1879, **12**, 426–428.

70. T. Malinski, Z. Taha, *Nature*, 1992, **358**, 676–678.

71. P. Vallance, K. Bhagat, R. MacAllister, S. Patton, T. Malinski, M. Radomski and S. Moncada, *Lancet,* 1995, **346**, 153–154.

72. Y. Y. Woldman, T. D. Eubank, A. J. Mock, N. C. Stevens, S. Varadharaj, J. Turco, M. A. Gavrilin, B. R. Branchini and V. V. Khramtsov, *Biochem. Biophys. Res. Commun.,* 2015, **465**, 232–238.

73. Y. Y. Woldman, J. Sun, J. L. Zweier and V. V. Khramtsov, *Free Radic. Biol. Med.,* 2009, **47**, 1339–1345.

74. T. Nagano, *Luminescence*, 1999, **14**, 283-290.

75. F. O. Brown, N. J. Finnerty, F. B. Bolger, J. Millar and J. P. Lowry, *Anal. Bioanal. Chem.,* 2005, **381**, 964–971.

76. Y. Katayama, N. Soh and M. Maeda, *ChemPhysChem.,* 2001, **2**, 655–661.

77. F. Bedioui and N. Villeneuve, *Electroanalysis*, 2003, **15**, 5–18.

78. S. Singha, Y. W. Jun, S. Sarkar and K. H. Ahn, *Acc. Chem.Res.*, 2019, **52**, 2571–2581.

79. Z. W. Ulissi, F. Sen, X. Gong, S. Sen, N. Iverson, A. A. Boghossian, L. C. Godoy, G. N. Wogan, D. Mukhopadhyay and M. S. Strano, *Nano Lett.,* 2014, **14**, 4887–4894

80. H. Kojima, N. Nakatsubo, K. Kikuchi, S. Kawahara, Y. Kirino, H. Nagoshi, Y. Hirata and T. Nagano, *Anal. Chem.,* 1998, **70**, 2446-2453.

81. H. Kojima, Y. Urano, K. Kikuchi, T. Higuchi, Y. Hirata and T. Nagano, *Angew. Chem. Int. Ed.,* 1999, **38**, 3209-3212.

82. H.-W. Yao, X.-Y. Zhu, X.-F. Guo and H. Wang, *Anal. Chem.,* 2016, **88**, 9014–9021.

83. X. Liu, S. Liu and G. Liang, *Analyst*, 2016, **141**, 2600–2605.

84. C. Tang, Q. Zheng, S. Zong, Z. Wang and Y. Cui, *Sens. Actuators B Chem.,* 2014, **202**, 99–104.

85. C. Tang, M. Wang, X. Shang, X. Chen, D. Huang and Q. Zheng, *J. Mater. Chem. C,* 2019, **7**, 3246–3252.

86. Z. Mao, W. Feng, Z. Li, L. Zeng, W. Lv and Z. Liu, *Chem. Sci.,* 2016, **7**, 5230–5235.

87. W. Feng, Q.-L. Qiao, S. Leng, L. Miao, W.-T. Yin, L.-Q. Wang and Z.-C. Xu, *Chin. Chem. Lett.,* 2016, **27**, 1554–1558.

88. F. Wang, S. Yu, Z. Xu, L. Li, Y. Dang, X. Xu, Y. Luo,Z. Cheng, H. Yu, W. Zhang, A. Zhang and C. Ding, *Anal. Chem.,* 2018, **90**, 7953–7962.

89. S. Wang, Z. Li, Y. Liu, G. Feng, J. Zheng, Z. Yuan and X. Zhang, *Sens. Actuators B Chem.,* 2018, **267**, 403–411.

90. P. Vaupel and A. Mayer, *Cancer Metastasis Rev.,* 2007, **26**, 225–239.

91. S. J. Lunt, N. Chaudary and R. P. Hill, *Clin. Exp. Metastasis,* 2009, **26**, 19–34.

92. N. Burrows, G. Cane, M. Robson, E. Gaude, W. J. Howat, P. W. Szlosarek, R. B. Pedley, C. Frezza, M. Ashcroft and P. H. Maxwell, *Sci. Rep.,* 2016, **6**, 22950.

93. O. P. Mishra, S. Zanelli, S. T. Ohnishi and M. Delivoria-Papadopoulos, *Neurochem. Res.,* 2000, **25**, 1559–1565

94. S. Biswas, Y. Rajesh, S. Barman, M. Bera, A. Paul, M. Mandal and N. D. Pradeep Singh, *Chem. Commun.,* 2018, **54**, 7940–7943.

95. H. Li and A. Wan, *Analyst,* 2015, **140**, 7129–7141.

96. X. Zhang, B. Wang, Y. Xiao, C. Wang and L. He, *Analyst*, 2018, **143**, 4180–4188.

97. J. Tang, Z. Guo, Y. Zhang, B. Bai and W.-H. Zhu, *Chem. Commun.,* 2017, **53**, 10520-10523.

98. T. Gotoh and M. Mori, *Arterioscler. Thromb. Vasc. Biol.,* 2006, **26**, 1439–1446.

99. G. C. Brown, *Nitric Oxide,* 2010, **23**, 153–165.

100. K. Kawahara, S. Oyadomari, T. Gotoh, S. Kohsaka, H. Nakayama and M. Mori, *FEBS Lett.,* 2001, **506**, 135–139.

101. X.-X. Chen, L.-Y. Niu, N. Shao and Q.-Z. Yang, *Anal. Chem.,* 2019, **91**, 4301–4306.

102. Y. Huo, J. Miao, L. Han, Y. Li, Z. Li, Y. Shi and W. Guo, *Chem. Sci.*, 2017, **8**, 6857–6864.

103. W.-L. Jiang, Y. Li, H.-W. Liu, D.-Y. Zhou, J. Ou-Yang, L. Yi and C.-Y. Li, *Talanta*, 2019, **197**, 436–443.

104. B. Wang, S. Yu, X. Chai, T. Li, Q. Wu and T. Wang, *Eur. J. Chem.*, 2016, **22**, 5649–5656.

105. P. Zhang, Y. Tian, H. Liu, J. Ren, H. Wang, R. Zeng, Y. Long and J. Chen, *Chem. Commun.,* 2018, **54**, 7231-7234.

106. J. Miao, Y. Huo, X. Lv, Z. Li, H. Cao, H. Shi, Y. Shi and W. Guo, *Biomaterials,* 2016, **78**, 11–19.

107. Y. Huo, J. Miao, J. Fang, H. Shi, J. Wang and W. Guo, *Chem. Sci.,* 2019, **10**, 145–152.

108. Z. Yu, J. Zhou, X. Dong, W. Zhao and Z. Chen, *Anal. Chim. Acta,* 2019, **1067**, 88–97.

109. Z. Mao, H. Jiang, X. Song, W. Hu and Z. Liu, *Anal. Chem.,* 2017, **89**, 9620-9624.

110. Z. Mao, H. Jiang, Z. Li, C. Zhong, W. Zhang and Z. Liu, *Chem. Sci.,* 2017, **8**, 4533–4538.

111. C. J. Reinhardt, E. Y. Zhou, M. D. Jorgensen, G. Partipilo and J. Chan, *J. Am. Chem. Soc.*, 2018, **140**, 1011–1018.

112. Y. Liu, H. Fan, Y. Wen, T. Jia, Q. Su and F. Li, *Dyes Pigm.*, 2019, **166**, 211–216.

113. H. Li, Y. H. Hao, W. Feng, and Song, Q.H., *J. Mater. Chem. B.,* 2020, **8**, 9785-9793.

114. P. Liu, B. Li, J. Zheng, Q. Liang, C. Wu, L. Huang, P. Zhang, Y. Jia and S. Wang, *Sens. Actuators B Chem.,* 2021, **329**, 129147.

115. Y. Liu, C. Jiao, Y. Wei, W. Lu, P. Zhang and Y. Wang, *Tetrahedron,* 2020, **76**, 131622.

116. Q. Tang, P. Li, Z. Zhou, Q. Lu, B. Gu, S. Tang and Y. Zhang, *Spectrochim. Acta A Mol. Biomol. Spectrosc.,* 2022, **270**, 120728.

117. L. L. Wang, J. Y. Bai, X. F. Li, M. H. Zheng, Y. Miao and J. Y. Jin, *Anal. Chim. Acta,* 2021, **1183**, 338980.

118. T. Itoh, K. Nagata, Y. Matsuya, M. Miyazaki and A. Ohsawa, *J. Org. Chem.,* 1997, **62**, 3582–3585.

119. X.-Q. Zhu, B.-J. Zhao and J.-P. Cheng, *J. Org. Chem.,* 2000, **65**, 8158–8163.

120. T. Itoh, K. Nagata, M. Okada and A. Ohsawa, *Tetrahedron Lett.,* 1995, **36**, 2269–2272.

121. S.-F. Ma, Q.-H. Wang, F.-T. Liu, H.-L. Wang, D.-C. Fang, B. Gong, L. He and Z.-L. Lu, *RSC Adv.,* 2016, **6**, 85698–85703.

122. H.-L. Wang, F.-T. Liu, A.-X. Ding, S.-F. Ma, L. He, L. Lin and Z.-L. Lu, *Spectrochim. Acta A Mol. Biomol. Spectrosc.,* 2016, **169**, 1–6.

123. C. Gao, L. Lin, W. Sun, Z.-L. Tan, J.-R. Huang, L. He and Z.-L. Lu, *Talanta,* 2018, **176**, 382–388.

124. S. Ma, X. Sun, Q. Yu, R. Liu, Z. Lu and L. He, *Photochem. Photobiol. Sci.*, 2020, **19**, 1230-1235.

125. S. Ma, D. C. Fang, B. Ning, M. Li, L. He and B. Gong, *Chem. Commun.,* 2014, **50**, 6475-6478.

126. F. Tang, C. Gao, J. Y. Liu, Z. L. Lu, L. He and A. X. Ding, *Sens. Actuators B Chem.,* 2021, **339**, 129880.

127. A. K. Mahapatra, S. S. Ali, K. Maiti, S. Mondal, R. Maji, S. Manna, S. K. Manna, M. R. Uddin and S. Mandal, *RSC Adv.,* 2016, **6**, 113219-113227.

128. H. Li, D. Zhang, M. Gao, L. Huang, L. Tang, Z. Li, X. Chen and X. Zhang, *Chem. Sci.,* 2017, **8**, 2199-2203.

129. Y. Yang, S. K. Seidlits, M. M. Adams, V. M. Lynch, C. E. Schmidt, E. V. Anslyn and J. B. Shear, *J. Am. Chem. Soc.,* 2010, **132**, 13114–13116.

130. C.-G. Dai, J.-L. Wang, Y.-L. Fu, H.-P. Zhou and Q.-H. Song, *Anal. Chem.,* 2017, **89**, 10511–10519.

131. X. Zhu, J.-Q. Chen, C. Ma, X. Liu, X.-P. Cao and H. Zhang, *Analyst,* 2017, **142**, 4623–4628.

132. L. Chen, D. Wu and J. Yoon, *Sens. Actuators B Chem.,* 2018, **259**, 347–353.

133. T.-W. Shiue, Y.-H. Chen, C.-M. Wu, G. Singh, H.-Y. Chen, C.-H. Hung, W.-F. Liaw and Y.-M. Wang, *Inorg. Chem.,* 2012, **51**, 5400–5408.

134. Y. Huo, J. Miao, Y. Li, Y. Shi, H. Shi and W. Guo, *J. Mater. Chem. B,* 2017, **5**, 2483–2490.

135. A. Beltrán, M. I. Burguete, D. R. Abánades, D. Pérez-Sala, S. V. Luis, F. Galindo, *Chem. Commun.,* 2014, **50**, 3579-3581.

136. I. M. Resta, B. Bedrina, E. Martínez-Planes, A. Minguela and F. Galindo, *J. Mater. Chem. B.,* 2021, **9**, 9885-9892.

137. Y.-L. Fu, H. Li, X.-Z. Wei and Q.-H. Song, *J. Mater. Chem. B,* 2019, **7**, 3792–3795.

138. C. Xu, C. Xin, C. Yu, M. Wu, J. Xu, W. Qin, Y. Ding, X. Wang, L. Li, W. Huang, *Chem. Commun.,* 2018, **54**, 13491-13494.

139. A. S. M. Islam, R. Bhowmick, K. Pal, A. Katarkar, K. Chaudhuri and M. Ali, *Inorg. Chem.,* 2017, **56**, 4324–4331.

140. A. S. M. Islam, R. Bhowmick, B. Chandra Garain, A. Katarkar and M. Ali, *J. Org. Chem.*, 2018, **83**, 13287– 13295.

141. A. S. M. Islam, M. Sasmal, D. Maiti, A. Dutta, B. Show and M. Ali, *ACS omega*, 2018, **3**, 10306-10316.

142. A. Dutta, A. S. M. Islam, D. Maiti, M. Sasmal, C. Pradhan and M. Ali, *Org. Biomol. Chem.*, 2019, **17**, 2492-2501.

143. Q. Han, J. Liu, Q. Meng, Y. L. Wang, H. Feng, Z. Zhang, Z. P. Xu and R. Zhang, ACS sens., 2018, **4**, 309-316.

144. S. J. Kim, S. Y. Park, S. A. Yoon, C. Kim, C. Kang and M. H. Lee, *Anal. Chem.,* 2021, **93**, 4391-4397.

145. W. Su, L. Huang, X. Liang, L. Zhu and W. Lin, *J. Photochem. Photobiol. A.,* 2021, **412**, 113256.

146. S. A. Hilderbrand and S. J. Lippard, *Inorg. Chem.*, 2004, **43**, 5294-5301.

147. N. Soh, Y. Katayama and M. Maeda, *Analyst,* 2001, **126**, 564-566.

148. M. H. Lim and S. J. Lippard, *Inorg. Chem.*, 2004, **43**, 6366-6370.

149. S. A. Hilderbrand, M. H. Lim and S. J. Lippard, *J. Am. Chem. Soc*., 2004, *126*, 4972-4978.

150. R. C. Smith, A. G. Tennyson and S. J. Lippard, *Inorg. Chem.,* 2006, **45**, 6222-6226.

151. P. C. Ford, B. O. Fernandez, M. D. Lim, *Chem. Rev.,* 2005, **105**, 2439-2455.

152. K. J. Franz, N. Singh, B. Spingler and S. J. Lippard, *Inorg. Chem.*, **2000**, *39*, 4081-4092.

153. S. A. Hilderbrand, S. J. Lippard, *Inorg. Chem.,* 2004, **43**, 4674-4682.

154. M. H. Lim, C. Kuang and S. J. Lippard, *ChemBioChem.,* 2006, **7,** 1571-1576.

155. C. Khin, M. D. Lim, K. Tsuge, A. Iretskii, G. Wu and P. C. Ford, *Inorg. Chem.,* 2007, **46**, 9323-9331.

156. M. H. Lim, B. A. Wong, W. H. Jr. Pitcock, D. Mokshagundam, M. H. Baik and S. J. Lippard, *J. Am. Chem. Soc.,* 2006, **128**, 14364-14373.

157. M. H. Lim, D. Xu and S. J. Lippard, *Nat. Chem. Biol.,* 2006, **2**, 375-380.

158. K. Tsuge, F. DeRosa, M. D. Lim and P. C. Ford, *J. Am. Chem. Soc.,* 2004, **126**, 6564-6565.

159. M. Sarma, A. Singh, G. S. Gupta, G. Das and B. Mondal, *Inorganica. Chim. Acta.,* 2010, **363**, 63-70.

160. X. Chen, L. Sun, Y. Chen, X. Cheng, W. Wu, L. Ji and H. Chao, *Biomaterials*, 2015, **58**, 72–81.

161. C. Wu, K.-J. Wu, T.-S. Kang, H.-M. D. Wang, C.-H. Leung, J.-B. Liu and D.-L. Ma, *Sci. Rep.*, 2018, **8**, 12467.

162. Y. Li, H. Wang, J. Li, J. Zheng, X. Xu and R. Yang, *Anal. Chem.,* 2011, **83**, 1268–1274.

163. M. H. Lee, J. S. Kim and J. L. Sessler, *Chem. Soc. Rev.*, 2015, **44**, 4185–4191.

164. Z. Dai, L. Tian, B. Song, X. Liu and J. Yuan, *Chem. Sci.,* 2017, **8**, 1969–1976.

165. M. H. Lim and S. J. Lippard, *J. Am. Chem. Soc.,* 2005, **127**, 12170–12171.

166. M. D. Pluth, M. R. Chan, L. E. McQuade and S. J. Lippard, *Inorg. Chem.,* 2011, **50**, 9385-9392.

167. N. Wilson, L. H. Mak, A. Cilibrizzi, A. D. Gee, N. J. Long, R. Woscholski and R. Vilar, *Dalton Trans.*, 2016, **45**, 18177–18182.

168. X. Sun, G. Kim, Y. Xu, J. Yoon and T. D. James, *ChemPlusChem*, 2016, **81**, 30–34.

169. M. Barzegar Amiri Olia, A. Zavras, C. H. Schiesser and S.-A. Alexander, *Org. Biomol. Chem.,* 2016, **14**, 2272–2281.

170. M. M. Sadek, M. Barzegar Amiri Olia, C. J. Nowell, N. Barlow, C. H. Schiesser, S. E. Nicholson and R. S. Norton, *Bioorg. Med. Chem.,* 2017, **25**, 5743–5748.

171. A. Loas and S. J. Lippard, *J. Mater. Chem. B,* 2017, **5**, 8929–8933.

172. P. Srivastava, M. Verma, S. Sivakumar and A. K. Patra, *Sens. Actuators, B*, 2019, **291**, 478–484.

173. U. P. Apfel, D. Buccella, J. J. Wilson and S. J. Lippard, *Inorg. Chem.,* 2013, **52**, 3285-3294.

174. X. Hu, J. Wang, X. Zhu, D. Dong, X. Zhang, S. Wu and C. Duan, *Chem. Commun.,* 2011, **47**, 11507-11509.

175. B. Mondal, P. Kumar, P. Ghosh, A. Kalita, *Chem.Commun.,* 2011, **47**, 2964-2966.

176. X. Hu, X. Zhang, H. Song, C. He, Y. Bao, Q. Tang and C. Duan, *Tetrahedron,* 2012, **68**, 8371-8375.

177. R. Alam, T. Mistri, P. Mondal, D. Das, S. K. Mandal, A. R. Khuda-Bukhsh and M. Ali, *Dalton Trans.,* 2014, **43**, 2566–2576.

178. A. S. M. Islam, M. Sasmal, D. Maiti, A. Dutta, S. Ganguly, A. Katarkar, S. Gangopadhyay, and M. Ali, *ACS Appl. Bio Mater.,* 2019, **2**, 1944-1955.

179. V. Shafirovich and S.V. Lymar, *Proc. Natl. Acad. Sci. U. S. A.,* 2002, **99,** 7340-7345.

180. M. D. Bartberger, W. Liu, E. Ford, K. M. Miranda, C. Switzer, J. M. Fukuto, P. J. Farmer, D. A. Wink and K. N. Houk, *Proc. Natl. Acad. Sci. U. S. A.,* 2002, **99**, 10958–10963.

181. E. G. DeMaster, B. Redfern and H. T. Nagasawa, *Biochem. Pharmacol.,* 1998, **55**, 2007 – 2015.

182. N. M. Cook, M. Shinyashiki, M. I. Jackson, F. A. Leal and J. M. Fukuto, *Arch. Biochem. Biophys.,* 2003, **410**, 89– 95.

183. D. A. Wink, M. Feelisch, J. M. Fukuto, D. Christodoulou, D. Jourd'heuil, M. Grisham, V. Vodovotz, J. A. Cook, M. Krishna, W. DeGraff, S. Kim, J. Gamson and J. B. Mitchell, *Arch. Biochem. Biophys.,* 1998, **351**, 66– 74.

184. S. I. Liochev and I. Fridovich, *Free Radical Biol. Med.,* 2003, **34**, 1399 –1404.

185. K. M. Miranda, M. G. Espey, K. Yamada, M. Krishna, N. Ludwick, S. Kim, D.Jourd'heuil, M. Grisham, M. Feelisch, J. M. Fukuto and D. A. Wink, *J. Biol. Chem.,* 2001, **276**, 1720– 1727.

186. K. M. Miranda, K. I. Yamada, M. G. Espey, D. D. Thomas, W. DeGraff, J. B. Mitchell, M. C. Krishna, C. A. Colton and D. A. Wink, *Arch. Biochem. Biophysics.*, 2002, **401**, 134-144.

187. M. P. Doyle, S. N. Mahapatro, R. D. Broene and J. K. Guy, *J. Am. Chem. Soc.,* 1988, **110**, 593– 599.

188. N. Paolocci, T. Katori, H. C. Champion, M. E. St. John, K. M. Miranda, J. M. Fukuto, D. A. Wink and D. A. Kass, *Proc. Natl. Acad. Sci. U. S. A.,* 2003, **100**, 5537 –5542.

189. A. Arcaro, G. Lembo and C. G. Tocchetti, *Curr. Heart Fail. Rep.*, 2014, **11**, 227-235.

190. J. M. Fukuto, *Br. j. pharmacol.*, 2019, **176**, 135-146.

191. J. C. Irvine, J. L. Favaloro, R. E. Widdop and B. K. Kemp-Harper, *Hypertension,* 2007, **49**, 885−892.

192. J. M. Fukuto, C. J. Cisneros and R. L. Kinkade,. *J. Inorg. Biochem.,* 2013, **118**, 201-208.

193. (a) C. G. Tocchetti, W. Wang, J. P. Froehlich, S. Huke, M. A. Aon, G. M. Wilson, G. Di Benedetto, B. O'Rourke, W. D. Gao, D. A. Wink, J. P. Toscano, M. Zaccolo, D. M. Bers, H. H. Valdivia, H. Cheng, D. A. Kass and N. Paolocci, *Circ. Res.,* 2007, **100**, 96−104. (b)

T. Dai, Y. Tian, C. G. Tocchetti, T. Katori, A. M. Murphy, D. A. Kass, N. Paolocci and W. D. Gao, *J. Physiol.,* 2007, **580**, 951−960.

194. N. Paolocci and D.A. Wink, *Am. J. physiol. Heart Circ. Physiol.,* 2009, **296**, H1217–H1220.

195. F. T. Bonner and B. Ravid, *Inorg. Chem.,* 1975, **14**, 558−563.

196. F. T. Bonner and M. N. Hughes, *Comments Inorg. Chem.,* 1988, **7**, 215−234.

197. F. T. Bonner and Y. Ko, *Inorg. Chem.,* 1992, **31**, 2514−2519.

198. R. Zamora, A. Grzesiok, H. Weber and M. Feelisch, *Biochem. J.,* 1995, **312**, 333−339.

199. L. K. Keefer, R. W. Nims, K. M. Davies and D. A. Wink, *Meth. Enzymol.,* 1996, **268**, 281−292.

200. K. M. Miranda, T. Katori, C. L. Torres de Holding, L. Thomas, L. A. Ridnour, W. J. McLendon, S. M. Cologna, A. S. Dutton, H. C. Champion, D. Mancardi, and C.G. Tocchetti, *J. Med. Chem.,* 2005, **48**, 8220−8228.

201. K. M. Miranda, A. S. Dutton, L. A. Ridnour, C. A. Foreman, E. Ford, N. Paolocci, T. Katori, C. G. Tocchetti, D. Mancardi, D. D. Thomas and M. G. Espey, *J. Am. Chem. Soc.,* 2005, **127**, 722−731.

202. A. S. Dutton, C. P. Suhrada, K. M. Miranda, D. A. Wink, J. M. Fukuto and K. N. Houk,. *Inorg. Chem.,* 2006, **45**, 2448−2456.

203. K. M. Miranda, H. T. Nagasawa and J. P. Toscano, *Curr. Top. Med. Chem.,* 2005, **5**, 649−664.

204. S. Donzelli, M. G. Espey, D. D. Thomas, D. Mancardi, C. G. Tocchetti, L. A. Ridnour, N. Paolocci, S. B. King, K. M. Miranda and G. Lazzarino, *Free Radic. Biol. Med.,* 2006, **40**, 1056−1066.

205. M. Feelisch, *Proc. Natl. Acad. Sci. U.S.A.,* 2003, **100**, 4978−4980.

206. X. Sha, S. Isabell, R. P. Patel, C. S. Day and S. B. King, *J. Am. Chem. Soc.,* 2006, **128**, 9687−9692.

207. M. A. Marti, S. E. Bari, D. A. Estrin and F. Doctorovich, *J. Am. Chem. Soc.,* 2005, **127** 4680-4684.

208. J. Rosenthal and S.J. Lippard, *J. Am. Chem. Soc.,* 2010, **132**, 5536-5537.

209. Y. Zhou, K. Liu, J. Y. Li, Y. A. Fang, T. C. Zhao and C. Yao, *Org. Lett.,* 2011, **13,** 1290-1293.

210. Y. Zhou, Y. W. Yao, J. Y. Li, C. Yao and B. P. Lin, *Sens. Actuators B Chem.,* 2012, **174,** 414-420.

211. A. T. Wrobel, T. C. Johnstone, A. D. Liang, S. J. Lippard and P. Rivera-Fuentes, *J. Am. Chem. Soc.*, 2014, **136**, 4697-4705.

212. A. Loas, R. J. Radford, A. D. Liang and S.J. Lippard, *Chem. Sci.,* 2015, **6**, 4131-4140.

213. H. J. Lv, R. F. Ma, X. T. Zhang, M. H. Li, Y. T. Wang, S. Wang and G. W. Xing, *Tetrahedron,* 2016, **72**, 5495−5501.

214. S. Palanisamy, Y. L. Wang, Y. J. Chen, C. Y. Chen, F. T. Tsai, W.F. Liaw and Y. M. Wang, *Molecules*, 2018, **23**, 2551.

215. J. A. Reisz, E. B. Klorig, M. W. Wright and S. B. King, *Org. Lett.,* 2009, **11**, 2719−2721.

216. J. A. Reisz, C. N. Zink and S. B. King, *J. Am. Chem. Soc.,* 2011, **133**, 11675−11685.

217. H. Wang, M. Xian, H. Wang and M. Xian, *Angew. Chem.,* 2008, **120**, 6700-6703.

218. K. Kawai, N. Ieda, K. Aizawa, T. Suzuki, N. Miyata and H. Nakagawa, *J. Am. Chem. Soc.*, 2013, **135**, 12690−12696.

219. G. J. Mao, X. B. Zhang, X. L. Shi, H. W. Liu, Y. X. Wu, L. Y. Zhou, W. H. Tan and R. Q. Yu, *Chem. Commun.,* 2014, **50**, 5790−5792.

220. K. N. Bobba, Y. Zhou, L. E. Guo, T. N. Zang, J. F. Zhang and S. Bhuniya, *RSC Adv.,* 2015, **5**, 84543−84546

221. Z. Miao, J. A. Reisz, S. M. Mitroka, J. Pan, M. Xian and S. B. King, *Bioorg. Med. Chem. Lett.,* 2015, **25**, 16−19.

222. X. T. Jing, F. B. Yu and L. X. Chen, *Chem. Commun.,* 2014, **50**, 14253−14256.

223. P. Liu, X. T. Jing, F. B. Yu, C. J. Lv and L. X. Chen, *Analyst*, 2015, **140**, 4576−4583.

224. P. Liu, X.-Y. Han, F- B. Yu and L.-X. Chen, *J. Anal. Chem.,* 2015, **43**, 1829−1836.

225. Y. Tan, R. Liu, H. Zhang, R. Peltier, Y. W. Lam, Q. Zhu, Y. Hu and H. Sun, *Sci. Rep.,* 2015, 5, 16979.

226. X. Gong, X. F. Yang, Y. Zhong, Y. Chen and Z. Li, *Dyes Pigm.,* 2016, **131**, 24−32.

227. H. Niu, X. Mi, X. Hua, Y. Zhang, Y. Zhai, F. Qin, Y. Ye, and Y. Zhao, *Anal. Chim. Acta*, 2022, **1192**, 339341.

228. H. Zhang, Z. Qiao, N. Wei, Y. Zhang and K. Wang, *Talanta*, 2020, **206**, 120196.

229. C. Zhang, F. He, F. Huang, J. Xu, and Y. Hu, *Dyes Pigm.,* 2021, **185**, 108889.

230. C. Zhang, M. Qian, L.Zhang, H. Zheng, M. Zhang, Y. Jiao, Y. S. Kafuti, Q. Chen and Wang, J., *J. Lumin.*, 2022, **241**, 118496.

231. C. X. Zhang, M. H. Xiang, X. J. Liu, F. Wang, R. Q. Yu and J. H. Jiang, *Talanta,* 2019, **193**, 152-160.

232. W. Li, X. Wang, Y. M. Zhang and S. X. A. Zhang, *Dyes Pigm.,* 2018, **148**, 348-352.

233. T. Wang, Y. Chai, S. Chen, G. Yang, C. Lu, J. Nie, C. Ma, Z. Chen, Q. Sun, Y. Zhang and J. Ren, *Dyes Pigm.*, 2019, **166**, 260-265.

234. S. Palanisamy, L. F. Chen, S. C. Tzou and Y. M. Wang, *Sens. Actuators B Chem.,* 2020, **310**, 127839.

235. Z. Li, J. Li, D. Zhang, X. Zhu, Y. Ye and Y. Zhao, *Sens. Actuators B Chem.,* 2020, **312**, 127944.

236. S. Peng, Z. Li, Y. Zhang, W. Cao, J. Liu, W. Zhu and Y. Ye, *Sens. Actuators B Chem.,* 2020, **317**, 128211.

237. C. Wei, X. Wang, X. Li, X. Jia, X. Hao, J. Zhang, P. Zhang and X. Li, *Spectrochim. Acta A.,* 2020, **227**, 117765.

238. Z. Liu and Q. Sun, *Spectrochim. Acta A,* 2020, **241**, 118680.

239. Y. Kong, X. Wan, Z. Liu, F. Chen, F. Wu, G. Qin, D. Cao and Y. Cui, *Sens. Actuators B Chem.,* 2022, **350**, 130852

240. H. Li, Q. Yao, F. Xu, N. Xu, X. Ma, J. Fan, S. Long, J. Du, J. Wang and X. Peng, *Anal. Chem.,* 2018, **90**, 4641-4648.

241. Q. Ma, J. Xu, G. Mao, X. Guo, B. Liang, Y. Bai and C. Wang, *Anal. Methods, 2019,* **11***, 832-843.

242. P. Zhang, P. Lian, X. Wang, X. Li, C. Wei and X. Li, *Anal. Methods,* 2019, **11**, 1299-1303.

243. J. B .Li, Q. Wang, H. W. Liu, X. Yin, X. X. Hu, L. Yuan and X. B. Zhang, *Chem. Commun.,* 2019, **55**, 1758-1761.

244. M. Yang, J. Fan, W. Sun, J. Du, S. Long, K. Shao and X. Peng, *Chem. Commun.,* 2019, **55**, 8583-8586.

245. Z. Chai, D. Liu, X. Li, Y. Zhao, W. Shi, X. Li and H. Ma, *Chem. Commun.,* 2021, **57**, 5063-5066.

246. V. Staikopoulos, X. Zhang, B. P. Pullen, P. Reineck, A. K. Vidanapathirana, S. M. Lee, J. Liu, C. Bursill, M. R. Hutchinson and A. D. Abell, *Sens. Diagn.,* 2022, **1**, 280-293.

247. J. Wang, W. Zhu, C. Li, P. Zhang, G. Jiang, G. Niu and B. Z. Tang, *Sci. China Chem.,* 2020, **63**, 282-289.

248. C. Liu, H. Wu, Z. Wang, C. Shao, B. Zhu and X. Zhang, *Chem. Commun.,* 2014, **50**, 6013− 6016.

249. C. Liu, Y. Wang, C. Tang, F. Liu, Z. Ma, Q. Zhao, Z. Wang, B. Zhu and X. Zhang, *J. Mater. Chem. B,* 2017, **5**, 3557−3564.

250. K. Zheng, H. Chen, S. Fang and Y. Wang, *Sens. Actuators, B,* 2016, **233**, 193−198.

251. H. M. Lv, Y. Chen, J. Lei, C. T. Au and S. F. Yin, *Anal. Methods,* 2015, **7**, 3883−3887.

252. X. Jin, X. Sun, X. Di, X. Zhang, H. Huang, J. Liu, P. Ji and H. Zhu, *Sens. Actuators, B Chem.,* 2016, **224**, 209−216.

253. H. T. Zhang, R. C. Liu, Y. Tan, W. H. Xie, H. P. Lei, H. Y. Cheung and H. Y. Sun, *ACS Appl. Mater. Interfaces.,* 2015, **7**, 5438−5443.

254. X. Zhu, M. Xiong, H. W. Liu, G. J. Mao, L. Zhou, J. Zhang, X. Hu, X. B. Zhang and W. Tan, *Chem. Commun.*, 2016, **52**, 733−736.

255. Y. Zhou, X. Zhang, S. Yang, Y. Li, Z. Qing, J. Zheng, J. Li and R. Yang, *Anal. Chem.,* 2017, **89**, 4587−4594.

256. S. Yuan, F. Wang, G. Yang, C. Lu, J. Nie, Z. Chen, J. Ren, Y. Qiu, Q. Sun, C. Zhao and W. H. Zhu, *Anal. chem.,* 2018, **90**, 3914-3919.

257. H. Li, C. Wang, L. Cai, X. Yu, L. Wu, N. Yuan, Y. Zhu, N. Jia, T.D. James and C. Huang, *Ind. Eng. Chem. Res.,* 2021, **60**, 15913-15920.

258. J. Xu, Y. Bai, Q. Ma, J. Sun, M. Tian, L. Li, N. Zhu and S. Liu, *ACS omega*, 2022, **7,** 5264-5273.

259. C. Li, G. Jiang, X. Liu, Q. Lai, M. Kang, D. Wang, P. Zhang, J. Wang, and B. Z. Tang, *Mater. Chem. Front.,* 2021, **5**, 1817-1823.

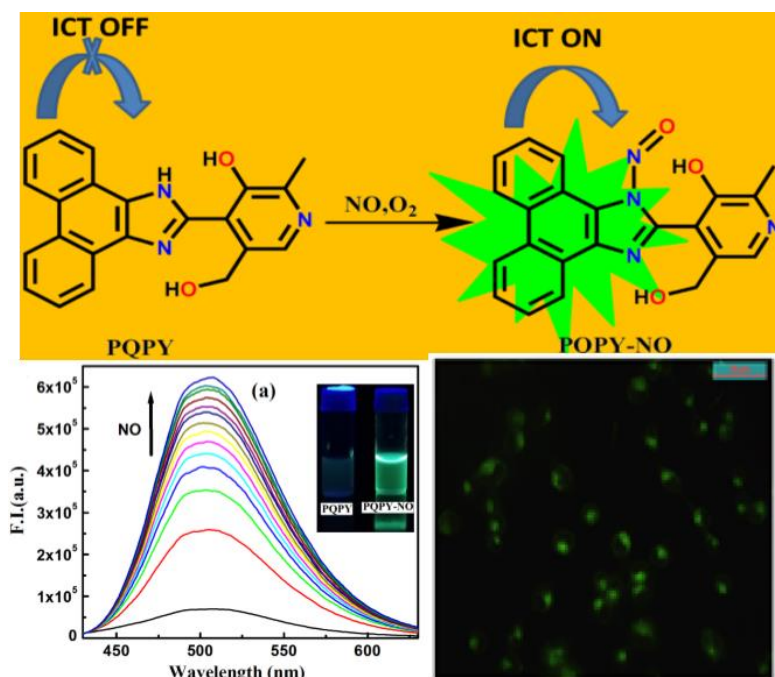260. M. R. Cline and J. P. Toscano, *J. Phys. Org. Chem.,* 2011, **24**, 993-998.

261. R. Smulik, D. Debski, J. Zielonka, B. Michalowski, J. Adamus, A. Marcinek, B. Kalyanaraman and A. Sikora, *J. Biol. Chem.,* 2014, **289**, 35570–35581.

262. N. W. Pino, J. Davis III, Z. Yu and J. Chan, *J. Am. Chem. Soc.,* 2017, **139**, 18476-18479.

263. A. Bachi, I. Dalle-Donne and A. Scaloni, *Chem. Rev.*, 2013, ***113***, 596-698.

264. Q. Xu, C. H. Heo, G. Kim, H. W. Lee, H. M. Kim and J. Yoon, *Angew. Chem. Int. Ed.,* 2015, **54**, 4890–4894.

265. A. B. Knott and E. Bossy-Wetzel, *Antioxid. Redox Signal,* 2009, **11**, 541 –553.

CHAPTER 2

Selective sensing of nitric oxide by a 9,10 phenanthroquinone–pyridoxal based fluorophore

Abstract:

In this article, we have designed and synthesized a new, convenient and efficient phenanthroquinone–pyridoxal based fluorogenic probe PQPY, highly suitable for the selective and sensitive detection of nitric oxide in an aerated aqueous (7 : 3 / H_2O: MeCN) medium at pH 7.0 (10 mM HEPES buffer). Upon addition of nitric oxide, this probe exhibits emission in the green region (λ_{em} = 505 nm) which is ascribed to ICT (intramolecular charge transfer) from the phenanthroquinone moiety to the imidazole –N–N=O fragment. The apparent formation constant, K_f of the NO product of the ligand is $(1.00 \pm 0.2) \times 10^5$ M^{-1} and the LOD is 78 nM. The substantial enhancement of the life-time of the ligand (τ_0 = 2.68 ns) occurs due to binding with nitric oxide (τ_0 = 3.96 ns). This probe is low cytotoxicity, cell permeable and suitable for living cell imaging application.

2.1 Introduction

Modern molecular biology has revealed that vast numbers of large and complex proteins and genes regulate the body functions. By contrast, a remarkably simple chemical, nitric oxide (NO), has been found to mediate the crucial features of neuronal communication, blood vessel modulation and immune response. NO can exist in a variety of molecular forms: free radical (NO^0), nitrosyl (NO^-) anion or nitrosonium (NO^+) cation depending on the NO source. Hence, the NO released from NO donors can differ from the NO produced in the endothelial cells. NO donors are pharmacologically active substances that release NO *in vivo* or *in vitro*. NO delivery can occur through many kinds of stimuli, depending on the NO donor structure. Among many physiological functions, NO induces vasodilation, inhibits platelet aggregation, prevents neutrophil/platelet adhesion to endothelial cells, inhibits smooth muscle cell proliferation and migration, regulates programmed cell death (apoptosis) and maintains the endothelial cell barrier function. NO generated by neurons acts as a neurotransmitter, whereas NO generated by macrophages in response to invading microbes acts as an antimicrobial agent. Therefore, its accurate detection and quantification are critical to understanding health and disease. The established paradigm of NO biochemistry from the production by NO synthases to the activation of soluble guanylyl cyclase (sGC) and to eventual oxidation to nitrite (NO_2^-) and nitrate (NO_3^-) may only represent part of NO's effects *in vivo*.[1,2] Due to the extremely short physiological half-life of this gaseous free radical (less than 1 second in circulating blood),[3] alternative strategies have been established for the detection of the reaction products of NO biochemistry. The quantification of NO metabolites in biological samples provides valuable information with regard to *in vivo* NO production, bioavailability and metabolism. Simply sampling a single compartment such as blood or plasma may not always provide an accurate assessment of the whole body NO status, particularly in tissues. Therefore, extrapolation of the plasma or blood NO status to specific tissues of interest is no longer a valid approach. As a result, methods continue to be developed and validated, which allow the detection and quantification of NO and NO-related products/metabolites in multiple compartments of experimental animals *in vivo*. Several analytical methods like electrochemical, fluorescence, electron spin resonance etc. have been proposed for the *in vitro* and *in vivo* analysis of NO.[4–12] In view of its sensitivity, selectivity, spatiotemporal resolution, and experimental feasibility, the fluorescence method has

been regarded as the most promising method to detect endogenous NO. A number of small organic and inorganic fluorescent NO sensors have been reported thus far. Many of them are involved in the reaction of *o*-diamino aromatics with NO in the presence of oxygen leading to the formation of triazole, which acts as a modulator in the photo-induced electron transfer (PET) mechanism resulting in fluorescence turn-on. Other mechanisms involve the oxidative deamination process[13] and NO/O_2 mediated diazotization with the concomitant ring formation.[9] However, they still have some undesired limitations, such as electron-rich aromatic diamines may undergo self-oxidation or react with other reactive oxygen/nitrogen species that may lead to the generation of fluorescent species.[13–21] Very recently, we have reported a new mechanism of NO sensing in which the thiosemicarbazide group, flanked by the carbonyl moiety, reacts with NO under aerobic conditions leading to the formation of the 1,3,4-oxadiazole moiety with the simultaneous elimination of thio-nitrous acid.[22] In the current paper we are planning to report another new strategy where NO directly reacts with the imidazolium NH group to generate the N–N=O moiety acting as an electron acceptor from the phenanthrone moiety as the electron donor group thereby resulting in a turn on fluorescent response by the ICT process.

2.2 Experimental section

2.2.1 Physical measurements

An IR 750 series-II FTIR (Nickolet Magna) spectrophotometer was used to record IR spectra in the range 400–4000 cm^{-1} on KBr pellets. Electronic spectra were recorded on an Agilent 8453 Diode-array UV-vis spectrophotometer using 7:3 HEPES buffer (10 mM) and MeCN as the solvent with a 1 cm quartz cuvette in the range 200–900 nm. Fluorescence studies were performed on a PTI (model QM-40) spectrofluorimeter and ^{1}H NMR spectra were recorded in DMSO-d_6 on a Bruker 300 MHz instrument using trimethylsilane ($\delta = 0$) as an internal standard. ESI-MS$^+$ (m/z) of the ligand was recorded using a high resolution mass spectrometer (Model: QTOF Micro YA263). Time correlated single photon counting (TCSPC) measurements using a picosecond diode laser (IBH nanoled-07) in an IBH fluorocube apparatus were performed to determine fluorescence lifetimes. A Hamamatsu MCP photomultiplier (R3809) was used to collect the fluorescence decay data which were further examined by using the IBH DAS6

software. To obtain cell images, a fluorescence microscope (Leica DM3000, Germany) was used.

2.2.2 Materials and methods

9,10-Phenanthroquinone, pyridoxal hydrochloride, ammonium acetate and glacial acetic acid were used to prepare the ligand. These reagents were purchased from Sigma-Aldrich. Salts of Cd^{2+}, Sm^{3+}, Co^{2+}, Mg^{2+}, Mn^{2+}, Na^+, Zn^{2+}, Dy^{3+}, Ni^{2+}, Cu^{2+}, Cr^{3+}, Hg^{2+}, Fe^{3+}, Pb^{2+}, Al^{3+}, F^-, $S_2O_3^{2-}$, HSO_4^-, IO_3^-, SO_4^{2-}, NO_2^-, HCO_3^-, Br^-, S^{2-}, HS^-, OAc^-, N_3^-, I^-, SCN^-, and ADP and biological anions like H_2O_2, O^{2-}, TEMPO radical, NO_3^-, ClO^-, AA, $NOBF_4$, glyoxal, formaldehyde, cysteine, homocysteine, glutathione etc. were obtained either from Sigma-Aldrich or from other commercial suppliers and used without further purification. Solvents like MeOH, N,N-dimethylformamide (DMF), MeCN, etc., (Merck, India) were of reagent grade and dried before use.

2.2.3 Synthesis of the ligand

The ligand 5-hydroxymethyl-2-methyl-4-(1H-phenanthro[9,10-d]imidazole-2-yl)-pyridin-3-ol (designated as PQPY) was synthesized by the reported procedure with slight modification.[23] Excess ammonium acetate (25 mmol, 1.927 g) was dissolved in 5 mL glacial acetic acid, and then 9,10-phenanthroquinone (5 mmol, 1.041 g) solution (in glacial acetic acid) was added to the ammonium acetate solution at 70 °C by heating under stirring conditions. After 10 minutes, pyridoxal hydrochloride (5 mmol, 1.018 g) solution in glacial acetic acid was added dropwise to the reaction mixture. Then this reaction was continued for 6 hours under refluxing conditions. A blackish crude solid product was obtained by filtration and washed with a small volume of glacial acetic acid. From this crude product, the ligand was obtained by methanol extraction. Then the methanol part was evaporated to dryness to get a pure pale yellow product confirmed by ^1H NMR **(Figure 2.1)**, HRMS **(Figure 2.2)** and FTIR **(Figure 2.3)**. (Yield,76%). ESI-MS^+(m/z): 357.1221 (PQPY + H^+), ^1H NMR (in DMSO-d_6) (δ, ppm):11.752 (s, 1H, –NH), 8.88–8.97 (m, 2H, –ArH), 8.55 (1H, d,–ArH), 8.36–8.34 (1H, d, –ArH), 8.29 (1H, S, –ArH), 7.64–7.87(4H, m, –ArH), 5.41 (1H, S, –OH), 5.11 (S, 2H, –CH$_2$), 1.21 (S, 3H, –CH$_3$).
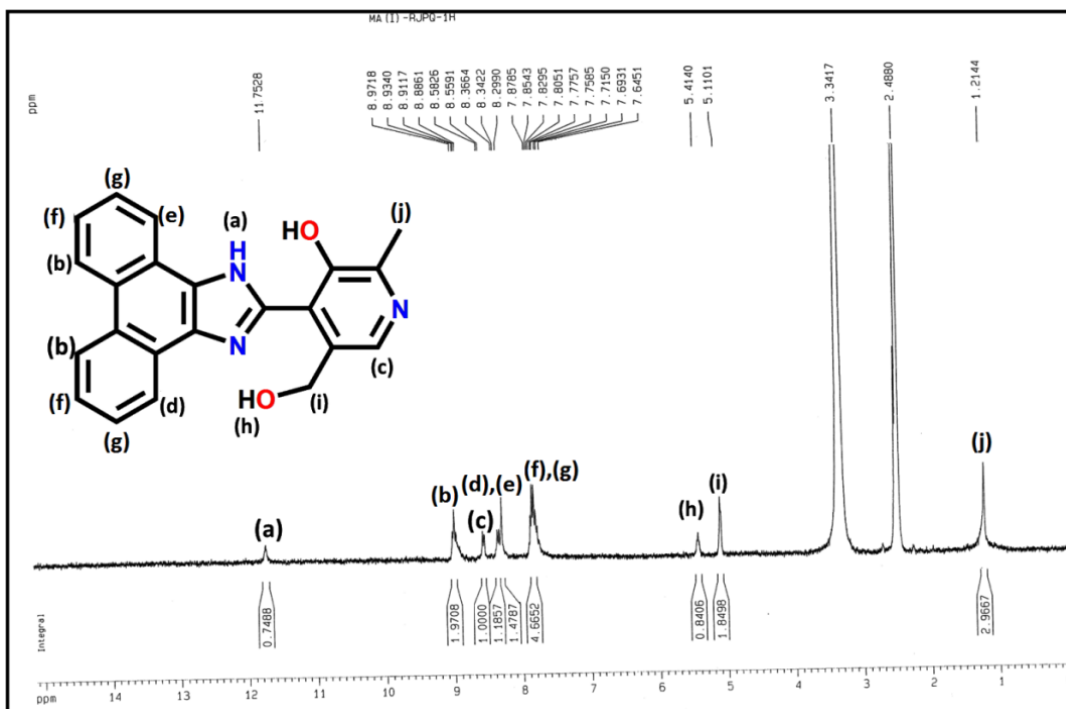
Figure 2.1 ^{1}H-NMR spectrum of PQPY in DMSO-d$_6$.
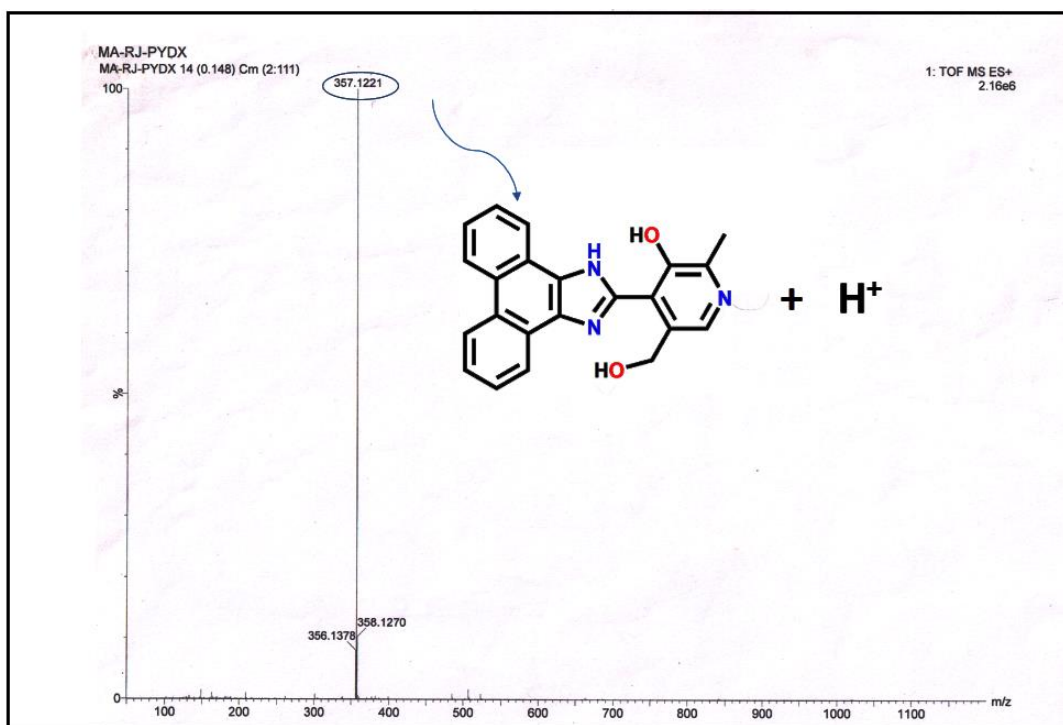
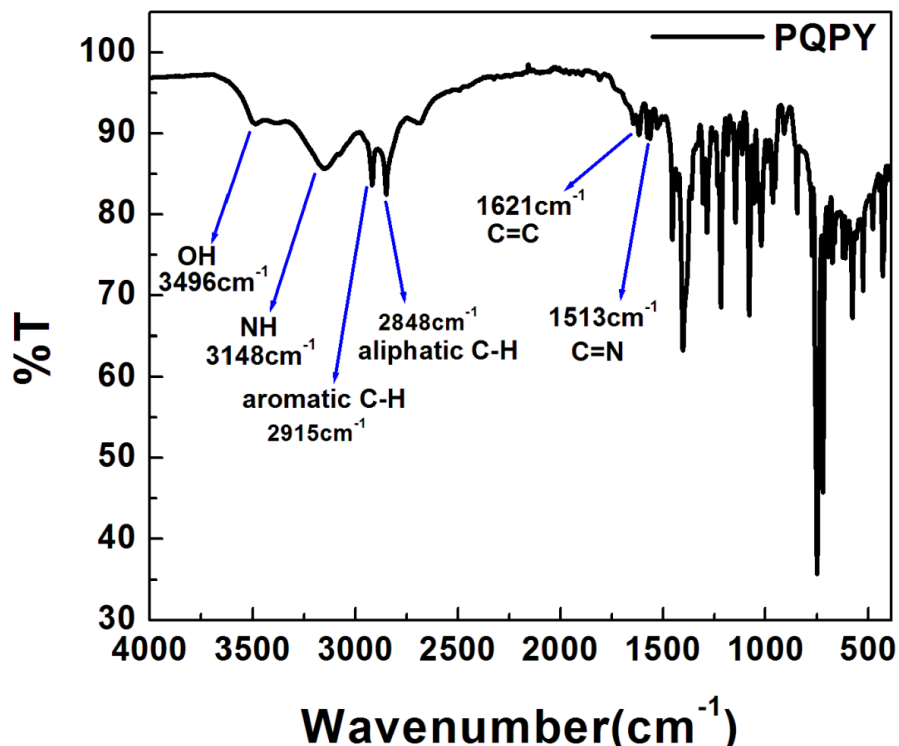**Figure 2.2** Mass spectrum of PQPY in MeCN.

Figure 2.3 IR spectrum of ligand (PQPY).

2.2.4 Solution preparation for fluorescence studies

A 10 mL 1.0×10^{-3} M stock solution of the ligand PQPY was prepared in DMF by slight heating for fluorescence titrations. The solutions of other metal ions and other anions were prepared in H_2O. A stock solution of nitric oxide was prepared in deoxygenated deionized water by purging nitric oxide gas for 15 min in a sealed vial with a syringe. The concentration of nitric oxide was 1.74×10^{-3} M. The nitric oxide gas was purified by passing it through a drying tube containing solid NaOH pellets.[24] HNO solution was prepared from Angeli's salt[25] and •OH and ONOO$^-$ solutions were prepared following a reported method.[26] A 100 mL solution of 10.0 mM 4-(2-hydroxyethyl)-1-piperazineethanesulfonic acid (HEPES) buffer was prepared adjusting pH to 7.0 using HCl and NaOH and ionic strength of the buffer solution was maintained at 0.10 M (NaCl) throughout the measurements. In this work, 20 μM ligand was taken in a cuvette containing a 2.5 ml mixture solution of HEPES buffer and MeCN in 7 : 3 ratio (v/v) and titrated with 0 to 75 μM NO solution incrementally in a regular time interval with $\lambda_{ex} = 400$ nm and 2, 2 slits.

2.2.5 Calculation of LOD

To know the limit of detection (LOD) of the ligand PQPY we used the following equation by the 3σ method.

$$\text{LOD} = 3 \times S_d/ S$$

S_d is the standard deviation obtained from the intercept of the plot of F.I. vs. [PQPY]. From the linear part of the titration plot, the value of the slope (S) is obtained.

2.2.6 Calculation of the quantum yield

Fluorescence quantum yields (Φ) were determined by using the equation:

$$\Phi_{sample} = [(OD_{std} \times A_{sample})/(OD_{sample} \times A_{std})] \times \Phi_{std}$$

Here, A_{sample} and A_{std} represent the areas under the fluorescence spectral curves. The optical densities of the sample and standard are designated as OD_{sample} and OD_{std}, respectively, at the excitation wavelength. Here, acidic quinine sulfate was taken as the standard ($\Phi_{std} = 0.54$) for the quantum yield calculation of ligands PQPY and PQPY-NO.

2.2.7 Cell culture

Human hepatocellular liver carcinoma (HepG2) cell lines (NCCS, Pune, India) were grown in DMEM supplemented with 10% FBS and antibiotics (penicillin-100 µg ml^{-1}; streptomycin-50 µg ml^{-1}). Cells were cultured at 37 °C in a 95% air, 5% CO_2 incubator.

2.2.8 Cell imaging study

HepG2 cells were cultured in a 35 × 10 mm culture dish on a coverslip for 24 h at 37 °C. The cells were treated with 5µM solutions of PQPY, prepared by dissolving PQPY in the mixed solvent HEPES buffer: acetonitrile = 7:3 (v/v) and incubated for 1 hour at 37 °C. For NO sensing study, HepG2 cells were pre-incubated with 5µM, 10µM and 20µM sodium nitroprusside (SNP)

for 60 min at 37 °C followed by washing three times with 1× PBS and subsequent incubation with 5µM of PQPY for 60 min at 37 °C. Fluorescence images of HepG2 cells were obtained by using a fluorescence microscope (Leica DM3000, Germany) with an objective lens of 40× magnification.

2.2.9 Cell cytotoxicity assay

Cytotoxicity for the ligand PQPY was assessed by the 3-(4,5-dimethylthiazol-2-yl)-2,5-diphenyltetra-zolium bromide (MTT) cell viability assay. HepG2 cells (1×10^5 cells per well) were cultured in a 96-well plate and incubated at 37 °C and were exposed to varying concentrations of PQPY (1, 5, 10, 20, 30, 40, 50, 60, 70, 80 and 100µM) for 24 hours. After the incubation, 10µl of MTT solution [5 mg ml^{-1}, dissolved in 1× phosphate-buffered saline (PBS)] was added to each well of a 96-well culture plate and then incubated at 37 °C for 4 hours. Media were decanted from wells and 100µL of 0.04 N acidic isopropyl alcohol was added into each well to solubilize the intracellular formazan crystals (blue-violet) formed. The absorbance of the solution was measured at 595 nm wavelength (EMax Precision MicroPlate Reader, Molecular Devices, U.S.A.). Values were calculated as mean ± standard errors of three independent experiments. The cell viability was expressed as the optical density ratio of the treatment to control.

2.3 Results and discussion
2.3.1 Design of the NO probe PQPY

For a few decades, the development of *ortho*-phenylene diamine (OPD) based probes using fluoresceins, anthraquinones, rhodamines, BODIPYs and cyanines **(Figure 2.4)** as fluorophore have emerged for the detection of nitric oxide but still there exist some serious limitations.[9] At first, in the presence of reactive oxygen and nitrogen species the electron rich diamino-benzene portion is readily Oxidized. The second important drawback is that the OPD moiety shows a false positive response towards glyoxal, dehydroascorbic acid (DHA) and ascorbic acid (AA)[27] like NO which misguides the researchers towards wrong interpretations of observations. Another

important shortcoming is that fluorescence enhancement occurs in the OPD moiety via benzotriazole formation, a secondary amine. Consequently, this is pH sensitive owing to
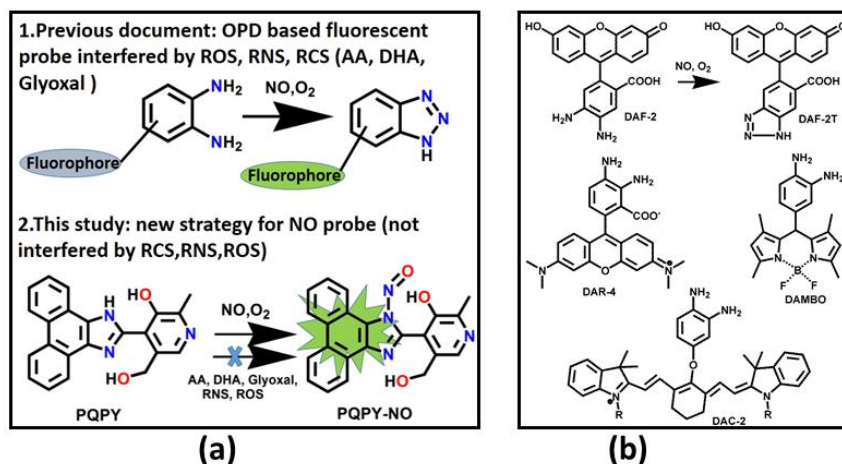
Figure 2.4 (a) Scheme of the N-nitrosation reactivity based NO probe PQPY and (b) some previously reported NO probes.

protonation to the secondary amine of triazole. So, the poor selectivity and the above mentioned limitations are broad concerns in the design of fluorescent NO probes. In our present work, taking the aforementioned concerns into account, we strategically designed a new type of fluorescent probe PQPY based on N-nitrosation[27] of a secondary amine taking 9,10-phenanthroquinone as a fluorophore. The reactivity of PQPY was assessed with biological carbonyl species (RCS (glyoxal, formaldehyde (FA), ascorbic acid (AA), dehydroascorbic acid (DHA)) and also with cysteine (CYS), homocysteine (HCY) and glutathione (GSH). Even a large excess of each biological intercellular molecule cannot light up our present probe except NO. So, N-nitrosation based PQPY shows an improved selectivity towards NO over RNS, ROS, and RCS compared to OPD based NO probes, which makes it useful as a superior NO sensor. Our ligand is also cell permeable, low cytotoxic, and pH independent with a very low detection limit (78 nM) and has an easy synthetic procedure which make it highly useful as a nitric oxide sensor. As illustrated in **Scheme 2.1**, the probe PQPY was synthesized by the reaction between 9,10-phenanthroquinone and pyridoxal-hydrochloride in the presence of ammonium acetate in glacial acetic acid medium.
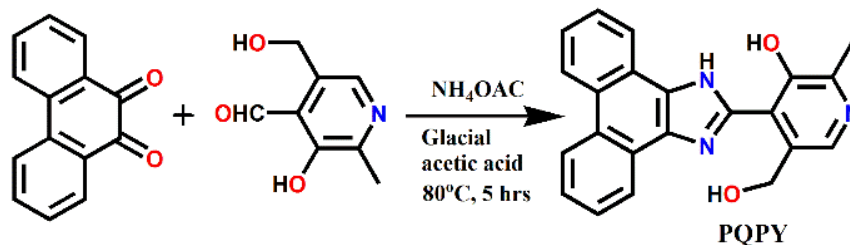
Scheme 2.1 Synthesis of the probe 5-hydroxymethyl-2-methyl-4-(1Hphenanthro [9,10-d]imidazole-2-yl)-pyridin-3-ol (hereafter designated as **PQPY**).

The probe was nicely analyzed by ^{1}H NMR **(Figure 2.1)**, HRMS **(Figure 2.2)** and IR **(Figure 2.3)** spectroscopy. The probe PQPY displayed a high fluorogenic response towards NO in the aerated aqueous buffer medium. In the present work, pyridoxal (one form of vitamin B$_6$) is taken as one part of the probe having a great significance in the growth of some medically relevant bacteria.

2.3.2 Spectral response of PQPY to NO

The sensitivity and selectivity of the probe PQPY are distinct only towards nitric oxide in aqueous acetonitrile medium at pH 7.0, as clearly demonstrated by the turn-on fluorescence response (λ_{em} = 505 nm) to nitric oxide upon excitation at 400 nm. The probe (20μM) was taken in a cuvette containing 2.5 mL of 10mM HEPES buffer: acetonitrile =7:3 (v/v), pH = 7.0 and μ = 0.10 M NaCl. Then the previously prepared nitric oxide solution (1.74×10^{-3} M) was added incrementally. For the deduction of the apparent formation constant (K_f) of the reaction between PQPY and NO, fluorescence titration was performed with the fixed concentration of PQPY (20 μM) with variable concentrations of NO (0–75 μM) at 25 °C. There was a gradual development of an emission band at ~505 nm (λ_{ex} = 400 nm) with the incremental addition of NO resulting in an approximately 9-fold enhancement in fluorescence intensity which is sufficient to detect intracellular nitric oxide in live cells (*vide infra*) **(Figure 2.5)**. A plot of F.I. versus [NO] at 505 nm gives a nonlinear curve, which was solved by adopting the equation $y = (a + b \times c \times x^n)/(1 + c \times x^n)$,[28] where *a* represents F.I. of the free ligand, *b* is F.I. of the ligand in the presence of excess NO, *c* is the formation constant, K_f, and n represents the stoichiometry. The evaluated parameters are n = 0.93 ± 0.01 and K_f = $(1.00 \pm 0.2) \times 10^5$ M^{-1}.
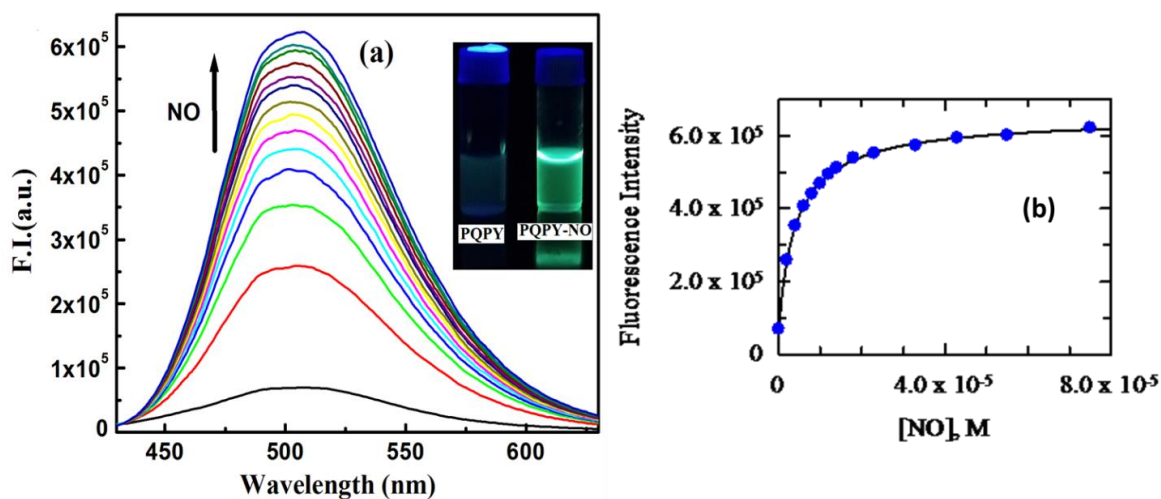
Figure 2.5 (a) Fluorescence titration of the ligand PQPY (20 μM) at 25 °C by the gradual addition of nitric oxide (0–75μM) in 7:3 HEPES buffer (10 mmol): acetonitrile medium at pH = 7.0 with λ_{ex} = 400 nm and λ_{em} = 505 nm. The inset shows the UV exposed emission image of PQPY and PQPY-NO; (b) nonlinear plot of F.I. vs. [NO].

2.3.3 Mechanism

In this research endeavor, we have designed a new fluorescent molecular probe PQPY which contains phenanthroimidazole and pyridine moieties acting as a fluorescence turn-on nitric oxide sensor. As the phenanthroimidazole moiety is an electron rich system, it acts as an electron donor (D) as well as a fluorophore and the other part *i.e.*, pyridine moiety, behaves also as an electron donor too due to the presence of the phenolic –OH group. So, the flow of charge from the phenanthroimidazole moiety to pyridoxal (D–A) does not occur significantly and it becomes very weakly fluorescent. However, the system generates electron donor–acceptor property on introduction of NO into the –NH nitrogen atom of imidazole group and becomes highly suitable for the intramolecular charge transfer process. Here, NO is an electron withdrawing group and drags the electron density from the phenanthrene moiety to the imidazole system, causing a drastic fluorescence enhancement by the ICT mechanism. The intramolecular charge transfer (ICT) mechanism of the probe PQPY upon reaction with nitric oxide can be nicely understood by spectrofluorometric study in solvents of different polarities. The experiment shows a 24 nm red shift on increasing the polarity of the solvents which clearly suggests the occurrence of the

intramolecular charge transfer mechanism in the ligand upon reaction with nitric oxide **(Figure 2.6)**.
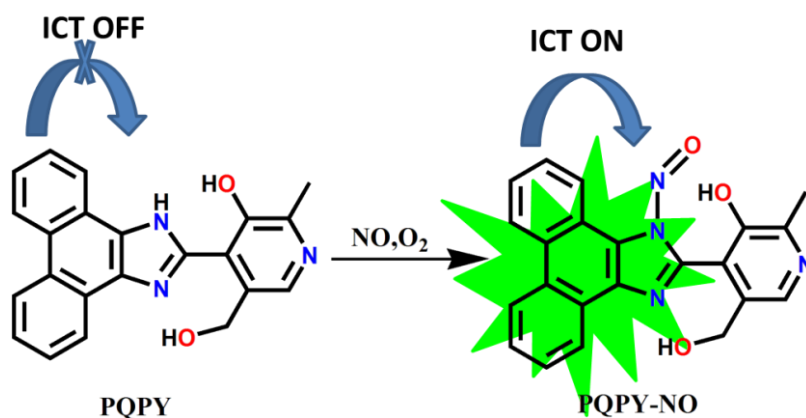
Scheme 2.2 Model describing the ICT on the fluorescence response of PQPY on interaction with NO in the presence of oxygen.
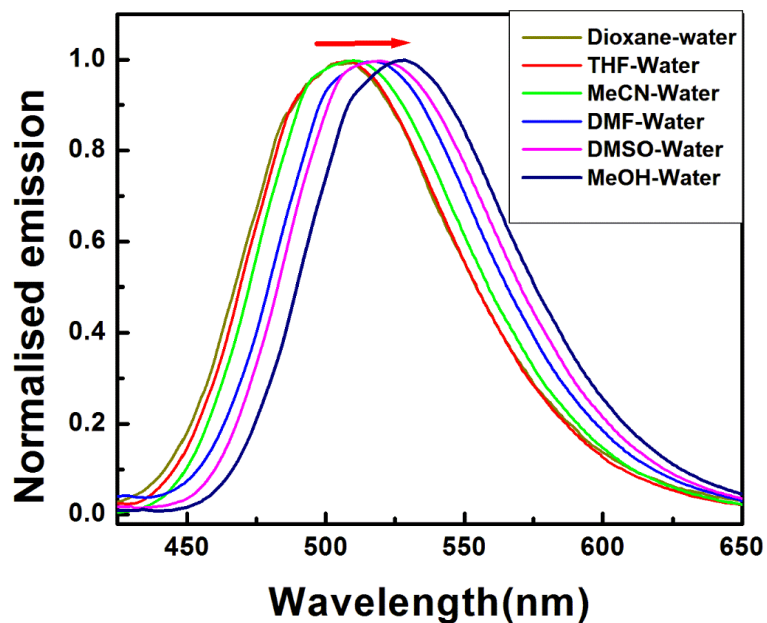
Figure 2.6 Normalized emissions of probe PQPY upon reaction with NO in different solvent (7:3 HEPES buffer: solvent) of different polarity.

As delineated by DFT optimization (*vide infra*) the HOMO of PQPY and PQPY-NO bears all the electron density localized on the phenanthrene moiety, whereas the LUMO electron density is

solely distributed in the 1-nitrosoimidazole moiety of PQPY-NO, clearly manifesting the ICT mechanism of sensing **(Scheme 2.2)**.

2.3.4 Confirmation of the sensing mechanism

To interpret the probable mechanism responsible for the fluorescence enhancement of the probe in the presence of nitric oxide, detailed product analysis was carried out by reacting PQPY with excess NO gas in the aerated MeCN medium. Then the solution was allowed to evaporate and the product PQPY-NO was isolated and characterized by using ^{1}H NMR **(Figure 2.7)** and FTIR **(Figure 2.8)** spectrometers. The molecular ion peak of PQPY-NO in the mass-spectrum was not found may be due to the breakdown of the N–N=O bond to give the parent probe PQPY and NO and thus we find only the molecular ion peak of the ligand PQPY.
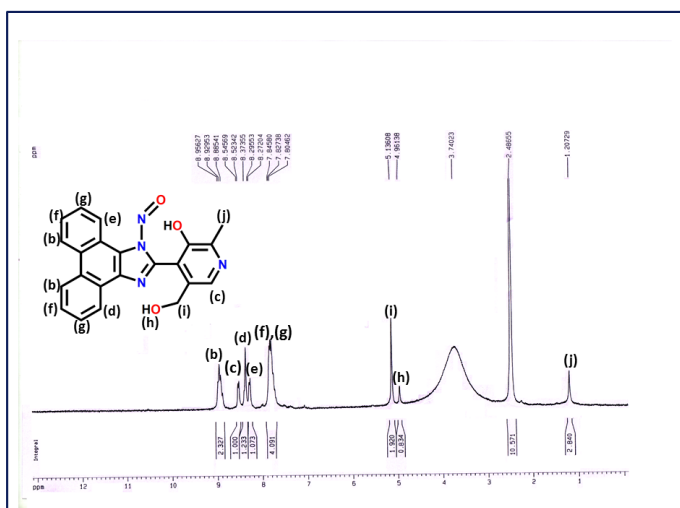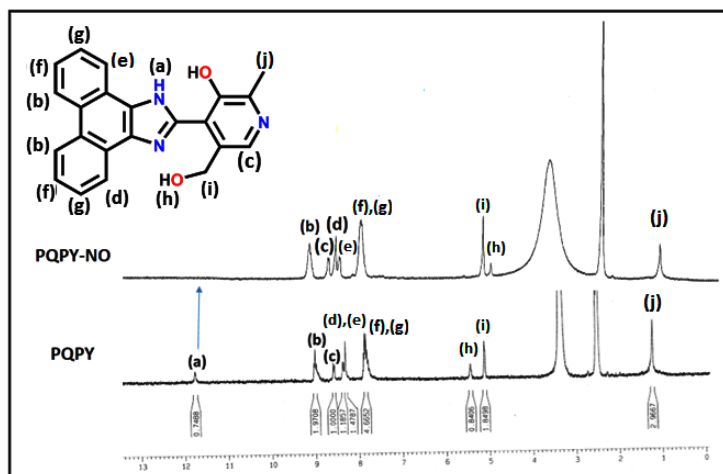

Figure 2.7 ^{1}H-NMR spectrum of PQPY-NO in DMSO-d$_6$.

But the proton NMR spectra **(Figure 2.8)** of PQPY and PQPY-NO clearly suggest that the imidazole –NH proton of PQPY exhibiting a single peak at 11.75 ppm vanished after the treatment with NO. So proton NMR depicts that NO is attached to the secondary amine of the imidazole system. This fact is further confirmed from the IR spectrum **(Figure 2.9)**. The N–H stretching frequency at 3148 cm^{-1} disappeared and a new peak at 1424 cm^{-1} for the –N=O group[29] was generated which confirms the formation of imidazole-N–N=O. So we can conclude that the nitric oxide was attached directly to the imidazole N atom causing a turn-on fluorescence

response and it is also evidenced from the substantial increase of the lifetime of the ligand (τ_0 = 2.68 ns) in the presence of nitric oxide (τ_0 = 3.96 ns). The non-existence of the ^{1}H NMR peak for phenolic –OH protons may arise due to the strong hydrogen bonding interaction between phenolic–OH and tertiary imidazole–N atoms (O–H···N). The quantum yield of compound

**Figure 2.8** ^{1}H NMR spectra of PQPY and PQPY-NO.
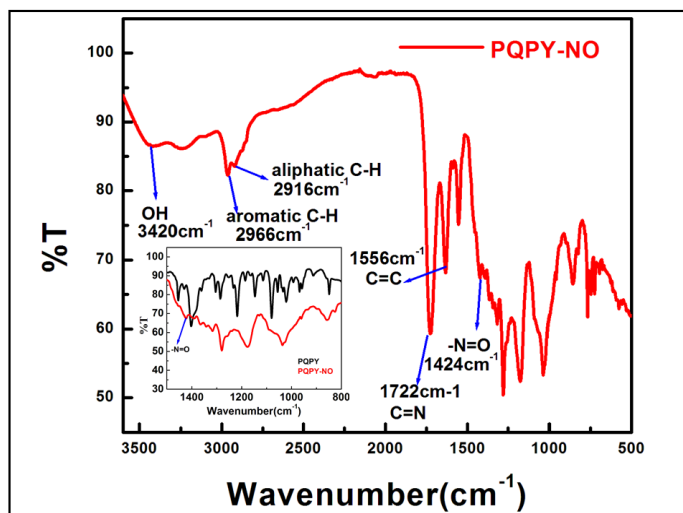
Figure 2.9 IR spectrum of PQPY-NO.

PQPY-NO was Φ = 0.1006 and that of the ligand (PQPY) was 0.02 (quinine sulfate in the acidic medium was taken as the standard). The analytical limit of detection (LOD) of nitric oxide was deduced by the 3σ method **(Figure 2.10)**, which was found to be as low as 78 nM further

indicating the high efficiency of the probe to detect nitric oxide. So, all the above experiments, results and discussions highly support the probe as an efficient nitric oxide sensor.
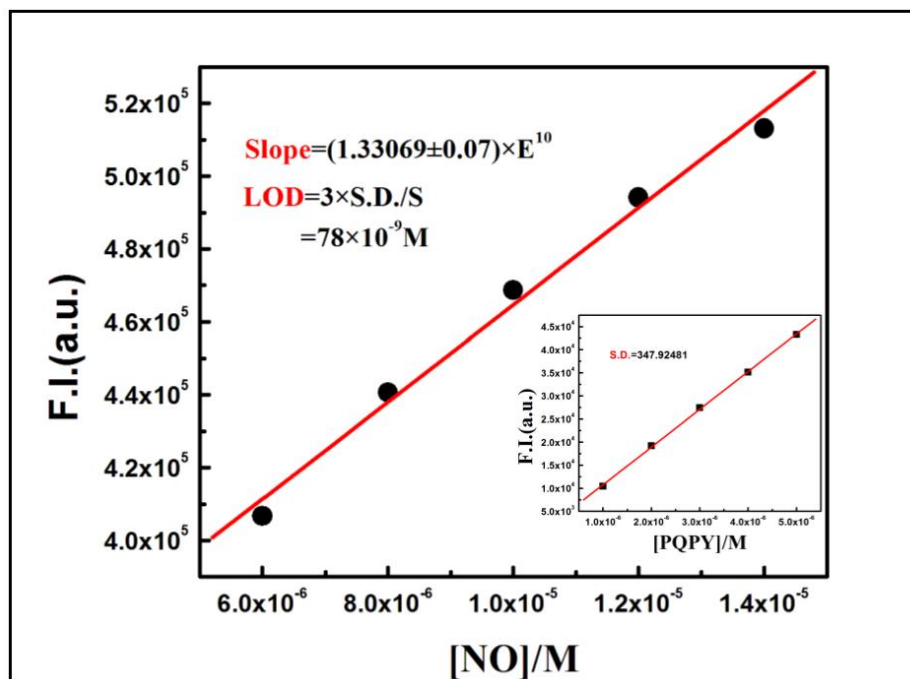
Figure 2.10 Determination of LOD of PQPY+ NO.

2.3.5 TCSPC studies

The average life-time of the probe (τ_0 = 2.68 ns) increases upon addition with 75 µM nitric oxide (τ_0 = 3.96 ns) and the bi-exponential decay curve of the ligand changes to mono-exponential upon reaction with NO **(Figure 2.11)**. This study signifies the NO addition and greater stability of the product in the excited state.
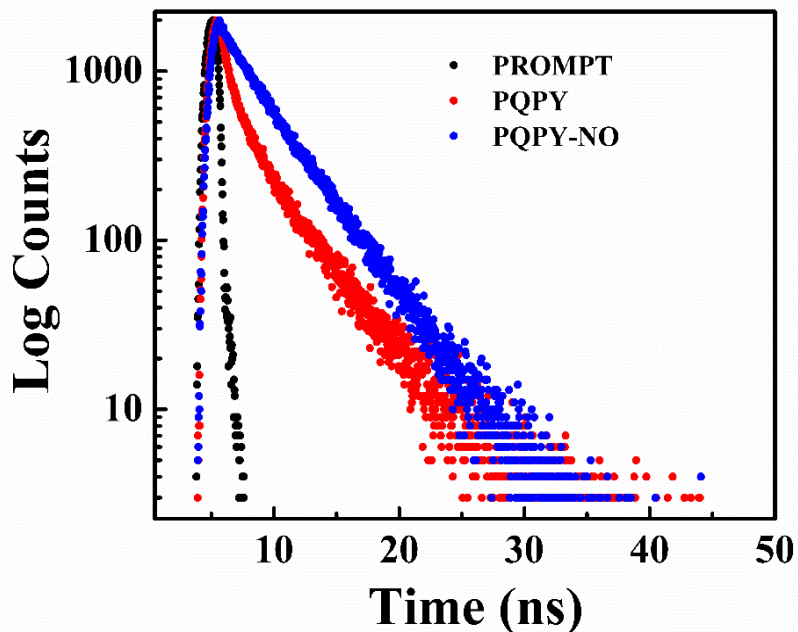
Figure 2.11 Life time plot for PQPY (20 µM) and PQPY+NO (75 µM) at pH 7.0 in HEPES buffer/MeCN (7: 3, v/v) at room temperature.

2.3.6 pH stability checking

To know the practical applicability and stability of the ligand PQPY and product PQPY-NO under different environmental and physiological conditions, a plot of F.I. vs. pH was drawn **Figure 2.12 (a)** which clearly reveals that PQPY exhibits a slight enhancement in fluorescence
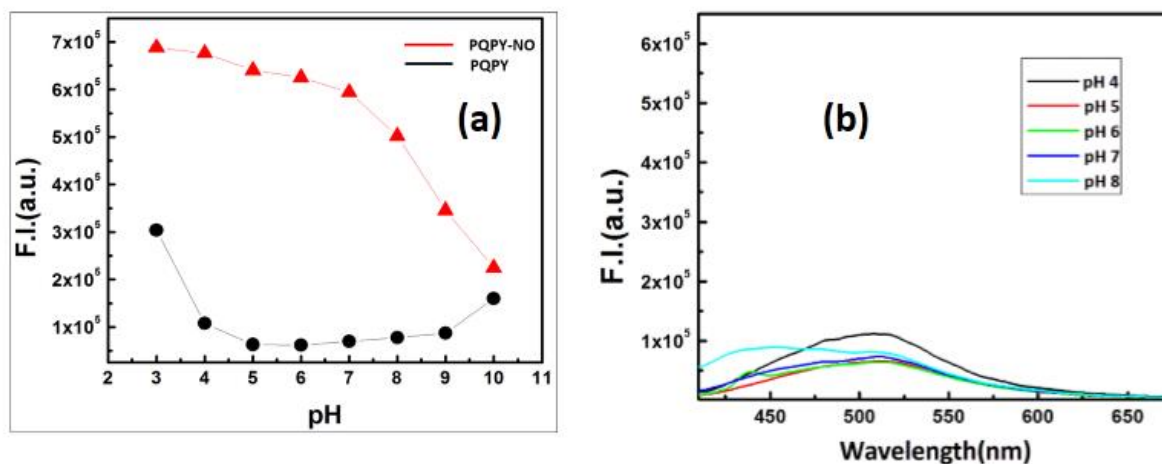

Figure 2.12 (a) pH dependent fluorescence responses of PQPY and PQPY-NO in 7: 3 (v/v) HEPES buffer/MeCN medium. **(b)** Emission profile of the probe at different pH.

intensity at low pH ($\leq$ 3.0) due to protonation of imidazole NH atoms but it remains practically indifferent within a wide range of pH (pH 4.0–9.0) as also demonstrated in **Figure 2.12 (b)** where fluorescence spectra were recorded at different pH (4.0, 5.0, 6.0 7.0 and 8.0) and FI were found to be invariant with pH. However, the product PQPY-NO shows high fluorescence intensity in a wide range of biological pH 4.0–9.0. As at pH $\approx$ 7.0, the fluorescence intensity is sufficiently high, it can be safely used under physiological conditions for monitoring NO **Figure 2.12 (a)**.

2.3.7 Selectivity study

To check the selectivity of PQPY, we have examined the response of PQPY towards commonly known metal ions (Cd^{2+}, Sm^{3+}, Co^{2+}, Mg^{2+}, Mn^{2+}, Na^+, Zn^{2+}, Dy^{3+}, Ni^{2+}, Cu^{2+}, Cr^{3+}, Hg^{2+}, Fe^{3+}, Pb^{2+}, Al^{3+}), anions (F^-, $S_2O_3^{2-}$, HSO_3^-, IO_3^-, SO_4^{2-}, NO_2^-, HCO_3^-, Br^-, S^{2-}, HS^-, OAc^-, N_3^-, I^-,
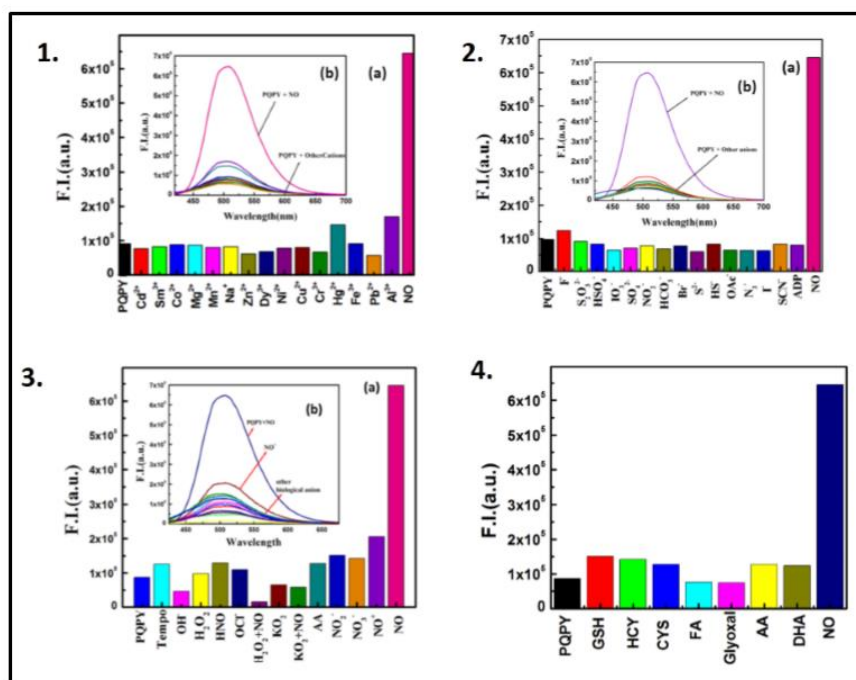
Figure 2.13 1(a), 2(a), 3(a), 4(a) are bar plot illustrating the fluorescence responses of PQPY at 505 nm (λ_{ex} = 400 nm) towards different cations, anions, reactive oxygen-nitrogen species, and thiols respectively. 1(b), 2(b), 3(b), 4(b) are the corresponding spectral plot. These experiments

are performed in HEPES buffer at pH 7.0 in H_2O–MeCN (7: 3, v/v) at room temperature. PQPY = 20 μM, X^{n-} =100 μM.

SCN^-, ADP) and biologically relevant species (Tempo, •OH, H_2O_2, NO, OCl^-, AA, $ONOO^-$, O^{2-}, NO_3^-, NO^+, DHA, FA, glyoxal, etc.). The fluorescence emission spectra **(Figure 2.13)** clearly imply that PQPY exhibits high selectivity towards nitric oxide in aqueous–acetonitrile (7:3) medium at pH = 7.0. Even the presence of a large excess of each cation, anion, and biological intercellular molecule cannot enhance the fluorescence intensity of our present probe except for NO suggesting its high selectivity towards nitric oxide.

2.3.8 Theoretical studies

To better understand the photophysical properties of the probe and NO product, we performed quantum chemical computations using the DFT/B3LYP/6-31G(d) level of theory. We optimized the energy of the probe and NO product to find the distribution of electron density within aromatic rings. All the calculations were performed with the Gaussian 09W software package.[30] The optimized geometry of the probe (PQPY) and its NO product (PQPY-NO) is shown in **Figure 2.14 A**. Both have a C1point group. The nature of all stationary points for both the free probe and it's NO product was confirmed by carrying out normal mode analysis. All the
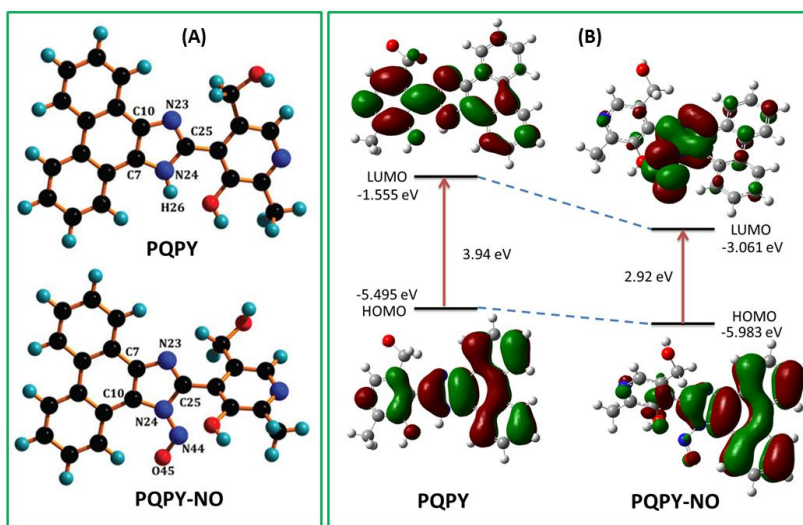
Figure 2.14 A. Optimized geometry of PQPY and the PQPY–NO product. **B.** Frontier molecular orbital of the probe (PQPY) and NO product (PQPY-NO).

frequencies turned out to be positive, which proved the global minima of PQPY and PQPY-NO. The important optimized geometrical parameters of the free PQPY and PQPY-NO are listed in **Table 1** and **Table 2** The highest occupied molecular orbital (HOMO) and the lowest unoccupied molecular orbital (LUMO) energies of the probe and NO product are shown in **Figure 2.14 B**. In the case of the probe as well as the NO product the HOMO electron densities are localized in the 2-(1H-phenanthro[9,10-d]imidazol-2-yl)-prop-2-en-1-ol moiety, whereas LUMO electron clouds reside in 5-hydroxymethyl-6-methylpyridin-3-ol for the probe but on the 1-nitroso-1H-imidazole moiety for the NO product. This delocalization of excited electronic energy to the 1-nitroso-1H-imidazole for the NO product is responsible for enhancing the fluorescence intensity due to the electron withdrawing nature of the –NNO group. The calculated HOMO and LUMO energy gap is found to be 2.92 eV for the NO product, which is lower than that of the calculated HOMO–LUMO gap of the probe (3.94 eV). Therefore, the NO product is more stable than that of the free probe.

Table 1: List of some selected bond lengths of Probe (PQPY) in the ground state calculated at B3LYP Levels. **Table 2:** Some selected geometrical parameters for NO product (PQPY-NO) in the ground state calculated at B3LYP Levels.

Table 1.

Bond Lengths (Å)			
N24-H26	1.429	N23-C25	1.345
C7-N24	1.393	C10-C23	1.384
C25-N24	1.237	C7-C10	1.390
Bond Angles (º)			
N24-C7-C10	105.49	N24-C25-N23	110.36
C25-N23-C10	105.93	C25-N24-N26	122.23

Table 2.

Bond Lengths (Å)			
N24-C25	1.429	N23-C25	1.310
C24-N44	1.393	C10-C23	1.406
N44-O45	1.237	C7-C10	1.390
Bond Angles (º)			
N24-C7-C10	103.33	N24-N44-O45	117.46
C25-N23-C10	106.67	C25-N24-C7	107.19
C25-N24-C44	114.95		

2.3.9 Cell imaging study

In order to assess the ability of PQPY to detect nitric oxide (NO) *in vitro*, it has been further checked for its properties to form a product with NO in living cells. Before that we have explored the cytotoxic effects of PQPY on live HepG2 cells by cell viability assay using MTT **(Figure 2.15 A)**. There was no significant reduction in the tetrazolium salt reflecting a decrease in formazan production for PQPY up to 10μM, thus suggesting that below 10μM ligand concentration would be much more effective for the analysis of its product formation with NO *in vitro*. Around 80% cell viability was observed for PQPY at 5μM, after which the viability of the HepG2 cells decreased. Hence, further experiments were carried out with 5μM of PQPY for treatment. The ligand PQPY showed the absence of intracellular fluorescence in HepG2 cells treated with 5μM of the ligand and incubated for 1 h **(Figure 2.15 B)**; however, a prominent intracellular green fluorescence signal was observed in cells when the HepG2 cells were incubated with 5μM of SNP for 60 min at 37 °C to produce exogenous NO, followed by incubation with 5μM of PQPY. The intracellular fluorescence was found to be prominently
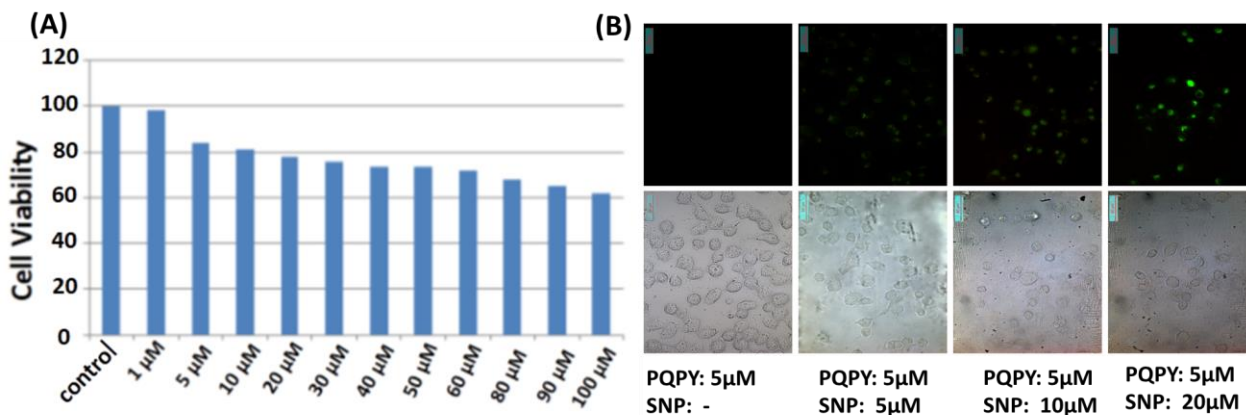
Figure 2.15 A. Percent (%) cell viability of HepG2 cells treated with different concentrations (1–100 μM) of PQPY for 24 hours determined by MTT assay. **B.** The fluorescence images of HepG2 cells were captured (40×) after incubation with 5 μM of PQPY for 60 min at 37 °C, followed by washing thrice with 1× PBS, and incubation with 5 μM, 10 μM and 20 μM of SNP for 60 min at 37 °C followed by incubation with 5 μM of PQPY for 60 min at 37 °C. The fluorescence images show no fluorescence signal by the fluorophore PQPY (5 μM) in the

absence of the NO donor, while the fluorescence gradually increases with higher concentration of the NO donor.

localized in the cytoplasmic region. Keeping the ligand PQPY concentration constant at 5μM and increasing the concentration of NO donor SNP (5μM, 10μM and 20μM), a NO concentration-dependent enhancement in the intracellular green fluorescence is observed, caused by the formation of the product between PQPY and NO. An intense intracellular fluorescence was observed due to the formation of PQPY-NO nearly at 20μM of SNP. Altogether, the present results suggest that the probe with low cytotoxicity and the property of enhanced fluorescence with increasing concentration of intracellular NO can be used for NO detection in biological samples.

2.4 Conclusion

In summary, we have been able to synthesize novel 5-hydroxymethyl-2-methyl-4-(1H-phenanthro[9,10-d]imidazole-2-yl)-pyridin-3-ol (PQPY) in a facile manner as a highly selective turn-on *in vitro* NO probe and characterize it by various spectroscopic techniques. The probe can detect nitric oxide efficiently and selectively in a wide range of physiological pH at room temperature in 70% water. The highly electron withdrawing group –N–N=O drags the electron density from the whole system (PQPY-NO) towards itself converting the probe to a donor–acceptor one giving the credit for intramolecular charge transfer which results in a large fluorescence enhancement. The formation constant $(1.00 \pm 0.2) \times 10^5$ obtained from the titration Supports the stability of the NO product (PQPY-NO). The 78 nM analytical detection limit deduced by the 3σ method reassures the potentiality of the ligand as a NO probe in biological systems. The ligand is also biocompatible due to its solubility in mixed aqueous–organic (water–acetonitrile; 7: 3) solutions and also it has cell permeability and the low cytotoxicity towards living cells magnifying its biological applicability.

References

1. N. S. Bryan and M. B. Grisham, *Free Radicals Biol. Med.*, 2007, **43**, 645–657.

2. D. S. Bredt, *Free Radicals Biol. Med.*, 1999, **31**, 577–596.

3. M. Kelm, *Biochim. Biophys. Acta*, 1999, **1411**, 273–289.

4. B. Brune, S. Dimmeler, L. M. Vedia and E. G. Lapetina, *Life Sci.*, 1994, **54**, 61–70.

5. B. J. Privett, J. H. Shin and M. H. Schoenfisch, *Chem. Soc. Rev.*, 2010, **39**, 1925–1935.

6. W. Hu, D. Boateng, J. Kong and X. Zhang, *Austin J. Biosens. Bioelectron.*, 2015, **1**, 1–9.

7. Y. Gabe, Y. Urano, K. Kikuchi, H. Kojima and T. Nagano, *J. Am. Chem. Soc.*, 2004, **126**, 3357–3367.

8. E. Sasaki, H. Kojima, H. Nishimatsu, Y. Urano, K. Kikuchi, Y. Hirata and T. Nagano, *J. Am. Chem. Soc.*, 2005, **127**, 3684–3685.

9. Y. Yang, S. K. Seidlits, M. M. Adams, V. M. Lynch, C. E. Schmidt, E. V. Anslyn and J. B. Shear, *J. Am. Chem. Soc.*, 2010, **132**, 13114–14116.

10. L. E. McQuade, M. D. Pluth and S. J. Lippard, *Inorg. Chem.*, 2010, **49**, 8025–8033.

11. L. E. McQuade and S. J. Lippard, *Inorg. Chem.*, 2010, **49**, 7464–7471.

12. M. H. Lim and S. J. Lippard, *Inorg. Chem.*, 2004, **43**, 6366–6370.

13. A. Beltrán, M. I. Burguete, D. R. Abánades, S. D. Pérez-Sala, V. Luis and F. Galindo, *Chem. Comm.*, 2014, **50**, 3579–3581.

14. M. H. Lim and S. J. Lippard, *J. Am. Chem. Soc.*, 2005, **127**, 12170–12171.

15. M. H. Lim and S. J. Lippard, *Inorg. Chem.*, 2006, **45**, 8980–8989.

16. C. Sun, W. Shi, Y. Song, W. Chen and H. Ma, *Chem. Commun.*, 2011, **47**, 8638–8640.

17. R. C. Smith, A. G. Tennyson, M. H. Lim and S. J. Lippard, *Org. Lett.*, 2005, **7**, 3573–3575.

18. T. W. Shiue, Y. H. Chen, C. M. Wu, G. Singh, H. Y. Chen, C. H. Hung, W. F. Liaw and Y. M. Wang, *Inorg. Chem.*, 2012, **51**, 5400–5408.

19. H. Kojima, M. Hirotani, N. Nakatsubo, K. Kikuchi, Ys. Urano, T. Higuchi, Y. Hirata and T. Nagano, *Anal. Chem.*, 2001, **73**, 1967–1973.

20. H. Yu, X. Zhang, Y. Xiao, W. Zou, L. Wang and L. Jin, *Anal. Chem.*, 2013, **85**, 7076–7084.

21. X. Dong, C. H. Heo, S. Chen, H. M. Kim and Z. Liu, *Anal. Chem.*, 2014, **86**, 308–311.
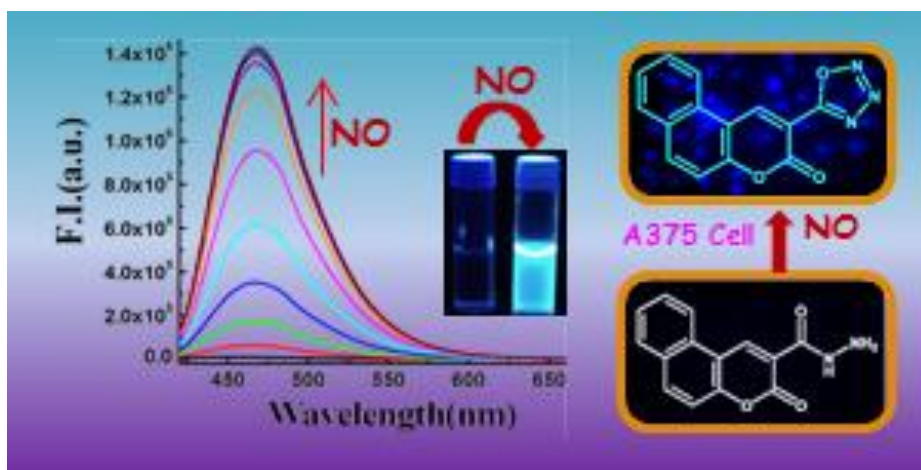
22. A. S. M. Islam, R. Bhowmick, K. Pal, A. Katarkar, K. Chaudhuri and M. Ali, *Inorg. Chem.*, 2017, **56**, 4324–4331.

23. A. J. Beneto, V. Thiagarajanb and A. Siva, *RSC Adv.*, 2015, **5**, 67849.

24. Š. Mesároš, S. Grunfeld, A. Mesárošová, D. Bustin and T. Malinski, *Anal. Chim. Acta*, 1997, **339**, 265–270.

25. A. T. Wrobel, T. C. Johnstone, A. Deliz Liang, S. J. Lippard and P. Rivera-Fuentes, *J. Am. Chem. Soc.*, 2014, **136**, 4697–4705.

26. S. Miyamoto, G. R. Martinez, A. P. B. Martins, M. H. G. Medeiros and P. DiMascio, *J. Am. Chem. Soc.*, 2003, **125**, 4510–4517.

27. Z. Mao, H. Jiang, Z. Li, C. Zhong, W. Zhang and Z. Liu, *Chem. Sci.*,2017, **8**, 4533.

28. A. S. M. Islam, R. Alam, A. Katarkar, K. Chaudhuri and M. Ali, *Analyst*, 2015, **140**, 2979–2983.

29. K. Tsuge, F. DeRosa, M. D. Lim and P. C. Ford, *J. Am. Chem. Soc.*, 2004, **126**, 6564–6565.

30. M. J. Frisch, G. W. Trucks, H. B. Schlegel, G. E. Scuseria, M. A. Robb, J. R. Cheeseman, G. Scalmani, V. Barone, B. Mennucci, G. A. Petersson, H. Nakatsuji, M. Caricato, X. Li, H. P. Hratchian, A. F. Izmaylov, J. Bloino, G. Zheng, J. L. Sonnenberg, M. Hada, M. Ehara, K. Toyota, R. Fukuda, J. Hasegawa, M. Ishida, T. Nakajima, Y. Honda, O. Kitao, H. Nakai, T. Vreven, J. A. Montgomery Jr., J. E. Peralta, F. Ogliaro, M. Bearpark, J. J. Heyd, E. Brothers, K. N. Kudin, V. N. Staroverov, R. Kobayashi, s. J. Normand, K. Raghavachari, A. Rendell, J. C. Burant, S. S. Iyengar, J. Tomasi, M. Cossi, N. Rega, J. M. Millam, M. Klene, J. E. Knox, J. B. Cross, V. Bakken, C. Adamo, J. Jaramillo, R. Gomperts, R. E. Stratmann, O. Yazyev, A. J. Austin, R. Cammi, C. Pomelli, J. W. Ochterski, R. L. Martin, K. Morokuma, V. G. Zakrzewski, G. A. Voth, P. Salvador, J. J. Dannenberg, S. Dapprich, A. D. Daniels, Ö. Farkas, J. B. Foresman, J. V. Ortiz, J. Cioslowski and D. J. Fox, Gaussian 09, revision A.1, Gaussian, Inc., Wallingford, CT, 2009.

CHAPTER 3

A coumarin embedded highly sensitive nitric oxide fluorescent sensor: kinetic assay and bio-imaging applications

Abstract:

Fluorescence spectroscopy is a significant bio-analytical technique for specific detection of nitric oxide (NO) and for broadcasting the *in vitro* and *in vivo* biological activities of this gasotransmitter. Herein, a benzo-coumarin embedded smart molecular probe (BCM) is employed for NO sensing through detailed fluorescence studies in purely aqueous medium. All the spectroscopic analysis and literature reports clearly validate the mechanistic insight of this sensing strategy *i.e.*, the initial formation of 1,2,3,4-oxatriazole on treatment of the probe with NO which finally converted to its carboxylic acid derivative. This oxatriazole formation results in a drastic enhancement in fluorescence intensity due to the photoinduced electron transfer (PET) effect. The kinetic investigation unveils the second and first-order dependency on [NO] and [BCM] respectively. The very low detection limit (16 nM), high fluorescence enhancement (123 fold) in aqueous medium and good formation constant ($K_f = (4.33 \pm 0.48) \times 10^4$ M^{-1}) along with pH invariability, non-cytotoxicity, biocompatibility and cell permeability make this probe a very effective one for tracking intracellular NO.

3.1 Introduction

Over a few decades, biologically abundant reactive nitrogen species (RNS) have played their pivotal role as a cell signaling molecule in the course of diverse physiological and pathological processes.[1] Nitric oxide (NO), a prime member of this class, is a pervasive gasotransmitter and is associated with numerous physiological processes in many bio-organisms. Endogenous production of NO takes place through the conversion of L-arginine to L-citrulline which is catalyzed by eNOS, nNOS and iNOS (NO synthase enzymes).[2] Physiologically, NO (i) functions as a stimulator in vascular smooth muscle relaxation, (ii) prevents infections functioning on the immune system and (iii) serves as a neurotransmitter.[3,4] The pathological impact on malfunctioning of NO homeostasis occurs due to carcinogenesis, neurodegenerative injury, endothelial dysfunction, diabetes, chronic liver inflammation etc.[5,6] Nitric oxide is involved in the modulation of gene transcription and acts as a controlling factor in the translation of m-RNA.[7,8] Considering the unambiguous significance of this bio-regulatory molecule, several methods like chemi-luminescence, electrochemistry, colorimetric assay, electron-paramagnetic resonance spectroscopy, fluorimetric techniques[9–14] etc. are widely used to comprehend the NO biology. But among these analytical methods, the fluorescence technique is considered as the most conducive one for endogenous NO detection owing to its high sensitivity, non-destructive and real-time imaging properties, minimal invasiveness, sophisticated instrumentation and high spatio-temporal resolution.[15–19] Thereby, by exploiting the fluorescence spectroscopic technique plenty of nitric oxide probes have been developed: (i) organic probes, (ii) single-walled nanotube (SWNT) probes, (iii) quantum dot (QD) probes and (iv) metal complex based probes.[20–27] The o-phenylene diamine (OPD) moiety, from the class of organic probes, is one of the promising receptors for NO leading to the formation of triazole with a significant enhancement of fluorescence intensity.[20–33] Though this strategy has attracted the deep attention of researchers, its applications are limited by some serious shortcomings. As for example, (a) the vicinal diamine may suffer from oxidation by various oxidants present in the biological system; (b) the triazole formed in the reaction with NO may show different fluorescence responses at different pH values due to the presence of the secondary –NH group, which may lead to misinterpretation of fluorescence data.[30,31,33] Considering all these limitations, our group has disclosed a novel strategy for nitric oxide sensing by employing quinolone as a fluorophore moiety and acyl

hydrazide as a receptor. Upon treatment with nitric oxide this probe primarily forms 1,2,3,4 oxatriazole causing a substantial enhancement in fluorescence intensity[34] and it finally converted to a carboxylic acid.[34] In our present work, we have used coumarin as a fluorophore which is a planar, rigid and pi-conjugated heterocycle. Over a few decades it was clearly recognized that the active site at 3 position of coumarin with its benzo counterpart is strongly fluorescent.[35] It is a naturally occurring organic compound found in plants and oil, like the oil of cassia, sweet clover, woodruff, tonka beans and lavender. Coumarin derivatives are well recognized due to their numerous activities in pharmaceuticals, insecticides, agrochemicals, fragrances, and polymer sciences and they are also identified as important organic fluorescent materials.[36] It is also used in the treatment of burns, brucellosis, rheumatic disease etc.[37] In respect of photophysical activities, coumarin and its derivatives exhibit high photostability, easy synthesis, an extended spectral range and good solubility.[38–40] So, considering all these significances, we developed our pioneering strategy by using a coumarin fluorophore joined with the benzo-counterpart which is synthesized by the well-known Knoevenagel condensation followed by hydrazination. Herein, a relevant study to comprehend the selectivity and sensitivity of BCM towards NO along with a plausible mechanism has been delineated by a concentration and time dependent kinetic studies. We have also performed a detailed cell imaging and theoretical studies. A very high sensitivity to nitric oxide along with a 123 fold fluorescence enhancement in purely aqueous medium at physiological pH and a very low detection limit (16 nM) qualify the efficacy of the probe for intracellular NO detection.

3.2 Experimental section

3.2.1 Materials

The reagents like 2-hydroxy-1-naphthaldehyde, diethyl-malonate, piperidine, glacial acetic acid, hydrazine hydrate are of reagent grade and purchased from Sigma Aldrich. The sodium salts of anions, the salts of metal ions (Pb^{2+}, Mn^{2+}, Co^{2+}, Ni^{2+}, Zn^{2+}, Cu^{2+}, Al^{3+}, Hg^{2+}, Mg^{2+}, Fe^{3+}, La^{3+}, Cr^{3+} and Cd^{2+}) and biologically reactive species (H_2O_2, O^{2-}, TEMPO radical, NO_3^-, NO_2^-, ClO^-, AA, NO^+, DEA-NONOate (sodium salt) were obtained either from Sigma-Aldrich or from other commercial suppliers and used without further purification. Solvents like DMF, MeCN etc., (Merck, India) were of reagent grade and dried using standard methods.

3.2.2 Synthesis of ligand

The ligand 3-oxo-3H-benzo[f]chromene-2-carboxylic acid hydrazide (designated as BCM) was synthesized by two step easy procedures.

Step-1: synthesis of 3-oxo-3H-benzo[f]chromene-2-carboxylic acid ethyl ester (L1)

2-Hydroxy-1-naphthaldehyde (10 mmol, 1.72 g) and di-ethyl malonate (20 mmol, 3.2 g) are mixed in a round bottom flask in 20 ml ethanol under heating and stirring conditions in the presence of 1 ml piperidine and 2 drops of glacial acetic acid. This reflux was continued for 6 h. After cooling at room temperature, the precipitate was filtered. After washing it with the mix solvent (hexane and ethyl acetate) a light yellow colour solid was obtained and characterized by ^{1}H NMR **(Figure 3.1)** and ^{13}C NMR **(Figure 3.2)**.^{1}H NMR (in DMSO-d$_6$) (δ, ppm): 9.24 (d, 1H, –CH), 8.50–8.47 (m, 1H, –ArH), 8.26–8.23(1H, m, –ArH), 8.02 (1H, d, –ArH), 7.75–7.72 (1H, m, –ArH), 7.63–7.60 (1H, m, –ArH), 7.53–7.50 (1H, m, –ArH), 4.34 (q, 2H,–CH$_2$), 1.37 (t, 3H, –CH$_3$). ^{13}C NMR (in DMSO-d$_6$) (δ, ppm):162.8, 155.9, 155.0, 143.7, 135.9, 129.6, 128.9, 126.3, 122.0, 116.4, 111.7, 61.2, 14.0.

Step-2: synthesis of 3-oxo-3H-benzo[f]chromene-2-carboxylic acid hydrazide (BCM)

The compound obtained from step-1 was dissolved in 20 ml of ethanol (5 mmol, 1.34 g) and hydrazine hydrate was added in an equimolar ratio (5 mmol) under refluxing conditions for 6 h. A yellow solid was formed during the reaction. The product BCM was collected and analyzed by ^{1}H NMR **(Figure 3.3)**, ^{13}C NMR **(Figure 3.4)** and mass spectroscopy **(Figure 3.5)**. ESI-MS+ (m/z): 277 (BCM + Na$^+$), ^{1}H NMR (in DMSO-d$_6$) (δ, ppm): 9.68 (1H, S, –CH), 9.39 (1H, S, –NH), 8.58 (1H, d,–ArH), 8.31 (1H, d, –ArH), 8.09 (1H, d, –ArH), 7.79 (1H, t,–ArH), 7.69–7.63 (2H, m, –ArH), 4.79 (2H, m, –NH2). ^{13}C NMR (in DMSO-d$_6$) (δ, ppm): 160.2, 159.7, 154.0, 141.7, 135.4, 129.9, 128.9, 128.8, 126.5, 122.2, 117.5, 116.3, 112.6.

3.2.3 Physical instrumentation and experimental methods

For analysis, the IR spectra of the compound within 400-4000 cm^{-1} has been obtained using IR 750 series-II FTIR (Nickolet Magna) spectrophotometer on solid KBr discs. ^{1}H and ^{13}C NMR

spectra were recorded taking solvent DMSO-d_6 in a Bruker 300 MHz and 400 MHz instrument using trimethylsilane ($\delta = 0$) as an internal standard. To record ESI-MS+ (m/z) spectra the mass spectrometer having Model: QTOF Micro YA263 was used. pH was maintained through-out the study using a digital pH meter (Model: Systronics 335, India) in the pH range 2–11 which was already calibrated using buffers of pH 4, 7 and 10. For all the fluorescence studies, a PTI (Model QM-40) spectrofluorimeter was used and UV−Vis spectra were recorded on an Agilent 8453 Diode-array spectrophotometer.

3.2.4 Kinetic Studies

We have performed the kinetic studies of NO detection maintaining the pseudo-first order conditions taking fixed 5 μM BCM (minor component) and varying the NO concentration in the range 20 μM and 100 μM at pH 7.0, at 15 °C. The rate of the reaction also depends on the [BCM] which is evaluated keeping NO (5μM) as minor component. The plot of logk_{obs} vs. log[BCM] and logk_{obs} vs. log[NO] shows about the first order and second order dependency of reaction upon [BCM] and [NO] respectively.

3.2.5 Stock solution preparation for photophysical studies

The stock solution of the probe BCM was prepared in a 10 ml of volumetric flux of 1.0×10^{-3} M in minimum DMF adjusted with CH_3CN. For Nitric Oxide solution preparation, Nitric Oxide gas (purified previously by passing through solid NaOH pellets) was purged for 15 min in a sealed vial containing deoxygenated deionized water.[41] This solution gives the NO concentration 1.74×10^{-3} M. For nitroxyl (HNO), Angeli's salt was taken.[42] By adopting the reported literature, ·OH and ONOO⁻ solutions were prepared.[43] The solutions of different cations, anions and biological species were prepared in H_2O. Throughout the experiments, a 10.0 mM HEPES buffer was taken maintaining pH 7.0 and ionic strength at 0.10 M (NaCl). In this work, 20 μM of the probe BCM, was added in a 2.5 ml of the 10.0 mM HEPES buffer upon which, nitric oxide solution (~40 μM) was added incrementally in a regular time interval and the fluorescence spectra were recorded in each case with slits 2 X 2 nm, $\lambda_{ex} = 410$ nm.

3.2.6 Calculation of Detection Limit (LOD)

For the determination of analytical limit of detection, we have adapted the 3σ method, narrated below:

$$LOD = 3 \times S_d/S$$

S_d denotes the standard deviation obtained from the intercept of the plot of fluorescence intensity (F.I.) vs. [BCM] where, S represents the slope found from the linear plot of F.I. vs. [NO].

3.2.7 Computational Details

For theoretical investigation we have performed the computational data analysis by DFT method [44] which is incorporated with the conductor-like polarizable continuum model (CPCM).[45-47] In this study, the Becke's hybrid function[48] with the Lee-Yang-Parr (LYP) correlation function[49] are also utilized. To get the fully optimized geometry of BCM and BCM-NO we have taken 6-31G(d,p) basis set and for electron density plots Gauss View 5.1 software was used. The absorption spectra of both the compound were also calculated by TD-DFT method using the 6-31G(d,p) basis set. All the related calculations were made applying Gaussian 09W software package[50] and for the calculation of molecular orbital contributions we have used Gauss Sum 2.1 programe.[51]

3.2.8 Cell culture and Cytotoxicity Assay

Human cancer cell line A375 (malignant skin melanoma) and Raw 264.7 murine macrophages cells were grown in DMEM (Dulbecco's modified Eagle's) medium furnished with 10% FBS and 1% antibiotic at 37 °C with 5% CO_2.[52] We have investigated the cell viability of the probe BCM in A375 and Raw 264.7 cells with the gradually incremented concentration (ranging from 10−100 μM/mL) of BCM for 24 h by the MTT assay.[53]

3.2.9 Cell Incubation, Imaging and Flow Cytometry Analysis

Cell imaging for exogenous and endogenous NO monitoring were carried out by exploiting reported method[52, 53] with A375 and Raw 264.7 cells respectively. Exogenously, A375 cells were incubated on a glass coverslip, followed by the treatment with DEA-NONOate (NO donor, 2 μM, 5 μM and 10 μM) for 30 min. Then the coverslip was washed with 1X PBS for three times and afterwards treated with BCM for 30 min. Endogenously, Raw 264.7 cells were co-stimulated with or without LPS (1.0 mg/ mL) and IFN-γ (1000 U/mL) for 6h and furthermore incubated with BCM (5 μM) for 30 min and with or without NO scavenger PTIO (2-phenyl-4,4,5,5-tetramethylimidazoline-1-oxyl 3-oxide). The cellular fluorescence was accompanied only through NO generation which was assured by NO scavenger PTIO (2- Phenyl-4,4,5,5-tetramethylimidazoline-1-oxyl-3-oxide) treatment. Then the live cell imaging by using fluorescence microscope (Carl Zeiss, Germany) was furnished. Next, 1×106 Raw 264.7 cells were seeded in a T25 flask (BD Falcon) maintaining 37 °C. Again the cells were incubated with our probe BCM for 30 min, afterwards, co-stimulated with or without LPS and IFN-γ for 6 h and also taking the NO scavenger PTIO (2-phenyl-4,4,5,5-tetramethylimidazoline-1-oxyl 3- oxide) live cell images were collected. Nextly, treated and untreated control cells were washed with icecold $1\times$ PBS which was resuspended in 500 μL of binding buffer and the flow cytometric analysis was carried out with FACS LSR (Becton Dickinson). The Flow cytometry analysis was performed by using Flowing Software, version 2.5.1.

3.3 Results and discussion

Scheme 3.1 displays a two steps synthetic pathway for the synthesis of 3-oxo-3H-benzo[f]chromene-2-carboxylic acid hydrazide (hereafter, designated as BCM). The first step is a very well-known Knoevenagel condensation between 2-hydroxy napthaldehyde and di-ethyl malonate in the presence of piperidine and glacial acetic acid under refluxing conditions. After 8 h, the reaction mixture is cooled to room temperature whereupon a pure product (L^1) was formed which was collected by filtration and well analyzed by ^{1}H NMR **(Figure 3.1)** and ^{13}C NMR **(Figure 3.2).** The second step comprises the treatment of the corresponding ester with hydrazine
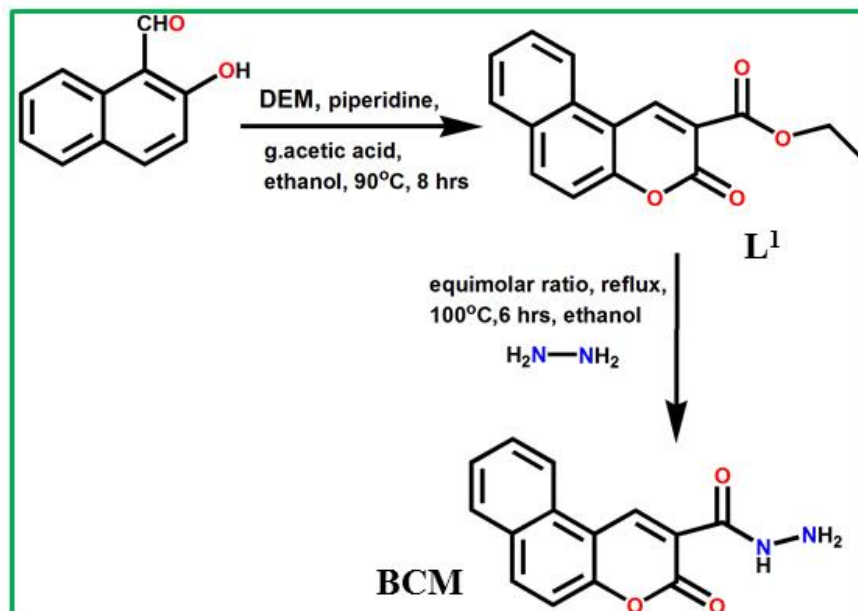
Scheme 3.1 Pathway for the synthesis of probe BCM.
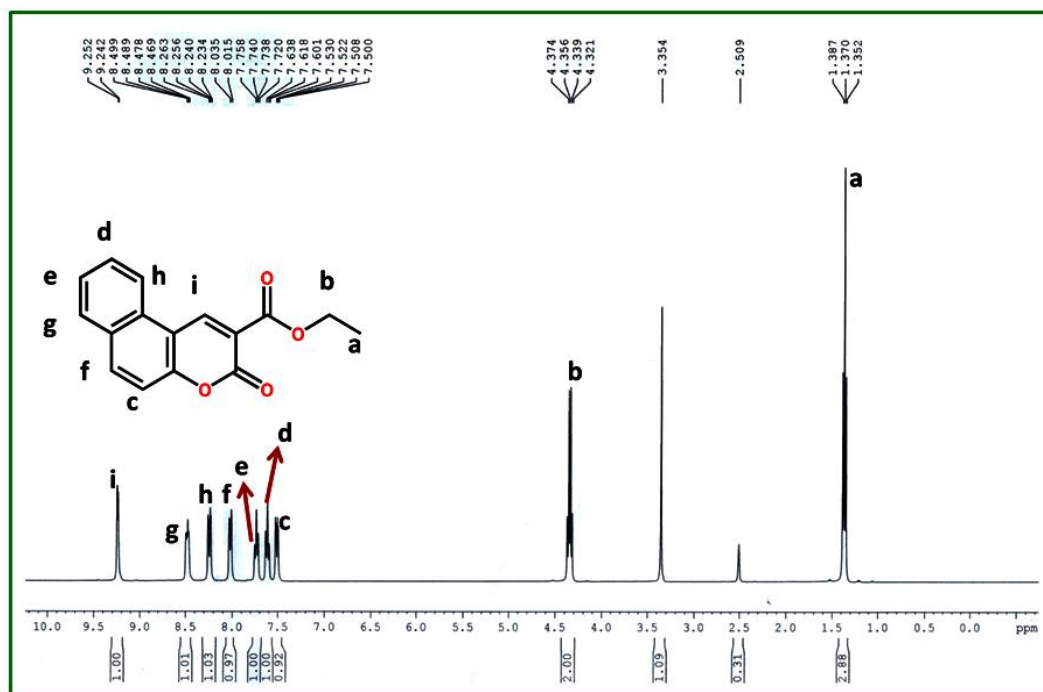
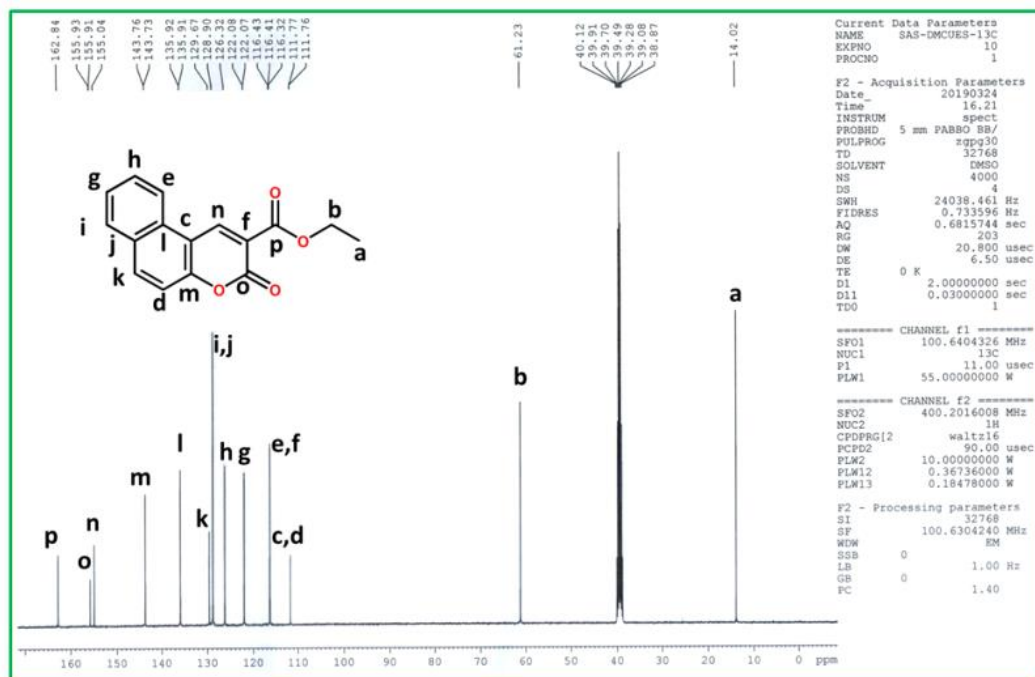**Figure 3.1** ^{1}H NMR of L^1.
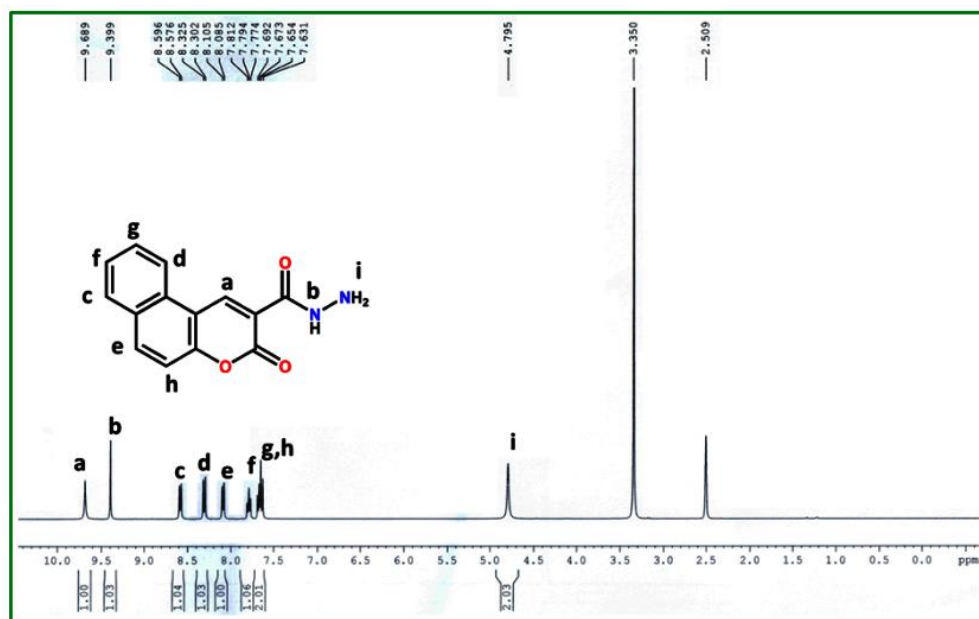
hydrate in an equimolar ratio. The targeted fluorescent probe was well characterized by common spectroscopic studies, i.e., ^{1}H NMR **(Figure 3.3),** ^{13}C NMR **(Figure 3.4),** mass spectroscopy

(Figure 3.5), and FTIR **(Figure 3.6).** The receptor exhibits very high affinity and selectivity towards NO in aqueous medium.
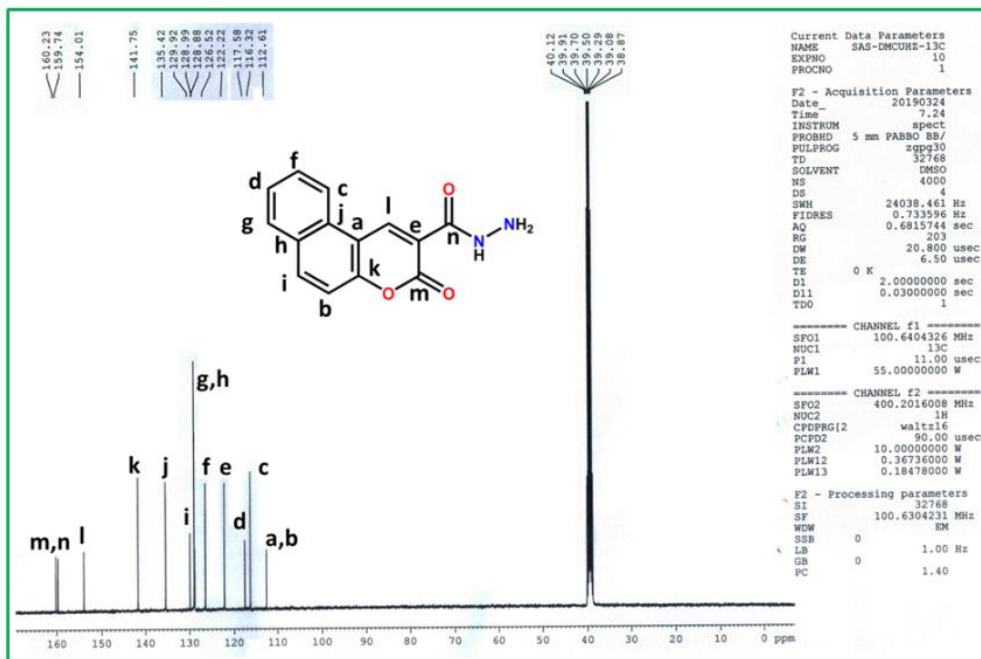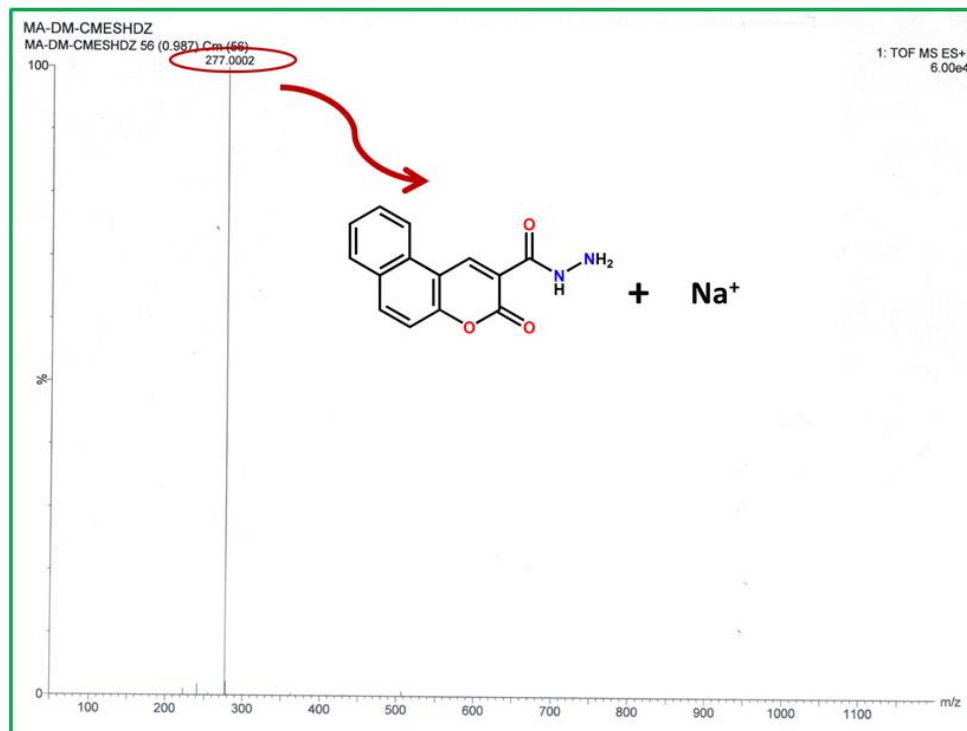

Figure 3.2 ^{13}C NMR of L^1.

Figure 3.3 ^{1}H NMR of BCM.

Figure 3.4 ^{13}C NMR of BCM.

Figure 3.5 Mass spectrum of BCM.
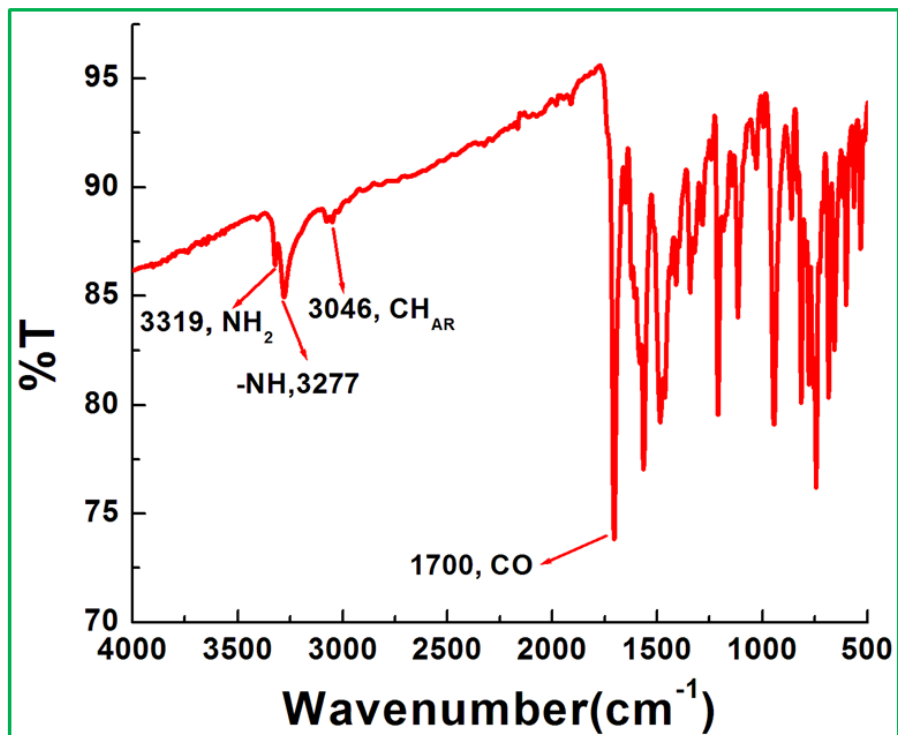
Figure 3.6 IR spectrum of BCM.

3.3.1 Photophysical response of BCM towards NO

The fluorescence properties of the probe BCM and affinity towards nitric oxide were analyzed by performing fluorescence titration, **(Figure 3.7)**. For this experiment, a fixed concentration (20 µM) of BCM was added into a cuvette containing 2.5 ml of aqueous HEPES buffer at 25 °C. Then, the NO solution was added progressively in the concentration range from 0 to 40 µM.
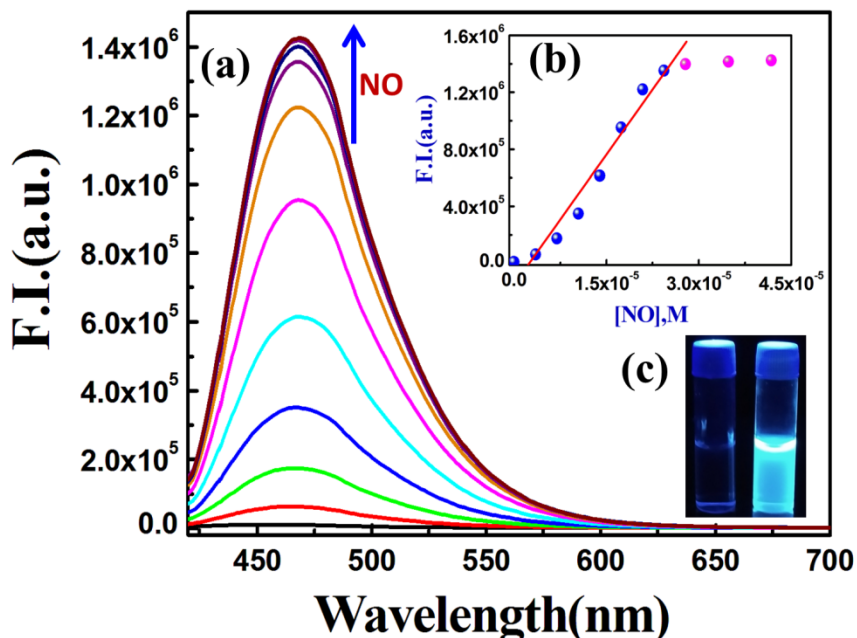
Figure 3.7 (a) Fluorescence emission spectra recorded by taking only fixed 20 μM BCM and also gradual addition of NO (0–40 μM) at 25 °C in 10 mM HEPES buffer at pH 7.0, λ_{ex} = 410 nm and λ_{em} = 470 nm. (b) Linear plot of F.I. vs. [NO]. (c) The image of probe BCM (left) and NO treated product (right) exposed to UV light.

BCM alone exhibits a very weak fluorescence in aqueous HEPES buffer, whereas gradual addition of NO causes a steady generation of fluorescence intensity resulting in an~123 fold enhancement at λ_{em} ~470 nm (λ_{ex} = 410 nm). To determine the apparent formation constant we have carried out a fluorescence titration experiment and a plot of F.I. vs. [NO] shows an excellent linearity of the curve up to 25 μM after which the plot gets saturated (maximum NO 40 μM). The linear part was easily solved by utilizing eqn. (1) [54] under the condition $1 \gg cx^n$ and n = 1.

$$y = \frac{(a+b \times c \times x^n)}{1+c \times x^n} \tag{1}$$

Where, parameters a and b denote the F.I. of the probe in the absence and presence of excess NO respectively, and c is the formation constant designated as K_f. The slope ($b \times c$) obtained from the curve gives c = K_f = (4.33 ± 0.48) × 10^4 M^{-1} (using b = F.I. in the presence of a large excess of NO).

3.3.2 Mechanistic view of fluorescence sensing of the receptor BCM towards NO

To gain insight into the mechanism which is responsible for fluorescence enhancement, we collected the product of the reaction between BCM and NO. For this purpose, BCM was dissolved (1 mmol, 0.254 g) in a minimum volume of dichloromethane (DCM) and finally with 20 ml acetonitrile under aerobic conditions. Then nitric oxide gas was bubbled through the probe solution for 15 minutes. A vivid fluorescence was noticed throughout the solution. The solvent was evaporated under pressure. A brown solid was collected and further purified by recrystallization in ethanol. The pure crystalline compound was filtered and characterized by ESI-MS$^+$ **(Figure 3.8),** ^{1}H NMR **(Figure 3.9)** and IR spectroscopy **(Figure 3.10).**
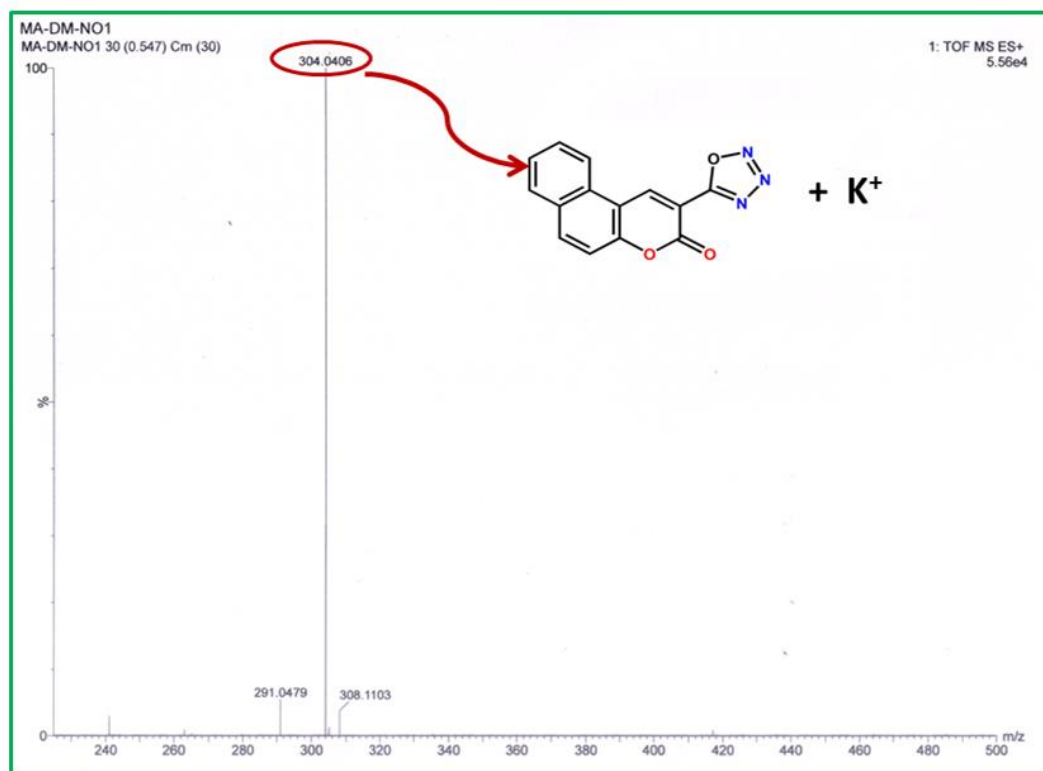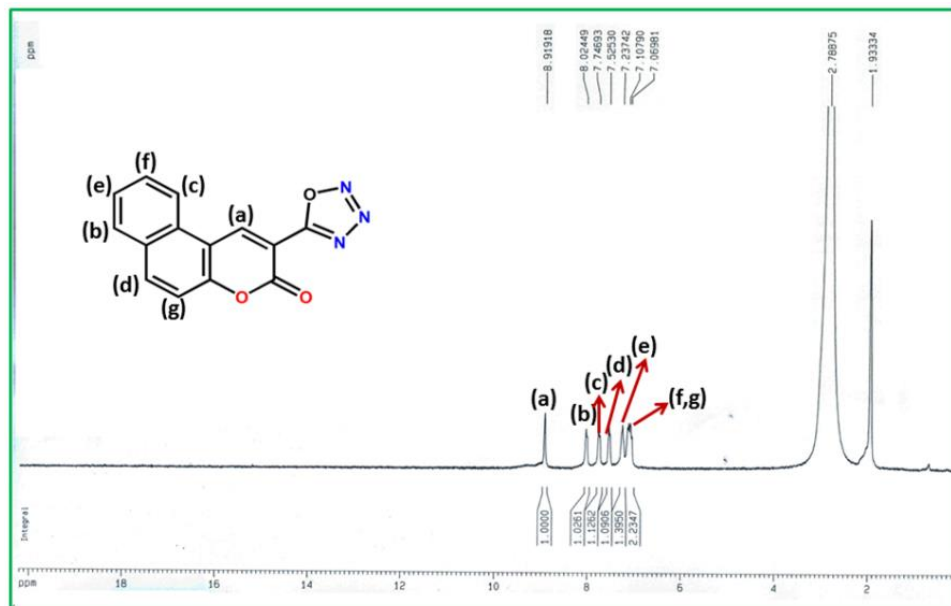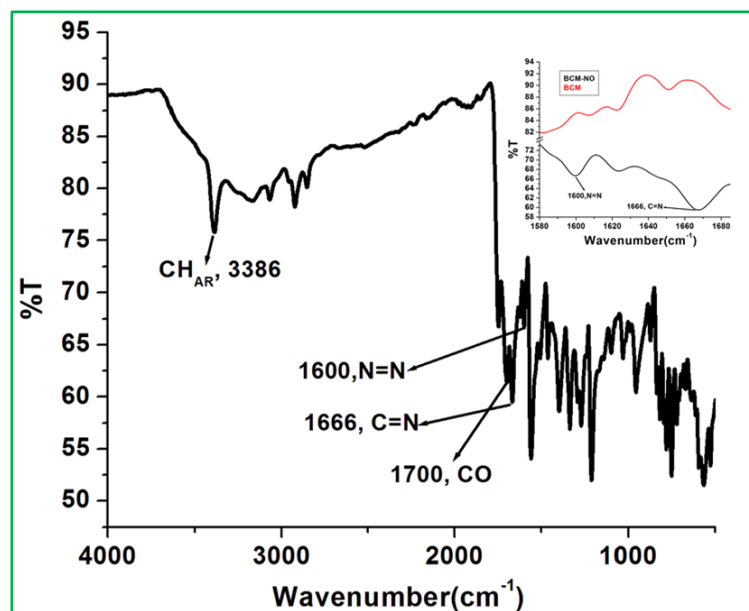

Figure 3.8 Mass spectrum of BCM-NO.

Figure 3.9 ^{1}H NMR spectrum of BCM-NO in MeCN (minimum DMSO-d_6).


Figure 3.10 IR of BCM-NO.

The ESI-MS^{+} spectrum **(Figure 3.8)** shows a peak at 304.0406 (1,2,3,4-oxatriazole+ K^{+}) suggesting the generation of 1,2,3,4-oxatriazole (BCM-NO) which was further ensured by the disappearance of –NH (9.39 ppm) and –NH$_2$ (4.79 ppm) peaks in the ^{1}H NMR spectra **(Figure 3.9)**. The generation of the IR peak at 1600 cm^{-1} (–N=N) and 1666 cm^{-1} (–C=N) also

strengthens the formation of the oxatriazole moiety **(Figure 3.10).** The predicted mechanism is outlined in **Scheme 3.2**, where NO first reacts with O_2 to generate N_2O_3 under aerobic conditions
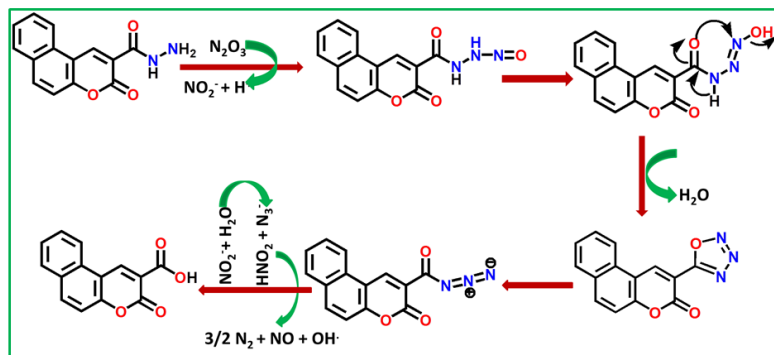
Scheme 3.2 Possible reaction mechanism for the reaction between BCM and NO.

which nitrosylates $-NH_2$ of BCM, to generate $-NH-NO$ which ultimately generates 1,2,3,4-oxatriazole (BCM-NO) as a stable product. The formation of the electron deficient oxatriazole moiety causes a large enhancement in fluorescence intensity at λ_{em} = 470 nm. It is interesting to note that the formed oxatriazole is finally transformed to a carboxylic acid through the formation of azide after keeping it in
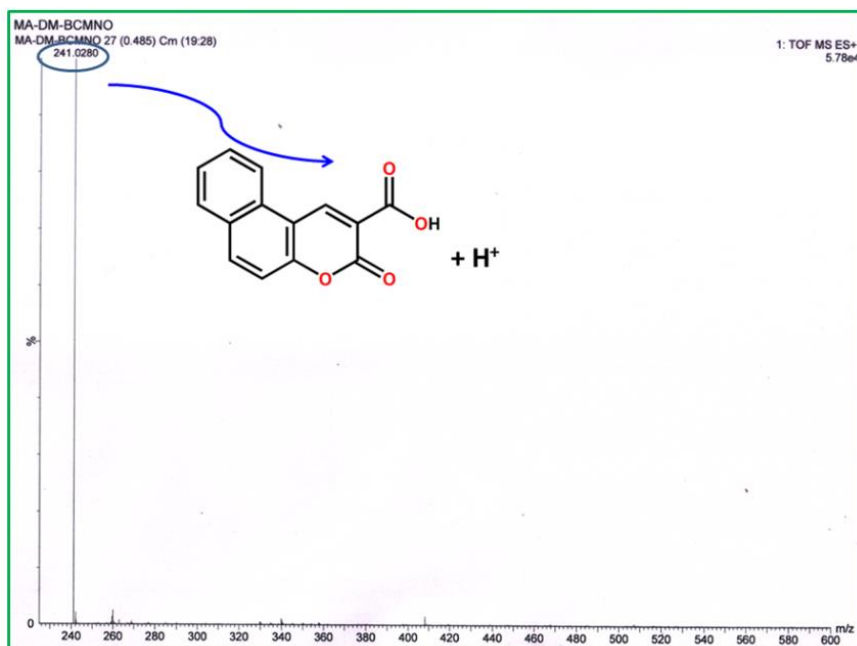
Figure 3.11 Mass spectrum of BCM-NO after long time (acid product).

solution for a long time and was ensured from the mass spectra (**Figure 3.11**) and ^{1}H NMR spectrum (**Figure 3.12**). From the electronic point of view the main-stream mechanism for NO sensing by OPD based probes is based upon the PET block process.[55–57] Very recently; our group
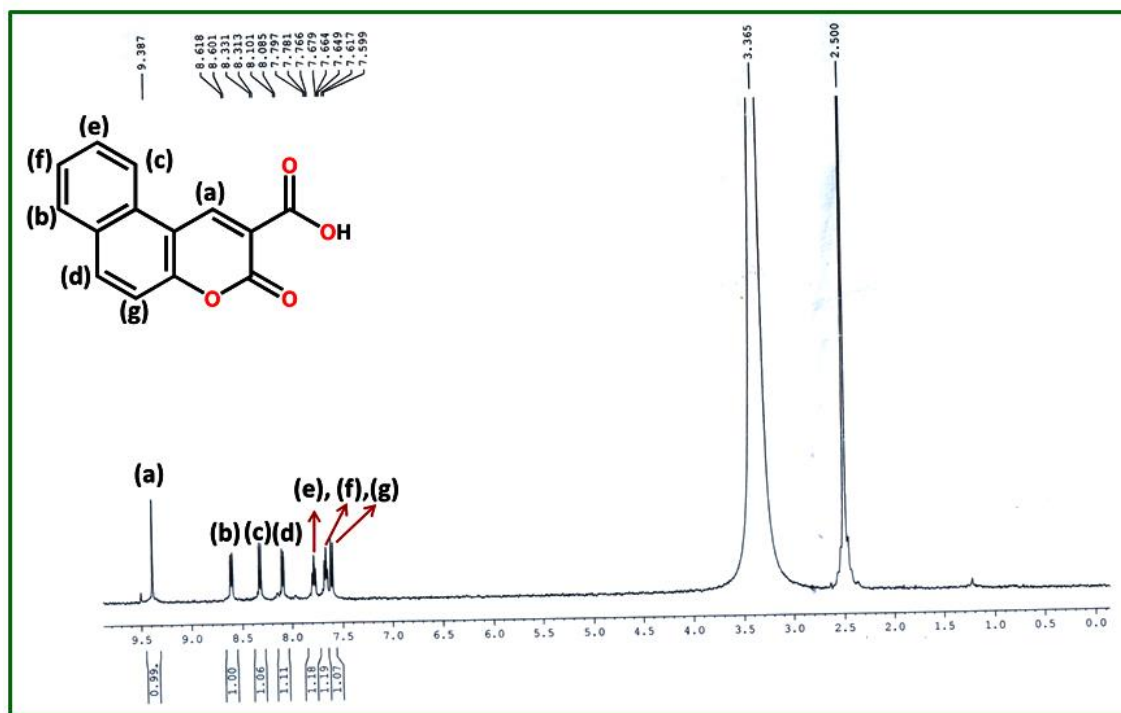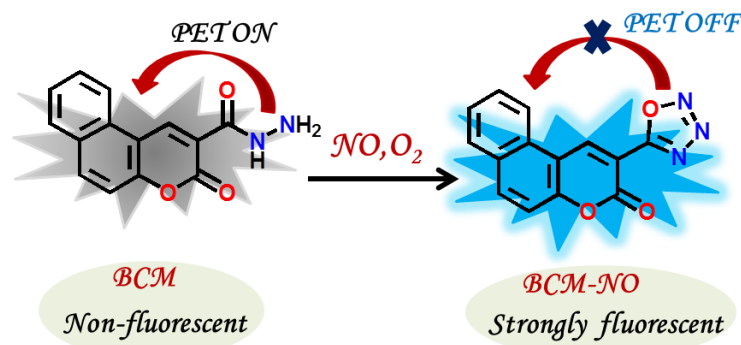

Figure 3.12 ^{1}H NMR spectrum of BCM-NO after long time (acid product) in DMSO-d_6.

reported a quinolone based NO sensor containing the acyl hydrazide moiety where the PET effect[34] was operative. In the current report, we propose that the PET-ON mechanism due to electron push from the hydrazide part to the coumarin fluorophore makes the probe BCM weakly


Scheme 3.3. Presentation of PET effect responsible for NO sensing.

fluorescent. However, upon reaction with NO a remarkable fluorescence enhancement has been perceived which may arise due to the generation of the electron deficient 1,2,3,4-oxatriazole moiety that restricts the above PET-ON process **(Scheme 3.3).**

3.3.3 Time dependent reaction of BCM with NO, a kinetic approach

To ensure a clear view of the operative mechanism of the reaction between BCM and NO, we have thoroughly performed kinetic studies at pH 7.0 (10 mM HEPES buffer, 0.10 M NaCl), 15 °C, under pseudo-first-order conditions using the fluorometric technique (**Figure 3.13**). In this study, we have taken a fixed concentration of BCM (5 µM) and variable [NO] (20–100 µM). The
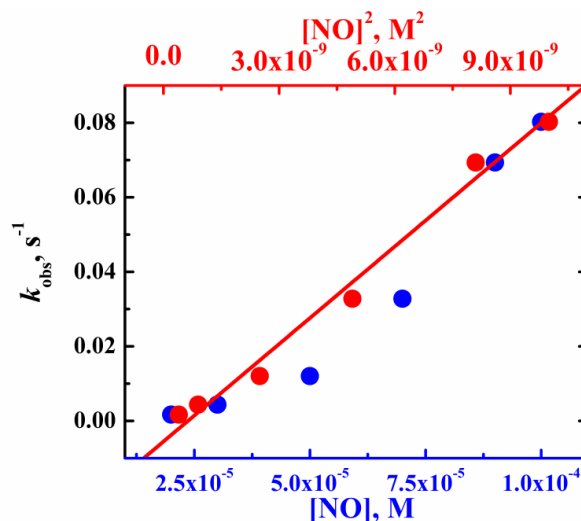

Figure 3.13 The k_{obs} vs. [NO] plot gives an upward curvature (blue solid circles), while a plot of k_{obs} vs. $[NO]^2$ gives a straight line (red solid circles). Experimental conditions are: [BCM] = 5 µM and [NO] = (20–100) µM, temperature = 15 °C in 10 mM HEPES buffer (pH = 7.0, NaCl = 0.10M). All the data were collected using the fluorescence technique.

kinetic traces at 470 nm unveil single exponential growth curves assigning the first-order dependency of the reaction rate on [BCM]. The time dependent fluorescence study also shows that the fluorescence intensities at 470 nm increase with time and reach a plateau within ~5 min
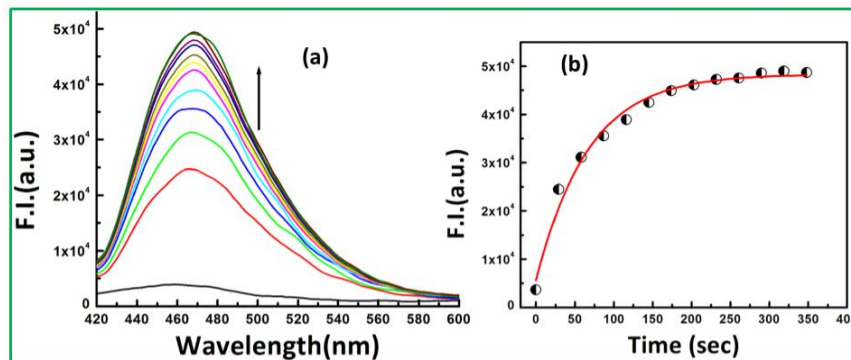
Figure 3.14 (a) Time-dependent fluorescence response and (b) corresponding growth curve for [BCM] = 5.0 µM and [NO] = 5.0 µM at 15 °C.

(Figure 3.14). The pseudo-first-order rate constants (k_{obs}) obtained from the growth curves have been plotted against [NO], which yields a nonlinear upward curvature. However, a plot of k_{obs} vs. [NO]^2 displayed a well fitted straight line which delineates the second-order dependency upon [NO] **(Figure 3.15)**. The log(k_{obs}) vs. log[NO] plot furnishes a straight line with a slope = (2.42 ± 0.08) with R = 0.997 which also supports the second order kinetics with respect to [NO]
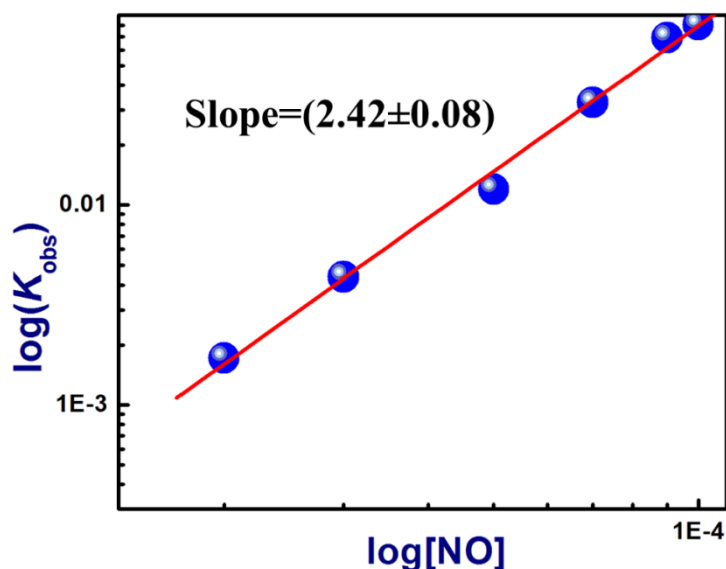
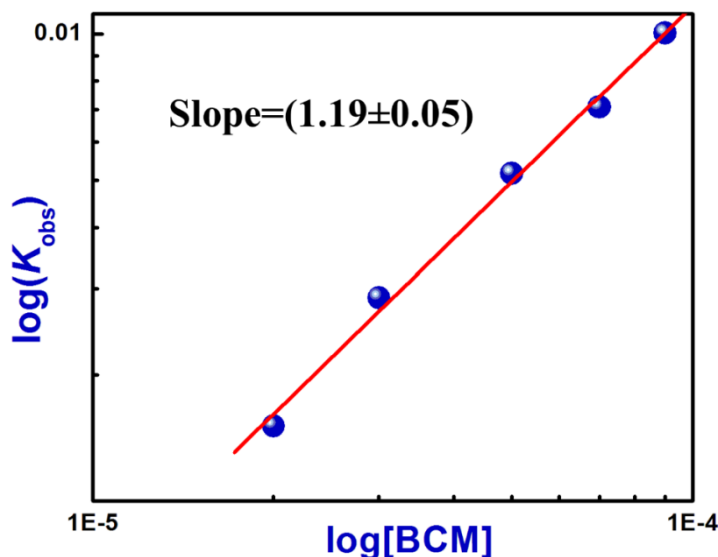**Figure 3.15**. Plot of log(k_{obs}) vs. log [NO].

(Figure 3.15). We have accomplished a second experiment to evaluate the dependency of rate upon [BCM] taking a fixed 5 µM [NO] with variable [BCM] in the range between 20 and 100
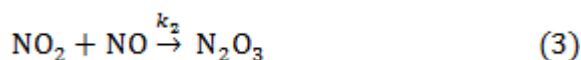
µM. Here, a plot of log(k_{obs}) vs. log[BCM] clearly demonstrates a first-order dependence on [BCM] with slope = (1.19 ±0.05) **(Figure 3.16)** and R = 0.997.

Figure 3.16 Plot of log(k_{obs}) vs. log [BCM].

Here, a provisional reaction sequence is formulated as follows:
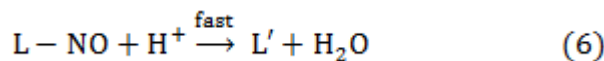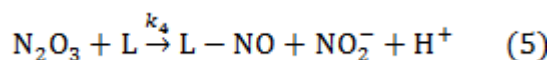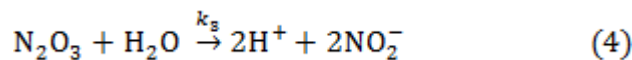
$$2NO + O_2 \xrightarrow{k_1} 2NO_2 \qquad (2)$$

$$NO_2 + NO \xrightarrow{k_2} N_2O_3 \qquad (3)$$

$$N_2O_3 + H_2O \xrightarrow{k_3} 2H^+ + 2NO_2^- \qquad (4)$$

$$N_2O_3 + L \xrightarrow{k_4} L-NO + NO_2^- + H^+ \qquad (5)$$

$$L-NO + H^+ \xrightarrow{fast} L' + H_2O \qquad (6)$$

The above reaction sequence clearly demonstrates that NO interacts firstly with its oxidized product NO_2 to form N_2O_3 that acts as a NO^+ donor in the next step under aerobic conditions. Then the formed N_2O_3 nitrosylates the amine hydrazide to generate L-NO which results in the synthesis of a closed ring 1,2,3,4-oxatriazole moiety in a fast step (**Scheme 3.2**). We have surveyed the literature to afford the rate constants of the above-mentioned reactions as: $k_1 = 6.33 \times 10^6$ M^{-2} s^{-1},[58] $k_2 = 1.1 \times 10^9$ $M^{-1}s^{-1}$,[59] and $k_3[H_2O] = 1.6 \times 10^3$ s^{-1}.[60] With the knowledge of these rate constants we can stipulate that NO_2 and N_2O_3 are present in very negligible amount as reactive intermediates. By applying a steady-state approximation eqn. (7) can be attained for the formation of L′ (BCM-NO).

$$\frac{d[L']}{dt} = \frac{k_1 k_4 [L]}{2(k_3[H_2O]) + k_4[L])}[NO]_t^2[O_2]_t \qquad (7)$$

From the previously illustrated kinetic studies, it was found that the reaction kinetics follows the second and first order dependence with respect to [NO] and [L] ([BCM]) respectively which lead us to make an assumption that $k_3[H_2O] \gg k_4[L]$. Now eqn. (7) reduces to eqn. (8).

$$\frac{d[L']}{dt} = \frac{k_1 k_4 [L]}{2 k_3[H_2O]}[NO]_t^2[O_2]_t \qquad (8)$$

As the kinetics was performed maintaining the pseudo first-order conditions, taking L (BCM) as a minor component (the dissolved $[O_2]_t = 2.5$ mM at 25 °C) eqn (8) reduces to eqn(9), where k_{obs} = {d[L']/dt}/[L]

$$k_{obs} = k'[NO]_t^2 \qquad (9)$$

taking,

$$k' = \frac{k_1 k_4}{2 k_3[H_2O]}[O_2]_t \qquad (10)$$

The value of k_4 is evaluated by utilizing the previously observed values of k_1 and $k_3[H_2O]$ mentioned above along with $k' = 8.60 \times 10^6$ M^{-2} s^{-1}, achieved from the linear plot of k_{obs} vs. $[NO]^2$ at 15 °C. From all of these data the value of k_4 was estimated to be 17.3×10^5 M^{-2} s^{-1} and found to be very much similar in order to some analogous reactions of N_2O_3 as follows: HSA $(0.3 \times 10^5$ M^{-1} s$^{-1})$, N-acetyl cysteine $(1.5 \times 10^5$ M^{-1} s$^{-1})$, GSH $(2.9 \times 10^5$ M^{-1} s$^{-1})$, Cys $(2.6 \times 10^5$ M^{-1} s$^{-1})$, and BSA $(0.06 \times 10^5$ M^{-1} s$^{-1})$. Interestingly, this result is also in accord with our reported works.[34, 53]

3.3.4 Limit of detection

We have also performed a study to evaluate the detection limit of NO by BCM which is revealed to be very low ~16 nM **(Figure 3.17)** making the probe very sensitive towards NO in macrophase cultures,[61] where nitric oxide is present in the micromolar to nanomolar range. So the concerned NO probe (BCM) is highly applicable for monitoring NO quantitatively in these cell types.
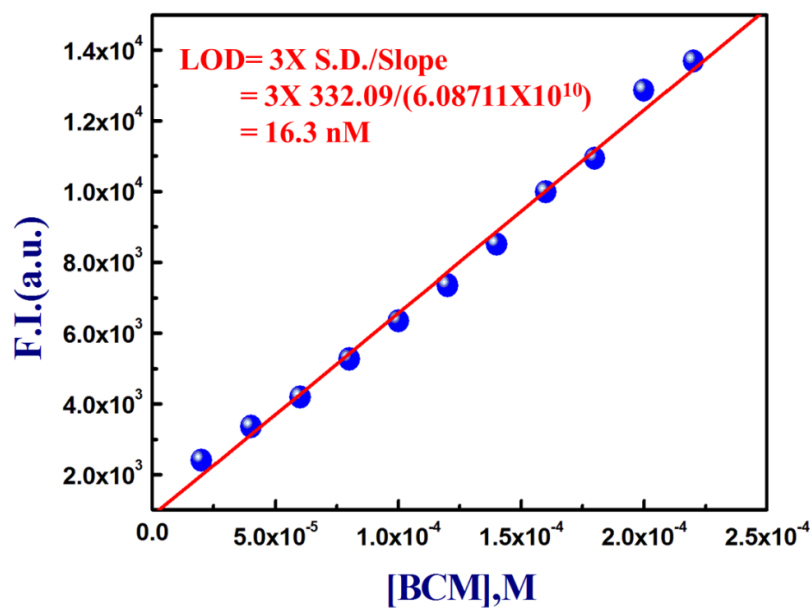
Figure 3.17 LOD of BCM + NO.

3.3.5 pH stability

To be an efficient fluorescent probe, it should show pH tolerance in the physiological range of pH so that it is easily applicable in bio-organisms. For this purpose we have assessed the pH effect on the photophysical behavior of BCM in the absence and presence of excess NO. **(Figure 3.18)** shows a very high fluorescence intensity of the probe and it's NO treated product in a low pH range (2–3). Probably the PET based probe BCM, due to the presence of an electron donor group (–NH-NH$_2$) is converted to its protonated form which would block the PET process generating the fluorescence intensity at a lower pH range. In the pH range 4–8 the probe shows very weak fluorescence, however on treatment with NO it displays a drastic enhancement in fluorescence intensity due to the oxatriazole formation. Moreover, at alkaline pH (>8) the fluorescence intensity of the NO treated product is inhibited likely due to the rapid decomposition of N$_2$O$_3$ **(reaction 4)**, formed in the reaction of NO$_2$ and NO **(reaction 3)** causing the availability of smaller and smaller amounts of reactive species (N$_2$O$_3$) towards the probe BCM **(reaction 5)**. Overall the pH study displays the well applicability of the probe at biological pH for tracing nitric oxide.
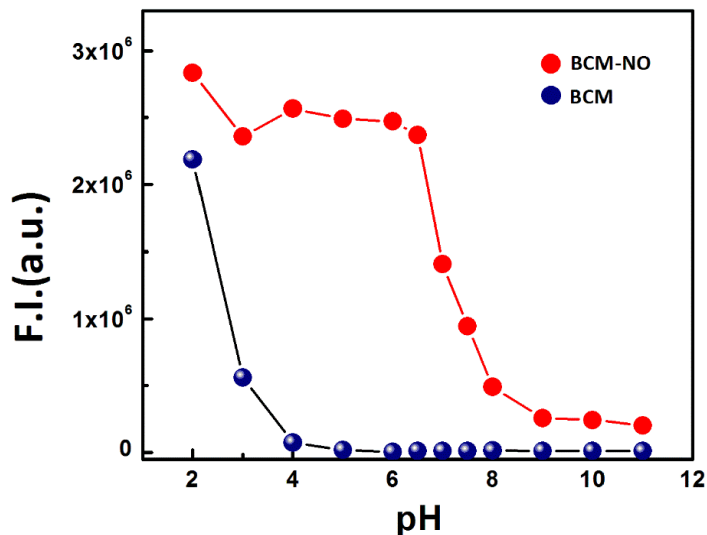
Figure 3.18 pH dependent NO detection by BCM at 470 nm λ_{ex} = 410 nm at 25 °C in 10 mM HEPES buffer.

3.3.6 Analyte selectivity experiment

The selectivity of a fluorescent probe towards a particular analyte is ensured by providing an appropriate binding site and some special chemical properties. Herein, the reactivity assay of probe BCM towards NO was conducted by using a broad array of putative interfering species like reactive species, important metal ions, and anions in 10 mM HEPES buffer, at 25 °C at pH 7.0. **(Figure 3.19)** clearly show that BCM is silent in fluorescence response towards essential metal ions and anions. Likewise, the selectivity of BCM towards NO was ensured by reacting BCM with relevant biologically reactive species like H_2O_2, ClO^-, KO_2, $^\bullet OH$, NO, NO_2^-, NO_3^-, TEMPO, glyoxal, $ONOO^-$, HNO, AA (ascorbic acid), and HCHO which revealed that none of these potential analytes triggered a fluorescence enhancement, except for NO **(Figure 3.20)**. To our delight, important cellular metabolites like AA, glyoxal and HCHO interact hardly with the concerning probe. So, this high selectivity is very much advantageous for precise detection of NO in biological milieu.
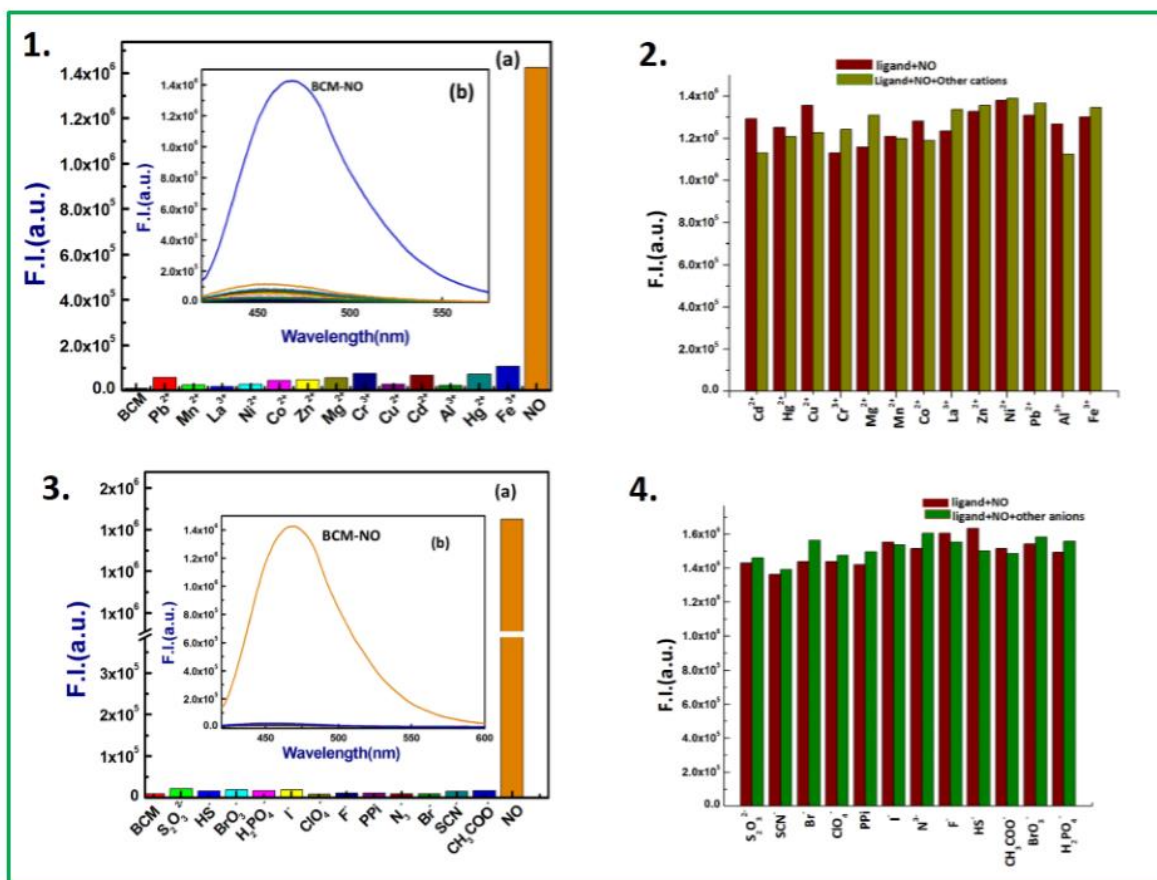
Figure 3.19 1.(a) Bar plot illustrating the fluorescence responses of BCM at 470 nm (λ_{ex} = 410 nm) towards different cations in HEPES buffer at pH 7.0, BCM = 20 μM, M^{n+} = 50 μM at 25 °C; **(b)** corresponding spectral responses. **2.** Bar plot of the BCM-NO in presence of different cations. **3. (a), (b)** bar plot and spectral plot for the selectivity study of the probe towards anions at same conditions. **4.** Over-selectivity study of BCM to NO in presence of anions.
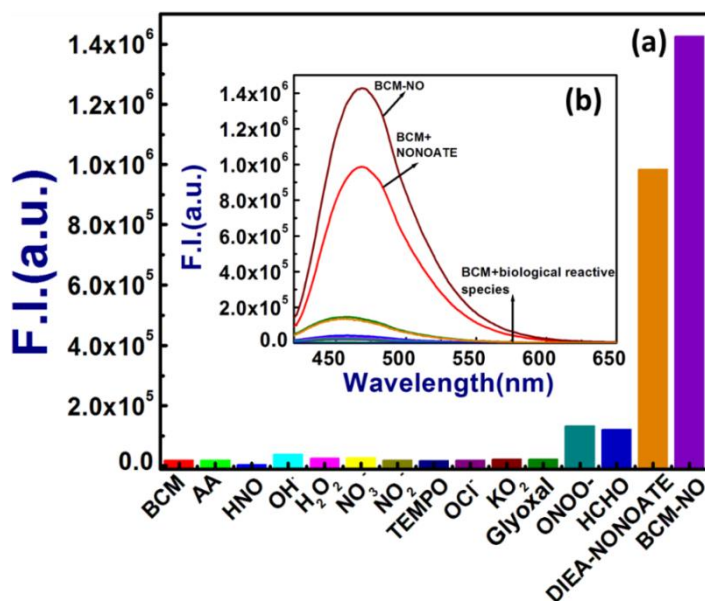
(Figure 3.20) (a) Bar plot presents the fluorescence responses of BCM at 470 nm (λ_{ex} = 410 nm) towards various biologically reactive species in HEPES buffer at pH 7.0, BCM = 20 µM, X^{n-} = 50 µM at 25 °C; (b) corresponding spectral responses.

3.3.7 Geometry optimization with an electronic structure

To get a theoretical overview on the interaction between BCM and NO we have conducted the DFT and TDDFT calculations of the probe (BCM) and its NO mediated product (BCM-NO). **(Figure 3.21)** presents the optimized geometry of both the compounds having the C1 point group. The structural compositions of these compounds have been established using mass spectroscopy which indicates the formation of oxatriazole from carbohydrazide in the presence of NO. All the important geometrical parameters of the probe BCM and BCM-NO are tabulated in **Tables 3.1 and 3.2.** For the BCM-NO product the N–O bond distance is 1.43 Å, whereas the C–O bond distances lie in the range of 1.2–1.4 Å.

In the ground state the density of electron clouds mainly prevails on the HOMO and LUMO of the 3-oxo-3H-benzo[f]chromene-2-carbaldehyde and 3-oxo-3H-benzo[f]-chromene-2-carboxylic acid amide moiety respectively in the probe BCM. In the case of BCM-NO, the
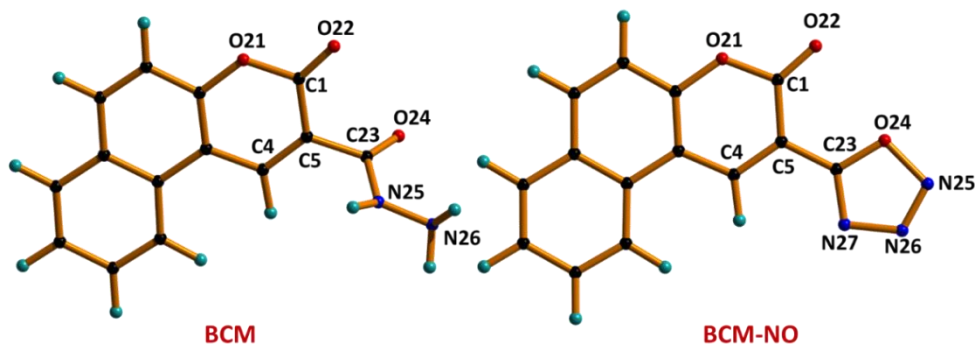
Figure 3.21 optimized geometry of BCM and BCM-NO.

electron clouds mainly reside on the HOMO and LUMO of the benzo[f]chromen-3-one and 3-[1,2,3,4]oxatriazol-5-yl-chromen-2-one moiety respectively **(Figure 3.22)**. These compositions are important to know the behaviour of the transition as well as the absorption spectra of both BCM
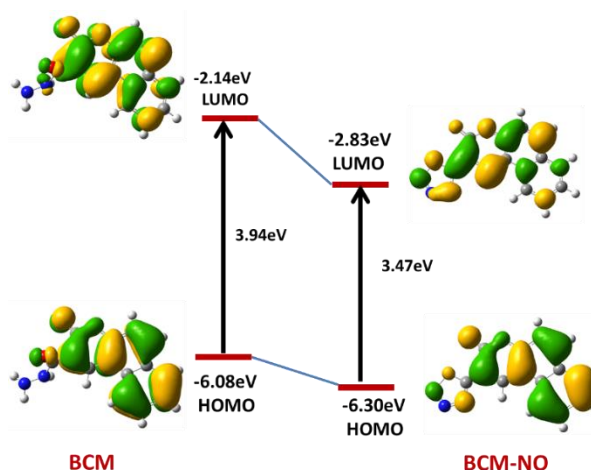
Figure 3.22 Frontier molecular orbitals of probe BCM and BCM-NO.

and BCM-NO. The calculated HOMO–LUMO energy gap associated with BCM and BCM-NO is 3.94 eV and 3.47 eV respectively **(Figure 3.22)**. By exploiting the TDDFT method, the UV-Vis absorption spectra of BCM and BCM-NO were obtained at room temperature in aqueous medium (**Figure 3.23A**). The absorption band of BCM at 374 nm in pure aqueous medium
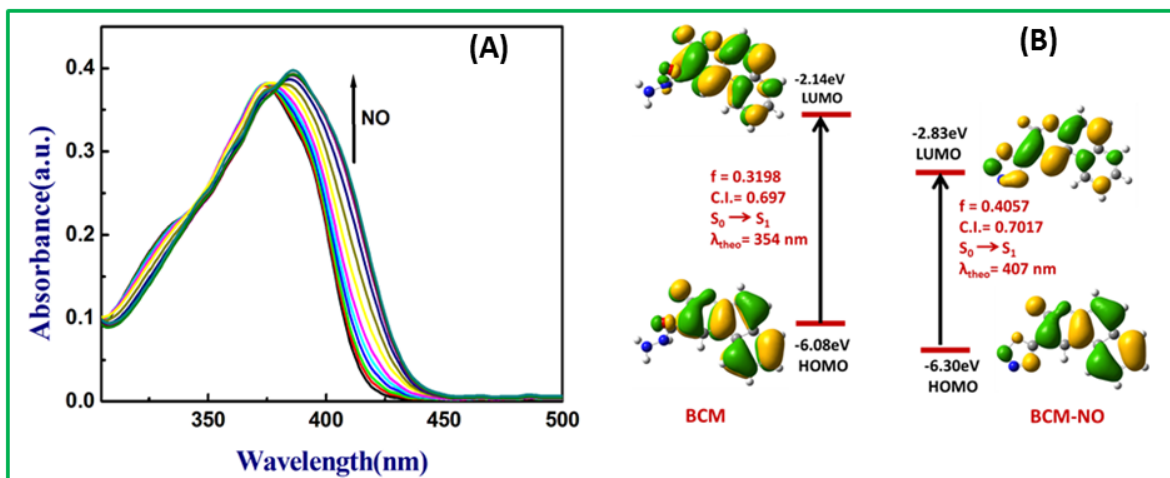
Figure 3.23 (A) UV response of BCM towards nitric oxide. **(B)** Frontier molecular orbitals of BCM and BCM-NO in UV-vis absorption.

corresponds to the peak at 354 nm (**Figure 3.23B**) obtained from the TDDFT calculation which is assigned to the $S_0 \rightarrow S_1$ electronic transitions with significant oscillator strength (**Tables 3.3 and 3.4**), whereas for BCM-NO the theoretically evaluated absorption band at 407 nm is ascribed to the peak at 386 nm also associated with the $S_0 \rightarrow S_1$ electronic transitions (**Figure 3.23B**). So, from this information it can be speculated that the experimental results have good agreement with the theoretical results.

Table 3.1 Some selected geometrical parameters (bond lengths and bond angles) of BCM in ground state calculated at B3LYP/6-31G (d,p) Levels.

Bond Lengths (Å)		Bond Angles (°)	
O21-C1	1.40	O22-C1-C5	127.16
C1-O22	1.20	C1-C5-C23	117.27
C5-C23	1.51	C5-C23-O24	122.09
C23-O24	1.21	O24-C23-N25	125.47
C23-N25	1.38	C23-N25-N26	119.59

Table 3.2 Some selected geometrical parameters (bond lengths and bond angles) of BCM-NO in ground state calculated at B3LYP/6-31G (d,p) Levels.

Bond Lengths (Å)		Bond Angles (°)	
O21-C1	1.40	O21-C1-O22	117.61
C1-O22	1.20	O22-C1-C5	127.89
C1-C5	1.46	C5-C23-O24	122.79
C5-C23	1.45	C23-O24-N25	104.10
C23-O24	1.32	O24-N25-N26	106.54
O24-N25	1.43	N25-N26-N27	112.77
N25-N26	1.25	C23-N27-N26	104.42
N26-N27	1.36		
N27-C23	1.31		

Table 3.3 Vertical excitation energy and oscillator strength (f_{cal}) of low-lying excited singlet states obtained from TDDFT// B3LYP/6-31G(d,p) calculations of BCM which is matched with the experimental one.

Electronic transition	Composition	Excitation energy	Oscillator strength (f_{cal})	CI	λ_{exp} (nm)
$S_0 \rightarrow S_1$	HOMO→LUMO (66 ->67)	3.499eV (354.29nm)	0.3198	0.69768	374

Table 3.4 Vertical excitation energy and oscillator strength (f_{cal}) of low-lying excited singlet states obtained from TDDFT// B3LYP/6-31G (d,p) calculations of BCM-NO which is matched with the experimental one.

Electronic transition	Composition	Excitation energy	Oscillator strength (f_{cal})	CI	λ_{exp} (nm)
$S_0 \rightarrow S_1$	HOMO→LUMO (68 ->69)	3.043eV (407.42nm)	0.4057	0.70177	386

3.3.8 NO detection in live cells

Fluorescence imaging studies were executed to explore the detecting capability of BCM as a NO sensor in living cells. The probe's cytotoxicity has been assessed in A375 and Raw 264.7 cells **(Figure 3.24).** The cell lines showed the evidence of well admissibility of BCM (more than 80% of the cell is viable up to 60 μM of BCM), indicating its effectiveness as a NO sensor in live cells
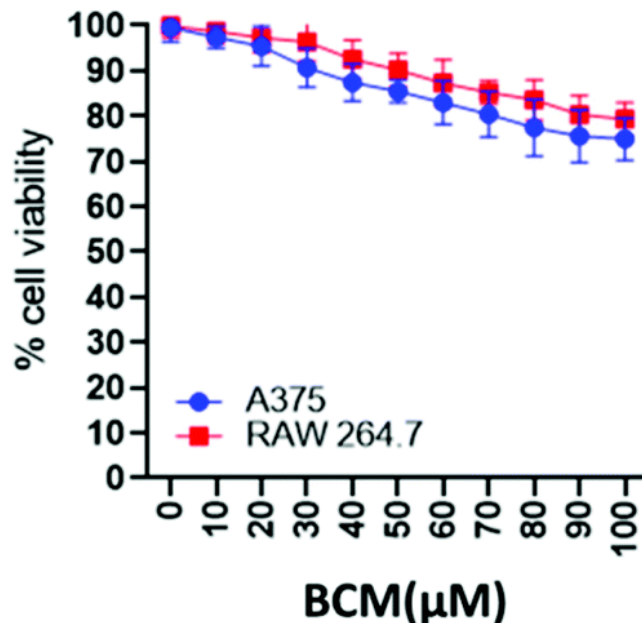
Figure 3.24 Graphical picture of the cell viability study of BCM

also. Exogenously stimulated NO sensing practicability of BCM was measured in A375 cells. The live cells were treated with the NO donor DEA-NONOate followed by incubation with the probe. BCM-NO showed intracellular fluorescence compared to the BCM probe only **(Figure 3.25)**. Likewise, endogenously stimulated NO sensing of the BCM probe has been estimated in Raw 264.7 cells where the cells were treated with LPS (1.0 mg mL^{-1}) and IFN-γ (1000 U mL^{-1})
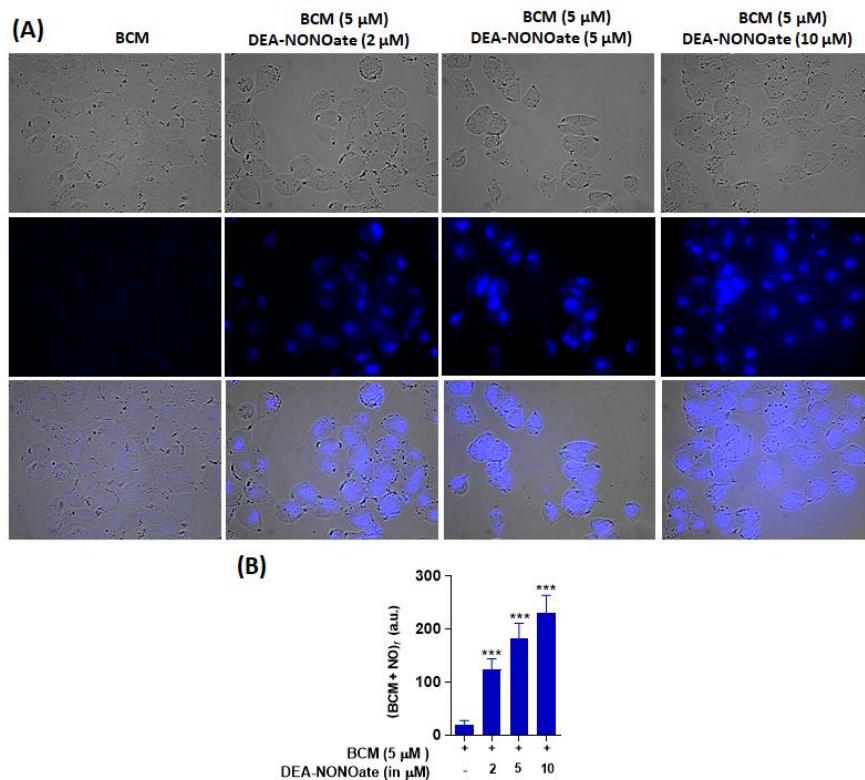
Figure 3.25 (A) Images of A375 cells incubated with 5 µM BCM for 30 min and then incubated with DEA-NONOate (2, 5 and 10 µM) for 30 min. The blue fluorescence was observed owing to the reaction of NO with BCM. Images were captured at 63x objective. (B) Quantification of fluorescence intensity in response to the intracellular NO interaction with BCM.

for 6 h and then treated with probe BCM **(Figure 3.26)**. Very obviously, in the presence of the NO stimulator the cells exhibited high fluorescence compared to the non-stimulated and PTIO (NO scavenger) treated ones. Additionally, flow cytometric studies were performed in Raw 264.7 cells for the evaluation of NO, showing a positive shift in the fluorescence peak for LPS + IFN-γ stimulated cells in contrast to the non-stimulated cells and PTIO (200 mM) **(Figure 3.26 C)**. So finally it can be concluded that BCM showed an excellent nontoxic fluorescence response towards NO for the purpose of cell imaging exogenously and endogenously.
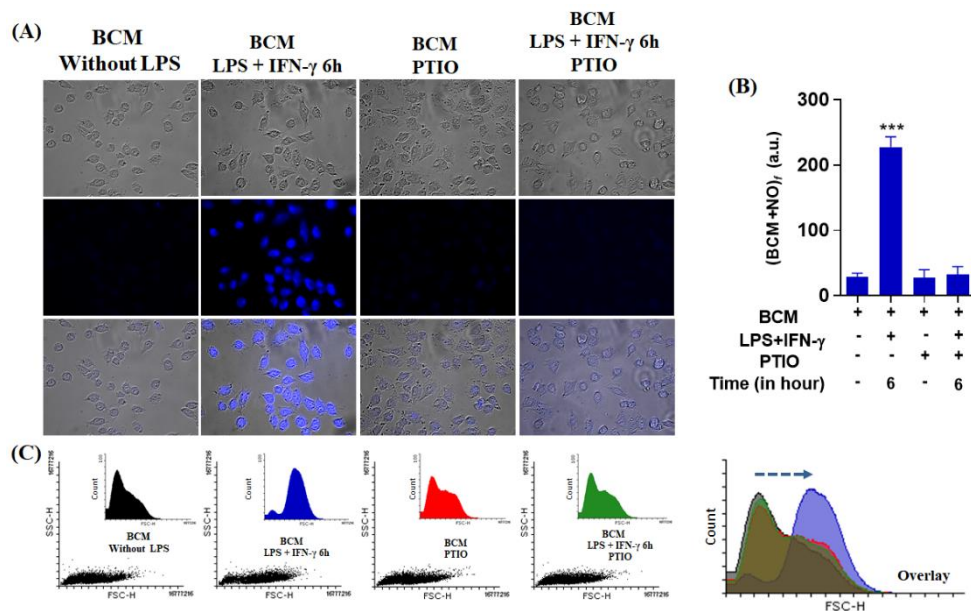
Figure 3.26 Endogenous recognition of NO with flow cytometry assay: **(A)** fluorescence images of Raw 264.7 macrophage cells incubated with BCM in the absence of LPS and stimulated with LPS + IFN-γ for 6 h followed by the addition of PTIO, a NO scavenger. The corresponding images were captured at 63× objective. **(B)** The characteristic bar plots display the changes in the fluorescence intensity of BCM upon interaction with LPS + IFN-γ, PTIO and LPS + IFN-γ + PTIO, respectively. The experiments were performed thrice and related data are presented as mean ± SD. For statistical importance the estimated results were verified with the student's t test. P values ≤0.05 were statistically significant. **(C)** Flow cytometry experiment of NO with BCM by using Flowing Software version 2.5.1. The representative dot plot of forward (FSC-H) versus side (SSC-H) scatter and the corresponding histogram plot displaying a positive response for gated Raw 264.7 macrophage cells towards NO. The overlap histogram plot indicates a positive shift in the fluorescence intensity peak of LPS + IFN-γ stimulated NO taken by BCM compared to without LPS + IFN-γ and PTIO.
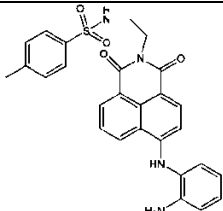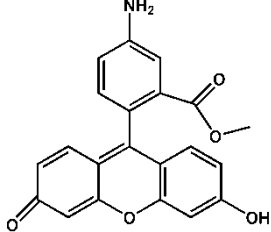
3.4 Conclusion

In brief, we are reporting herewith a smart fluoregenic probe BCM on the benzocoumarin platform which selectively recognizes NO under physiological conditions. From the linear F.I. vs. [NO] plot obtained from the fluorescence titration experiment yields $K_f = (4.33 \pm 0.48) \times 10^4$
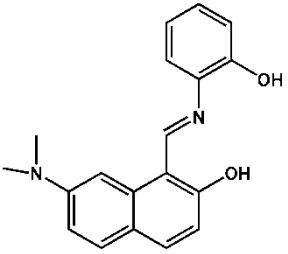
M^{-1}. Here, the acid-hydrazide moiety of probe BCM reacts with NO/O_2 to form the electron deficient 1,2,3,4-oxatrizole moiety which is solely responsible for fluorescence enhancement through the PET blocking mechanism. The outstanding sensing performance of BCM towards NO is also illustrated by its very low detection limit (16 nM), and specific response to NO with desirable selectivity and sensitivity in the presence of other biologically reactive species which makes the probe highly potent for NO detection in the biological environment. The reaction mechanism of BCM and NO was confirmed by kinetic studies which reveal the 1st order dependence on BCM and the 2nd order dependence on NO. The pH variation study for NO detection also supports BCM as an efficient NO sensor in a wide range of pH. Beside these, the bio-imaging implication of this probe is also appreciable owing to its least cytotoxicity and biocompatibility for *in vitro* NO detection. The application of BCM can also be extended to flow cytometric analysis of exogeneous and endogeneous NO in living cells. So, all the above mentioned experiments and information confirm BCM as a very appropriate probe for the tracking of NO.
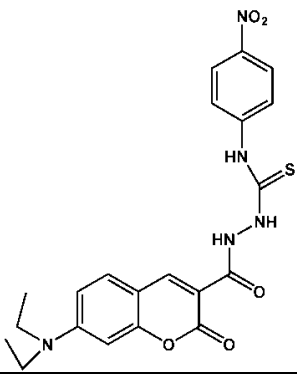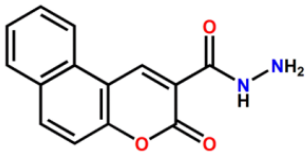
Table 3.5 Comparison table of some previously reported nitric oxide probes.

Serial no.	Structure of probe	LOD	fold	medium	mechanism	Emission wavelength	kinetics	Reference
1.		3.3 nM	22	PBS buffer	OPD- based	538nm	Not done	ACS Sens. 2018,3, 11, 2311
2.		44 nM	_	Hepes buffer	De-amination	524nm	Not done	Inorg. Chem. 2012, 51, 5400

3.		97.8 nM	7.5	PBS Buffer (5%DMSO+0.2% Triton X-100)	Breaking of Schiff base	590nm	Not done	Chem. Commun., 2018, 54, 13491
4.		30 nM	5	Ethanol + PBS buffer 1:1	Through diazonium intermediate	518nm	Not done	*Chem. Commun.,* 2014, 50, 7499
5.		37 nM	–	PBS+10%MeCN	N-Nitrosation	613nm	Not done	**Chem. Sci.,** 2017, 8, 4533
6.		25 nM	63	PBS buffer	Hanstch ester synthesis	525nm	Not done	**Talanta** 176 (2018) 382
7.		21 nM	11	PBS buffer	Metal based sensor	522nm	Not done	*J. Mater.Chem. B,* 2017, 5, 8929
8.		2.1 µM	83	Aerated H_2O	Deamination	550nm	Not done	*Chem. Commun.,* 2014, 50, 3579

9.		47.6 nM	5	DMSO+ Hepes buffer 3:7	1,3,4-oxadiazole formation	475nm	Not done	*ACS Sens.* 2019, 4,2, 309
10.		16 nM	123	Hepes buffer	1,2,3,4 oxatriazole	470nm	Done	This work

References

1. (a) P. F. Bove and A. D. V. Vliet, *Free Radical Biol. Med.,* 2006, **41**, 515–527; (b) A. H. Ashoka, F. Ali, R. Tiwari, R. Kumari, S. K. Pramanik and A. Das, *ACS Omega,* 2020, **5**, 1730–1742.

2. D. J. Stuehr, J. Santolini, Z. Q. Wang, C. C. Wei andS. Adak, *J. Biol. Chem.,* 2004, **279**, 36167–36170.

3. (a) P. Pacher, J. S. Beckman and L. Liaudet, *Physiol. Rev.,* 2007, **87**, 315–424; (b) Y. Liu, H. Fan, Y. Wen, T. Jia, Q. Su and F. Lia, *Dyes Pigm.,* 2019, **166**, 211–216.

4. A. De Mel, F. Murad and A. M. Seifalian, *Chem. Rev.,* 2011, **111**, 5742–5767.

5. Y. Iwakiri and M. Y. Kim, *Trends Pharmacol. Sci.,* 2015, **36**, 524–536.

6. S. P. Hussain, L. J. Hofseth and C. C. Harris, *Nat. Rev. Cancer,* 2003, **3**, 276–285.

7. B. V. Khan, D. G. Harrison, M. T. Olbrych, R. W. Alexander and R. M. Medford, *Proc. Natl. Acad. Sci. U. S. A.,* 1996, **93**, 9114–9119.

8. K. Pantopoulos and M. W. Hentze, *Proc. Natl. Acad.Sci. U. S. A.,* 1995, **92**, 1267–1271.

9. (a) B. J. Privett, J. H. Shin and M. H. Schoenfisch, *Chem. Soc. Rev.,* 2010, **39**, 1925–1935; (b) S. Biswas, Y. Rajesh,S. Barman, M. Bera, A. Paul, M. Mandal and N. D. P. Singh, *Chem. Commun.,* 2018, **54**, 7940–7943.

10. S. R-Nuévalos, M. Parra, S. Ceballos, S. Gil and A. M. Costero, *J. Photochem. Photobiol. A*, 2020, **388**, 112132.

11. (a) E. Sasaki, H. Kojima, H. Nishimatsu, Y. Urano, K. Kikuchi, Y. Hirata and T. Nagano, *J. Am. Chem. Soc.,* 2005, **127**, 3684–3685; (b) Z. Yu, J. Zhou, X. Dong, W. Zhao and Z. Chen, *Anal. Chim. Acta,* 2019, **1067**, 88–97.

12. Y. Yang, S. K. Seidlits, M. M. Adams, V. M. Lynch,C. E. Schmidt, E. V. Anslyn and J. B. Shear, *J. Am. Chem. Soc.,* 2010, **132**, 13114–14116.

13. L. E. McQuade and S. J. Lippard, *Inorg. Chem.,* 2010, **49**, 7464–7471.

14. M. H. Lim and S. J. Lippard, *Inorg. Chem.,* 2004, **43**, 6366–6370.

15. L. Y. Niu, Y. Z. Chen, H. R. Zheng, L. Z. Wu, C. H. Tung and Q. Z. Yang, *Chem. Soc. Rev.,* 2015, **44**, 6143–6160.

16. M. Gao, F. Yu, C. Lv, J. Choo and L. Chen, *Chem. Soc. Rev.,*2017, **46**, 2237–2271.

17. N. Zhang, Y. Si, Z. Sun, L. Chen, R. Li, Y. Qiao and H. Wang, *Anal. Chem.,* 2014, **86**, 11714–11721.

18. F. Yu, P. Li, G. Zhao, T. Chu and K. Han, *J. Am. Chem. Soc.,* 2011, **133**, 11030–11033.

19. G. Chen, Q. Fu, F. Yu, R. Ren, Y. Liu, Z. Cao, G. Li, X. Zhao, L. Chen, H. Wang and J. You, *Anal. Chem.,* 2017, **89**, 8509–8516.

20. (a) W. Hu, D. Boateng, J. Kong and X. Zhang, Austin *J. Biosens. Bioelectron.,* 2015, **1**, 1–9; (b) T. Zhou, J. Wang, J. Xu, C. Zheng, Y. Niu, C. Wang, F. Xu, L. Yuan, X. Zhoa, L. Liang and P. Xu, *Anal. Chem.,* 2020**, 92**, 5064–5072.

21. (a) C. J. Reinhardt, E. Y. Zhou, M. D. Jorgensen, G. Partipilo and J. Chan, *J. Am. Chem. Soc.,* 2018, **140**, 1011–1018;(b) Y. Huo, J. Miao, J. Fang, H. Shi, J. Wang and W. Guo, *Chem. Sci.,* 2019, **10**, 145–152.

22. (a) C. Xu, C. Xin, C. Yu, M. Wu, J. Xu, W. Qin, Y. Ding, X. Wang, L. Li and W. Huang, *Chem. Commun.,* 2018, **54**, 13491–13494; (b) X. Lv, Y. Wang, S. Zhang, Y. Liu, J. Zhang and W. Guo, *Chem. Commun.,* 2014, **50**, 7499–7502.

23. M. H. Lim and S. J. Lippard, *J. Am. Chem. Soc.,* 2005, **127**, 12170–12171.

24. D. A. Jose, N. Sharma, R. Sakla, R. Kaushik and S. Gadiyaram, *Methods,* 2019, **168**, 62–75.

25. A. S. M. Islam, M. Sasmal, D. Maiti, A. Dutta, S. Ganguly, A. Katarkar, S. Gangopadhyay and M. Ali, *ACS Appl. Bio Mater.,* 2019, **2**, 1944–1955.

26. D. Maiti, A. S. M. Islam, M. Sasmal, C. Prodhan and M. Ali, *Photochem. Photobiol. Sci.,* 2018, **17**, 1213–1221.

27. (a) A. Dutta, A. S. M. Islam, D. Maiti, M. Sasmal,C. Prodhan and M. Ali, *Org. Biomol. Chem.,* 2019, **17**, 2492–2501; (b) P. Srivastava, M. Verma, S. Sivakumar and A. K. Patra, *Sens. Actuators, B,* 2019, **291**, 478–484.

28. X. Zhang, B. Wang, Y. Xiao, C. Wang and L. He, *Analyst,* 2018, **143**, 4180–4188.

29. X.-X. Chen, L.-Y. Niu, N. Shao and Q.-Z. Yang, *Anal. Chem.,* 2019, **91**, 4301–4306.

30. A. Beltrán, M. I. Burguete, D. R. Abánades, S. D. Pérez-Sala, V. Luis and F. Galindo, *Chem. Commun.,* 2014, **50**, 3579–3581.

31. Q. Wang, X. Jiao, C. Liu, S. He, L. Zhaoab and X. Zeng, *J. Mater. Chem. B,* 2018, **6**, 4096–4103.

32. S.-J. Li, D.-Y. Zhou, Y. Li, H.-W. Liu, P. Wu, J. Ou-Yang, W.-L. Jiang and C.-Y. Li, *ACS Sens.,* 2018, **3**, 2311–2319.

33. (a) C. Sun, W. Shi, Y. Song, W. Chen and H. Ma, *Chem. Commun.,* 2011, **47**, 8638–8640; (b) A. V. Latha,M. Ayyappan, A. R. Kallar, R. V. Kakkadavath, S. P. Victor and S. Selvam, *Mater. Sci. Eng. C,* 2020, **108**, 110463.

34. (a) A. S. M. Islam, R. Bhowmick, B. C. Garain, A. Katarkar and M. Ali, *J. Org. Chem.,* 2018, **83**, 13287–13295;(b) C. M. Wu, Y. H. Chen, K. Dayananda, T. W. Shiue,C. H. Hung, W. F. Liaw, P. Y. Chen and Y. M. Wang, *Anal. Chim. Acta,* 2011, **708**, 141–148; (c) M. E. Azab, H. M. F. Madkour and M. A. E. Ibraheem, *Phosphorus, Sulfur Silicon Relat. Elem.,* 2006, **181**, 1299–1313;(d) M. K. Ibrahim, K. El-Adl, M. F. Zayed and H. A. Mahdy, *Med. Chem. Res.,* 2015, **24**, 99–114.

35. (a) H. Ammar, S. Fery-Forgues and R. El. Gharbi, *Dyes Pigm.,* 2003, 57, 259; (b) S. Sastry, *Biophys. Chem.,* 2001, **91**,191; (c) M. Chiyomi, M. Toshinobu, K. Yasuko,T. Kenichiro, Y. Hideyuki, N. Hitoshi, Y. Masatoshi and T. Akira, *Chem. Pharm. Bull.,* 2005, **53**, 750.

36. (a) M. A. Saleh, A. Kamel, A. El-Demerdash and J. Jones, *Chemosphere,* 1998, **36**, 1543–1552; (b) H. Yu, H. Mizufune, K. Uenaka, T. Moritoki and H. Koshima, *Tetrahedron Lett.,* 2005, **61**, 8932–8938; (c) S. Xiao, T. Yi, F. Li and C. Huang, *Tetrahedron Lett.,* 2005, **46**, 9009–9012.

37. M. Walshe, J. Howarth, M. T. Kelly, R. O'Kennedy and M. R. Smyth, *J. Pharm. Biomed. Anal.,* 1997, **16**, 319–325.

38. (a) B. Kovac and I. Novak, *Spectrochim. Acta, Part A,* 2002, **58**, 1483; (b) B. A. Elsayeda, I. A. Ibrahema, M. S. Attia, S. M. Shaabana and M. M. Elsenety, *Sens. Actuators. B*, 2016, **232**, 642–652.

39. (a) R. Zhang, H. Zheng and J. Shen, *Synth. Met.,* 1999, 106,157–160; (b) N. Mishra, V. Patil, A. Asrondkar, A. S. Bobade and A. S. Chowdhary, *World J. Pharm. Res.,* 2015, **4**, 627–636.

40. (a) J. Preat, D. Jacquemin and E. A. Perpète,Chem. *Phys. Lett.,* 2005, **415**, 20–24; (b) Rajesha, H. S. B. Naik, H. N. H. Kumar, K. M. Hosamani and K. M. Mahadevan, *ARKIVOC,* 2009, **2**, 11–19; (c) R. M. Zaki,Y. A. Elossaily and A. M. Kamal El-Dean, *Russ. J. Bioorg. Chem.,* 2012, **38**, 639–646.

41. Š. Mesároš, S. Grunfeld, A. Mesárošová, D. Bustin and T. Malinski, *Anal. Chim.Acta,* 1997, **339**, 265−270.

42. A. T. Wrobel, T. C. Johnstone, A. D. Liang, S. J. Lippard and P. A. Rivera-Fuentes, *J. Am. Chem. Soc.,* 2014, **136**, 4697−4705.

43. M. Grätzel, S. Taniguchi and A. Henglein, *Ber. Bunsen-Ges. Phys. Chem.,* 1970, **74**, 488–492.

44. R. G. Parr and W. Yang, *Density Functional Theory of Atoms and Molecules, Oxford University Press,* Oxford,1989.

45. V. Barone and M. Cossi, *J. Phys. Chem. A,* 1998, **102**, 1995-2001.

46. V. Barone and M.Cossi, *J. Chem. Phys.,* 2001, **115**, 4708-4717.

47. M. Cossi, N. Rega, G. Scalmani and V. Barone, *J. Comput. Chem.*, 2003**,** 24, 669-681.

48. A. D. Becke, Density-functional thermochemistry. III. The role of exact exchange. *J. Chem. Phys*., 1993, **98**, 5648-5652.

49. C. Lee, W. Yang and R. G. Parr, *Phys. Rev. B: Condens. Matter Mater. Phys.*, 1988, **37**, 785-789.

50. M. J. Frisch, G. W. Trucks, H. B. Schlegel, G. E. Scuseria, M. A. Robb, J. R. Cheeseman, G. Scalmani, V. Barone, B. Mennucci, G. A. Petersson, H. Nakatsuji, M. Caricato, X. Li, H. P. Hratchian, A. F. Izmaylov, J. Bloino, G.Zheng, J. L. Sonnenberg, M. Hada, M. Ehara, K. Toyota, R. Fukuda, J. Hasegawa, M. Ishida, T. Nakajima, Y. Honda, O. Kitao,
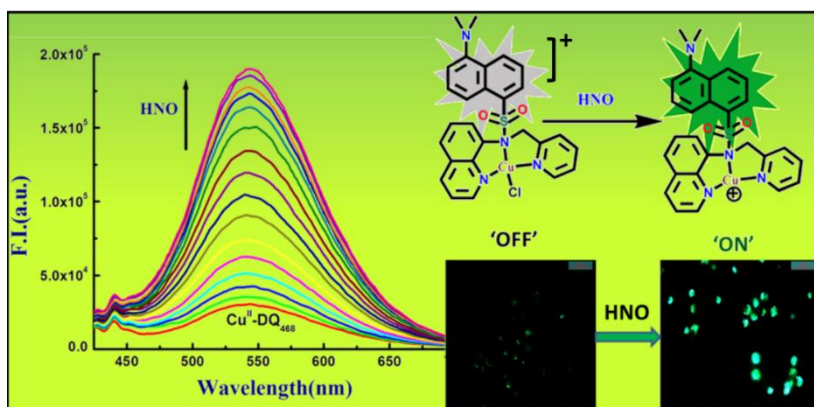
H. Nakai, T. Vreven, J. A. Montgomery Jr., J. E. Peralta, F. Ogliaro, M. Bearpark, J. J. Heyd, E. Brothers, K. N. Kudin, V. N. Staroverov, R. Kobayashi, J. Normand, K. Raghavachari, A. Rendell, J. C. Burant, S. S. Iyengar, J. Tomasi, M. Cossi, N. Rega, J. M. Millam, M. Klene, J. E. Knox, J. B. Cross, V. Bakken, C. Adamo, J. Jaramillo, R. Gomperts, R. E. Stratmann, O. Yazyev, A. J. Austin, R. Cammi, C. Pomelli, J. W. Ochterski, R. L. Martin, K. Morokuma V. G. Zakrzewski, G. A. Voth, P. Salvador, J. J. Dannenberg, S. Dapprich, A. D. Daniels, Ö. Farkas, J. B. Foresman, J. V. Ortiz, J. Cioslowski and D. J. Fox, Gaussian 09, (Revision A.1), Gaussian, Inc., Wallingford, CT, 2009.

51. N. M. O'Boyle, A. L. Tenderholt, K. M. Langner, *J. Comput. Chem.*, 2008, **29**, 839-845.

52. A. S. M. Islam, R. Bhowmick, B. C. Garain, A. Katarkar and M. Ali, *J. Org. Chem.,* 2018, **83**, 13287−13295.

53. A. S. M. Islam, R. Bhowmick, K. Pal, A. Katarkar, K. Chaudhuri and M. Ali, *Inorg. Chem.* 2017, **56**, 4324−4331.

54. A. S. M. Islam, R. Alam, A. Katarkar, K. Chaudhuri and M. Ali, *Analyst,* 2015, **140**, 2979–2983.

55. H. Kojima, N. Nakatsubo, K. Kikuchi, S. Kawahara, Y. Kirino, H. Nagoshi, Y. Hirata and T. Nagano, *Anal. Chem.,* 1998, **70**, 2446–2453.

56. H. Kojima, M. Hirotani, N. Nakatsubo, K. Kikuchi, Y. Urano, T. Higuchi, Y. Hirata and T. Nagano, *Anal. Chem.,* 2001, **73**, 1967–1973.

57. E. Sasaki, H. Kojima, H. Nishimatsu, Y. Urano, K. Kikuchi, Y. Hirata and T. Nagano, *J. Am. Chem. Soc.,* 2005, **127**, 3684–3685.

58. V. G. Kharitonov, A. R. Sundquist and V. S. Sharma, *J. Biol. Chem.,* 1994, **269**, 5881–5883.

59. M. Grätzel, S. Taniguchi and A. Henglein, *Ber. Bunsen-Ges. Phys. Chem.,* 1970, **74**, 488−492.

60. W. R. Licht, S. R. Tannenbaum and W. M. Deen, *Carcinogenesis,* 1988, **9**, 365–372.

61. T. Chen, R. Zamora, B. Zuckerbraun and T. R. Billiar, *Curr. Mol. Med.,* 2003, **3**, 519–526.

CHAPTER 4

Dansyl-appended Cu^{II}-complex-based nitroxyl (HNO) sensing with living cell imaging application and DFT studies

Abstract: We introduce herein, a novel copper complex based fluorescent probe $[Cu^{II}(DQ_{468})Cl]^+$ that exhibits a significant fluorescence turn-on response towards nitroxyl (HNO) with high selectivity over other biological reactive oxygen, nitrogen and sulfur species, including nitric oxide (NO). A smart strategy, involving HNO-induced reduction of paramagnetic $[Cu^{II}(DQ_{468})Cl]^+$ to diamagnetic $[Cu^{I}(DQ_{468})]^+$ with concomitant fluorescence enhancement via a PET mechanism is discussed here. This metal ion reduction-based strategy was also supported by X-band EPR response and mass spectrometry. The metal free probe (DQ_{468}) showed high affinity towards Cu^{2+} to form $[Cu^{II}(DQ_{468})Cl]^+$ with a 0.091 μM detection limit, which subsequently enabled the detection of HNO in an organo-aqueous medium at biological pH (7.4) in the green wavelength region ($\lambda_{em} = 543$ nm) with a LOD of 0.41 μM. The ground-state geometries of DQ_{468}, $[Cu^{II}(DQ_{468})Cl]^+$ and $[Cu^{I}(DQ_{468})]^+$ were optimized by DFT calculations, which revealed that the central metal ion in $[Cu^{II}(DQ_{468})Cl]^+$ is in a distorted tetrahedral geometry with the C1 point group. Additionally, the negligible cytotoxicity and good biocompatibility make the developed probe useful for the *in vitro* detection of HNO.

4.1 Introduction

Over the past few decades, the development of a fluorescent probe for the detection of metal ions[1] has attracted a great deal of attention from chemists and biologists due to the key role these ions play in chemistry and biology and due to their effects on the environment.[2] For instance, cupric ion (Cu^{2+}) is an environmental pollutant at high concentration[3] and one of the most abundant essential trace metal ions[4] in the human body, with the highest concentration found in the liver. The dysregulation of copper homeostasis causes various diseases, like Menkes,[5] amyotrophic lateral sclerosis[6] and Alzheimer's disease.[7] The EPA (U.S. Environmental Protection Agency) has set the maximum level of copper in drinking water at 1.3 ppm ($\sim$20 μM). So, the sensitive detection of copper levels in biological systems and in the environment is highly necessary. Very recently, copper-bound fluorescent probes have been developed for the detection of some biological reactive nitrogen species, like nitric oxide (NO) and nitroxyl (HNO).[8–12] Nitric oxide(NO) is a very reactive gaseous free-radical, responsible for both the physiological and pathological activities of various biological organisms[13–19] and being present in the nervous,[20] immune[21] and cardiovascular[22] systems. Another species of concern is the nitroxyl (HNO) biomolecule, which is the protonated and one-electron reduced analogue of NO. Though HNO and NO are very closely related species, they have distinct chemical and biochemical properties.[23] So, the development of chemical tools that can distinguish HNO over NO is very necessary. From recent advances in the medical activities of HNO, it has also been reported that HNO confers vasoprotective effects,[24] enhances heart muscle contractility[25] and inhibits platelet aggregation.[26] Significantly, HNO regulates cardiovascular functions and also acts as an important tool for the treatment of heart failure.[25,27] In spite of the aforementioned progress made on HNO, still the roles of it in biology are largely unknown. So, some probe that could monitor HNO sensitively and selectively over other interfering reactive species is highly desired for the further analysis of HNO. Frequently, some difficulties are encountered in the sensing of HNO, such as:[28–30] (i) the detection of HNO may be interfered by some biologically reducing agents; (ii) the very low concentration of HNO in biological systems may not be sufficient to produce a visible response towards a probe; and (iii) the pH-dependent response of HNO towards a probe. There are many varieties of techniques for HNO detection, i.e. chromatography, electrochemical analysis,[31] high performance liquid chromatography (HPLC),[32] chemiluminescence,[33] etc.

Although these methods are sensitive, they are associated with sophisticated instrumentation, complicated sample preparation and can cause the destruction of tissues or cells. So, they are not suitable for living cell applications. Very recently, the technique associated with fluorescence spectroscopy is considered the gold standard due to its direct and precise measurement and also due to its sensitivity and well defined spatiotemporal resolution.[34] Using the fluorescence method, an HNO-detecting probe should have some properties, e.g. high affinity for HNO without any interference from other biological reactive species, work downstream the NO oxidation products, water solubility and membrane permeability. To date, a number of fluorescent sensors that can track HNO in live cells have been developed. One of the common types is Staudinger ligation-based HNO sensing (**Scheme 4.1(i)**). Here, a chemo-specific reaction occurs with a triphenyl phosphine moiety to form an aza-ylide intermediate, which in turn reacts with an adjacent ester moiety, leading to the removal of alcohol and an enhancement of the fluorescence intensity.[35–39] Another common
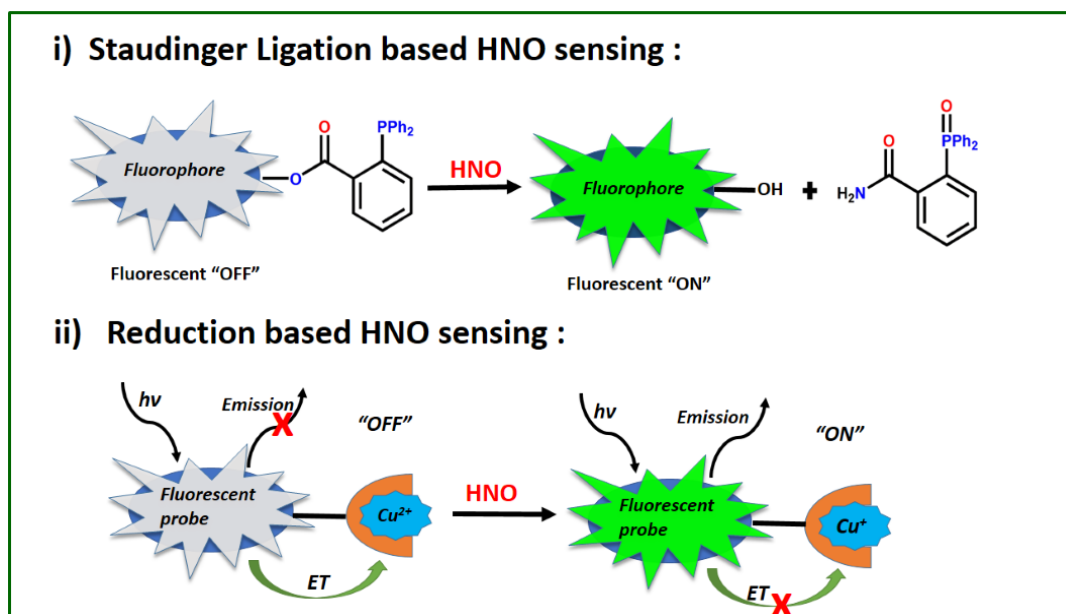
Scheme 4.1 General mechanism of sensing HNO using: **(i)** Staudinger ligation-based mechanism involving the release of a fluorophore; **(ii)** HNO-induced reduction of Cu^{II} complex. The electron transfer (ET) from the fluorophore (in the photoexcited state) to the metal centre (paramagnetic Cu^{2+}) makes the probe nonfluorescent (OFF state). The selective reduction of Cu(II) to Cu(I) by HNO stops the ET, thereby restoring the emission of the fluorophore (ON state).

design of HNO probe involves the HNO induced reduction of Cu(II) to Cu(I) **(Scheme 4.1(ii))**.[40–42] Here, the fluorescence of the photo-emissive ligand is quenched due to binding with the paramagnetic cupric ion, and the regeneration of fluorescence intensity occurs upon HNO treatment due to the conversion of paramagnetic Cu(II) to diamagnetic Cu(I). The unpaired electron in the d orbital of the Cu(II) centre can reliably achieve this quenching by either electron or energy transfer (**Scheme 4.1**). Exploiting this strategy, Lippard and Rosenthal pioneered the building of a BODIPY-based nitroxylsensor.[40] Yao et al. also reported a similar type of Cu^{2+}-chelating system using coumarin fluorophore.[42] Besides, a number of related Cu-complex-based nitroxyl probes have been developed so far using this redox-based strategy, but most of them are prone to being sensitive towards other biological reductive species, like cysteine(CYS), homocysteine (HCY), glutathione (GSH), ascorbate, H_2S, etc., along with HNO present in the living matrices.[29,30]

To overcome the lack of selectivity of the so-called Cu^{II}complex-based HNO probe, we have synthesized $[Cu^{II}\text{-}DQ_{468}]$ as an HNO probe upon a dansyl-quinoline platform, which is highly sensitive and selective towards HNO but remains almost indifferent towards other biologically abundant reducing agents. DQ_{468} shows typical dansyl green emission, which is
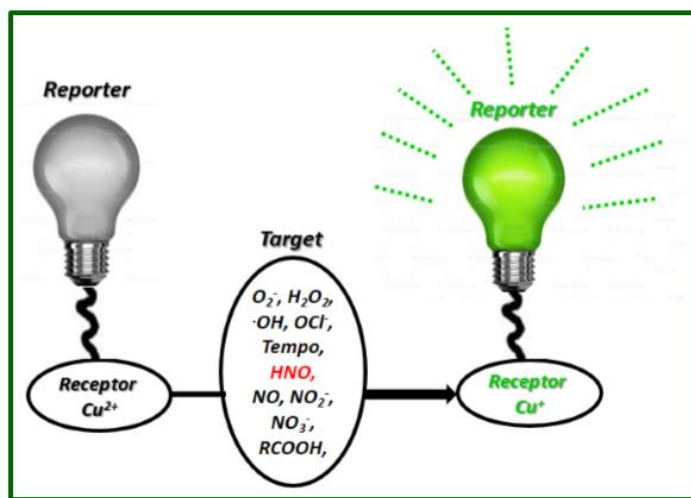
Scheme 4.2 Schematic representation of the copper-complex-based sensor for the detection of HNO. Here, the copper complex shows a weak fluorescence (light bulb off); and the only target HNO reduces the PET effect and enhances the fluorescence intensity (light bulb on).

better for living samples. Moreover, Cu^{II}-DQ_{468} detects HNO effectively in the biological pH range and it is water friendly, low cytotoxic and cell permeable, thus offering better detection of HNO in living cells. Dansyl is a classical fluorophore, and is used widely for its solvatochromism and high emission quantum yields.[43–45] Additionally, we employed 8-amino-quinoline as an excellent receptor for coordination to Cu(II) ions[41,46] and methyl pyridine as an auxiliary group for strong coordination with Cu(II). This new probe, in the presence of Cu^{2+}, displayed excellent sensitivity and selectivity towards HNO over other biologically reactive species **(Scheme 4.2)** and it was successfully applied to intracellular HNO detection. The coordination mode of the metal-free probe towards Cu^{2+} was established by ground-state DFT calculations on both the ligand and copper complexes.

4.2 Experimental section

4.2.1 Physical measurements

To record the IR spectra, an IR 750 series-II FTIR (Nickolet Magna) spectrophotometer was used in the range 400–4000 cm^{-1} on KBr pellets. An Agilent 8453 Diode-array UV-Vis spectrophotometer was used for recording the electronic spectra using 8:2 MeCN and HEPES buffer (10 mM) as the solvent in a 1 cm quartz cuvette in the range 200–900 nm. Fluorescence studies were carried out in a PTI (model QM-40) spectrofluorimeter. ESI-MS+ (m/z) spectra were recorded using a high-resolution mass spectrometer (Model: QTOF MicroYA263). ^{1}H NMR spectra were recorded in DMSO-d_6 with a Bruker 300 MHz instrument using trimethylsilane ($\delta = 0$) as an internal standard. The X-band EPR spectral studies were performed on an EPR-Spectrometer (Model: JEOL, JES-FA 200). The interaction of the copper complex towards HNO at different pH values was investigated. The pH of these solutions were recorded on a digital pH meter (Model: Systronics 335, India) in the pH range 2–11, which was previously calibrated using buffers of pH 4, 7 and 10. For the cell imaging study, a fluorescence microscope (Leica DM3000, Germany) was used.

4.2.2 Materials and methods

8-Aminoquinoline, 2-chloromethyl pyridine hydrochloride, dansyl chloride and potassium carbonate were used to prepare the ligand. These reagents were purchased from Sigma-Aldrich. Reactive biological species (H_2O_2, O^{2-}, TEMPO radical, NO_3^-, NO_2^-, ClO^-, AA), metal ions (Co^{2+}, Mn^{2+}, Na^+, Ni^{2+}, Zn^{2+}, Cu^{2+}, Al^{3+}, Hg^{2+}, Pb^{2+}, Sm^{3+}, Mg^{2+}, K^+, Fe^{3+}, Cr^{3+} and Cd^{2+}) and all the tested amino acids were obtained either from Sigma-Aldrich or from other commercial suppliers and used without further purification. Solvents like MeOH, MeCN, THF, etc., (Merck, India) were of reagent grade and dried before use.

4.2.3 Synthesis of the ligand

The ligand 5-dimethylamino-naphthalene-1-sulfonic acid pyridin-2-ylmethyl-quinolin-8-yl-amide (designated as DQ_{468}) was synthesized by a facile two-step procedure.

Step 1: Synthesis of pyridin-2-ylmethyl-quinolin-8-yl-amine, L1

Excess potassium carbonate (30 mmol) was added to the solution of 8-aminoquinoline (1 g, 6.93 mmol) in 20 ml dry acetonitrile with stirring for 1 h at room temperature. Then, a solution of 2-chloromethyl pyridine hydrochloride (1.13 g, 6.93 mmol) in acetonitrile was added drop wise to the reaction mixture under refluxing conditions at 120 °C. The reaction was continued for 8 h. and then solvent was evaporated and the residual part was purified through column chromatography using ethyl-acetate and hexane (v/v = 3: 7) as the eluent to obtain the pure yellow oily product, which was characterized and analyzed by ^{1}H NMR (**Figure 4.1**), ^{13}C NMR (**Figure 4.2**) and HRMS (**Figure 4.3**). ESI-MS+ (m/z): 236.1119 (L1 +H^+), ^{1}H NMR (in DMSO-d_6) (δ, ppm): 8.76 (s, 1H, –NH), 8.57 (d,1H, –ArH), 8.20 (1H, t, –ArH), 7.71 (1H, d, –ArH), 7.49 (1H, m,–ArH), 7.39 (2H, d, –ArH), 7.26 (2H, m, –ArH), 7.04 (d, 1H,–ArH), 6.56 (d, 1H, –ArH), 4.58 (d, 2H, –CH$_2$).
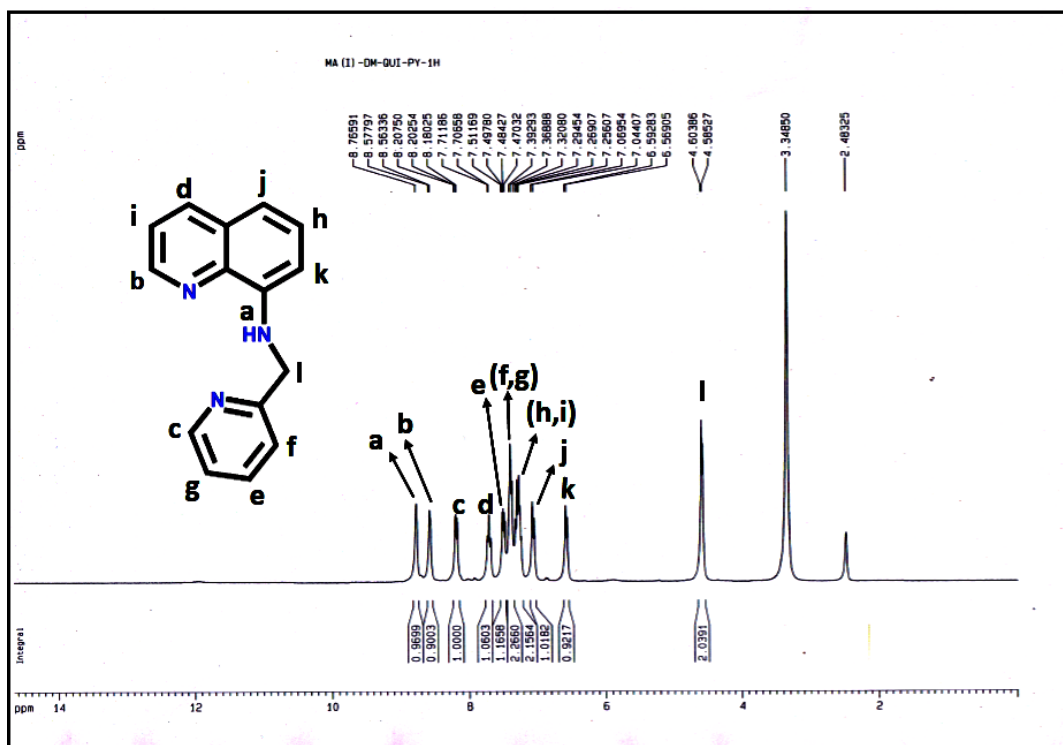
Figure 4.1. ^{1}H NMR spectrum of (**L1**) in DMSO-d_6.

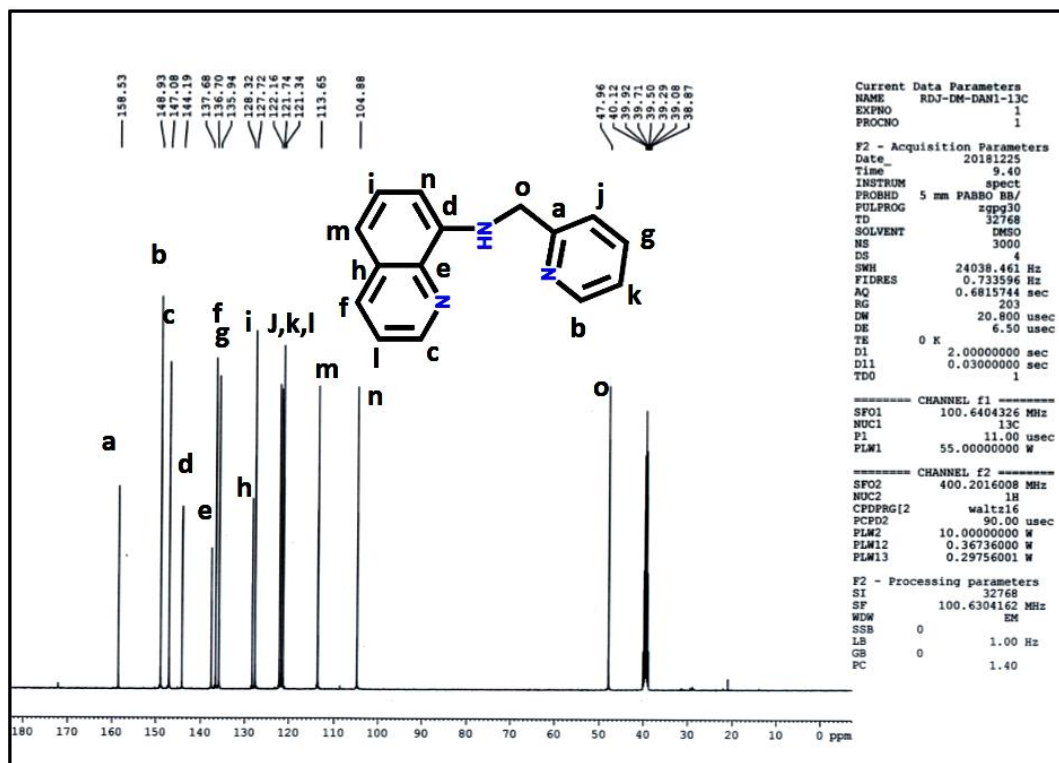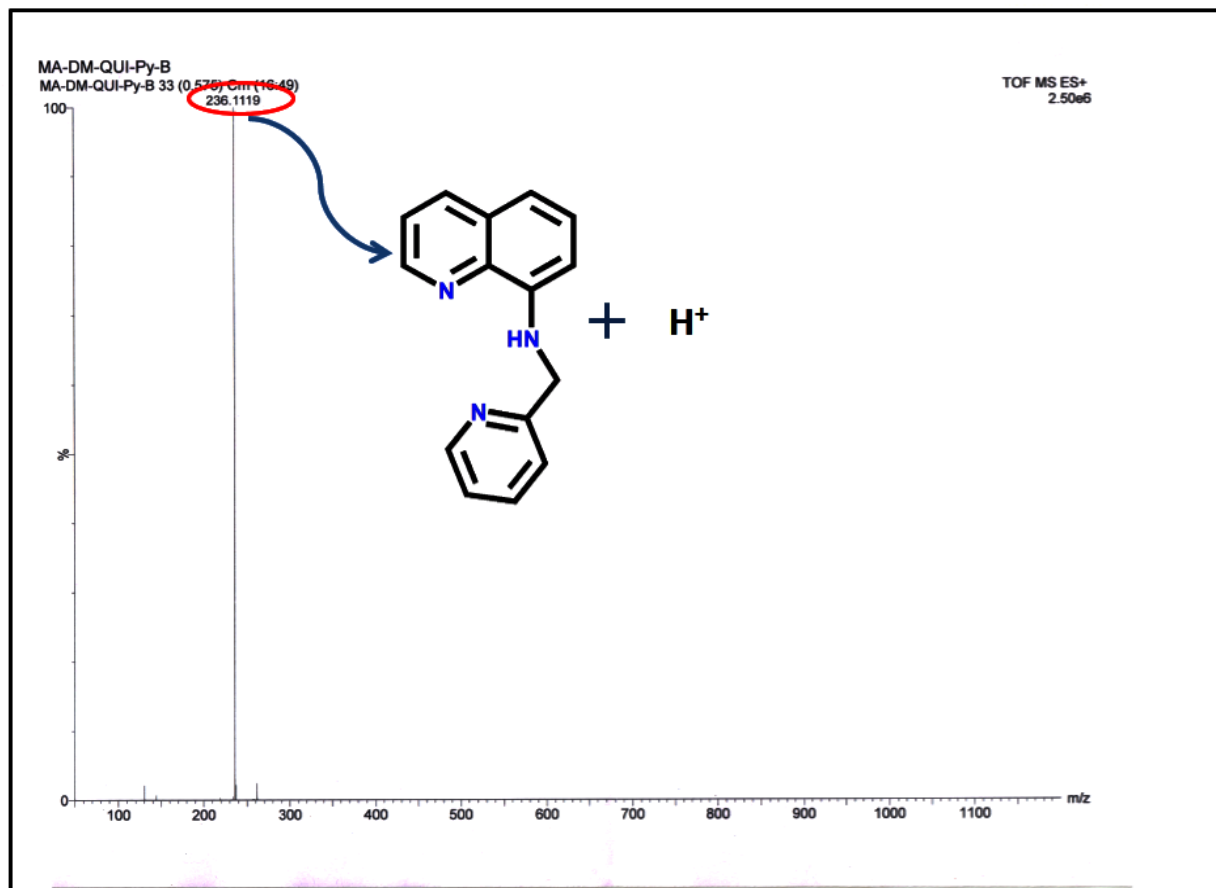**Figure 4.2.** ^{13}C NMR spectrum of (**L1**) in DMSO-d_6.

Figure 4.3 Mass spectrum of (**L1**) in MeCN.

Step 2: Synthesis of 5-dimethylamino-naphthalene-1-sulfonic acid pyridin-2-ylmethyl-quinolin-8-yl-amide, DQ$_{468}$

The compound obtained from step 1 (3 mmol) was further treated with excess potassium carbonate (15 mmol) in dry acetonitrile for 1 h under stirring. Dansyl chloride (3 mmol) was added to it in a cold condition under a nitrogen atmosphere. The reaction was allowed to continue overnight at room temperature. Then, the solvent was evaporated and the solid product was purified by column chromatography using ethyl-acetate and hexane (v/v = 3 : 7) as the eluent to obtain a pure solid product (DQ$_{468}$), which was characterized and analyzed by ^{1}H NMR (**Figure 4.4**), ^{13}C NMR (**Figure 4.5**), HRMS (**Figure 4.6**) and FTIR (**Figure 4.7**) ESI-MS+ (m/z): 469.2234 (DQ$_{468}$ + H$^+$), ^{1}H NMR (in DMSO-d$_6$) (δ, ppm): 8.38 (d, 1H, –ArH), 8.31 (s, 1H, –ArH), 8.18–8.21 (3H, t, –ArH), 7.90 (1H, d, –ArH), 7.76 (3H, t, –ArH), 7.53 (3H, m, –ArH), 7.26 (1H, t, –ArH), 7.17 (1H, d, –ArH), 7.02(d, 2H, –ArH), 5.28 (s, 2H, –CH$_2$), 2.77 (d, 6H, –CH$_3$).
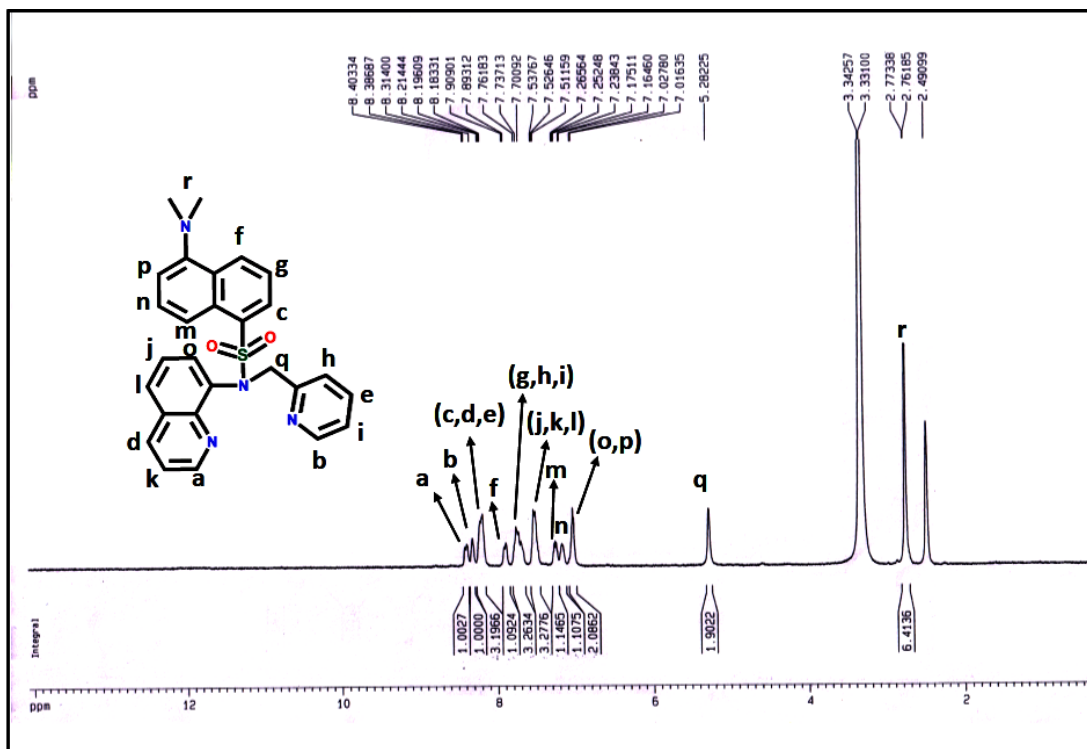
Figure 4.4 ^{1}H NMR spectrum of DQ$_{468}$ in DMSO-d_6.
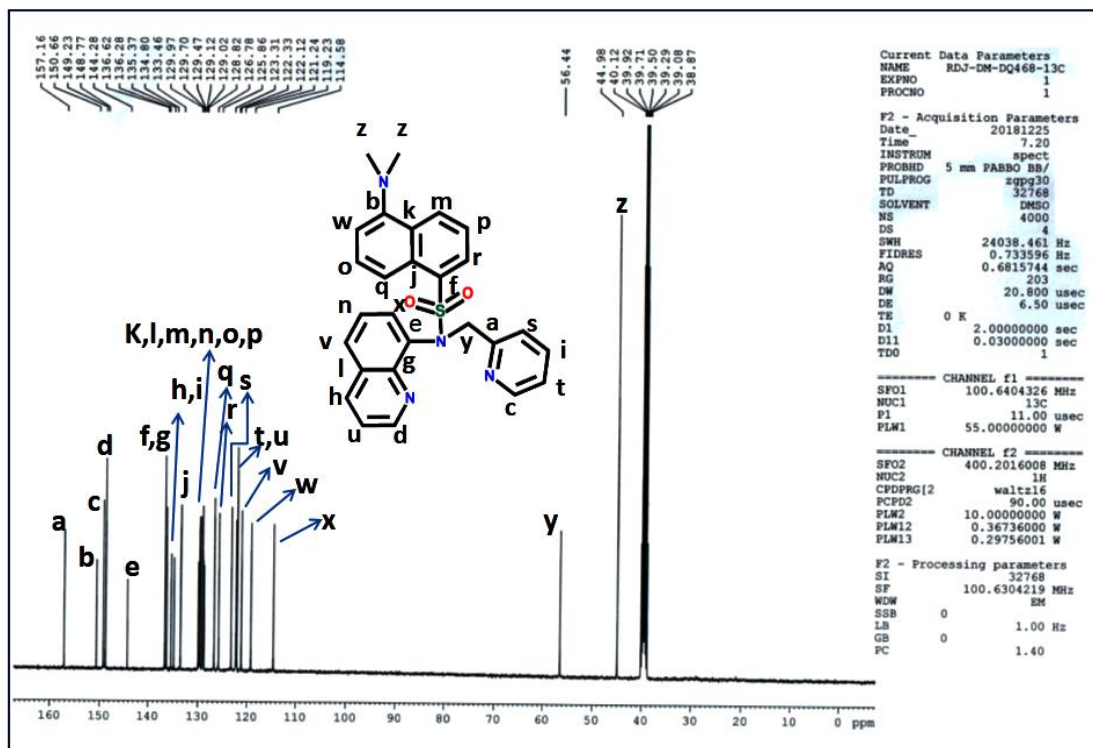
Figure 4.5 ^{13}C NMR of (DQ$_{468}$) in DMSO-d_6.

Figure 4.6 HRMS spectra of DQ$_{468}$

Figure 4.7 IR spectra of DQ$_{468}$

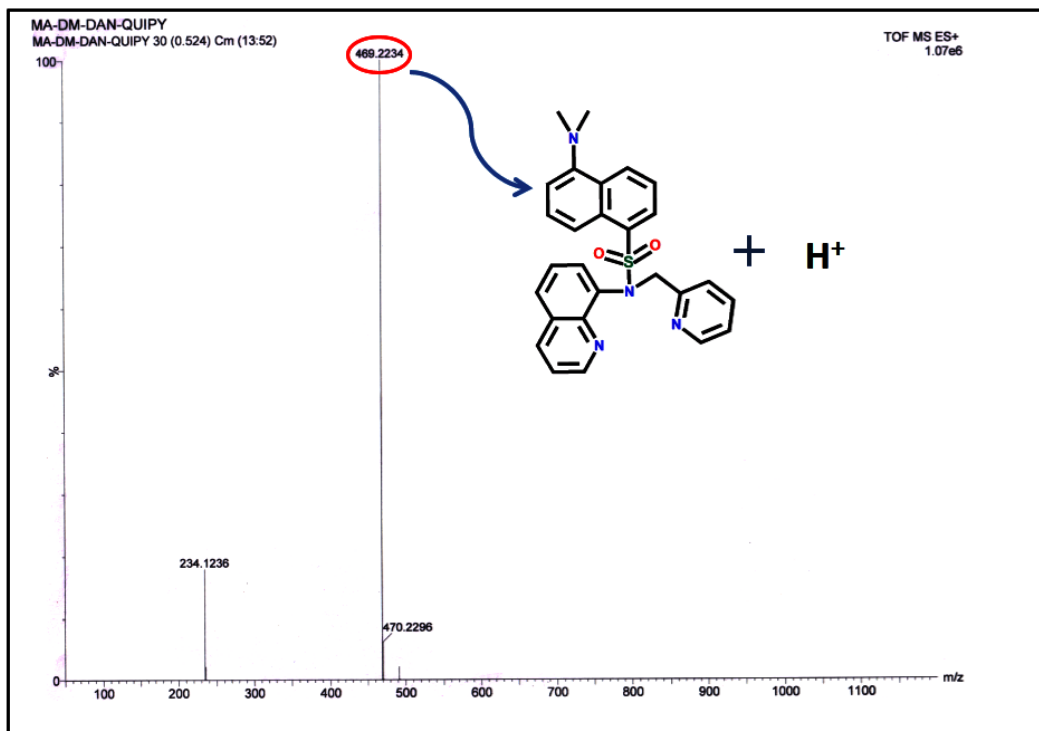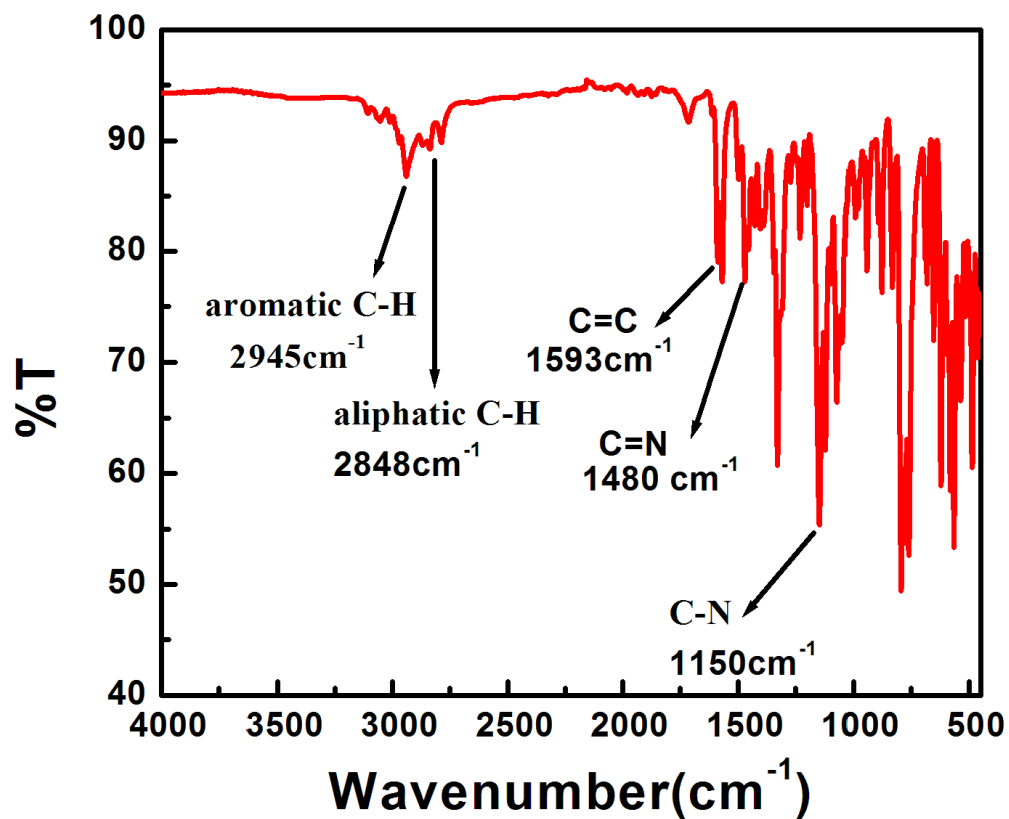## 4.2.4 Solution preparation for the UV-Vis absorption and fluorescence studies

A 10 mL 1.0×10^{-3} M stock solution of the ligand DQ_{468} was prepared in acetonitrile for the spectral studies. A stock solution of 1.0×10^{-2} M $CuCl_2 \cdot 2H_2O$ and Angeli's salt[9] in water were prepared in deoxygenated, deionized water separately under a N_2 atmosphere. A nitric oxide solution was prepared by purging nitric oxide gas for 15 min in a sealed vial with a syringe in deoxygenated water to give a resultant concentration of 1.74×10^{-3} M.[47,48] $ONOO^-$ and $^{\bullet}OH$ solutions were prepared using reported methods.[49] A 100 mL, 10.0 mM (4-(2-hydroxyethyl)-1-piperazineethanesulfonic acid) (HEPES) buffer solution was prepared with adjusting its pH to 7.0 using HCl and NaOH and the ionic strength of this solution was maintained at 0.10 M (NaCl) throughout the measurements. In this work, 20 μM DQ_{468} solution was taken in a cuvette containing 2.5 ml solution of MeCN–HEPES buffer (v/v = 8: 2 ratio) and titrations were carried out with Cu^{2+} solution for maximum fluorescence quenching and with the subsequent incremental addition of HNO in regular time intervals for fluorescence regeneration at $\lambda_{ex} = 390$ nm with slits 5 nm × 3 nm.

4.2.5 Calculation of the LOD

To determine the analytical limit of detection (LOD) of the ligand DQ_{468} and $[Cu^{II}(DQ_{468})Cl]^+$, we have followed the 3σ method.

$$LOD = 3 \times S_d/S$$

where, S_d is the standard deviation of the intercept for the plot of F.I. vs. $[DQ_{468}]$ for detection of Cu^{2+} and S is the slope obtained from the linear part of the FI vs. $[Cu^{2+}]$ plot. For HNO detection, S_d is the standard deviation of the intercept obtained from a plot of F.I. vs. $[Cu^{II}(DQ_{468})Cl]^+$ and S is the slope obtained from the linear part of the plot of FI vs. [HNO] .

4.2.6 Calculation of the quantum yield

For the determination of fluorescence quantum yields (Φ), we used the following equation

$$\Phi_{sample} = [(OD_{std} \times A_{sample})/ (OD_{sample} \times A_{std})] \times \Phi_{std}$$

where, A_{sample} and A_{std} represent the areas under the fluorescence spectral curves of the sample and standard, respectively. The optical densities of the sample and standard are designated as OD_{sample} and OD_{std}, respectively, at the excitation wavelength. Here, quinine sulfate was taken as the standard (Φ_{std} = 0.54) for the quantum yield calculation of the ligand DQ_{468} and $[Cu(DQ_{468})Cl]^+$.

4.2.7 Job's plot

We determined the composition of the complex with the help of Job's method. In this method, fluorescence intensities were measured for a series of solutions where the sum of DQ_{468} and $CuCl_2$ remains constant in a fixed volume, but changing the individual molar concentration and then plotted the fluorescence intensity against the mole fraction of Cu^{2+}. A break point was found at 0.5 mole fraction, indicating a (1:1) complex formation between DQ_{468} and Cu^{2+}.

4.2.8 Cell culture

Human hepatocellular liver carcinoma (HepG2) cell lines (NCCS, Pune, India) were grown in DMEM supplemented with 10% FBS and antibiotics (penicillin, 100 µg ml^{-1}; streptomycin, 50 µg ml^{-1}). Cells were cultured at 37 °C in a 95% air, 5% CO_2 incubator.

4.2.9 Cell cytotoxicity assay

The cytotoxicity for ligand DQ_{468} was assessed by the 3-(4,5-dimethylthiazol-2-yl)-2,5-diphenyltetrazolium bromide (MTT) cell viability assay. HepG2 cells (1 × 105 cells per well) were cultured in a 96-well plate incubated at 37 °C, and were exposed to varying concentrations of DQ_{468} (5, 10, 20, 30, 40, 50, 60, 70, 80, 90 and 100 µM) for 24 h. After the incubation, 10 µL of MTT solution [5 mg ml^{-1}, dissolved in 1× phosphate-buffered saline (PBS)] was added to each well of the 96-well culture plate, and then incubated at 37 °C for 4 h. The media were decanted from the wells and 100 µL of 0.04 N acidic isopropyl alcohol was added into each well to solubilize the intracellular formazan crystals (blue-violet) formed. Absorbance of the solutions was measured at 595 nm (EMax Precision MicroPlate Reader, Molecular Devices, USA). Values

were calculated as the mean ± standard errors of three independent experiments. The cell viability was expressed as the optical density ratio of the treatment to control.

4.2.10 Cell imaging study

HepG2 cells were cultured in a 35 × 10 mm culture dish on a cover-slip for 24 h at 37 °C. The cells were treated with 5 μM and 10 μM solutions of DQ_{468}, prepared by dissolving it in a mixed solvent of DMSO: water = 1 : 9 (v/v) and incubated for 1 h at 37 °C. For the complex formation study with Cu^{2+} ions, HepG2 cells were pre-incubated with 10 μM of DQ_{468} for 60 min at 37 °C, followed by washing three times with 1× PBS and subsequent incubation with 10 μM of Cu^{2+} for 60 min at 37 °C. To study the nitroxyl (HNO) sensing property of the ligand, HepG2 cells were pre-incubated with 10 μM of DQ_{468} for 60 min at 37 °C, followed by washing three times with 1×PBS and subsequent incubation with 10 μM of Cu^{2+} for 60 min at 37 °C again, followed by washing three times with 1× PBS and subsequent incubation with 10 μM of Angeli's salt $[Na_2N_2O_3]$, for 60 min at 37 °C. Fluorescence images of HepG2 cells were taken by a fluorescence microscope (Leica DM3000, Germany) with an objective lens of 40× magnification.

4.2.11 Computational details

Ground-state electronic structures of the ligand and complexes were calculated in acetonitrile solution using the DFT method[50] associated with the conductor-like polarizable continuum model (CPCM).[51] Becke's hybrid function[52] with the Lee–Yang–Parr (LYP) correlation function[53] were utilized throughout the study. The fully optimized geometries of the ligand and complexes were determined without any symmetry restrictions. The nature of all the stationary points for both the metal-free ligand DQ_{468} and its Cu^{2+} complex were recognized by using normal mode analysis. The UV-Vis absorption spectral properties of DQ_{468} and the complexes $[Cu^{II}(DQ_{468})Cl]^+$ and $[Cu^{I}(DQ_{468})]^+$ in acetonitrile were estimated on the basis of their optimized ground-state geometries, by time-dependent density functional theory (TDDFT)[54] related to the conductor-like polarizable continuum model (CPCM).[51] We computed the lowest 40 singlet–singlet transitions and the electronic excitation energies were obtained accurately due to the

presence of electronic correlation in the TDDFT (B3LYP) method.[55] For ground-state optimization, we used the 6-31G(d) basis set. Gauss View 5.1 software was used for the calculation of the electron density plots in the frontier molecular orbital. All the calculations were obtained using Gaussian 09W software package.[56] We also used the Gauss Sum 2.1 programe[57] for the calculation of the molecular orbital contributions from atoms or groups.

4.3 Results and discussion

4.3.1 Synthesis and photophysical properties

Figure 4.8 A displays the synthetic pathway of the present probe DQ_{468}. It involves two steps nucleophilic substitution reactions. In the initial step, 8-aminoquinoline was allowed to react with commercially accessible 2-(chloromethyl) pyridine in the presence of K_2CO_3 in MeCN in a 1 : 1 mole ratio under refluxing conditions for 24 h to obtain L^1 (pyridin-2-ylmethyl-quinolin-8-yl-amine)., This compound was then treated with dansyl chloride, a fluorophoric moiety, in a 1:1
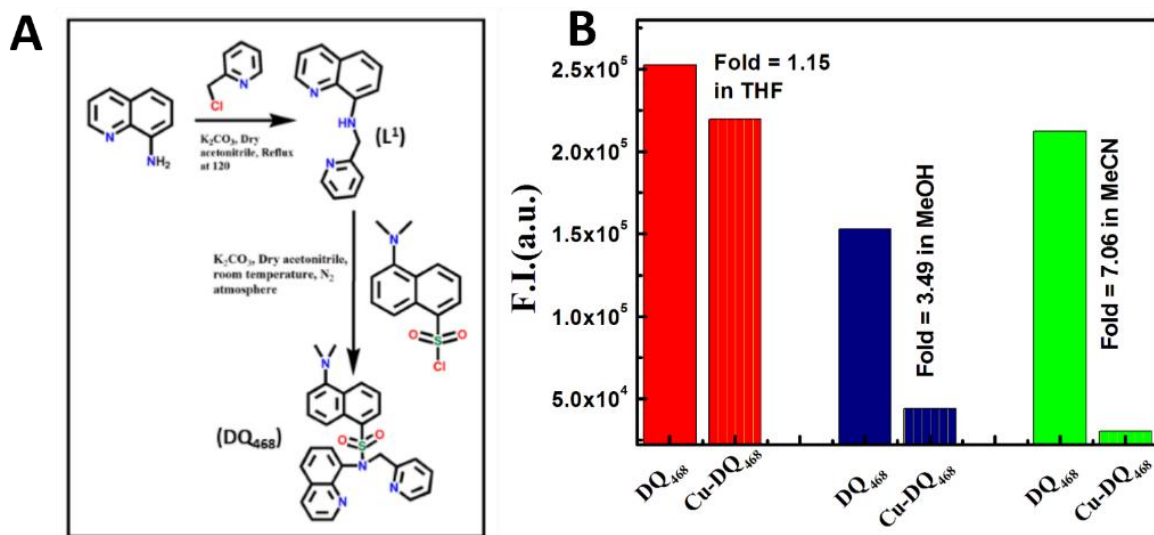
Figure 4.8 A. Schematic representation of synthesis of probe DQ_{468} **B**. Solvent selectivity of Cu(II)-complex formation of probe DQ_{468}.

mole ratio under a N_2 atmosphere in a cold condition and allowed to proceed overnight, under constant stirring condition to get the solid product on vacuum evaporation. The intermediate (L^1) and target compound were thoroughly characterized by different spectroscopic techniques. The

complex Cu^{II}-DQ$_{468}$ was prepared by the stoichiometric reaction of CuCl$_2$·2H$_2$O and DQ$_{468}$ in MeCN and characterized by mass and EPR analysis. These studies are in good agreement with the chemical formula [Cu^{II}(DQ$_{468}$)Cl]Cl of the complex. Before going for more detailed experiments, we have checked the fluorescence responses of DQ$_{468}$ towards Cu^{II} in various solvents, like THF, MeOH and MeCN. It was observed that the complex formation of DQ$_{468}$ with Cu(II) occurred in MeCN efficiently, while in THF and MeOH, a large excess of Cu^{2+} was needed to quench the fluorescence intensity (**Figure 4.8 B**). So we have selected MeCN as an organic solvent for the more detailed studies. There is also a previous report where MeCN was used as a solvent for the reduction of Cu(II) to Cu(I).[58]

4.3.2 UV-Vis study

The spectrophotometric titration of the probe was performed with the gradual addition of Cu^{2+} in an aqueous–organic medium (10 mM HEPES buffer: acetonitrile = 2:8 solution, v/v) at pH
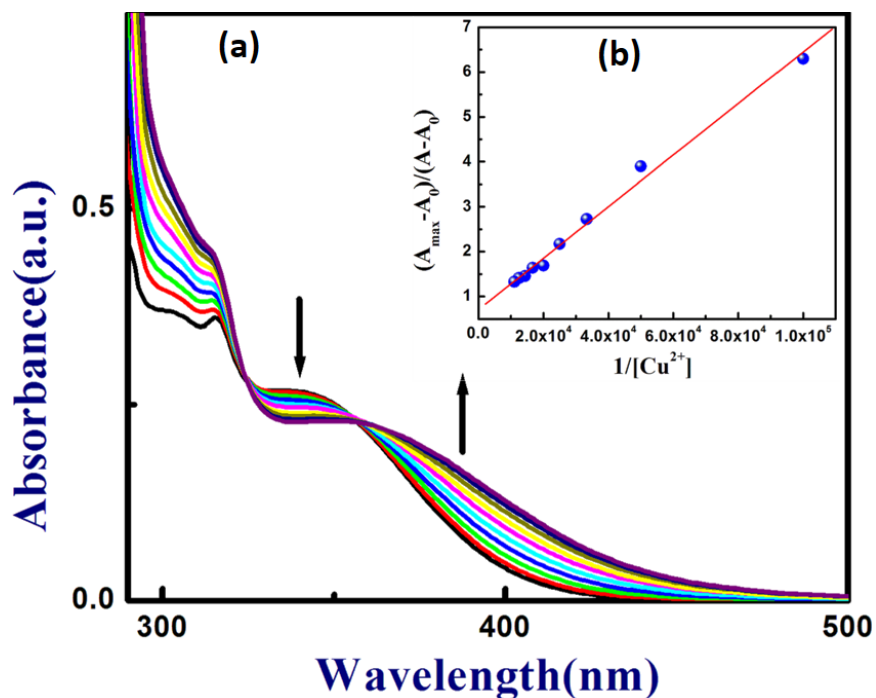
Figure 4.9 (a) Absorption titration of DQ$_{468}$ with the gradual addition of Cu^{2+} in MeCN : HEPES buffer medium (v : v = 8 : 2) at pH 7.0 at 25 °C; (b) Benesi–Hildebrand plot.

7.0. This study clearly demonstrated that the absorption of DQ_{468} at 337 nm vanishes gradually, with the concomitant development of a new peak at 370 nm upon the incremental addition of Cu^{2+} (**Figure 4.9 a**). This occurrence is expected due to the coordination of DQ_{468} towards Cu^{2+}. The data obtained from the UV-Vis titration was solved easily using the Benesi–Hildebrand equation, where A_0 and A_{max} are the absorbances of the ligand in the absence and presence of excess Cu^{2+}. By considering eqn. (1), a linear fit was obtained from the plot of $(A_{max} - A_0)/(A - A_0)$ vs. $1/[M]$, which clearly manifests the 1:1 complex formation (n = 1) and provided an apparent formation constant K_f of $(1.74 \pm 0.17) \times 10^4\ M^{-1}$ (**Figure 4.9 b**).

$$\frac{(A_{max}-A_0)}{(A-A_0)} = 1 + \frac{1}{K[M]^n} \qquad (1)$$

4.3.3 Fluorescence quenching studies

The emission spectral pattern of the probe DQ_{468} exhibited a typical dansyl green fluorescence at λ_{em} = 543 nm on excitation at 390 nm. The fluorescence titration of DQ_{468} with Cu^{2+} was performed taking a fixed concentration of DQ_{468} (20 µM) in aqueous–acetonitrile medium (10 mM HEPES buffer: acetonitrile = 2: 8 solution, v/v) at pH 7.0 and µ = 0.10 M NaCl. Then, freshly prepared Cu^{2+} solution was added progressively, which led to the gradual decrease in the fluorescence intensity of DQ_{468}. The complete complex formation occurred upon the addition of ~5 equivalent of Cu^{2+}, yielding almost a 7-fold decrease in fluorescence intensity, which was sufficient to detect Cu^{2+} (**Figure 4.10 a**). The degree of fluorescence quenching was evaluated by obtaining a linear Stern–Volmer eqn. 2, between the ratio of the relative fluorescence intensities, (F_{max}/F) and [Q] [59] where F_{max} and F are the steady state fluorescence intensities in the absence and presence of the quencher (Cu^{2+}), respectively, and [Q] is the Cu^{2+} ion concentration. The estimated (K_{SV}, quenching constant Stern–Volmer constant) was found to be K_{SV} = (7.32 ±0.08) $\times 10^4\ M^{-1}$ (**Figure 4.10 b**).

$$\frac{F_{max}}{F} = 1 + K_{SV}[Q] \qquad (2)$$

A Job's plot was constructed to determine the mole ratio of reaction between Cu^{2+} and DQ_{468} by following the change in fluorescence intensity at 543 nm (**Figure 4.10 c**). The Job's plot clearly exhibited the 1:1 complex formation by a break point at 0.5. This was further supported by the mass spectrum of this species, m/z =566.168, which corresponds to $[Cu(DQ_{468})Cl]^{+}$ (**Figure 4.11**). We have also calculated the quantum yield of the metal free DQ_{468} and $[Cu(DQ_{468})Cl]^{+}$, which were found to be 0.135 and 0.026, respectively.
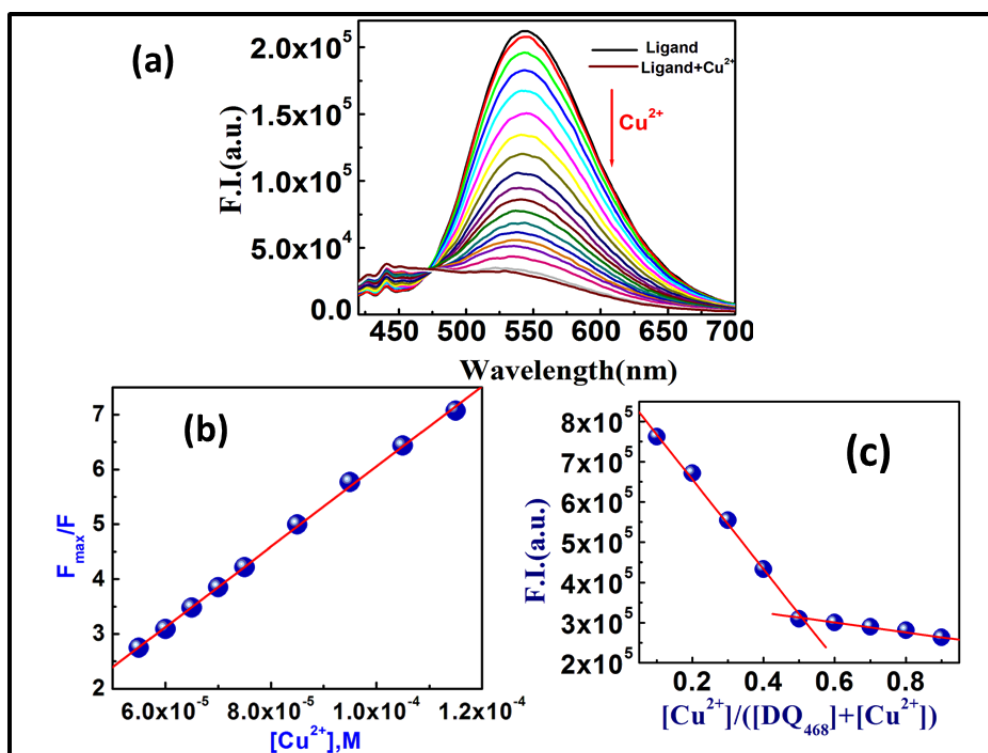
Figure 4.10 (a) Fluorescence titration of DQ_{468} (20 µM) at 25 °C by the incremental addition of Cu^{2+} (0–100 µM) in HEPES buffer (10 mmol) : acetonitrile medium (2 : 8) at pH 7.0 with λ_{ex} = 390 nm and λ_{em} = 543 nm. (b) Linear Stern–Volmer plot, (c) Job's plot.

From the literature reports, [60,61] we could presume that a strong interaction has been taken place between DQ_{468} and doubly charged copper ion, leading to the effective quenching of the fluorescence intensity of DQ_{468}, which could be ascribed to the photoinduced electron transfer (PET) mechanism from the dansyl fluorophore to the chelated Cu^{2+}. Additionally, this probe exhibits the limit of detection of 0.091 µM (**Figure 4.12**).
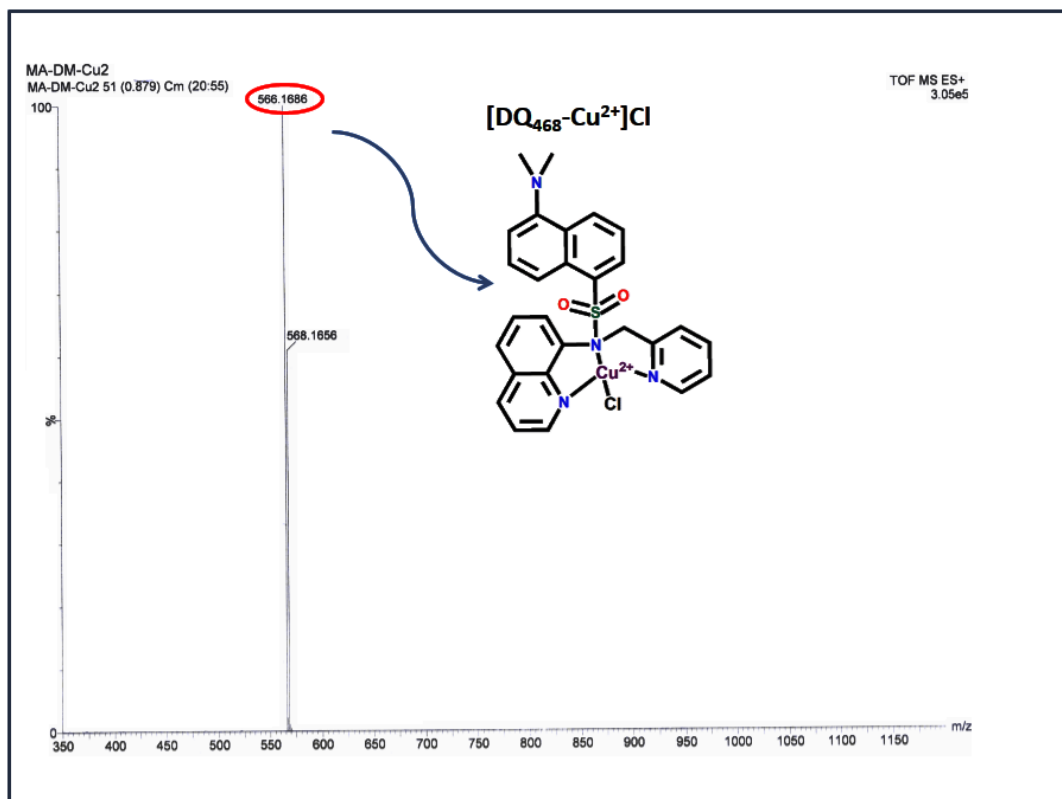
Figure 4.11 Mass spectra of Cu^{2+} complex of probe DQ$_{468}$.
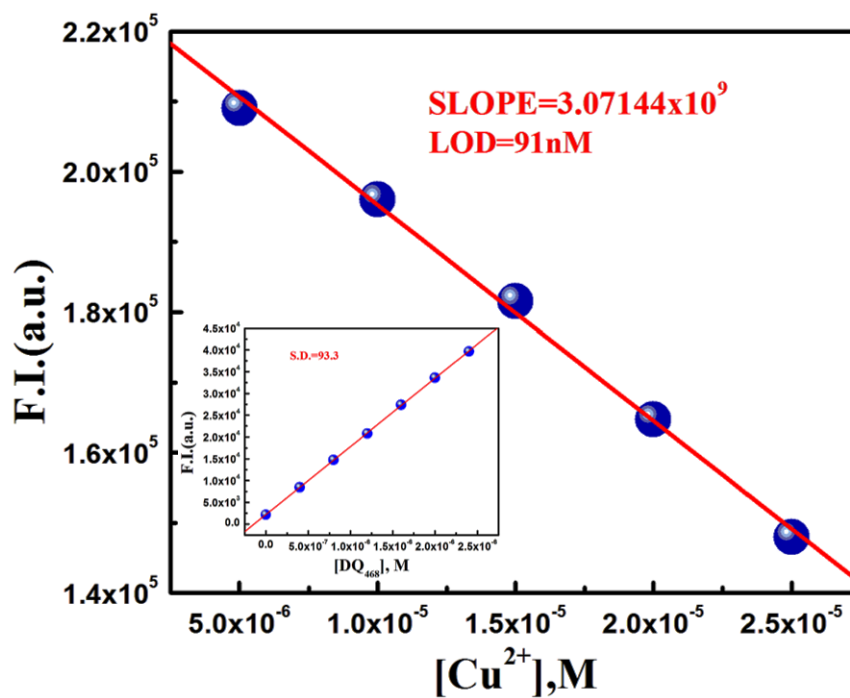
Figure 4.12 LOD of DQ$_{468}$ to Cu^{2+}.

4.3.4 Analyte selectivity and HNO-induced reduction of $[Cu(DQ_{468})Cl]^+$

The ability of a fluorescent probe to sense a particular analyte depends on the specificity of its chemical reactions and chemical properties. We have checked the reactivity of the probe (DQ_{468}) towards some commonly known metal ions. This study exhibited a high affinity of the probe only towards Cu^{2+} (**Figure 4.13**) without any interference from other metal ions, except Fe^{3+}, which showed a slight quenching of F.I. of DQ_{468}, but it was interesting to see that the further addition of HNO produced no influence on its F.I. Thus, the recognition of HNO by $[Cu^{II}(DQ_{468})Cl]^+$ complex is highly selective. This Cu^{II}-complex is also inert towards other commonly known biological reactive oxygen, nitrogen and sulfur species (ROS, RNS, RSS) present in the live cells. The selectivity tests were performed in aqueous–acetonitrile (v/v = 2 : 8) medium (pH 7.0 and μ =0.10 M NaCl), taking a fixed concentration of DQ_{468} (20 μM). Here, we have screened a wide array of reactive oxygen, nitrogen and sulfur species, like NO, H_2O_2, NO_3^-, NO_2^-, AA, ClO^-, O^{2-}, •OH, TEMPO, $ONOO^-$, HS^-, S^{2-} in excess (10 equivalence) upon the probe DQ_{468}. But none other than HNO could induce an enhancement of the fluorescence intensity of $[Cu^{II}(DQ_{468})Cl]^+$ (**Figure 4.14 A**). Upon treatment with Angeli's salt (HNO donor), the fluorescence intensity was restored up to 90% (6-fold). In aqueous solution (pH 7,) Angeli's
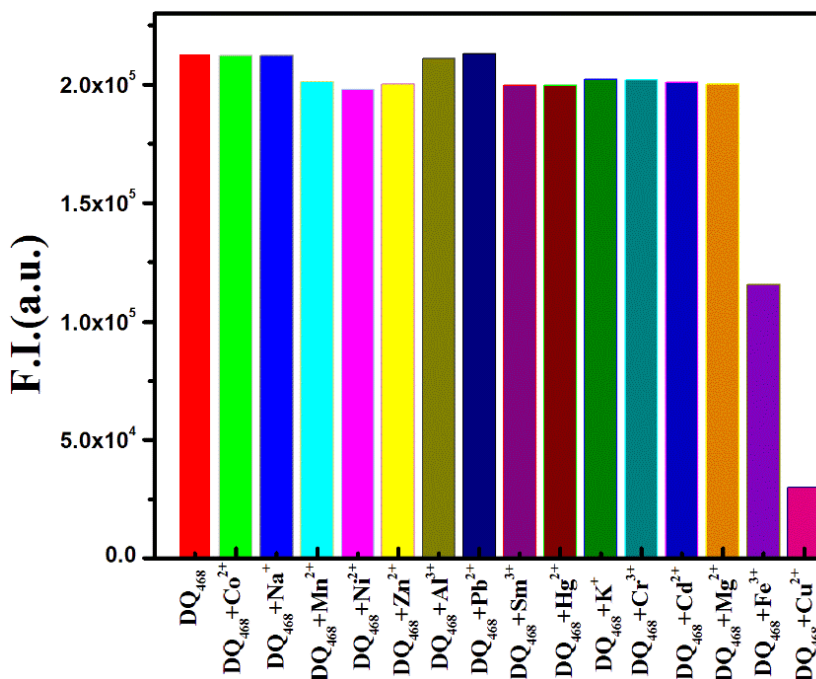
Figure 4.13 Metal ion selectivity test of DQ_{468}
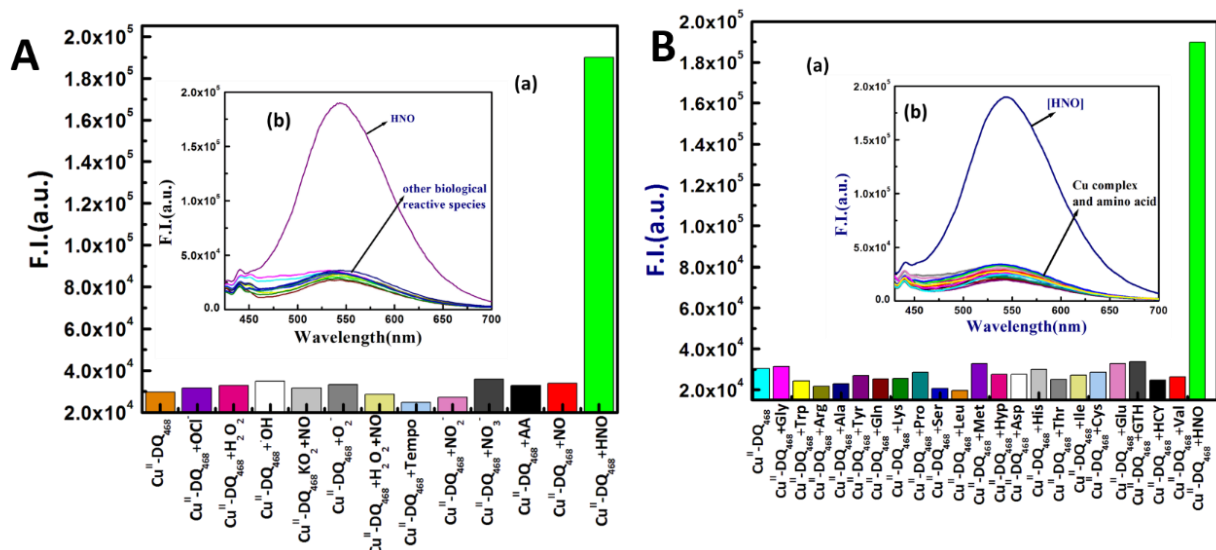
Figure 4.14.A. (a) Bar plot representing the fluorescence responses of $[Cu^{II}(DQ_{468})Cl]^+$ at 543 nm (λ_{ex} = 390 nm) towards various biological reactive species in MeCN : HEPES buffer (8 : 2, v/v) at room temperature at pH 7.0, DQ_{468} = 20 μM, X^n = 200 μM. (b) Corresponding spectral responses of DQ_{468}. **B.** (a) Bar plot representing the fluorescence responses of $[Cu^{II}(DQ_{468})Cl]^+$ at 543 nm (λ_{ex} = 390 nm) towards various amino acids with the conditions: (8 : 2, v/v) MeCN/HEPES buffer; 25 °C, pH 7.0 $[Cu^{II}(DQ_{468})Cl]^+$ = 20 μM, amino acid = 200 μM. (b) Corresponding spectral responses of $[Cu^{II}(DQ_{468})Cl]^+$ towards different amino acids.

salt ($Na_2N_2O_3$) undergoes dissociation to form HNO as well as $NaNO_2$ [62] which may be the reason behind the reduction of metal ions. To verify that HNO was solely responsible for the regeneration of fluorescence through reduction, the reactivity of $[Cu(DQ_{468})Cl]^+$ towards $NaNO_2$ was checked. But here, no detectable fluorescence enhancement was observed (**Figure 4.14 A**) leading to the conclusion that the fluorescence enhancement occurred only due to HNO, not by the side product (NO_2^-). Interestingly, the probe $[Cu(DQ_{468})Cl]^+$ showed no significant change in fluorescence intensity upon the addition of saturated NO solution even though HNO and NO are very closely related biological species. So, the difference in the interaction of $[Cu(DQ_{468})Cl]^+$ towards NO and HNO magnifies the beauty of our system towards HNO detection over NO. Our probe also showed inertness towards biologically abundant reactive sulfur species, like L-(+)-cysteine, GSH and HCY (**Figure 4.14 B**), and also towards important amino acids. All these experiments showed that our Cu-complex-based HNO probe was highly specific towards HNO over other reactive species present in the biological milieu.

4.3.5 Fluorescence studies on HNO-induced reduction of $[Cu(DQ_{468})Cl]^+$

HNO is a sufficiently strong reducing reagent for the quantitative reduction of Cu(II) to Cu(I). So in our present work, there was an adequate possibility for the formation of diamagnetic Cu(I) from paramagnetic Cu(II) with the concomitant regeneration of the fluorescence intensity under the influence of HNO. This redox-based HNO sensing strategy is a useful pathway for the detection of HNO in living cells also. We found that there was a marked increase in fluorescence response (30-fold) of $[Cu(DQ_{468})Cl]^+$ upon the incremental addition of HNO in pure MeCN, but when the same experiment was performed in 10% and 20% HEPES buffer at pH 7.0, the fluorescence enhancement was observed to be 8-fold and 6-fold respectively (**Figure 4.15 A**). We have used MeCN–H_2O (8: 2 v/v) throughout the experiments as the extent
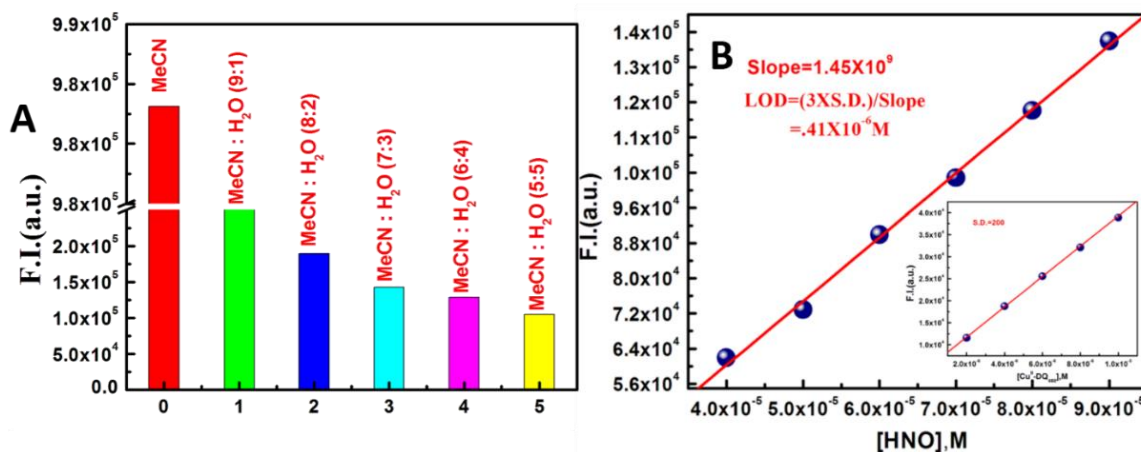
Figure 4.15 A Water variation on HNO induced reduction of $[Cu^{II}(DQ_{468})Cl]^+$. **B.** LOD of $[Cu^{II}(DQ_{468})Cl]^+$ to HNO.

of fluorescence regeneration in this solvent mixture was sufficient to detect HNO in living cells also. It was noteworthy that the fluorescence intensity of DQ_{468} dramatically reduced (almost 7-fold) upon addition of $\sim$5 equivalent of Cu^{2+} due to paramagnetic Cu^{2+} complex formation, which upon exposure to HNO, gets reduced to Cu(I), restoring the fluorescence intensity up to 90% to that of DQ_{468} and limit of detection for HNO sensing was calculated to be 0.41 μM (**Figure 4.15 B**). The formation constant of $[Cu^{I}(DQ_{468})]^+$ was determined by the Benesi–Hildebrand equation, and was found to be $(3.096 \pm 0.08) \times 10^3$ M^{-1} (**Figure 4.16**).
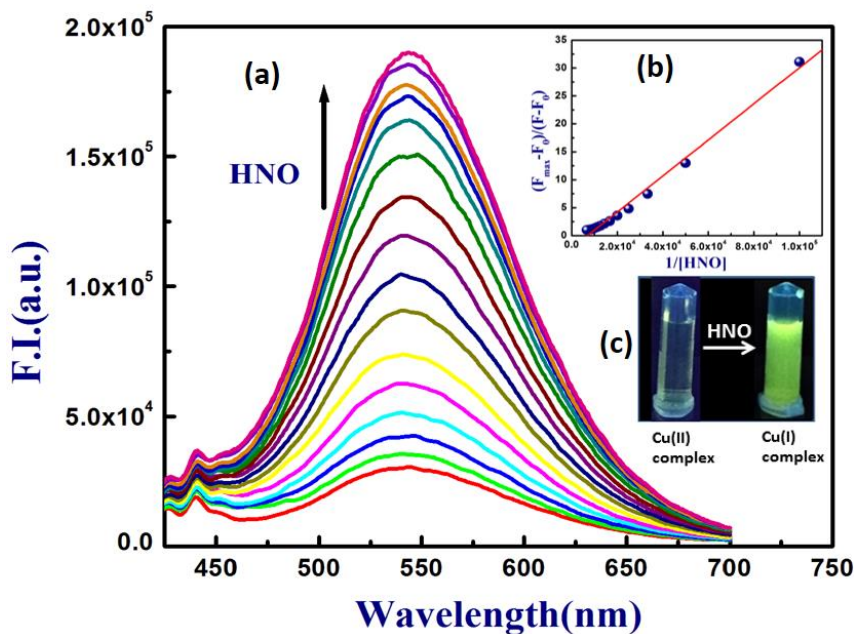
Figure 4.16 (a) Fluorescence titration of $[Cu^{II}(DQ_{468})Cl]^+$ at 25 °C by the incremental addition of HNO in acetonitrile : HEPES buffer (8 : 2) (10 mmol) at pH = 7.0 with λ_{ex} = 390 nm and λ_{em} = 543 nm; (b) Benesi–Hildebrand plot. (c) UV exposed emission image of $[Cu^{II}(DQ_{468})Cl]^+$ and Cu(I)-DQ$_{468}$.

4.3.6 Mechanistic view of HNO sensing

Till date, the regeneration of the fluorescence intensity of the previously reported Cu^{2+} complex towards HNO, occurred in one of three following ways (**Scheme 4.3**):[10,40–42,46] (a) turn-on sensing by the reduction of the metal center with a simultaneous displacement of the probe; in
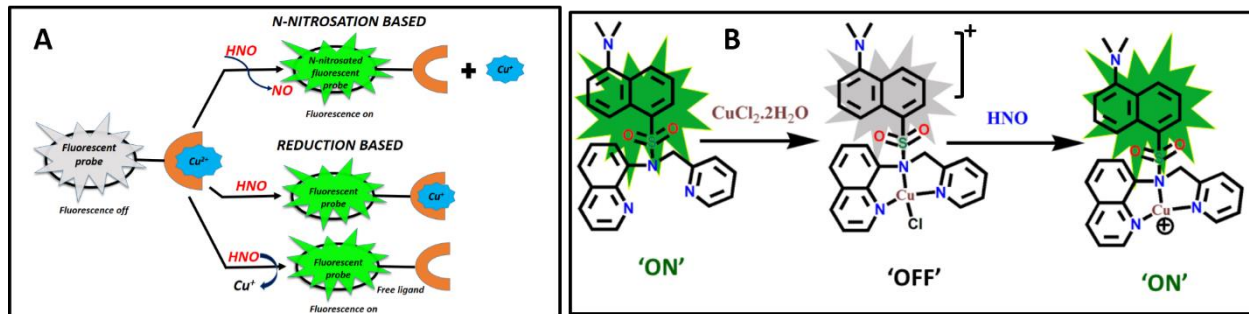
Scheme 4.3 A. Established mechanisms for HNO detection. **B**. Working mechanism in the present work.

this process a N-nitrosation reaction occurs on the secondary nitrogen atom with concomitant removal of Cu(I). In this case, the fluorescence emission property of the probe may change; (b) turn-on sensing due to the reduction of Cu^{2+} without removal of the fluorophore; in this mechanism, 100% recovery of the fluorescence intensity of the probe may not occur because the PET from the fluorophore to the Cu^+ is not fully blocked, leading to lowering of the electron
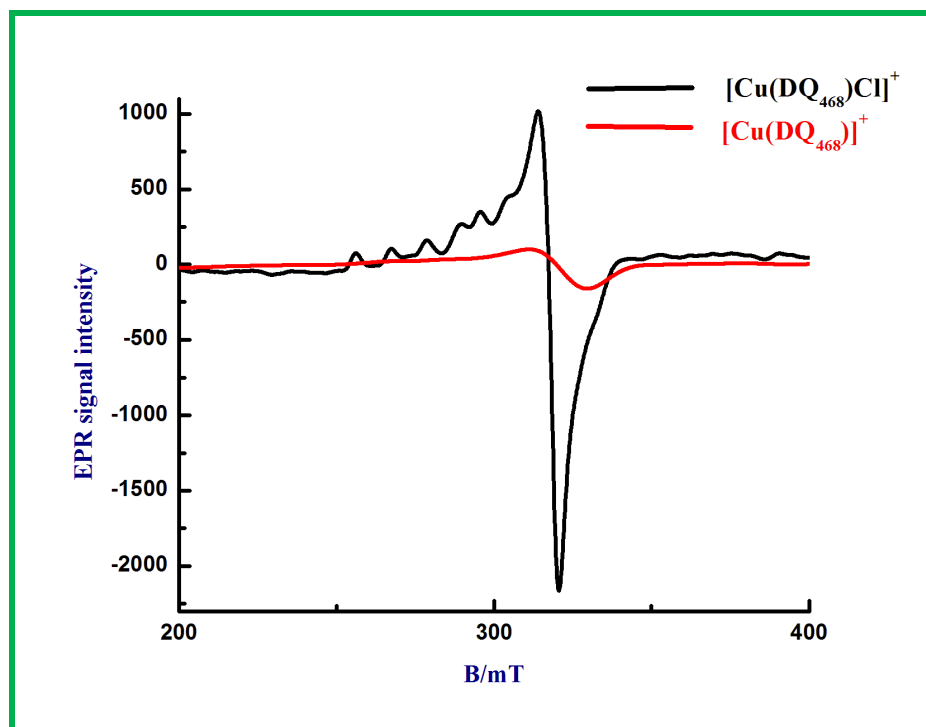
Figure 4.17 EPR spectrum of $[Cu^{II}(DQ_{468})Cl]^+$ (20 μM) and $[Cu^I(DQ_{468})]^+$ (in situ reduction with excess $Na_2N_2O_3$) at 77 K.

density on the probe; and (c) turn-on sensing caused by the formation of diamagnetic Cu^+ species from paramagnetic Cu^{2+} with subsequent removal of the probe; this mechanism results in ~100% recovery of the fluorescent intensity. Among the above-said probable mechanisms, particularly (b) is operative in our present investigation (**Scheme 4.3 B**). Here, DQ_{468} forms a Cu^{II}-complex leading to fluorescence quenching (PET-ON), and subsequent regeneration of fluorescence was achieved by the nitroxyl (HNO) addition, transforming Cu(II) to Cu(I) (PET OFF).[40,42,63,64] This phenomenon was justified by the EPR spectroscopy (**Figure 4.17**) and mass spectrometric (**Figure 4.18**) analysis. The EPR spectrum of $[Cu(DQ_{468})Cl]^+$ is a typically axial type with $g\perp$ = 2.051 and $g\parallel$ = 2.321, indicating the presence of a paramagnetic Cu^{2+} ion. Upon treatment with

Angeli's salt ($Na_2N_2O_3$) the spectrum clearly showed that the previous characteristic signals of Cu^{2+} was vanished to base-line, i.e. the newly formed product was EPR silent, indicating the presence of the metal ion in its reduced form (Cu^I). Here, as the metal is
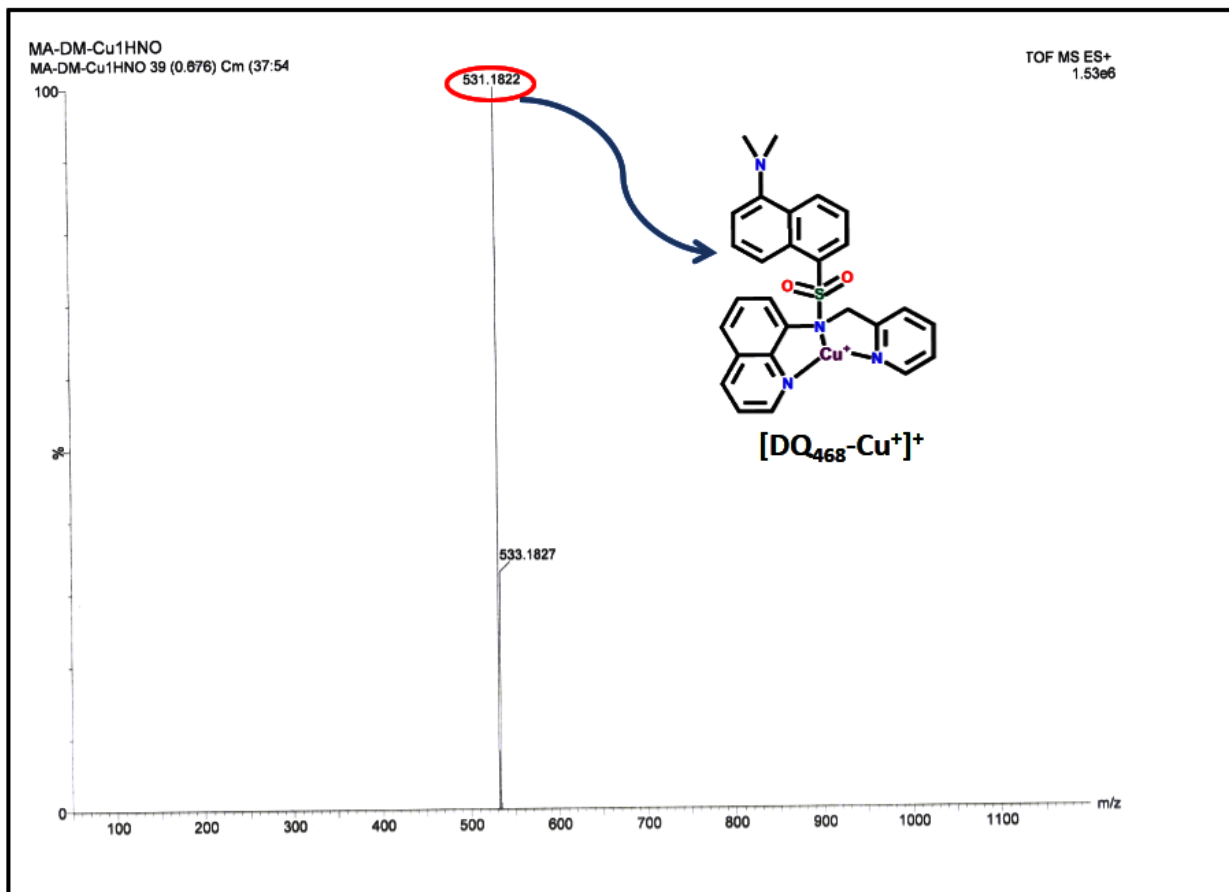
Figure 4.18 Mass spectrum of $[Cu(DQ_{468})Cl]^+$ $Na_2N_2O_3$.

still coordinated to the probe as Cu^+, PET is not blocked fully, resulting in a lowering of the fluorescence intensity with respect to metal-free DQ_{468}. We have also checked the fluorescence response of DQ_{468} towards CuCl salt. The corresponding spectrum was very much similar to that of the HNO-treated spectrum of Cu^{II}-DQ_{468} (**Figure 4.19 A**). This HNO-induced reduction was further supported by the mass spectroscopy, where, ESI-MS+ of $[Cu(DQ_{468})Cl]^+$ corresponds to (m/z): 566.1152 (**Figure 4.11**) and ESI-MS+ of $[Cu(DQ_{468})]^+$ corresponds to (m/z): 531.1822 (**Figure 4.18**).
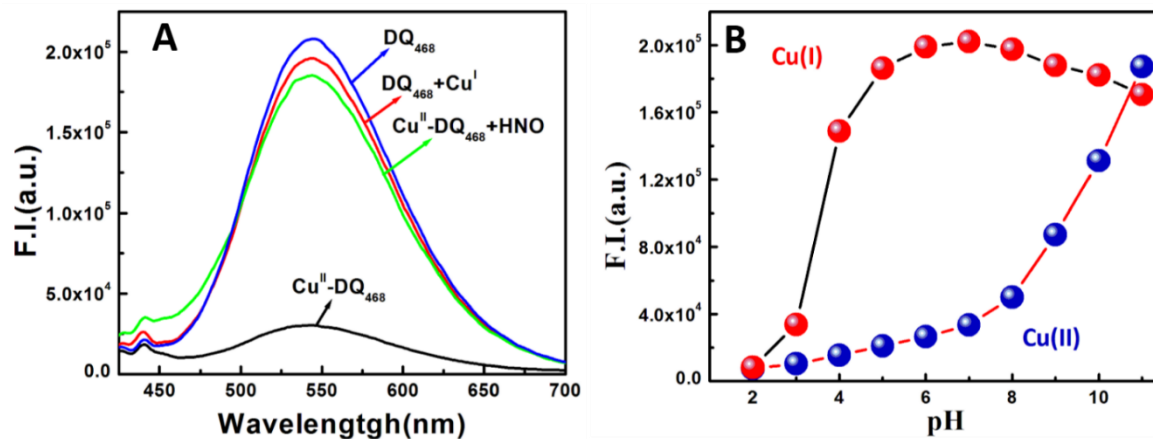
Figure 4.19 A. Emission spectra of DQ$_{468}$ in presence of CuI. **B.** pH-Dependent fluorescence responses of [Cu^{II}(DQ$_{468}$)Cl]$^+$ and [Cu^{I}(DQ$_{468}$)]$^+$ in 8 : 2 (v/v) MeCN/HEPES buffer medium.

4.3.7 pH effect on [Cu^{II}(DQ$_{468}$)Cl]$^+$ and [Cu^{I}(DQ$_{468}$)]$^+$

For the proper biological application of any fluorescent sensor, the sensing should occur in a wide array of pH because different cells or different compartments of a same cell, may have different pH values. However, in the presence of copper(II) chloride, the fluorescence of DQ$_{468}$ was of low intensity and exhibited almost an invariant emission profile over a pH range from 2 to 8 (**Figure 4.19 B**). Then upon treatment with HNO, the Cu(II) bound probe exhibited a drastic enhancement in fluorescence intensity in a wide scale of pH (4–10). This large increase in fluorescence intensity in a wide range of pH suggests that our Cu-complex-based probe [Cu(DQ$_{468}$)Cl]$^+$ could safely be used in HNO detection in living cells at different pH.

4.3.8 Theoretical studies (Geometry optimization and electronic structure)

To get some idea about the interaction of Cu^{2+} complex and HNO, we have carried out DFT and TDDFT calculations on DQ$_{468}$, [Cu^{II}(DQ$_{468}$)Cl]$^+$ and [Cu^{I}(DQ$_{468}$)]$^+$.[65,66] **Figure 4.20** shows the optimized geometries of DQ$_{468}$, [Cu^{II}(DQ$_{468}$)Cl]$^+$ and [Cu^{I}(DQ$_{468}$)]$^+$ with the *C1* point group. The nature of all stationary points for both the free ligand DQ$_{468}$ and its Cu-complexes
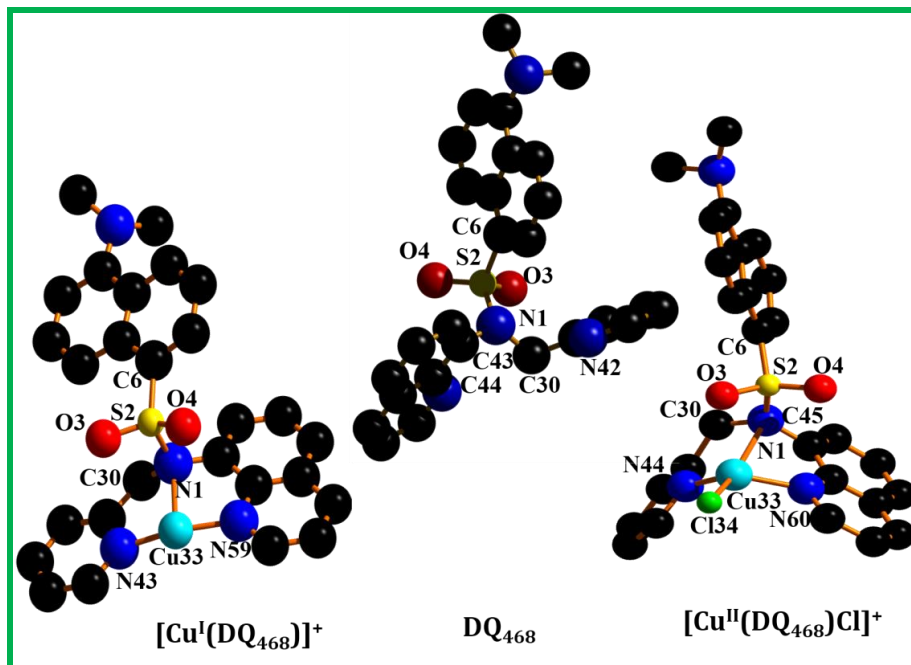
Figure 4.20 Optimized geometry of ligand and Cu-complexes.
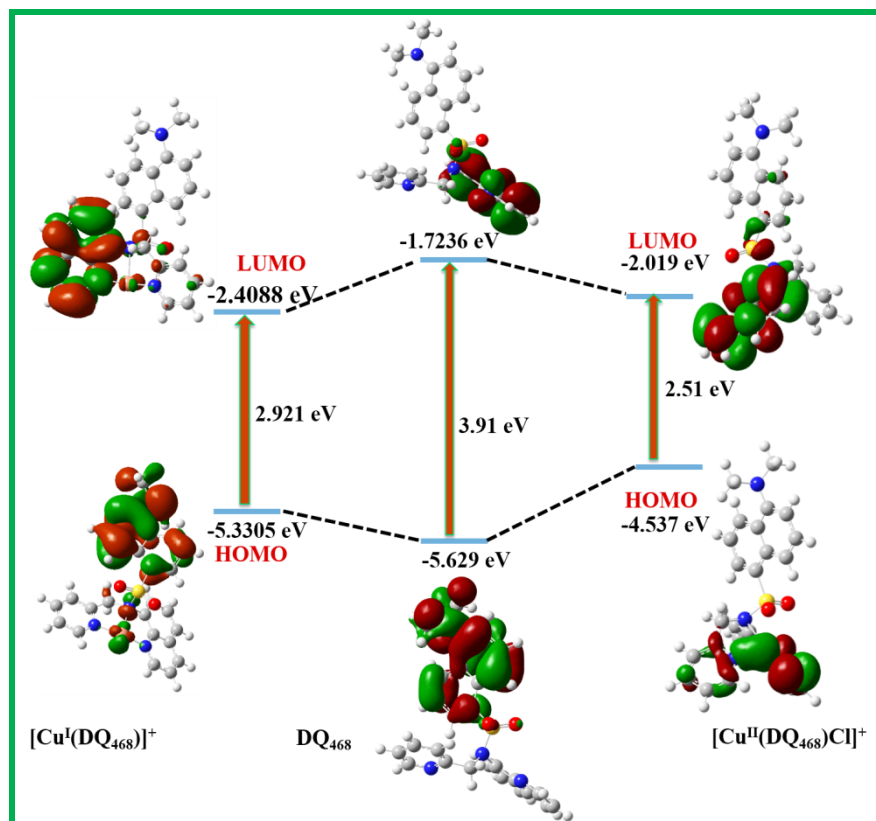
Figure 4.21 Frontier molecular orbitals of DQ$_{468}$, [Cu^{II}(DQ$_{468}$)Cl]$^+$ and [Cu^I(DQ$_{468}$)]$^+$.

were recognized by using normal mode analysis. The global minima of DQ_{468}, $[Cu^{II}(DQ_{468})Cl]^+$ and $[Cu^{I}(DQ_{468})]^+$ were confirmed by the positive values of all the frequencies. The compositions of the Cu-complexes were determined by mass spectroscopy as $[Cu^{II}(DQ_{468})Cl]^+$ and $[Cu^{I}(DQ_{468})]^+$, which displayed the presence of one chlorine in the molecular fragment of Cu^{2+} complex and the absence of the same in its reduced product. The central metal ion Cu^{2+} was in the distorted tetrahedral arrangement, while the metal ion was coordinated through naphthalene-1-sulfonic acid methylamide-N1, 2-methyl-pyridine-N44 and quinoline-N60 along with one chlorine atom (Cl34).

Figure 4.22 Frontier molecular orbitals of DQ_{468} and $[Cu^{II}(DQ_{468})Cl]^+$ in UV-Vis absorption**.**

Similarly, **Figure 4.21** depicts the HOMO–LUMO energy gaps of $[Cu^{II}(DQ_{468})Cl]^+$, $[Cu^{I}(DQ_{468})]^+$ and DQ_{468} were 2.51 eV, 2.92 and 3.91 eV, respectively. Now, all the calculated important geometrical parameters of the free ligand DQ_{468}, $[Cu^{II}(DQ_{468})Cl]^+$ and $[Cu^{I}(DQ_{468})]^+$ are listed in **Table 4.1 A, B, C**. From which it is found that the calculated Cu–N bond distances fall in the range 1.94–2.81 Å in the Cu^{2+} complex. The Cu33–N1 bond length was slightly larger than other Cu–N bond lengths, which may be due to weak coordination through N1, as it is directly attached to the highly electron withdrawing –SO_2R group. After complex formation, there are changes in some C–S, S–N and N–C bond lengths with respect to the free ligand. In the

ground state of DQ$_{468}$, the electron density resides mainly on the HOMO, LUMO and LUMO+1 molecular orbitals of the dansyl, quinoline and naphthalene fragments of the ligand, respectively (**Figure 4.22**). For the [Cu^{II}(DQ$_{468}$)Cl]$^+$ complex, the electron density was mainly localized on the HOMO and HOMO−5 molecular orbitals of the dimethyl-naphthalen-1-ylamine fragment and for LUMO, it resided on the quinoline- 8yl-amine moiety. HOMO−5
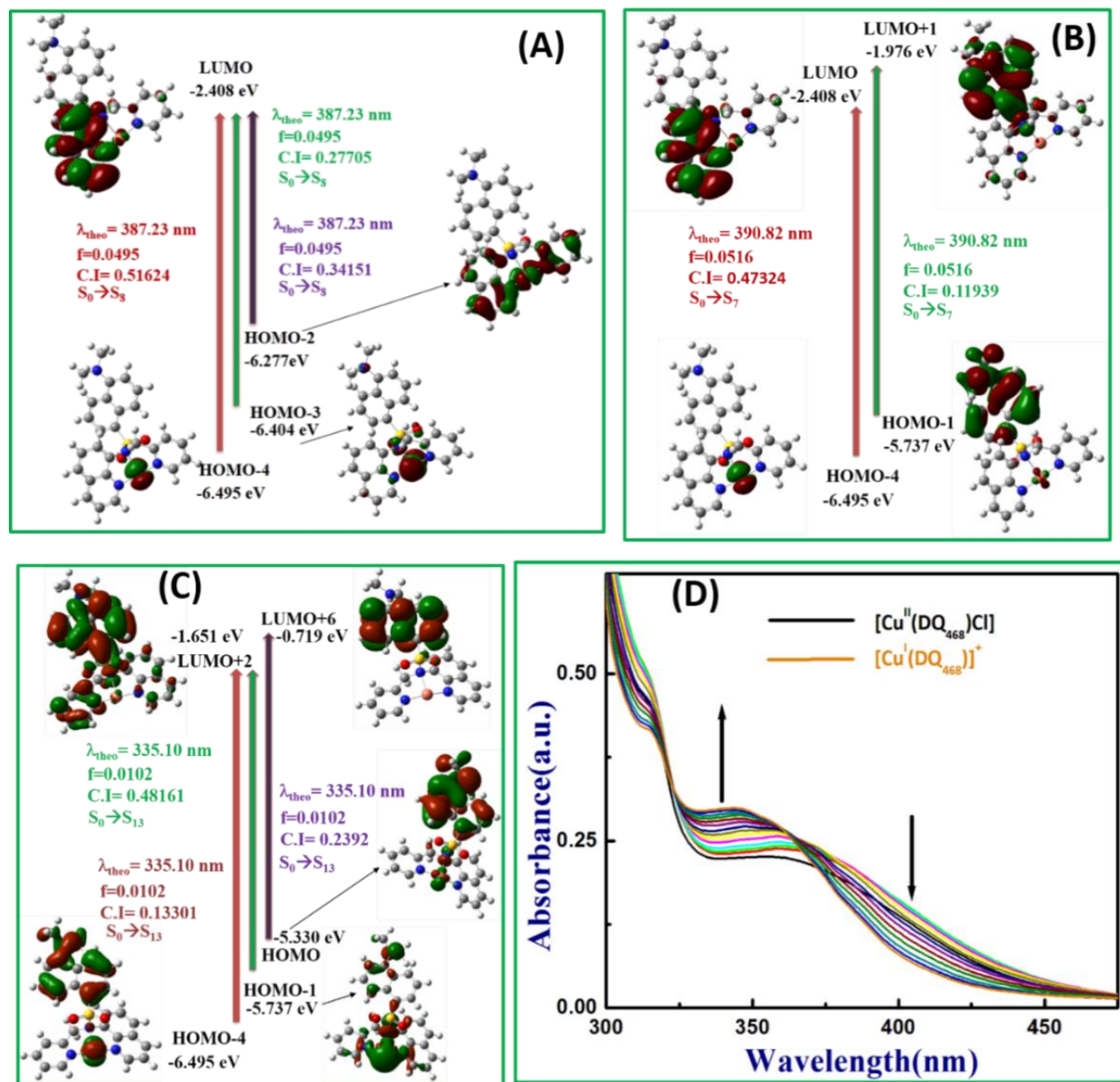
Figure 4.23 A, B, C Frontier molecular orbitals of [Cu^{I}(DQ$_{468}$)]$^+$ in UV-Vis absorption. **D.** UV-Vis spectra of [Cu^{II}(DQ$_{468}$)Cl]$^+$ towards HNO.

molecular orbital was mainly originated from ligand π and π* orbital contributions, while the HOMO and LUMO orbitals were originated from the metal d orbital along with ligand π orbital contributions (**Figure 4.22**). For the reduced species $[Cu^I(DQ_{468})]^+$, the electron cloud resides mainly on HOMO, HOMO−3, HOMO−2 and HOMO−4 molecular orbitals of the dimethyl-naphthalen-1-yl-amine moiety with Cu atom. Also, the HOMO−1, LUMO, LUMO+2, LUMO+1 and LUMO+6 molecular orbitals were originated from the Cu^{2+} coordination sphere, quinoline moiety, 5-dimethylamino-naphthalene-1-sulfonic acid (pyridin-2-ylmethyl)-amide fragment and naphthalene moiety, respectively (**Figure 4.23 A, B, C**). These compositions are useful in understanding the nature of transition as well as the absorption property of both the free ligand and its Cu-complexes. The ligand DQ_{468} has showed an absorption band at 337 nm in acetonitrile–water (8:2) at room temperature, which corresponds to the absorption band at 354.85 obtained from TDDFT calculations as given in **Table 4.2** This band was assigned to S0 → S1 electronic transitions (**Figure 4.22**). The absorption energy along with their oscillator strengths are given in **Table 4.2.** The complex $[Cu^{II}(DQ_{468})Cl]^+$ showed an absorption band at

370 nm (**Figure 4.22**) in acetonitrile–water (8 : 2) at room temperature and the corresponding calculated absorption band was located at 375.33 (**Table 4.3**), ascribed to the electronic transition S0 → S20. The reduced complex $[Cu^I(DQ_{468})]^+$ displayed an absorption band at 340 nm, which is ascribed to the transitions S0 → S13, S0 → S7 and S0 → S8 (**Figure 4.23 A, B, C**) in the range of 335 nm to 391 nm, with a significant oscillator strength, which were in agreement with our experimental results (**Table 4.4, Figure 4.23 D**).

Table 4.1 A, B, C. Some selected geometrical parameters (bond lengths and bond angles) of DQ_{468}, $[Cu^{II}(DQ_{468})Cl]^+$ and $[Cu^I(DQ_{468})Cl]^+$ in ground state calculated at B3LYP/6-31G (d) Levels.

(A)	Bond Length(Å)		
C6- S2	1.81	S2-N1	1.70
S2-O4	1.46	N1-C43	1.43
S2-O3	1.46	N1-C30	1.48
Bond Angles(°)			
C6-S2-N1	104.68	S2-N1-C43	116.03
O4-S2-O3	120.27	S2-N1-C30	116.48
N1-C43-C44	120.49	N1-C30-C33	113.16

(B)	Bond Length(Å)		
S2-C6	1.808	Cu33-N60	1.949
S2-N1	1.695	N1-Cu33	2.816
N1-C45	1.431	Cu33-Cl34	2.278
N1-C30	1.468	Cu33-N44	1.944
Bond Angles(°)			
S2-N1-C30	118.446	N60-Cu33-Cl34	112.665
S2-N1-C45	120.096	N44-Cu33-Cl34	114.493
N1-Cu33-N44	73.925	N1-Cu33-N60	71.219

(C)	Bond Length(Å)		
C6-S2	1.7928	N43-Cu33	1.8746
S2-O4	1.4629	N1-Cu33	2.1991
S2-O3	1.4629	N59-Cu33	1.8749
S2-N1	1.7599		
Bond Angles(°)			
C6-S2-N1	108.5100	N1-Cu33-N59	86.7645
S2-N1-Cu33	98.1251	N43-Cu33-N59	156.9166
N1-Cu33-N43	87.3255		

Table 4.2 A. Vertical excitation energy and oscillator strength (f_{cal}) of low-lying excited singlet states obtained from TDDFT// B3LYP/6-31G(d) calculations of DQ_{468} which is matched with the experimental one**. B.** All vertical excitation energies and oscillator strengths ($f$cal) of some low-lying excited singlet states obtained from TDDFT// B3LYP/6-31G(d) calculations of DQ_{468}**.**

(A)

Electronic Transition	Composition	Excitation energy	Oscillator strength (f_{cal})	CI	λ_{exp} (nm)
S0 → S1	HOMO→ LUMO+1 (123 ->125)	3.494 eV (354.85nm)	0.1310	0.68978	337

(B)

Electronic Transition	Composition	Excitation energy	Oscillator strength (f_{cal})	CI	λ_{exp} (nm)
S0 → S2	123 →124	3.5588 eV	0.0009	0.69982	348.38
S0 → S3	122 →124	4.1961 eV	0.1322	0.62435	295.48
	123 →128			0.14947	
S0 → S4	123 →126	4.2099 eV	0.0162	0.17684	294.51
	123 →128			0.48177	

S0 → S5	123 →126	4.3426 eV	0.0002	0.67979	285.51
S0 → S6	116 →124	4.3549 eV	0.0189	0.51975	284.70
	117 →124			0.15908	
	118 →124			0.36919	
	122 →124			0.18026	
S0 → S7	122 →125	4.4352 eV	0.0010	0.68757	279.55
S0 → S8	117 →124	4.5105 eV	0.0352	0.10643	274.88
	119 →124			0.50113	
S0 → S9	121 →124	4.5430 eV	0.0066	0.6754	272.91
S0 → S10	121 →125	4.5719 eV	0.0394	0.66793	271.19

Table 4.3 A. Vertical excitation energy and oscillator strength (*f*cal) of low-lying excited singlets obtained from TDDFT// B3LYP/6-31G (d) calculations of $[Cu^{II}(DQ_{468})Cl]^{+}$ complex which is matched with the experimental one. **B.** All vertical excitation energies and oscillator strengths (*f*cal) of some low-lying excited singlets obtained from TDDFT// B3LYP/6-31G (d) calculations of $[Cu^{II}(DQ_{468})Cl]^{+}$ complex.

(A)

Electronic Transition	Composition	Excitation energy	Oscillator strength (*f*cal)	CI	λ_{exp} (nm)
S0 →S20	HOMO-5 →LUMO (141→147)	3.3033 eV (375.33nm)	0.0508	0.629	370

(B)

Electronic Transition	Composition	Excitation energy	Oscillator strength (*f*cal)	CI	λ_{exp} (nm)
S0 →S10	144→149	2.7669 eV	0.0013	0.661	448.10
S0 →S11	144 ->148	2.8810 eV	0.0021	0.667	430.36
	144 ->149			0.212	
S0 →S12	146 ->150	2.9085 eV	0.0030	0.680	426.28
	146 ->151			0.114	
S0 →S13	142 ->149	2.9834 eV	0.0039	0.468	415.59
	143 ->148			0.213	
S0 →S14	142 ->149	3.0358 eV	0.0029	0.128	408.40
	143 ->148			0.100	
	145 ->150			0.603	
	145 ->151			0.110	
S0 →S15	143 ->148	3.0578 eV	0.0049	0.13245	405.47
	145 ->150			0.29261	
	146 ->151			0.29932	

	146 ->152			0.52448	
S0 →S16	143 ->148	3.0652 eV	0.0030	0.62561	404.49
S0 →S17	142 ->148	3.1582 eV	0.0003	0.68404	392.58
	142 ->149			0.13745	
S0 →S18	145 ->151	3.1867 eV	0.0013	0.34507	389.07
	145 ->152			0.59806	
S0 →S19	142 ->149	3.2509 eV	0.0042	0.32038	381.39
	143 ->147			0.10125	
	143 ->148			0.14708	
	143 ->149			0.37583	
S0 →S20	141 ->147	3.3033 eV	0.0508	0.62904	375.33

Table 4.4 A. Vertical excitation energies and oscillator strength (f_{cal}) of low-lying excited singlets obtained from TDDFT// B3LYP/6-31G (d) calculations of $[Cu^I(DQ_{468})]^+$ complex which is matched with the experimental one. **B.** All vertical excitation energies and oscillator strengths (f_{cal}) of some low-lying excited singlets obtained from TDDFT// B3LYP/6-31G(d) calculations of $[CuI(DQ_{468})]+$ complex .

(A)

Electronic Transition	Composition	Excitation energy	Oscillator strength (f_{cal})	CI	λ_{exp} (nm)
S0 → S13	HOMO-4 →LUMO+2 (133→140) HOMO-1→LUMO+2 (136→140) HOMO→LUMO+6 (137 →144)	3.699 eV (335.10nm)	0.0102	0.13301 0.48161 0.23920	
S0 → S7	HOMO-4→LUMO (133->138)	3.1724 eV (390.82 nm)	0.0516	0.47324	
	HOMO-1→LUMO+1 (136 ->139)			0.11939	340
S0 → S8	HOMO-4→LUMO (133 ->138)	3.2018 eV (387.23nm)	0.0495	0.51624	
	HOMO-3→LUMO (134 ->138)			0.27705	
	HOMO-2→LUMO (135 ->138)			0.34151	

(B)

Electronic Transition	Composition	Excitation energy	Oscillator strength (f_{cal})	CI	λ_{exp} (nm)
S0 → S7	133->138	3.1724 eV	0.0516	0.47324	390.82
	136 ->139			0.11939	

S0 → S8	133 ->138	3.2018 eV	0.0495	0.51624	387.23
	134 ->138			0.27705	
	135 ->138			0.34151	
S0 → S9	137 ->141	3.3675 eV	0.0002	0.67789	368.18
S0 →S10	132 ->138	3.3891 eV	0.0005	0.67855	365.83
	137 ->141			0.16656	
S0 → S11	137 ->142	3.5407 eV	0.0015	0.69295	350.17
	137 ->143			0.10158	
S0 → S12	134 ->139	3.6471 eV	0.0032	0.14748	339.95
	134 ->140			0.37982	
	135 ->139			0.17712	
	135 ->140			0.24647	
	136 ->140			0.44043	
S0 → S13	133->140	3.6999 eV	0.0102	0.13301	335.10
	136 ->140			0.48161	
	137 ->144			0.23920	
S0 → S14	135 ->139	3.7298 eV	0.0015	0.37668	332.42
	135 ->140			0.14490	
	137 ->143			0.11738	
	137 ->144			0.52594	
S0 → S15	134 ->139	3.7414 eV	0.0080	0.23671	331.39
	134 ->140			0.44980	
	137 ->144			0.28323	
S0→ S16	133 ->139	3.7803 eV	0.0019	0.26571	327.98
	133 ->140			0.60691	
	135 ->139			0.19626	

4.3.9 Cytotoxicity studies and cell imaging

Considering the fluorescence emitting property of DQ_{468} in the absence of Cu^{2+} ions, it was further checked for its sensing ability in living cells. To determine whether DQ_{468} has cytotoxic effects, a cell viability assay using MTT was performed with calculating the % cell viability on HepG2 cells (**Figure 4.24 A**.). There was no significant reduction in the tetrazolium salt (reflected by a decrease in formazan production) for DQ_{468} up to 20 μM, thus suggesting that bellow 20 μM ligand concentration, DQ_{468} would be much more effective for the analysis of its fluorescence emissions in vitro. More than 80% cell viability was observed for DQ_{468} at 5 μM and 10 μM, after which the viability of the HepG2 cells decreased. Hence, further experiments were carried out with 5 μM and 10 μM of DQ_{468} for treatment. The ligand DQ_{468} exhibited
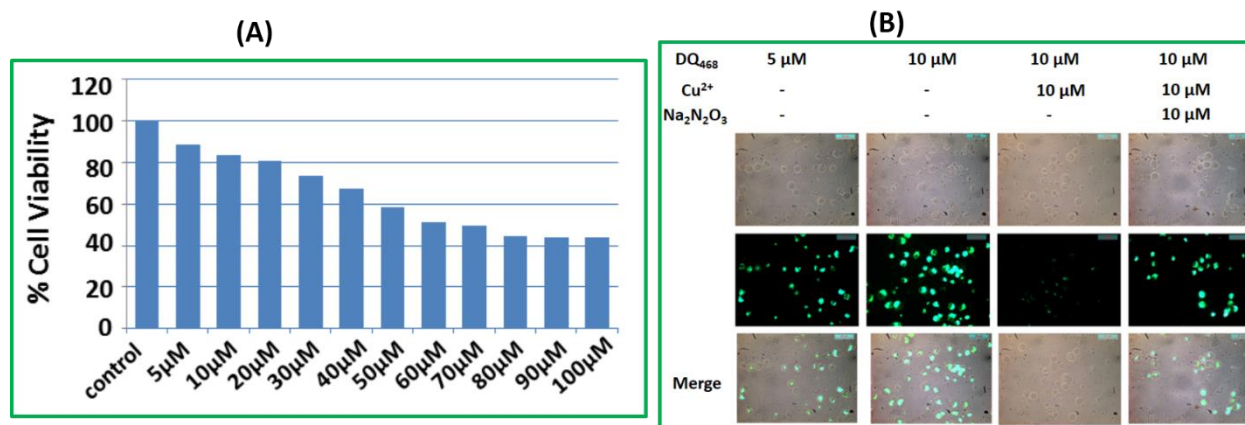
Figure 4.24 A. Percent (%) cell viability of HepG2 cells treated with different concentrations (1–100 μM) of DQ_{468} for 24 h, as determined by MTT assay. **B.** The fluorescence images of HepG2 cells were captured (40×) after incubation with 5 and 10 μM of DQ_{468} for 60 min at 37 °C, which showed green fluorescence emission. The emission quenches in the presence of Cu^{2+} ions, as the HepG2 cells were treated with 10 μM of Cu^{2+} ions, followed by washing three times with 1× PBS, and incubation with 10 μM of DQ_{468} for 60 min at 37 °C. The fluorescence emission reappeared in the presence of 10 μM of $Na_2N_2O_3$ for 60 min at 37 °C, which reduces the Cu^{2+} ions concentration by converting them to Cu^+ ions.

prominent intracellular green fluorescence in HepG2 cells treated with 5 μM of the ligand and incubated for 1 h; which was found to be increased when the HepG2 cells were incubated with 10 μM of DQ_{468} for 60 min at 37 °C (**Figure 4.24 B**.). However, the fluorescence emission was significantly quenched in the presence of 10 μM Cu^{2+} ions. Upon the further addition of Angeli's salt (10 μM) at 37 °C, the green fluorescence emission was recovered due to the reduction of Cu^{2+} ions to Cu^+ ion. So, our present ligand DQ_{468} was able to detect Cu^{2+} and HNO sequentially in biological samples with low cytotoxicity.
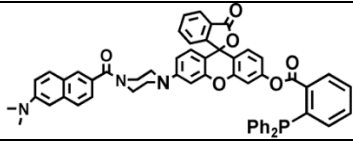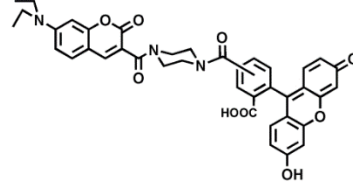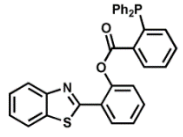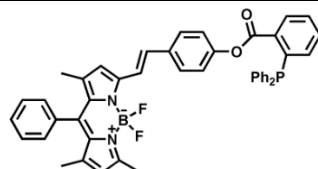
4.4 Conclusion

In summary, we have synthesized a fluorogenic probe DQ_{468} in a facile manner on a dansyl-quinoline platform. Here, first the metal-free probe DQ_{468} showed high fluorescence intensity, which gets quenched by the coordination with paramagnetic Cu^{2+} (7-fold) with K_{SV} = (7.32 ± 0.08) × 10^4 M^{-1}. The composition of complex formation was obtained by Job's method and by

mass spectroscopy showing 1: 1 complex formation with a limit of detection of 0.091 μM. This Cu^{II} complex-based system was allowed to react with Angeli's salt (HNO donor), an ample reducing agent. Very obviously, the Cu^{II} was converted to the diamagnetic Cu^{I} and fluorescence intensity was regenerated. This reduction based turn-on sensing was well established by mass spectroscopy as well as EPR spectroscopy, which showed that the previously observed peak for Cu^{II} gets dropped to the base line in the presence of HNO, indicating the reduction of the metal centre. This [Cu^{II}(DQ$_{468}$)Cl]$^{+}$ complex-based probe also showed high affinity only towards HNO, being inert towards other commonly known RNS, ROS and RSS, and even towards NO abundant in biological milieu, thus signifying it's efficiency as a good nitroxyl sensor in a wide range of physiological pH. In view of its proper biological activity, our present system also qualified under the eligibility criteria due to its negligible cytotoxicity and biocompatibility with in vitro sensing ability in living cells. So, all these above experiments and discussions certify our probe as a good candidate for nitroxyl sensing.

Table 4.5. Comparative table of some previously reported HNO probes.

HNO Probes	λ_{em}	LOD (μM)	REFERENCE
	541nm	.59	*Chem. Commun.,* 2016, **52**, 733
	517nm	1.4	*ACS Appl. Mater. Interfaces,* 2015, **7**, 5438
	460nm	.98	*Anal. Methods*, 2015, **7**, 3883
	586nm	2	*Anal. Chem.* 2017, **89**, 12087.

Structure	λ	Value	Reference
	450nm	9	*Molecules,* 2018, **23**, 2551
	595nm	23	*Tetrahedron,* 2016, **72** , 5495
	543nm	0.4	**THIS WORK**
	546nm	0.5	*Chem. Commun.,* 2014, **50**, 6013
	512nm	0.59	*Chem. Commun.,* 2015, **51**, 5754
	490nm	0.64	*J. Mater. Chem. B,* 2016, **4**, 1263

References

1. (a) A. P. D. Silva, H. Q. N. Gunaratne, T. Gunnlaugsson, A. J. M. Huxley, C. P. McCoy, J. T. Rademacher and T. E. Rice, *Chem. Rev.,* 1997, **97**, 1515-1566; (b) T. Gunnlaugsson, J. P. Leonard and J. N. S. Murray, *Org. Lett.,* 2004, **6**, 1557-1560; (c) C. Yu, J. Zhang, J. Li, P. Liu, P. Wei and L. Chen, *Microchim. Acta,* 2011, **174**, 247-255.
2. J. S. Kim and D. T. Quang, *Chem. Rev.,* 2007, **107**, 3780-3799.

3. (a) B. High, D. Bruce and M. M. Richter, *Anal. Chim. Acta,* 2001, **449**, 17-22; (b) L. Tapia, M. Suazo, C. Hödar,V. Cambiazo and M. González, *BioMetals,* 2003, **16**, 169-174.

4. (a) M. C. Linder and M. Hazegh-Azam, *Am. J. Clin. Nutr.,* 1996, **63**, 797S-811S; (b) R. Uauy, M. Olivares and M. Gonzalez, *Am. J. Clin. Nutr.,* 1998, **67**, 952S-959S.

5. (a) Z. Xu, S. J. Han, C. Lee, J. Yoon and D. R. Spring, *Chem. Commun.,* 2010, **46**, 1679-1681; (b) X. Cao, W. Lin and W. Wan, *Chem. Commun.,* 2012, **48**, 6247-6249; (c) C. S. Lim, J. H. Han, C. W. Kim, M. Y. Kang, D. W. Kang and B. R. Cho, *Chem. Commun.,* 2011, **47,** 7146-7148; (d) Y. Zhao, X. B. Zhang, Z. X. Han, L. Qiao, C. Y. Li, L. X. Jian, G. L. Shen and R. Q. Yu, *Anal. Chem.,* 2009, **81**, 7022-7030.

6. (a) T. P. Thomas, M. T. Myaing, J. Y. Ye, K. Candido, A. Kotlyar, J. Beals, P. Cao, B. Keszler, A. K. Patri, T. B. Norris and J. R. Baker, *Biophys. J.,* 2004, **86,** 3959-3965; (b) Y. Liu, X. H. Dong, J. Sun, C. Zhong, B. Li, X. You, B. Liu and Z. Liu, *Analyst,* 2012, **137**, 1837-1845.

7. (a) D. W. Domaille, L. Zeng and C. J. Chang, *J. Am. Chem. Soc.,* 2010, **132**, 1194-1195; (b) Q. Qu, A. Zhu, X. Shao, G. Shi and Y. Tian, *Chem. Commun.,* 2012, **48**, 5473-5475.

8. (a) M. H. Lim, D. Xu and S. J. Lippard, *Nat. Chem. Biol.,*2006, **2**, 375-380; (b) S. Kim, M. A. Minier, A. Loas, S. Becker,F. Wang and S. J. Lippard, *J. Am. Chem. Soc.,* 2016, **138**, 1804-1807; (c) M. D. Pluth, M. R. Chan, L. E. McQuade and S. J. Lippard, *Inorg. Chem.,* 2011, **50**, 9385-9392.

9. A. T. Wrobel, T. C. Johnstone, A. D. Liang, S. J. Lippard and P. Rivera-Fuentes, *J. Am. Chem. Soc.,* 2014, **136**, 4697-4705.

10. X. Sun, G. Kim, Y. Xu, J. Yoon and T. D. James, *ChemPlusChem,* 2016, **81**, 30-34.

11. (a) A. Dutta, R. Alam, A. S. M. Islam, A. Dutta and M. Ali, *Dalton Trans.,* 2018, **47**, 11563-11571; (b) T. Anand, G. Sivaraman and D. Chellappa, *J. Photochem. Photobiol. A,* 2014, **281**, 47-52.

12. (a) A. Kalita, P. Kumar, R. C. Deka and B. Mondal, *Inorg.Chem.,* 2011, **50**, 11868-11876; (b) P. Kumar, A. Kalita and B. Mondal, *Dalton Trans.,* 2012, **41**, 10543-10548.

13. D. D. Thomas, L. A. Ridnour, J. S. Isenberg, W. Flores-Santana, C. H. Switzer, S. Donzelli, P. Hussain, C. Vecoli, N. Paolocci, S. Ambs, C. A. Colton, C. C. Harris, D. D. Roberts and D. A. Wink, *Free Radicals Biol. Med.,*2008, **45**, 18-31.

14. G. A. Blaise, D. Gauvin, M. Gangal and S. Authier, *Toxicology,* 2005, **208**, 177-192.

15. C. Q. Li and G. N. Wogan, *Cancer Lett.,* 2005, **226**, 1-15.

16. V. Calabrese, C. Mancuso, M. Calvani, E. Rizzarelli,D. A. Butterfield and A. M. G. Stella, *Nat. Rev. Neurosci.,* 2007**, 8**, 766-775.

17. A. S. Vidwans, S. Kim, D. O. Coffin, D. A. Wink and S. J. Hewett, *J. Neurochem.,* 1999, **72**, 1843-1852.

18. L. A. Ridnour, D. D. Thomas, C. Switzer, W. Flores-Santana, J. S. Isenberg, S. Ambs, D. D. Roberts and D. A. Wink, *Nitric Oxide,* 2008, **19**, 73-76.

19. M. B. Grisham, D. Jourd'Heuil and D. A. Wink, *Am. J. Physiol.: Gastrointest. Liver Physiol.,* 1999, **276,** G315-G321.

20. D. S. Bredt, P. M. Hwang and S. H. Snyder, *Nature,* 1990, **347**, 768-770.

21. C. Bogdan, *Nat. Immunol.,* 2001, **2**, 907-916.

22. R. O. Cannon, *Clin. Chem.,* 1998, **44,** 1809-1819.

23. J. M. Fukuto, C. J. Cisneros and R. L. Kinkade, *J. Inorg. Biochem.,* 2013, **118**, 201-208.

24. M. L. Bullen, A. A. Miller, K. L. Andrews, J. C. Irvine, R. H. Ritchie, C. G. Sobey and B. K. Kemp-Harper, *Antioxid. Redox Signaling,* 2011, **14**, 1675-1686.

25. N. Paolocci, W. F. Saavedra, K. M. Miranda, C. Martignani, T. Isoda, J. M. Hare, M. G. Espey, J. M. Fukuto, M. Feelisch, D. A. Wink and D. A. Kass, *Proc. Natl. Acad. Sci. U. S. A.,*2001, **98**, 10463-10468.

26. R. F. Dautov, D. T. M. Ngo, G. Licari, S. Liu, A. L. Sverdlov, R. H. Ritchie, B. K. Kemp-Harper, J. D. Horowitz and Y. Y. Chirkov, *Nitric Oxide,* 2013, **35**, 72-78.

27. C. H. Switzer, W. Flores-Santana, D. Mancardi, S. Donzelli, D. Basudhar, L. A. Ridnour, K. M. Miranda, J. M. Fukuto, N. Paolocci and D. A. Wink, *Biochim. Biophys. Acta, Bioenerg.,* 2009, **1787**, 835-840.

28. C. Liu, Z. Cao, Z. Wang, P. Jia, J. Liu, Z. Wang, B. Han, X. Huang, X. Li, B. Zhu and X. Zhang, *Sens. Actuators, B,* 2015, **220**, 727-733.

29. Y. Zhou, Y. W. Yao, J. Y. Li, C. Yao and B. P. Lin, *Sens. Actuators B,* 2012, **174**, 414-420.

30. M. Royzen, J. J. Wilson and S. J. Lippard, *J. Inorg. Biochem.,* 2013, **118**, 162-170.

31. (a) S. A. Suárez, D. E. Bikiel, D. E. Wetzler, M. A. Martí and F. Doctorovich, *Anal. Chem.,* 2013, **85**, 10262-10269; (b) V. K. Gupta, M. R. Ganjali, P. Norouzi, H. Khani, A. Nayak and S. Agarwal, *Crit. Rev. Anal. Chem.,* 2011, **41**, 282-313.

32. J. A. Reisz, C. N. Zink and S. B. King, *J. Am. Chem. Soc.,* 2011, **133**, 11675-11685.

33. (a) T. Malinski and Z. Taha, *Nature,* 1992, **358,** 676-678; (b) L. A. Ridnour, J. E. Sim, M. A. Hayward, D. A. Wink, S. M. Martin, G. R. Buettner and D. R. Spitz, *Anal. Biochem.,* 2000, **281**, 223-229; (c) T. Nagano and T. Yoshimura, *Chem. Rev.,* 2002, **102**, 1235-1270; (d) E. M. Hetrick and M. H. Schoenfisch, *Annu. Rev. Anal. Chem.,* 2009, **2**, 409.

34. (a) J. R. Lakowicz, Principles of Fluorescence Spectroscopy, *Springer-Verlag, Berlin, 3rd edn,* 2006; (b) X. Li, X. Gao, W. Shi and H. Ma, *Chem. Rev.,* 2014, **114**, 590-659; (c) L. Yuan, W. Lin, K. Zheng and S. Zhu, *Acc. Chem. Res.,* 2013, **46**, 1462-1473.

35. H. Zhang, R. Liu, Y. Tan, W. H. Xie, H. Lei, H. Cheung and H. Sun, *ACS Appl. Mater. Interfaces,* 2015, **7**, 5438-5443.

36. K. Zheng, H. Chen, S. Fang and Y. Wang, *Sens. Actuators, B,* 2016, **233**, 193-198.

37. K. Kawai, N. Ieda, K. Aizawa, T. Suzuki, N. Miyata and H. Nakagawa, *J. Am. Chem. Soc.,* 2013, **135,** 12690-12696.

38. B. Dong, K. Zheng, Y. Tang and W. Lin, *J. Mater. Chem. B,* 2016, **4**, 1263-1269.

39. (a) P. Liu, X. Han, F. Yu and L. Chen, Chin. *J. Anal. Chem.,* 2015, **43**, 1829-1836; (b) P. Liu, X. Jing, F. Yu, C. Lv and L. Chen, *Analyst,* 2015, **140,** 4576-4583; (c) X. Jing, F. Yu and L. Chen, *Chem. Commun.,* 2014, **50**, 14253-14256.

40. J. Rosenthal and S. J. Lippard, *J. Am. Chem. Soc.,* 2010, **132**, 5536-5537.

41. U. P. Apfel, D. Buccella, J. J. Wilson and S. J. Lippard, *Inorg. Chem.,* 2013, **52**, 3285-3294.

42. Y. Zhou, K. Liu, J.-Y. Li, Y. Fang, T.-C. Zhao and C. Yao, *Org. Lett.,* 2011, **13**, 1290-1293.

43. A. Dhir, V. Bhalla and M. Kumar, *Org. Lett.,* 2008, **10**, 4891-4894.

44. Y. Hu, B. Wang and Z. Su, *Polym. Int.,* 2008, **57**, 1343-1350.

45. M. H. Lee, H. J. Kim, S. Yoon, N. Park and J. S. Kim, *Org. Lett.,* 2008, **10**, 213-216.

46. M. H. Lim, B. A. Wong, W. H. Pitcock, D. Mokshagundam, M. H. Baik and S. J. Lippard, *J. Am. Chem. Soc.,* 2006, **128,** 14364-14373.

47. D. Maiti, A. S. M. Islam, M. Sasmal, C. Prodhan and M. Ali, *Photochem. Photobiol. Sci.,* 2018, **17**, 1213-1221.

48. A. S. M. Islam, M. Sasmal, D. Maiti, A. Dutta, B. Show and M. Ali, *ACS Omega,* 2018, **3**, 10306-10316.

49. S. Miyamoto, G. R. Martinez, A. P. B. Martins, M. H. G. Medeiros and P. DiMascio, *J. Am. Chem. Soc.,2003,* **125**, 4510-4517.

50. R. G. Parr and W. Yang, Density Functional Theory of Atoms and Molecules, *Oxford University Press, Oxford,* 1989.

51. (a) V. Barone and M. Cossi, *J. Phys. Chem. A,* 1998, **102**, 1995-2001; (b) M. Cossi and V. Barone, *J. Chem. Phys.,* 2001, **115**, 4708-4717; (c) M. Cossi, N. Rega, G. Scalmani and V. Barone, *J. Comput. Chem.,* 2003, **24**, 669-681.

52. A. D. Becke, *J. Chem. Phys.,* 1993, **98**, 5648-5652.

53. C. Lee, W. Yang and R. G. Parr, Phys. Rev. B: Condens. *Matter Mater. Phys.,* 1988, **37**, 785-789.

54. (a) M. E. Casida, C. Jamoroski, K. C. Casida and D. R. Salahub, *J. Chem. Phys.,* 1998, **108**, 4439-4449; (b) R. E. Stratmann, G. E. Scuseria and M. J. Frisch, *J. Chem. Phys.,* 1998, **109**, 8218-8224; (c) R. Bauernschmitt and R. Ahlrichs, *Chem. Phys. Lett.,* 1996, **256**, 454-464.

55. (a) T. Liu, H. X. Zhang and B. H. Xia, *J. Phys. Chem. A,* 2007, **111**, 8724-8730; (b) X. Zhou, H. X. Zhang, Q. J. Pan, B. H. Xia and A. C. Tang, *J. Phys. Chem. A,* 2005, **109**, 8809-8818; (c) X. Zhou, A. M. Ren and J. K. Feng, *J. Organomet. Chem.,* 2005, **690**, 338-347; (d) A. Albertino, C. Garino, S. Ghiani, R. Gobetto, C. Nervi, L. Salassa, E. Rosenverg, A. Sharmin, G. Viscardi, R. Buscaino, G. Cross and M. Milanesio, *J. Organomet. Chem.,* 2007, **692**, 1377-1391.

56. M. J. Frisch, G. W. Trucks, H. B. Schlegel, G. E. Scuseria, M. A. Robb, J. R. Cheeseman, G. Scalmani, V. Barone, B. Mennucci, G. A. Petersson, H. Nakatsuji, M. Caricato,X. Li, H. P. Hratchian, A. F. Izmaylov, J. Bloino, G. Zheng,J. L. Sonnenberg, M. Hada, M. Ehara, K. Toyota, R. Fukuda,J. Hasegawa, M. Ishida, T. Nakajima, Y. Honda, O. Kitao,H. Nakai, T. Vreven, J. A. Montgomery Jr., J. E. Peralta,F. Ogliaro, M. Bearpark, J. J. Heyd, E. Brothers, K. N. Kudin,V. N. Staroverov, R. Kobayashi, J. Normand, K. Raghavachari,A. Rendell, J. C. Burant, S. S. Iyengar, J. Tomasi, M. Cossi,N. Rega, J. M.

Millam, M. Klene, J. E. Knox, J. B. Cross,V. Bakken, C. Adamo, J. Jaramillo, R. Gomperts,R. E. Stratmann, O. Yazyev, A. J. Austin, R. Cammi,C. Pomelli, J. W. Ochterski, R. L. Martin, K. Morokuma, V. G. Zakrzewski, G. A. Voth, P. Salvador, J. J. Dannenberg,S. Dapprich, A. D. Daniels, Ö. Farkas, J. B. Foresman,J. V. Ortiz, J. Cioslowski and D. J. Fox, Gaussian 09, (RevisionA.1), Gaussian, Inc., Wallingford, CT, 2009.

57. N. M. O'Boyle, A. L. Tenderholt and K. M. Langner, *J. Comput. Chem.,* 2008, **29**, 839-845.

58. M. Sarma, A. Kalita, P. Kumar, A. Singh and B. Mondal, *J. Am. Chem. Soc.,* 2010, **132**, 7846-7847.

59. Y. Liu, K. Ai, X. Cheng, L. Huo and L. Lu, *Adv. Funct. Mater.,* 2010, **20**, 951-956.

60. (a) X. Chen, S. W. Nam, G. H. Kim, N. Song, Y. Jeong, I. Shin, S. K. Kim, J. Kim, S. Park and J. Yoon, *Chem. Commun.,* 2010, **46**, 8953-8955; (b) M. Royzen, Z. Dai and J. W. Canary, *J. Am. Chem. Soc.,* 2005, **127**, 1612-1613.

61. Y. Q. Wang, H.-M. Zhang, G.-C. Zhang, W.-H. Tao, Z.-H. Fei and Z.-T. Liu, *J. Pharm. Biomed. Anal.,* 2007, **43**, 1869-1875.

62. M. E. Murphy and H. Sies, *Proc. Natl. Acad. Sci. U. S. A.,*1991, **88**, 10860-10864.

63. R. Alam, T. Mistri, P. Mondal, D. Das, S. K. Mandal, A. R. Khuda Bukhsh and M. Ali, *Dalton Trans.,* 2014, **43**, 2566-2576.

64. B. Dong, X. Kong and W. Lin, *ACS Chem. Biol.,* 2018, **13**,1714-1720.

65. M. A. Michael, G. Pizzella, L. Yang, Y. Shi, T. Evangelou, D. T. Burke and Y. Zhang, *J. Phys. Chem. Lett.,* 2014, **5**, 1022-1026.

66. W. Yang, X. Chen, H. Su, W. Fanga and Y. Zhang, *Chem. Commun.,* 2015, **51**, 9616-9619.

CHAPTER 5

Highlights of the Thesis

After the elaborate description, here the overall view of this thesis has been summarized chapterwise. This may be cooperative to focus the goal of our endeavor and will conclude how much we have fulfilled our aim for the entitled project.

Chapter 1

This chapter describes about the short introduction about reactive bio-molecule NO (Nitric Oxide) and HNO (nitroxyl). The synthetic pathways of their formation in human body and their key role in physiological and pathological processes has been elaborately explained along with the brief review of previously reported NO and HNO probes by fluoroscence method.

Chapter 2

In this chapter the detailed experimental studies, synthesis and application of the probe PQPY has been delineated in detail. PQPY is a phenanthroquinone–pyridoxal based fluorogenic probe. This probe is highly efficient for the selective and sensitive tracking of nitric oxide in semi-aqueous medium at pH 7.0. PQPY demonstrates about the very strong interaction with nitric oxide revealing the enhancement in fluorescence emission in green region (λ_{em} = 505 nm). Here the operative mechanism for NO sensing is ICT process (intramolecular charge transfer) occurring from the electron rich phenanthroquinone unit to the electron defficient imidazole –N–N=O fragment. The formation constant, K_f, of the NO mediated product of the ligand is $(1.00 \pm 0.2) \times 10^5$ M^{-1} showing LOD 78 nM. The life-time of the ligand (τ_0 = 2.68 ns) is enhanced due to binding with nitric oxide (τ_0 = 3.96 ns). Additionally from the application part, this probe is also least cytotoxic, cell permeable and suitable for living cell imaging application.

Chapter 3

In this chapter the nitric oxide is selectively and sensitively monitored by the fluorescence probe named as BCM. In this probe the fluorophore is taken as benzo-coumarin which is attached with the carbohydrazide moiety acting as the NO recognition unit. However, this smart molecular probe is employed for NO sensing with detailed fluorescence spectroscopic studies in aqueous medium. The mechanistic insight of this sensing strategy has been clearly validated by the spectroscopic analysis and literature reports. Here, upon treatment of the probe with NO, 1,2,3,4-oxatriazole is formed initially which ultimately released its carboxylic acid derivative. This oxatriazole formation executes the strong enhancement in fluorescence intensity due to the

photoinduced electron transfer (PET) effect. The kinetic study analysis displays that the reaction rate follows second and first-order dependency on [NO] and [BCM] respectively. BCM shows the key features like 16 nM detection limit, 123 fold high fluorescence enhancement in aqueous medium and good formation constant ($K_f = (4.33 \pm 0.48) \times 10^4$ M^{-1}) along with pH tolerable nature. This probe is also sufficiently potent for tracking of intracellular NO due to its non-cytotoxicity, biocompatibility and cell permeability.

Chapter 4

In this chapter the detailed description about the dansyl appended copper complex $[Cu^{II}(DQ_{468})Cl]^+$ has been provided. This non-fluorescent copper complex acts as a selective and sensitive nitroxyl probe. This probe displays a vivid turn-on fluorescence enlargement towards nitroxyl (HNO) devoiding of other biological reactive reductants, including nitric oxide (NO). The well-established strategy, associated here is HNO-influenced reduction of paramagnetic Cu^{II} complex to diamagnetic Cu^{I} complex which causes simultaneous fluorescence enhancement via PET blocking pathway. This HNO induced reduction was also evidenced by X-band EPR spectra and mass spectroscopy. The metal free probe (DQ_{468}) exhibits strong affection towards Cu^{2+} to form $[Cu^{II}(DQ_{468})Cl]^+$ with a 0.091 μM detection limit. This complex subsequently detects HNO in a semi aqueous medium at biological pH by the generation of fluorescence intensity in green region ($\lambda_{em} = 543$ nm) with detection limit of 0.41 μM. The ground-state geometries of all the related compounds were optimized by DFT calculations. Moreover, this probe is very negligibly cytotoxic and biocompatible, featuring the usefulness for the *in vitro* detection of HNO.

List of Publications

1. **D. Maiti,** A.S.M. Islam, M. Sasmal, C. Prodhan, M. Ali, *Photochem. Photobiol. Sci.,* 2018, 17, 1213-1221

2. **D. Maiti,** A.S.M. Islam, A. Dutta, M. Sasmal, C. Prodhan, M. Ali, *Dalton Trans.,* 2019, 48, 2760-27716.

3. **D. Maiti,** A.S.M. Islam, M. Sasmal, A. Dutta, A. Katarkar and M. Ali, *Org. Biomol. Chem.,* 2020, 18, 8450

4. A. S. M. Islam, M. Sasmal, **D. Maiti,** A. Dutta, B. Show, and M. Ali, *ACS Omega,* 2018, **3**, 10306−10316

5. A. S. M. Islam, M. Sasmal, **D. Maiti,** A. Dutta, S. Ganguly, A. Katarkar, S. Gangopadhyay and M. Ali, *ACS Appl. Bio Mater.,* 2019, 25, 1944-1955

6. A. Dutta, A.S.M. Islam, **D. Maiti,** M. Sasmal, C .Prodhan, M. Ali, *Org. Biomol. Chem .,* *2019,* 17, 2825-2825

7. M. Sasmal, A. S. M. Islam, R. Bhowmick, **D. Maiti**, A. Dutta, and M. Ali, *ACS Appl. Bio Mater.* 2019, 2, 8, 3551–3561

PAPER

Check for updates

Selective sensing of nitric oxide by a 9,10-phenanthroquinone–pyridoxal based fluorophore†

Debjani Maiti,[a] Abu Saleh Musha Islam,[a] Mihir Sasmal,[a] Chandraday Prodhan[b] and Mahammad Ali ★[a]

In this article, we have designed and synthesized a new, convenient and efficient phenanthroquinone–pyridoxal based fluorogenic probe **PQPY**, highly suitable for the selective and sensitive detection of nitric oxide in an aerated aqueous (7 : 3/H$_2$O : MeCN) medium at pH 7.0 (10 mM HEPES buffer). Upon addition of nitric oxide, this probe exhibits emission in the green region (λ_{em} = 505 nm) which is ascribed to ICT (intramolecular charge transfer) from the phenanthroquinone moiety to the imidazole –N–N═O fragment. The apparent formation constant, K_f, of the NO product of the ligand is (1.00 $\pm$ 0.2) $\times$ 10^5 M^{-1} and the LOD is 78 nM. The substantial enhancement of the life-time of the ligand (τ_0 = 2.68 ns) occurs due to binding with nitric oxide (τ_0 = 3.96 ns). This probe is low cytotoxicity, cell permeable and suitable for living cell imaging application.

Introduction

Modern molecular biology has revealed that vast numbers of large and complex proteins and genes regulate the body functions. By contrast, a remarkably simple chemical, nitric oxide (NO), has been found to mediate the crucial features of neuronal communication, blood vessel modulation and immune response. NO can exist in a variety of molecular forms: free radical (NO^0), nitrosyl (NO$^-$) anion or nitrosonium (NO$^+$) cation depending on the NO source. Hence, the NO released from NO donors can differ from the NO produced in the endothelial cells. NO donors are pharmacologically active substances that release NO *in vivo* or *in vitro*. NO delivery can occur through many kinds of stimuli, depending on the NO donor structure. Among many physiological functions, NO induces vasodilation, inhibits platelet aggregation, prevents neutrophil/platelet adhesion to endothelial cells, inhibits smooth muscle cell proliferation and migration, regulates programmed cell death (apoptosis) and maintains the endothelial cell barrier function. NO generated by neurons acts as a neurotransmitter, whereas NO generated by macrophages in response to invading microbes acts as an antimicrobial agent.

Therefore, its accurate detection and quantification are critical to understanding health and disease.

The established paradigm of NO biochemistry from the production by NO synthases to the activation of soluble guanylyl cyclase (sGC) and to eventual oxidation to nitrite (NO$_2^-$) and nitrate (NO$_3^-$) may only represent part of NO's effects *in vivo*.[1,2] Due to the extremely short physiological half life of this gaseous free radical (less than 1 second in circulating blood),[3] alternative strategies have been established for the detection of the reaction products of NO biochemistry. The quantification of NO metabolites in biological samples provides valuable information with regard to *in vivo* NO production, bioavailability and metabolism. Simply sampling a single compartment such as blood or plasma may not always provide an accurate assessment of the whole body NO status, particularly in tissues. Therefore, extrapolation of the plasma or blood NO status to specific tissues of interest is no longer a valid approach. As a result, methods continue to be developed and validated, which allow the detection and quantification of NO and NO-related products/metabolites in multiple compartments of experimental animals *in vivo*.

Several analytical methods like electrochemical, fluorescence, electron spin resonance *etc.* have been proposed for the *in vitro* and *in vivo* analysis of NO.[4–12] In view of its sensitivity, selectivity, spatiotemporal resolution, and experimental feasibility, the fluorescence method has been regarded as the most promising method to detect endogenous NO. A number of small organic and inorganic fluorescent NO sensors have been reported thus far. Many of them are involved in the reac-

[a]*Department of Chemistry, Jadavpur University, 188 Raja S.C. Mallick Road, Kolkata 700 032, India. E-mail: m_ali2062@yahoo.com*
[b]*Molecular & Human Genetics Division, CSIR-Indian Institute of Chemical Biology, 4 Raja S.C. Mallick Road, Kolkata-700032, India*

†Electronic supplementary information (ESI) available. See DOI: 10.1039/c8pp00115d

This journal is © The Royal Society of Chemistry and Owner Societies 2018

Photochem. Photobiol. Sci., 2018, **17**, 1213–1221 | 1213

tion of *o*-diamino aromatics with NO in the presence of oxygen leading to the formation of triazole, which acts as a modulator in the photoinduced electron transfer (PET) mechanism resulting in fluorescence turn-ON. Other mechanisms involve the oxidative deamination process[13] and NO/O_2 mediated diazotisation with the concomitant ring formation.[9] However, they still have some undesired limitations, such as electron-rich aromatic diamines may undergo self-oxidation or react with other reactive oxygen/nitrogen species that may lead to the generation of fluorescent species.[13–21] Very recently, we have reported a new mechanism of NO sensing in which the thiosemicarbazide group, flanked by the carbonyl moiety, reacts with NO under aerobic conditions leading to the formation of the 1,3,4-oxadiazole moiety with the simultaneous elimination of thionitrous acid.[22] In the current paper we are planning to report another new strategy where NO directly reacts with the imidazolium NH group to generate the N–N=O moiety acting as an electron acceptor from the phenanthrone moiety as the electron donor group thereby resulting in a turn on fluorescent response by the ICT process.

Experimental section

Physical measurements

An IR 750 series-II FTIR (Nickolet Magna) spectrophotometer was used to record IR spectra in the range 400–4000 cm^{-1} on KBr pellets. Electronic spectra were recorded on an Agilent 8453 Diode-array UV-vis spectrophotometer using 7 : 3 HEPES buffer (10 mM) and MeCN as the solvent with a 1 cm quartz cuvette in the range 200–900 nm. Fluorescence studies were performed on a PTI (model QM-40) spectrofluorimeter and ^{1}H NMR spectra were recorded in DMSO-d$_6$ on a Bruker 300 MHz instrument using trimethylsilane ($\delta = 0$) as an internal standard. ESI-MS$^+$ (*m/z*) of the ligand was recorded using a high resolution mass spectrometer (Model: QTOF Micro YA263). Time correlated single photon counting (TCSPC) measurements using a picosecond diode laser (IBH nanoled-07) in an IBH fluorocube apparatus were performed to determine fluorescence lifetimes. A Hamamatsu MCP photomultiplier (R3809) was used to collect the fluorescence decay data which were further examined by using the IBH DAS6 software. To obtain cell images, a fluorescence microscope (Leica DM3000, Germany) was used.

Materials and methods

9,10-Phenanthroquinone, pyridoxal hydrochloride, ammonium acetate, and glacial acetic acid were used to prepare the ligand. These reagents were purchased from Sigma-Aldrich. Salts of Cd^{2+}, Sm^{3+}, Co^{2+}, Mg^{2+}, Mn^{2+}, Na^+, Zn^{2+}, Dy^{3+}, Ni^{2+}, Cu^{2+}, Cr^{3+}, Hg^{2+}, Fe^{3+}, Pb^{2+}, Al^{3+}, F^-, $S_2O_3^{2-}$, HSO_4^-, IO_3^-, SO_4^{2-}, NO_2^-, HCO_3^-, Br^-, S^{2-}, HS^-, OAc^-, N_3^-, I^-, SCN^-, and ADP and biological anions like H_2O_2, O^{2-}, TEMPO radical, NO_3^-, ClO^-, AA, $NOBF_4$, glyoxal, formal-

dehyde, cysteine, homocysteine, glutathione *etc.* were obtained either from Sigma-Aldrich or from other commercial suppliers and used without further purification. Solvents like MeOH, *N,N*-dimethylformamide (DMF), MeCN, *etc.*, (Merck, India) were of reagent grade and dried before use.

Synthesis of the ligand

The ligand 5-hydroxymethyl-2-methyl-4-(1*H*-phenanthro[9,10-*d*]imidazole-2-yl)-pyridin-3-ol (designated as **PQPY**) was synthesized by the reported procedure with slight modification.[23] Excess ammonium acetate (25 mmol, 1.927 g) was dissolved in 5 mL glacial acetic acid, and then 9,10-phenanthroquinone (5 mmol, 1.041 g) solution (in glacial acetic acid) was added to the ammonium acetate solution at 70 °C by heating under stirring conditions. After 10 minutes, pyridoxal hydrochloride (5 mmol, 1.018 g) solution in glacial acetic acid was added dropwise to the reaction mixture. Then this reaction was continued for 6 hours under refluxing conditions. A blackish crude solid product was obtained by filtration and washed with a small volume of glacial acetic acid. From this crude product, the ligand was obtained by methanol extraction. Then the methanol part was evaporated to dryness to get a pure pale yellow product confirmed by ^{1}H NMR (Fig. S1†), HRMS (Fig. S2†) and FTIR (Fig. S4†). (Yield, 76%). ESI-MS$^+$ (*m/z*): 357.1221 (PQPY + H$^+$), ^{1}H NMR (in DMSO-d$_6$) (δ, ppm): 11.752 (s, 1H, –NH), 8.88–8.97 (m, 2H, –ArH), 8.55 (1H, d, –ArH), 8.36–8.34 (1H, d, –ArH), 8.29 (1H, S, –ArH), 7.64–7.87 (4H, m, –ArH), 5.41 (1H, S, –OH), 5.11 (S, 2H, –CH$_2$), 1.21 (S, 3H, –CH$_3$).

Solution preparation for fluorescence studies

A 10 mL 1.0×10^{-3} M stock solution of the ligand **PQPY** was prepared in DMF by slight heating for fluorescence titrations. The solutions of other metal ions and other anions were prepared in H_2O. A stock solution of nitric oxide was prepared in deoxygenated deionized water by purging nitric oxide gas for 15 min in a sealed vial with a syringe. The concentration of nitric oxide was 1.74×10^{-3} M. The nitric oxide gas was purified by passing it through a drying tube containing solid NaOH pellets.[24] HNO solution was prepared from Angeli's salt[25] and $^\bullet$OH and $ONOO^-$ solutions were prepared following a reported method.[26] A 100 mL solution of 10.0 mM 4-(2-hydroxyethyl)-1-piperazineethanesulfonic acid (HEPES) buffer was prepared adjusting pH to 7.0 using HCl and NaOH and ionic strength of the buffer solution was maintained at 0.10 M (NaCl) throughout the measurements. In this work, 20 μM ligand was taken in a cuvette containing a 2.5 ml mixture solution of HEPES buffer and MeCN in 7 : 3 ratio (v/v) and titrated with 0 to 75 μM NO solution incrementally in a regular time interval with $\lambda_{ex} = 400$ nm and 2, 2 slits.

Calculation of LOD

To know the limit of detection (LOD) of the ligand **PQPY** we used the following equation by the 3σ method.

$$LOD = 3 \times S_d / S$$

1214 | *Photochem. Photobiol. Sci.*, 2018, **17**, 1213–1221

This journal is © The Royal Society of Chemistry and Owner Societies 2018

S_d is the standard deviation obtained from the intercept of the plot of F.I. *vs.* [**PQPY**]. From the linear part of the titration plot, the value of the slope (S) is obtained.

Calculation of the quantum yield

Fluorescence quantum yields (Φ) were determined by using the equation:

$$\Phi_{sample} = (OD_{std} \times A_{sample})/(OD_{sample} \times A_{std}) \times \Phi_{std}$$

Here, A_{sample} and A_{std} represent the areas under the fluorescence spectral curves. The optical densities of the sample and standard are designated as OD_{sample} and OD_{std}, respectively, at the excitation wavelength. Here, acidic quinine sulfate was taken as the standard ($\Phi_{std} = 0.54$) for the quantum yield calculation of ligands **PQPY** and **PQPY-NO**.

Cell culture

Human hepatocellular liver carcinoma (HepG2) cell lines (NCCS, Pune, India) were grown in DMEM supplemented with 10% FBS and antibiotics (penicillin-100 µg ml^{-1}; streptomycin-50 µg ml^{-1}). Cells were cultured at 37 °C in a 95% air, 5% CO_2 incubator.

Cell imaging study

HepG2 cells were cultured in a 35 × 10 mm culture dish on a coverslip for 24 h at 37 °C. The cells were treated with 5 µM solutions of **PQPY**, prepared by dissolving **PQPY** in the mixed solvent HEPES buffer : acetonitrile = 7 : 3 (v/v) and incubated for 1 hour at 37 °C. For NO sensing study, HepG2 cells were preincubated with 5 µM, 10 µM and 20 µM sodium nitroprusside (SNP) for 60 min at 37 °C followed by washing three times with 1× PBS and subsequent incubation with 5 µM of **PQPY** for 60 min at 37 °C. Fluorescence images of HepG2 cells were obtained by using a fluorescence microscope (Leica DM3000, Germany) with an objective lens of 40× magnification.

Cell cytotoxicity assay

Cytotoxicity for the ligand **PQPY** was assessed by the 3-(4,5-dimethylthiazol-2-yl)-2,5-diphenyltetra-zolium bromide (MTT) cell viability assay. HepG2 cells (1×10^5 cells per well) were cultured in a 96-well plate and incubated at 37 °C and were exposed to varying concentrations of **PQPY** (1, 5, 10, 20, 30, 40, 50, 60, 70, 80 and 100 µM) for 24 hours. After the incubation, 10 µl of MTT solution [5 mg ml^{-1}, dissolved in 1× phosphate-buffered saline (PBS)] was added to each well of a 96-well culture plate and then incubated at 37 °C for 4 hours. Media were decanted from wells and 100 µL of 0.04 N acidic isopropyl alcohol was added into each well to solubilize the intracellular formazan crystals (blue-violet) formed. The absorbance of the solution was measured at 595 nm wavelength (EMax Precision MicroPlate Reader, Molecular Devices, USA). Values were calculated as mean ± standard errors of three independent experiments. The cell viability was expressed as the optical density ratio of the treatment to control.

Results and discussion

Design of the NO probe PQPY

For a few decades, the development of *ortho*-phenylene diamine (OPD) based probes using fluoresceins, anthraquinones, rhodamines, BODIPYs, and cyanines (Fig. 1) has emerged for the detection of nitric oxide but still there exist some serious limitations[9]. At first, in the presence of reactive oxygen and nitrogen species the electron rich diamino-benzene portion is readily oxidized. The second important drawback is that the OPD moiety shows a false positive response towards glyoxal, dehydroascorbic acid (DHA), and ascorbic acid (AA)[27] like NO which misguides the researchers towards wrong interpretations of observations. Another important shortcoming is that fluorescence enhancement occurs in the OPD moiety *via* benzotriazole formation, a secondary amine. Consequently, this is pH sensitive owing to protonation to the secondary amine of triazole. So, the poor selectivity and the above mentioned limitations are broad concerns in the design of fluorescent NO probes. In our present work, taking the aforementioned concerns into account, we strategically designed a new type of fluorescent probe **PQPY** based on *N*-nitrosation[27] of a secondary amine taking 9,10-phenanthroquinone as a fluorophore. The reactivity of **PQPY** was assessed with biological carbonyl species (RCS (glyoxal, formaldehyde (FA), ascorbic acid (AA), dehydroascorbic acid (DHA)) and also with cysteine (CYS), homocysteine (HCY), and glutathione (GSH). Even a large excess of each biological intercellular molecule cannot light up our present probe except for NO.

So, *N*-nitrosation based **PQPY** shows an improved selectivity towards NO over RNS, ROS, and RCS compared to OPD based NO probes, which makes it useful as a superior NO sensor. Our ligand is also cell permeable, low cytotoxicity, and pH independent with a very low detection limit (78 nM) and has an easy synthetic procedure which make it highly useful as a nitric oxide sensor.

As illustrated in Scheme 1, the probe **PQPY** was synthesized by the reaction between 9,10-phenanthroquinone and pyridoxal-hydrochloride in the presence of ammonium acetate in glacial acetic acid medium. The probe was nicely analyzed by
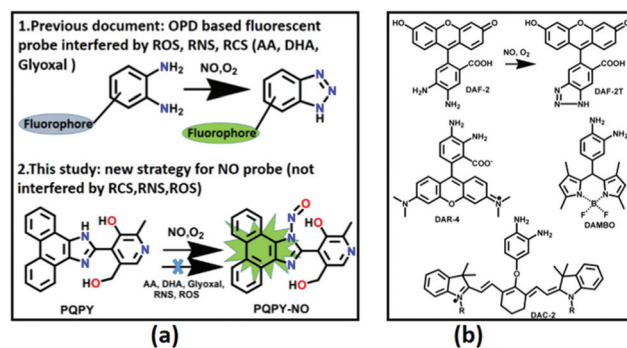

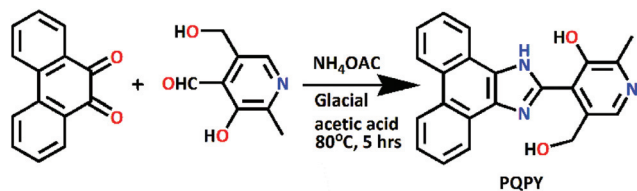**Fig. 1** (a). Scheme of the *N*-nitrosation reactivity based NO probe **PQPY** and (b) some previously reported NO probes.

This journal is © The Royal Society of Chemistry and Owner Societies 2018

Photochem. Photobiol. Sci., 2018, **17**, 1213–1221 | **1215**

Scheme 1 Synthesis of the probe 5-hydroxymethyl-2-methyl-4-(1*H*-phenanthro[9,10-*d*]imidazol-2-yl)-pyridin-3-ol (designated as **PQPY**).

---

¹H NMR (Fig. S1†), HRMS (Fig. S2†) and IR (Fig. S4†) spectroscopy.

The probe **PQPY** displayed a high fluorogenic response towards NO in the aerated aqueous buffer medium. In the present work, pyridoxal (one form of vitamin B₆) is taken as one part of the probe having a great significance in the growth of some medically relevant bacteria.

Spectral response of PQPY to NO

The sensitivity and selectivity of the probe **PQPY** are distinct only towards nitric oxide in aqueous acetonitrile medium at pH 7.0, as clearly demonstrated by the turn-on fluorescence response (λ_{em} = 505 nm) to nitric oxide upon excitation at 400 nm. The probe (20 μM) was taken in a cuvette containing 2.5 mL of 10 mM HEPES buffer : acetonitrile = 7 : 3 (v/v), pH = 7.0 and μ = 0.10 M NaCl. Then the previously prepared nitric oxide solution (1.74×10^{-3} M) was added incrementally.

For the deduction of the apparent formation constant (K_f) of the reaction between **PQPY** and NO, fluorescence titration was performed with the fixed concentration of **PQPY** (20 μM) with variable concentrations of NO (0–75 μM) at 25 °C. There was a gradual development of an emission band at ~505 nm (λ_{ex} = 400 nm) with the incremental addition of NO resulting in an approximately 9-fold enhancement in fluorescence intensity which is sufficient to detect nitric oxide intracellularly in live cells (*vide infra*) (Fig. 2). A plot of F.I. *versus* [NO] at 505 nm gives a nonlinear curve, which was solved by adopting the equation $y = (a + b \times c \times x^n)/(1 + c \times x^n)$,[28] where a represents F.I. of the free ligand, b is F.I. of the ligand in the presence of

excess NO, c is the formation constant, K_f, and n represents the stoichiometry. The evaluated parameters are $n = 0.93 \pm 0.01$ and $K_f = (1.00 \pm 0.2) \times 10^5$ M⁻¹.

Mechanism

In this research endeavor, we have designed a new fluorescent molecular probe **PQPY** which contains phenanthroimidazole and pyridine moieties acting as a fluorescence turn-on nitric oxide sensor. As the phenanthroimidazole moiety is an electron rich system, it acts as an electron donor (D) as well as a fluorophore and the other part *i.e.*, pyridine moiety, behaves also as an electron donor due to the presence of the phenolic –OH group. So, the flow of charge from the phenanthroimidazole moiety to pyridoxal (D–A) does not occur significantly and it becomes very weakly fluorescent, whereas the system is transferred to the electron donor–acceptor one being highly suitable for the intramolecular charge transfer mechanism upon reaction with nitric oxide. Here, NO is an electron withdrawing group and drags the electron density from the phenanthroquinone moiety to the imidazole system, causing a drastic fluorescence enhancement by the ICT mechanism. The intramolecular charge transfer (ICT) mechanism of the probe **PQPY** upon reaction with nitric oxide can be nicely understood by spectrofluorometric study in solvents of different polarities. The experiment shows a 24 nm red shift on increasing the polarity of the solvents which clearly suggests the occurrence of the intramolecular charge transfer mechanism in the ligand upon reaction with nitric oxide (Fig. S5†). As delineated by DFT optimization (*vide infra*) the HOMO of **PQPY** and **PQPY-NO** bears all the electron density localized on the phenanthrene moiety, whereas the LUMO electron density is solely distributed in the 1-nitrosoimidazole moiety of **PQPY-NO**, clearly manifesting the ICT mechanism of sensing (Scheme 2).

Confirmation of the sensing mechanism

To interpret the probable mechanism responsible for the fluorescence enhancement of the probe in the presence of nitric oxide, detailed product analysis was carried out by reacting **PQPY** with excess NO gas in the aerated MeCN medium. Then the solution was allowed to evaporate and the product
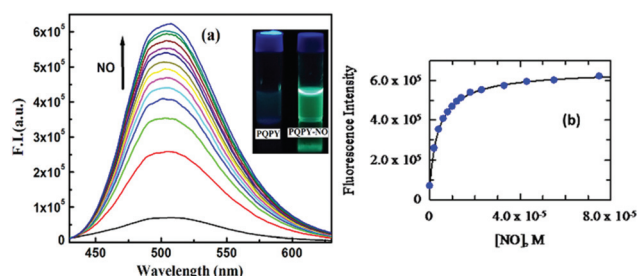
Fig. 2 (a). Fluorescence titration of the ligand **PQPY** (20 μM) at 25 °C by the gradual addition of nitric oxide (0–75 μM) in 7 : 3 HEPES buffer (10 mmol) : acetonitrile medium at pH = 7.0 with λ_{ex} = 400 nm and λ_{em} = 505 nm. The inset shows the UV exposed emission image of **PQPY** and **PQPY-NO**; (b) nonlinear plot of FI *vs.* [NO].
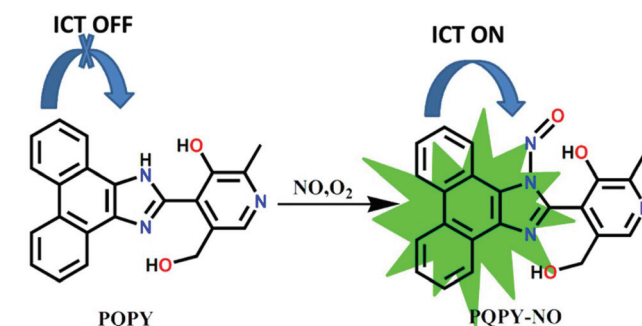
Scheme 2 Model describing the ICT on the fluorescence response of **PQPY** on interaction with NO in the presence of oxygen.

1216 | *Photochem. Photobiol. Sci.*, 2018, **17**, 1213–1221

This journal is © The Royal Society of Chemistry and Owner Societies 2018

PQPY-NO was isolated and characterized by using ^{1}H NMR (Fig. S6†) and FTIR (Fig. S7†) spectrometers. The molecular ion peak of **PQPY-NO** in the mass-spectrum was not found may be due to the breakdown of the N–N≡O bond to give the parent probe **PQPY** and NO and thus we find only the molecular ion peak of the ligand **PQPY**.

But the proton NMR spectra (Fig. 3) of **PQPY** and **PQPY-NO** clearly suggest that the imidazole –NH proton of **PQPY** exhibiting a single peak at 11.75 ppm vanished after the treatment with NO. So proton NMR depicts that NO is attached to the secondary amine of the imidazole system. This fact is further confirmed from the IR spectrum (Fig. S7†). The N–H stretching frequency at 3148 cm^{-1} disappeared and a new peak at 1424 cm^{-1} for the –N≡O group[29] was generated which confirms the formation of imidazole-N–N≡O. So we can conclude that the nitric oxide was attached directly to the imidazole N atom causing a turn-on fluorescence response and it is also evidenced from the substantial increase of the lifetime of the ligand (τ_0 = 2.68 ns) in the presence of nitric oxide (τ_0 = 3.96 ns). The non-existence of the ^{1}H NMR peak for phenolic –OH

protons may arise due to the strong hydrogen bonding interaction between phenolic–OH and tertiary imidazole–N atoms (O–H···N).

The quantum yield of compound **PQPY-NO** was Φ = 0.1006 and that of the ligand (**PQPY**) was 0.02 (quinine sulfate in the acidic medium was taken as the standard). The analytical limit of detection (LOD) of nitric oxide was deduced by the 3σ method (Fig. S8†) which was found to be as low as 78 nM further indicating the high efficiency of the probe to detect nitric oxide. So, all the above experiments, results and discussions highly support the probe as an efficient nitric oxide sensor.

TCSPC studies

The average life-time of the probe (τ_0 = 2.68 ns) increases upon addition with 75 µM nitric oxide (τ_0 = 3.96 ns) and the biexponential decay curve of the ligand changes to the monoexponential form on reaction with NO (Fig. 4). This study signifies the NO addition and greater stability of the product in the excited state.

pH stability checking

To know the practical applicability and stability of the ligand **PQPY** and product **PQPY-NO** under different environmental and physiological conditions, a plot of F.I. *vs.* pH was drawn which clearly reveals that **PQPY** exhibits a slight enhancement in fluorescence intensity at low pH, (≤3.0) due to protonation of imidazole NH atoms but it remains practically indifferent within a wide range of pH (pH 4.0–9.0). However, the product **PQPY-NO** shows high fluorescence intensity in a wide range of biological pH 4.0–9.0. As at pH ≈ 7.0, the fluorescence intensity is sufficiently high, it can be safely used under physiological conditions for monitoring NO (Fig. 5). Not only the NO product **PQPY-NO**, but our ligand also shows an almost invariable emission profile in a wide range of pH (Fig. S9†).

Selectivity study

To check the selectivity of **PQPY**, we have examined the response of **PQPY** towards commonly known metal ions (Cd^{2+},
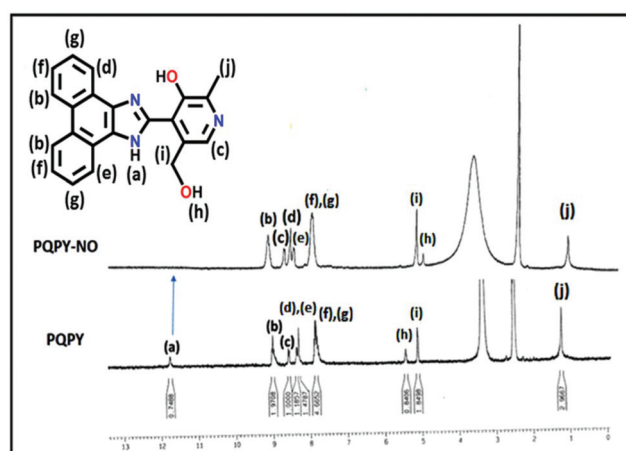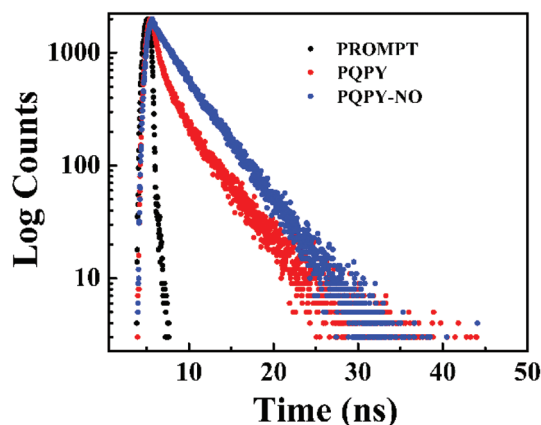

Fig. 3 NMR spectra of **PQPY** and **PQPY-NO**.

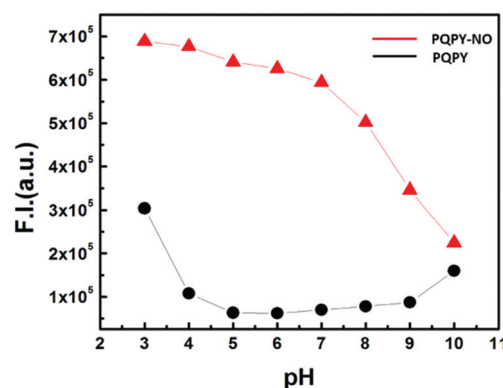**Fig. 4** Life time calculation plot for **PQPY** (20 µM) and **PQPY+NO** (75 µM) at pH 7.0 in HEPES buffer/MeCN (7 : 3, v/v) at room temperature.

Fig. 5 pH dependent fluorescence responses of **PQPY** and **PQPY-NO** in 7 : 3 (v/v) HEPES buffer/MeCN medium.

This journal is © The Royal Society of Chemistry and Owner Societies 2018

Photochem. Photobiol. Sci., 2018, **17**, 1213–1221 | **1217**

Sm^{3+}, Co^{2+}, Mg^{2+}, Mn^{2+}, Na^+, Zn^{2+}, Dy^{3+}, Ni^{2+}, Cu^{2+}, Cr^{3+}, Hg^{2+}, Fe^{3+}, Pb^{2+}, Al^{3+}), anions (F^-, $S_2O_3^{2-}$, HSO_3^-, IO_3^-, SO_4^{2-}, NO_2^-, HCO_3^-, Br^-, S_2^-, HS^-, OAc^-, N_3^-, I^-, SCN^-, ADP) and biologically relevant species (Tempo, $^\cdot OH$, H_2O_2, NO, OCl^-, AA, $ONOO^-$, O_2^-, NO_3^-, NO^+, DHA, FA, glyoxal, etc.). The fluorescence emission spectra (Fig. 6–9) clearly imply that **PQPY** exhibits high selectivity towards nitric oxide in aqueous–acetonitrile (7 : 3) medium at pH = 7.0. Even the presence of a large excess of each cation, anion, and biological intercellular molecule cannot enhance the fluorescence intensity of our present
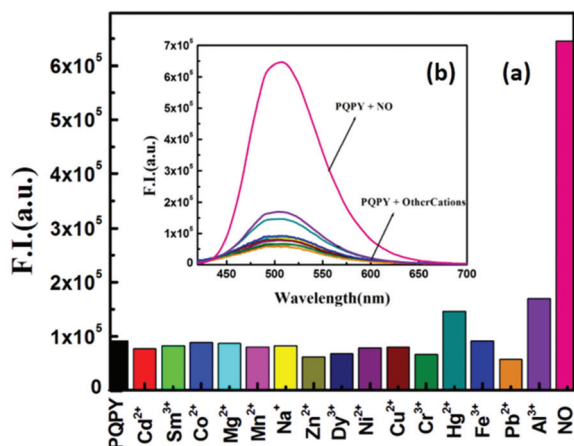

Fig. 8 (a) Bar plot illustrating fluorescence responses of **PQPY** at 505 nm (λ_{ex} = 400 nm) towards different biologically relevant species in HEPES buffer at pH 7.0 in H_2O−MeCN (7 : 3, v/v) at room temperature. **PQPY** = 20 μM, X^{n-} = 100 μM. (b) Spectral response of **PQPY** towards different biological anions.

Fig. 6 (a) Bar plot illustrating fluorescence responses of **PQPY** at 505 nm (λ_{ex} = 400 nm) towards different cations in HEPES buffer at pH 7.0 in H_2O−MeCN (7 : 3, v/v) at room temperature. **PQPY** = 20 μM, X^{n-} = 100 μM. (b) Spectral response of **PQPY** towards different cations.
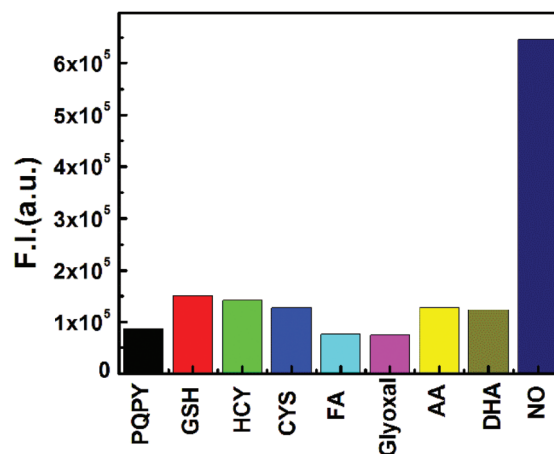
Fig. 9 Bar plot illustrating fluorescence responses of **PQPY** at 505 nm (λ_{ex} = 400 nm) towards different biologically relevant thiols and carbonyl species in HEPES buffer at pH 7.0 in H_2O−MeCN (7 : 3, v/v) at room temperature. **PQPY** = 20 μM, [X] = 100 μM.
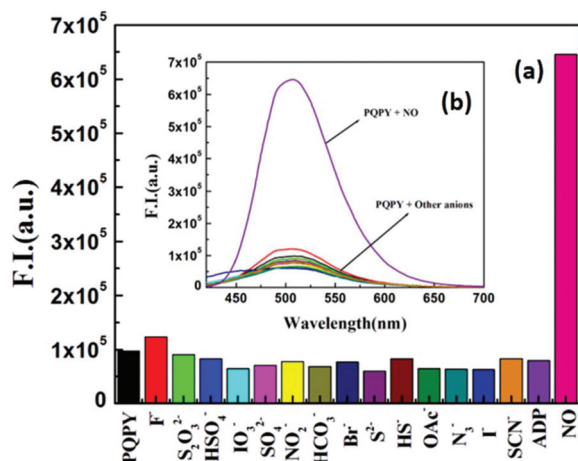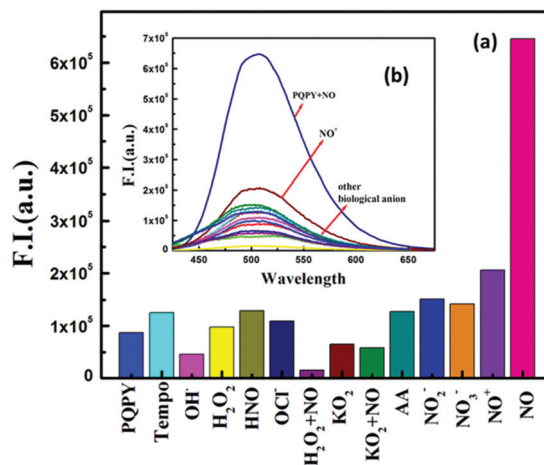

Fig. 7 (a) Bar plot illustrating fluorescence responses of **PQPY** at 505 nm (λ_{ex} = 400 nm) towards different anions in HEPES buffer at pH 7.0 in H_2O−MeCN (7 : 3, v/v) at room temperature. **PQPY** = 20 μM, X^{n-} = 100μM. (b) Spectral response of **PQPY** towards different anions.

probe except for NO suggesting its high selectivity towards nitric oxide.

Theoretical studies

To better understand the photophysical properties of the probe and NO product, we performed quantum chemical computations using the DFT/B3LYP/6-31G(d) level of theory. We optimized the energy of the probe and NO product to find the distribution of electron density within aromatic rings. All the calculations were performed with the Gaussian 09W software package.[30] The optimized geometry of the probe (**PQPY**) and its NO product (**PQPY-NO**) is shown in Fig. 10. Both have a C1

Fig. 10 Optimized geometry of PQPY and the PQPY−NO product.

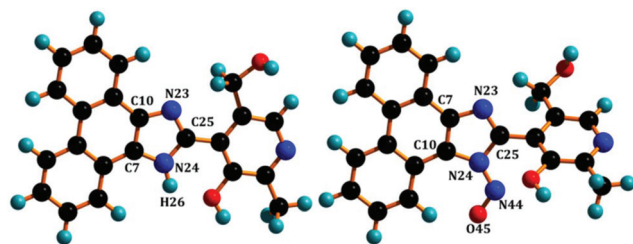point group. The nature of all stationary points for both the free probe and its NO product was confirmed by carrying out normal mode analysis. All the frequencies turned out to be positive, which proved the global minima of **PQPY** and **PQPY-NO**. The important optimized geometrical parameters of the free **PQPY** and **PQPY-NO** are listed in Tables S1 and S2.† The highest occupied molecular orbital (HOMO) and the lowest unoccupied molecular orbital (LUMO) energies of the probe and NO product are shown in Fig. 11.

In the case of the probe as well as the NO product the HOMO electron densities are localized in the 2-(1*H*-phenanthro[9,10-*d*]imidazol-2-yl)-prop-2-en-1-ol moiety, whereas LUMO electron clouds reside in 5-hydroxymethyl-6-methylpyridin-3-ol for the probe but on the 1-nitroso-1*H*-imidazole moiety for the NO product. This delocalization of excited electronic energy to the 1-nitroso-1*H*-imidazole for the NO product is responsible for enhancing the fluorescence intensity due to the electron withdrawing nature of the –NNO group. The calcu-

lated HOMO and LUMO energy gap is found to be 2.92 eV for the NO product, which is lower than that of the calculated HOMO–LUMO gap of the probe (3.94 eV). Therefore, the NO product is more stable than that of the free probe.

Cell imaging study

In order to assess the ability of **PQPY** to detect nitric oxide (**NO**) *in vitro*, it has been further checked for its properties to form a product with **NO** in living cells. Before that we have explored the cytotoxic effects of **PQPY** on live HepG2 cells by cell viability assay using MTT (Fig. 12). There was no significant reduction in the tetrazolium salt reflecting a decrease in formazan production for **PQPY** up to 10 μM, thus suggesting that below 10 μM ligand concentration **PQPY** would be much more effective for the analysis of its product formation with **NO** *in vitro*. Around 80% cell viability was observed for **PQPY** at 5 μM, after which the viability of the HepG2 cells decreased.
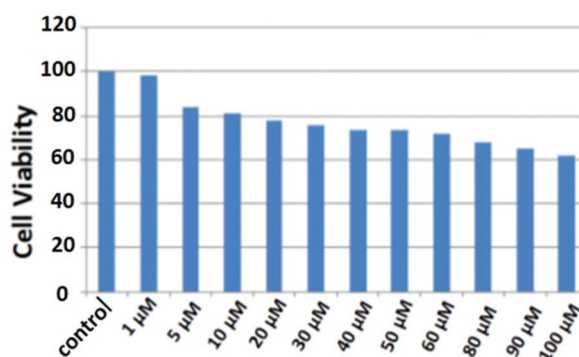
Fig. 12 Percent (%) cell viability of HepG2 cells treated with different concentrations (1−100 μM) of PQPY for 24 hours determined by MTT assay.

Fig. 11 Frontier molecular orbital of the probe (**PQPY**) and NO product (**PQPY-NO**).

| PQPY: 5μM | PQPY: 5μM | PQPY: 5μM | PQPY: 5μM |
| SNP: - | SNP: 5μM | SNP: 10μM | SNP: 20μM |

Fig. 13 The fluorescence images of HepG2 cells were captured (40×) after incubation with 5 μM of **PQPY** for 60 min at 37 °C, followed by washing thrice with 1× PBS, and incubation with 5 μM, 10 μM and 20 μM of SNP for 60 min at 37 °C followed by incubation with 5 μM of **PQPY** for 60 min at 37 °C. The fluorescence images show no fluorescence signal by the fluorophore **PQPY** (5 μM) in the absence of the NO donor, while the fluorescence gradually increases with higher concentration of the NO donor.

This journal is © The Royal Society of Chemistry and Owner Societies 2018

Photochem. Photobiol. Sci., 2018, **17**, 1213–1221 | **1219**

Hence, further experiments were carried out with 5 μM of **PQPY** for treatment.

The ligand **PQPY** showed the absence of intracellular fluorescence in HepG2 cells treated with 5 μM of the ligand and incubated for 1 h (Fig. 13); however, a prominent intracellular green fluorescence signal was observed in cells when the HepG2 cells were incubated with 5 μM of SNP for 60 min at 37 °C to produce exogenous NO, followed by incubation with 5 μM of **PQPY**. The intracellular fluorescence was found to be prominently localized in the cytoplasmic region.

Keeping the ligand **PQPY** concentration constant at 5 μM and increasing the concentration of NO donor SNP (5 μM, 10 μM and 20 μM), a NO concentration-dependent enhancement in the intracellular green fluorescence is observed, caused by the formation of the product between **PQPY** and NO. An intense intracellular fluorescence was observed due to the formation of **PQPY-NO** nearly at 20 μM of SNP. Altogether, the present results suggest that the probe with low cytotoxicity and the property of enhanced fluorescence with increasing concentration of intracellular NO can be used for NO detection in biological samples.

Conclusion

In summary, we have been able to synthesize novel 5-hydroxymethyl-2-methyl-4-(1*H*-phenanthro[9,10-*d*]imidazole-2-yl)-pyridin-3-ol (**PQPY**) in a facile manner as a highly selective turn-on *in vitro* NO probe and characterize it by various spectroscopic techniques. The probe can detect nitric oxide efficiently and selectively in a wide range of physiological pH at room temperature in 70% water. The highly electron withdrawing group –N–N=O drags the electron density from the whole system (**PQPY-NO**) towards itself converting the probe to a donor–acceptor one giving the credit for intramolecular charge transfer which results in a large fluorescence enhancement. The formation constant $(1.00 \pm 0.2) \times 10^5$ obtained from the titration supports the stability of the NO product (**PQPY-NO**). The 78 nM analytical detection limit deduced by the 3σ method reassures the potentiality of the ligand as a NO probe in biological systems. The ligand is also biocompatible due to its solubility in mixed aqueous–organic (water–acetonitrile; 7 : 3) solutions and also it has cell permeability and the low cytotoxicity towards living cells magnifying its biological applicability.

Conflicts of interest

There are no conflicts to declare.

Acknowledgements

References

1 N. S. Bryan and M. B. Grisham, Methods to detect nitric oxide and its metabolites in biological samples, *Free Radicals Biol. Med.*, 2007, **43**, 645–657.

2 D. S. Bredt, Endogenous nitric oxide synthesis: Biological functions and pathophysiology, *Free Radicals Biol. Med.*, 1999, **31**, 577–596.

3 M. Kelm, Nitric oxide metabolism and breakdown, *Biochim. Biophys. Acta*, 1999, **1411**, 273–289.

4 B. Brune, S. Dimmeler, L. M. Vedia and E. G. Lapetina, Nitric oxide: A signal for ADP-ribosylation of proteins, *Life Sci.*, 1994, **54**, 61–70.

5 B. J. Privett, J. H. Shin and M. H. Schoenfisch, Electrochemical nitric oxide sensors for physiological measurements, *Chem. Soc. Rev.*, 2010, **39**, 1925–1935.

6 W. Hu, D. Boateng, J. Kong and X. Zhang, Advancement of Fluorescent Methods for Detection of Nitric Oxide, *Austin J. Biosens. Bioelectron.*, 2015, **1**, 1–9.

7 Y. Gabe, Y. Urano, K. Kikuchi, H. Kojima and T. Nagano, Highly Sensitive Fluorescence Probes for Nitric Oxide Based on Boron Dipyrromethene Chromophore-Rational Design of Potentially Useful Bioimaging Fluorescence Probe, *J. Am. Chem. Soc.*, 2004, **126**, 3357–3367.

8 E. Sasaki, H. Kojima, H. Nishimatsu, Y. Urano, K. Kikuchi, Y. Hirata and T. Nagano, Highly Sensitive Near-Infrared Fluorescent Probes for Nitric Oxide and Their Application to Isolated Organs, *J. Am. Chem. Soc.*, 2005, **127**, 3684–3685.

9 Y. Yang, S. K. Seidlits, M. M. Adams, V. M. Lynch, C. E. Schmidt, E. V. Anslyn and J. B. Shear, A highly selective low-background fluorescent imaging agent for nitric oxide, *J. Am. Chem. Soc.*, 2010, **132**, 13114–14116.

10 L. E. McQuade, M. D. Pluth and S. J. Lippard, Mechanism of Nitric Oxide Reactivity and Fluorescence Enhancement of the NO-Specific Probe CuFL1, *Inorg. Chem.*, 2010, **49**, 8025–8033.

11 L. E. McQuade and S. J. Lippard, Fluorescence-Based Nitric Oxide Sensing by Cu(II) Complexes That Can Be Trapped in Living Cells, *Inorg. Chem.*, 2010, **49**, 7464–7471.

12 M. H. Lim and S. J. Lippard, Fluorescence-Based Nitric Oxide Detection by Ruthenium Porphyrin Fluorophore Complexes, *Inorg. Chem.*, 2004, **43**, 6366–6370.

13 A. Beltrán, M. I. Burguete, D. R. Abánades, S. D. Pérez-Sala, V. Luis and F. Galindo, Turn-on fluorescent probes for nitric oxide sensing based on the *ortho*-hydroxyamino structure showing no interference with dehydroascorbic acid, *Chem. Commun.*, 2014, **50**, 3579–3581.

14 M. H. Lim and S. J. Lippard, Copper Complexes for Fluorescence-Based NO Detection in Aqueous Solution, *J. Am. Chem. Soc.*, 2005, **127**, 12170–12171.

15 M. H. Lim and S. J. Lippard, Fluorescent Nitric Oxide Detection by Copper Complexes Bearing Anthracenyl and

1220 | *Photochem. Photobiol. Sci.*, 2018, **17**, 1213–1221

This journal is © The Royal Society of Chemistry and Owner Societies 2018

Dansyl Fluorophore Ligands, *Inorg. Chem.*, 2006, **45**, 8980–8989.

16 C. Sun, W. Shi, Y. Song, W. Chen and H. Ma, An unprecedented strategy for selective and sensitive fluorescence detection of nitric oxide based on its reaction with a selenide, *Chem. Commun.*, 2011, **47**, 8638–8640.

17 R. C. Smith, A. G. Tennyson, M. H. Lim and S. J. Lippard, Conjugated Polymer-Based Fluorescence Turn-On Sensor for Nitric Oxide, *Org. Lett.*, 2005, **7**, 3573–3575.

18 T. W. Shiue, Y. H. Chen, C. M. Wu, G. Singh, H. Y. Chen, C. H. Hung, W. F. Liaw and Y. M. Wang, Nitric Oxide Turn-on Fluorescent Probe Based on Deamination of Aromatic Primary Monoamines, *Inorg. Chem.*, 2012, **51**, 5400–5408.

19 H. Kojima, M. Hirotani, N. Nakatsubo, K. Kikuchi, Ys. Urano, T. Higuchi, Y. Hirata and T. Nagano, Bioimaging of Nitric Oxide with Fluorescent Indicators Based on the Rhodamine Chromophore, *Anal. Chem.*, 2001, **73**, 1967–1973.

20 H. Yu, X. Zhang, Y. Xiao, W. Zou, L. Wang and L. Jin, Targetable Fluorescent Probe for Monitoring Exogenous and Endogenous NO in Mitochondria of Living Cells, *Anal. Chem.*, 2013, **85**, 7076–7084.

21 X. Dong, C. H. Heo, S. Chen, H. M. Kim and Z. Liu, Quinoline-Based Two-Photon Fluorescent Probe for Nitric Oxide in Live Cells and Tissues, *Anal. Chem.*, 2014, **86**, 308–311.

22 A. S. M. Islam, R. Bhowmick, K. Pal, A. Katarkar, K. Chaudhuri and M. Ali, A Smart Molecule for Selective Sensing of Nitric Oxide: Conversion of NO to HSNO; Relevance of Biological HSNO Formation, *Inorg. Chem.*, 2017, **56**, 4324–4331.

23 A. J. Beneto, V. Thiagarajanb and A. Siva, A tunable ratiometric pH sensor based on phenanthro[9,10-*d*]imidazole covalently linked with vinylpyridine, *RSC Adv.*, 2015, **5**, 67849.

24 Š. Mesároš, S. Grunfeld, A. Mesárošová, D. Bustin and T. Malinski, Determination of nitric oxide saturated (stock) solution by chronoamperometry on a porphyrine microelectrode, *Anal. Chim. Acta*, 1997, **339**, 265–270.

25 A. T. Wrobel, T. C. Johnstone, A. Deliz Liang, S. J. Lippard and P. Rivera-Fuentes, A Fast and Selective Near-Infrared Fluorescent Sensor for Multicolor Imaging of Biological Nitroxyl (HNO), *J. Am. Chem. Soc.*, 2014, **136**, 4697–4705.

26 S. Miyamoto, G. R. Martinez, A. P. B. Martins, M. H. G. Medeiros and P. DiMascio, Direct Evidence of Singlet Molecular Oxygen $[O_2\ (^1\Delta_g)]$ Production in the Reaction of Linoleic Acid Hydroperoxide with Peroxynitrite, *J. Am. Chem. Soc.*, 2003, **125**, 4510–4517.

27 Z. Mao, H. Jiang, Z. Li, C. Zhong, W. Zhang and Z. Liu, An *N*-nitrosation reactivity-based two-photon fluorescent probe for the specific *in situ* detection of nitric oxide, *Chem. Sci.*, 2017, **8**, 4533.

28 A. S. M. Islam, R. Alam, A. Katarkar, K. Chaudhuri and M. Ali, Di-oxime based selective fluorescent probe for arsenate and arsenite ions in a purely aqueous medium with living cell imaging applications and H-bonding induced microstructure formation, *Analyst*, 2015, **140**, 2979–2983.

29 K. Tsuge, F. DeRosa, M. D. Lim and P. C. Ford, Intramolecular Reductive Nitrosylation: Reaction of Nitric Oxide and a Copper(II) Complex of a Cyclam Derivative with Pendant Luminescent Chromophores, *J. Am. Chem. Soc.*, 2004, **126**, 6564–6565.

30 M. J. Frisch, G. W. Trucks, H. B. Schlegel, G. E. Scuseria, M. A. Robb, J. R. Cheeseman, G. Scalmani, V. Barone, B. Mennucci, G. A. Petersson, H. Nakatsuji, M. Caricato, X. Li, H. P. Hratchian, A. F. Izmaylov, J. Bloino, G. Zheng, J. L. Sonnenberg, M. Hada, M. Ehara, K. Toyota, R. Fukuda, J. Hasegawa, M. Ishida, T. Nakajima, Y. Honda, O. Kitao, H. Nakai, T. Vreven, J. A. Montgomery Jr., J. E. Peralta, F. Ogliaro, M. Bearpark, J. J. Heyd, E. Brothers, K. N. Kudin, V. N. Staroverov, R. Kobayashi, s. J. Normand, K. Raghavachari, A. Rendell, J. C. Burant, S. S. Iyengar, J. Tomasi, M. Cossi, N. Rega, J. M. Millam, M. Klene, J. E. Knox, J. B. Cross, V. Bakken, C. Adamo, J. Jaramillo, R. Gomperts, R. E. Stratmann, O. Yazyev, A. J. Austin, R. Cammi, C. Pomelli, J. W. Ochterski, R. L. Martin, K. Morokuma, V. G. Zakrzewski, G. A. Voth, P. Salvador, J. J. Dannenberg, S. Dapprich, A. D. Daniels, Ö. Farkas, J. B. Foresman, J. V. Ortiz, J. Cioslowski and D. J. Fox, *Gaussian 09, revision A.1*, Gaussian, Inc., Wallingford, CT, 2009.

This journal is © The Royal Society of Chemistry and Owner Societies 2018

Photochem. Photobiol. Sci., 2018, **17**, 1213–1221 | **1221**

Check for updates

A coumarin embedded highly sensitive nitric oxide fluorescent sensor: kinetic assay and bio-imaging applications†

Debjani Maiti,[a] Abu Saleh Musha Islam, [ID][a] Mihir Sasmal, [ID][a] Ananya Dutta,[a] Atul Katarkar[b] and Mahammad Ali [ID] *[a,c]

Fluorescence spectroscopy is a significant bio-analytical technique for specific detection of nitric oxide (NO) and for broadcasting the *in vitro* and *in vivo* biological activities of this gasotransmitter. Herein, a benzo-coumarin embedded smart molecular probe (BCM) is employed for NO sensing through detailed fluorescence studies in purely aqueous medium. All the spectroscopic analysis and literature reports clearly validate the mechanistic insight of this sensing strategy *i.e.*, the initial formation of 1,2,3,4-oxatriazole on treatment of the probe with NO which finally converted to its carboxylic acid derivative. This oxatriazole formation results in a drastic enhancement in fluorescence intensity due to the photoinduced electron transfer (PET) effect. The kinetic investigation unveils the second and first-order dependency on [NO] and [BCM] respectively. The very low detection limit (16 nM), high fluorescence enhancement (123 fold) in aqueous medium and good formation constant ($K_f = (4.33 \pm 0.48) \times 10^4$ M^{-1}) along with pH invariability, non-cytotoxicity, biocompatibility and cell permeability make this probe a very effective one for tracking NO intracellularly.

Introduction

Over a few decades, biologically abundant reactive nitrogen species (RNS) have played their pivotal role as a cell signalling molecule in the course of diverse physiological and pathological processes.[1] Nitric oxide (NO), a prime member of this class, is a pervasive gasotransmitter and is associated with numerous physiological processes in many bio-organisms. Endogenous production of NO takes place through the conversion of L-arginine to L-citrulline which is catalysed by eNOS, nNOS and iNOS (NO synthase enzymes).[2] Physiologically, NO (i) functions as a stimulator in vascular smooth muscle relaxation, (ii) prevents infections functioning on the immune system and (iii) serves as a neurotransmitter.[3,4] The pathological impact on malfunctioning of NO homeostasis occurs due to carcinogenesis, neurodegenerative injury, endothelial dysfunction, diabetes, chronic liver inflammation *etc.*[5,6] Nitric oxide is involved in the modulation of gene transcription and

acts as a controlling factor in the translation of *m*-RNA.[7,8] Considering the unambiguous significance of this bio-regulatory molecule, several methods like chemi-luminescence, electrochemistry, colorimetric assay, electron-paramagnetic resonance spectroscopy, fluorimetric techniques[9–14] *etc.* are widely used to comprehend the NO biology.

But among these analytical methods, the fluorescence technique is considered as the most conducive one for endogenous NO detection owing to its high sensitivity, non-destructive and real-time imaging properties, minimal invasiveness, sophisticated instrumentation and high spatio-temporal resolution.[15–19] Thereby, by exploiting the fluorescence spectroscopic technique plenty of nitric oxide probes have been developed: (i) organic probes, (ii) single-walled nanotube (SWNT) probes, (iii) quantum dot (QD) probes and (iv) metal complex based probes.[20–27] The *o*-phenylene diamine (OPD) moiety, from the class of organic probes, is one of the promising receptors for NO leading to the formation of triazole with a significant enhancement of fluorescence intensity.[20–33] Though this strategy has attracted the deep attention of researchers, its applications are limited by some serious shortcomings. As for example, (a) the vicinal diamine may suffer from oxidation by various oxidants present in the biological system; (b) the triazole formed in the reaction with NO may show different fluorescence responses at different pH values due to the presence of the secondary –NH group, which may lead to misinterpretation of fluorescence data.[30,31,33]

[a]Department of Chemistry Jadavpur University, Kolkata 700 032, India.
E-mail: m_ali2062@yahoo.com; Fax: +91-33-2414-6223
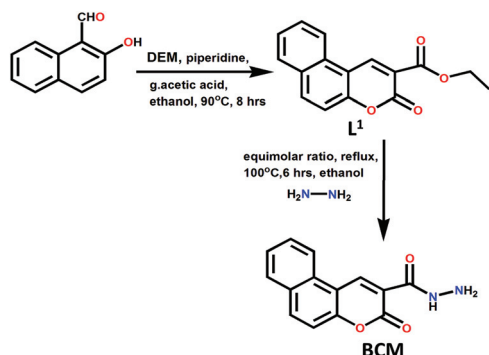*[b]Department of Biochemistry, University of Lausanne, Ch. des Boveresses 155, 1066 Epalinges, Switzerland*
[c]Vice-Chancellor, Aliah University, ll-A/27, Action Area II, Newtown, Action Area II, Kolkata, West Bengal 700160, India. E-mail: vc_au@aliah.ac.in
†Electronic supplementary information (ESI) available. See DOI: 10.1039/d0ob00567c

Considering all these limitations, our group has disclosed a novel strategy for nitric oxide sensing by employing quinoline as a fluorophore moiety and acyl hydrazide as a receptor. Upon treatment with nitric oxide this probe primarily forms 1,2,3,4 oxatrizole causing a substantial enhancement in fluorescence intensity[34] and it finally converted to a carboxylic acid.[34] In our present work, we have used coumarin as a fluorophore which is a planar, rigid and pi-conjugated heterocycle. Over a few decades it was clearly recognized that the active site at 3 position of coumarin with its benzo counterpart is strongly fluorescent.[35] It is a naturally occurring organic compound found in plants and oil, like the oil of cassia, sweet clover, woodruff, tonka beans and lavender. Coumarin derivatives are well recognized due to their numerous activities in pharmaceuticals, insecticides, agrochemicals, fragrances, and polymer sciences and they are also identified as important organic fluorescent materials.[36] It is also used in the treatment of burns, brucellosis, rheumatic disease, *etc*.[37] In respect of photophysical activities, coumarin and its derivatives exhibit high photostability, easy synthesis, an extended spectral range and good solubility.[38–40] So, considering all these significances, we developed our pioneering strategy by using a coumarin fluorophore joined with the benzo-counter part which is synthesized by the well-known Knoevenagel condensation followed by hydrazination. Herein, a relevant study to comprehend the selectivity and sensitivity of BCM towards NO along with a plausible mechanism has been delineated by a concentration and time dependent kinetic studies. We have also performed a detailed cell imaging and theoretical studies. A very high sensitivity to nitric oxide along with a 123 fold fluorescence enhancement in purely aqueous medium at physiological pH and a very low detection limit (16 nM) qualify the efficacy of the probe for intracellular NO detection.

Results and discussion

Scheme 1 displays a two steps synthetic pathway for the synthesis of 3-oxo-3*H*-benzo[*f*]chromene-2-carboxylic acid hydrazide (hereafter designated as BCM). The first step is a very well-known Knoevenagel condensation between 2-hydroxy napthal-

dehyde and di-ethyl malonate in the presence of piperidine and glacial acetic acid under refluxing conditions. After 8 h, the reaction mixture is cooled to room temperature whereupon a pure product (L[1]) was formed which was collected by filtration and well analyzed by ^{1}H NMR (Fig. S1†) and ^{13}C NMR (Fig. S2†).

The second step comprises the treatment of the corresponding ester with hydrazine hydrate in an equimolar ratio. The targeted fluorescent probe was well characterized by common spectroscopic studies, *i.e.*, ^{1}H NMR (Fig. S3†), ^{13}C NMR (Fig. S4†), mass spectroscopy (Fig. S5†), and FTIR (Fig. S6†). The receptor exhibits very high affinity and selectivity towards NO in aqueous medium.

Photophysical response of BCM towards NO

The fluorescence properties of the probe BCM and affinity towards nitric oxide were analyzed by performing fluorescence titration, Fig. 1. For this experiment, a fixed concentration (20 μM) of BCM was added into a cuvette containing 2.5 ml of aqueous HEPES buffer at 25 °C. Then, the NO solution was added progressively in the concentration range from 0 to 40 μM. BCM alone exhibits a very weak fluorescence in aqueous HEPES buffer, whereas gradual addition of NO causes a steady generation of fluorescence intensity resulting in an ~123 fold enhancement at λ_{em} ~470 nm (λ_{ex} = 410 nm). To determine the apparent formation constant we have carried out a fluorescence titration experiment and a plot of F.I. *vs.* [NO] shows an excellent linearity of the curve up to 25 μM after which the plot gets saturated (maximum NO 40 μM). The linear part was easily solved by utilizing eqn (1) [41] under the condition $1 \gg cx^n$ and $n = 1$.

$$y = \frac{(a + b \times c \times x^n)}{1 + c \times x^n} \tag{1}$$

where parameters a and b denote the F.I. of the probe in the absence and presence of excess NO respectively, and c is the

Scheme 1 Pathway for the synthesis of probe BCM.
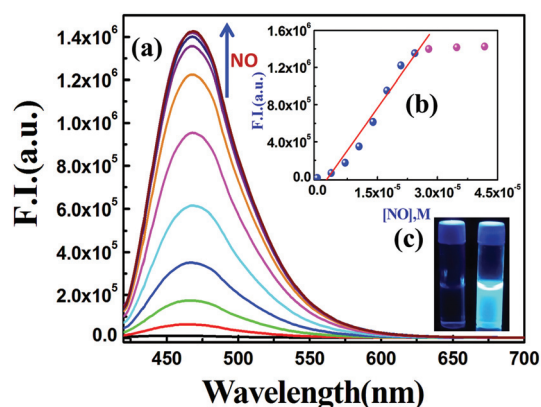
Fig. 1 (a) Fluorescence emission spectra recorded by taking only fixed 20 μM BCM and also gradual addition of NO (0–40 μM) at 25 °C in 10 mM HEPES buffer at pH 7.0, λ_{ex} = 410 nm and λ_{em} = 470 nm. (b) Linear plot of F.I. *vs.* [NO]. (c) The image of probe BCM (left) and NO treated product (right) exposed to UV light.
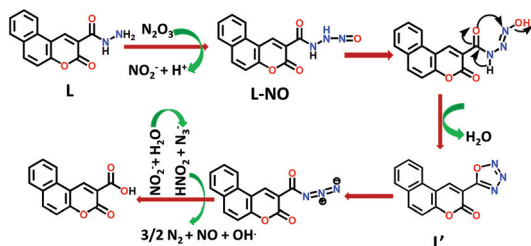
formation constant designated as K_f. The slope $(b \times c)$ obtained from the curve gives $c = K_f = (4.33 \pm 0.48) \times 10^4$ M^{-1} (using $b =$ F.I. in the presence of a large excess of NO).

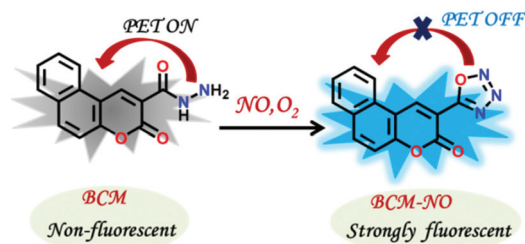**Mechanistic view of fluorescence sensing of the receptor BCM towards NO**

To gain insight into the mechanism which is responsible for fluorescence enhancement, we collected the product of the reaction between BCM and NO. For this purpose, BCM was dissolved (1 mmol, 0.254 g) in a minimum volume of dichloromethane (DCM) and finally with 20 ml acetonitrile under aerobic conditions. Then nitric oxide gas was bubbled through the probe solution for 15 minutes. A vivid fluorescence was noticed throughout the solution. The solvent was evaporated under pressure. A brown solid was collected and further purified by recrystallization in ethanol. The pure crystalline compound was filtered and characterized by ESI-MS$^+$ (Fig. S7†), ^{1}H NMR (Fig. S8†) and IR spectroscopy (Fig. S9†). The ESI-MS$^+$ spectrum (Fig. S7†) shows a peak at 304.0406 (1,2,3,4-oxatriazole + K$^+$) suggesting the generation of 1,2,3,4-oxatriazole (BCM-NO) which was further ensured by the disappearance of –NH (9.39 ppm) and –NH$_2$ (4.79 ppm) peaks in the ^{1}H NMR spectra (Fig. S8†). The generation of the IR peak at 1600 cm^{-1} (–N=N) and 1666 cm^{-1} (–C=N) also strengthens the formation of the oxatriazole moiety (Fig. S9†).

The predicted mechanism is outlined in Scheme 2, where NO first reacts with O$_2$ to generate N$_2$O$_3$ under aerobic conditions which nitrosylates –NH$_2$ of BCM to generate –NH-NO which ultimately generates 1,2,3,4-oxatriazole (BCM-NO) as a stable product. The formation of the electron deficient oxatriazole moiety causes a large enhancement in fluorescence intensity at $\lambda_{em} = 470$ nm. It is interesting to note that the formed oxatriazole is finally transformed to a carboxylic acid through the formation of azide after keeping it in solution for a long time and was ensured from the mass spectra (Fig. S10†) and ^{1}H NMR spectrum (Fig. S11†).

From the electronic point of view the main-stream mechanism for NO sensing by OPD based probes is based upon the PET block process.[42–44] Very recently, our group reported a quinoline based NO sensor containing the acyl hydrazide moiety where the PET effect[34] was operative. In the current report, we propose that the PET-ON mechanism due to electron push from the hydrazide part to the coumarin fluorophore makes the probe BCM weakly fluorescent. However, upon reaction
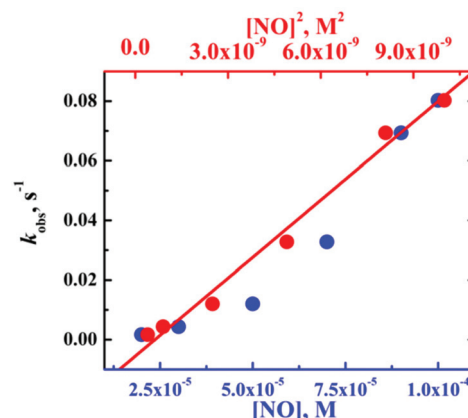

Scheme 3   Presentation of PET effect responsible for NO sensing.

with NO a remarkable fluorescence enhancement has been perceived which may arise due to the generation of the electron deficient 1,2,3,4-oxatriazole moiety that restricts the above PET-ON process (Scheme 3).

Time dependent reaction of BCM with NO, a kinetic approach

To ensure a clear view of the operative mechanism of the reaction between BCM and NO, we have thoroughly performed kinetic studies at pH 7.0 (10 mM HEPES buffer, 0.10 M NaCl), 15 °C, under pseudo-first-order conditions using the fluorometric technique (Fig. 2). In this study, we have taken a fixed concentration of BCM (5 μM) and variable [NO] (20–100 μM). The kinetic traces at 470 nm unveil single exponential growth curves assigning the first-order dependency of the reaction rate on [BCM]. The time dependent fluorescence study also shows that the fluorescence intensities at 470 nm increase with time and reach a plateau within ~5 min (Fig. S12†). The pseudo-first-order rate constants (k_{obs}) obtained from the growth curves have been plotted against [NO], which yields a nonlinear upward curvature.
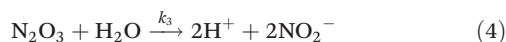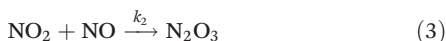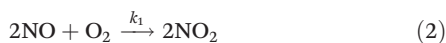
However, a plot of k_{obs} *vs.* [NO]^2 displayed a well fitted straight line which delineates the second-order dependency upon [NO] (Fig. 2†). The log(k_{obs}) *vs.* log[NO] plot furnishes a straight line with a slope = (2.42 ± 0.08) with $R = 0.997$ which

Fig. 2   The k_{obs} *vs.* [NO] plot gives an upward curvature (blue solid circles), while a plot of k_{obs} *vs.* [NO]^2 gives a straight line (red solid circles). Experimental conditions are: [BCM] = 5 μM and [NO] = (20−100) μM, temperature = 15 °C in 10 mM HEPES buffer (pH = 7.0, NaCl = 0.10 M). All the data were collected using the fluorescence technique.

Scheme 2   Possible reaction mechanism for the reaction between BCM and NO.

8452 | *Org. Biomol. Chem.*, 2020, **18**, 8450–8458

This journal is © The Royal Society of Chemistry 2020

also supports the second order kinetics with respect to [NO] (Fig. S13†). We have accomplished a second experiment to evaluate the dependency of rate upon [BCM] taking a fixed 5 μM [NO] with variable [BCM] in the range between 20 and 100 μM. Here, a plot of $\log k_{obs}$ vs. $\log$[BCM] clearly demonstrates a first-order dependence on [BCM] with slope = (1.19 ± 0.05) (Fig. S14†) and $R = 0.997$.

Here, a provisional reaction sequence is formulated as follows:

$$2NO + O_2 \xrightarrow{k_1} 2NO_2 \tag{2}$$

$$NO_2 + NO \xrightarrow{k_2} N_2O_3 \tag{3}$$

$$N_2O_3 + H_2O \xrightarrow{k_3} 2H^+ + 2NO_2^- \tag{4}$$

$$N_2O_3 + L \xrightarrow{k_4} L-NO + NO_2^- + H^+ \tag{5}$$

$$L-NO + H^+ \xrightarrow{fast} L' + H_2O \tag{6}$$

The above reaction sequence clearly demonstrates that NO interacts firstly with its oxidized product NO_2 to form N_2O_3 that acts as a NO^+ donor in the next step under aerobic conditions. Then the formed N_2O_3 nitrosylates the amine hydrazide to generate L-NO which results in the synthesis of a closed ring 1,2,3,4-oxatriazole moiety in a fast step (Scheme 2). We have surveyed the literature to afford the rate constants of the above-mentioned reactions as: $k_1 = 6.33 \times 10^6$ M^{-2} s^{-1},[45] $k_2 = 1.1 \times 10^9$ $M^{-1}s^{-1}$,[46] and $k_3[H_2O] = 1.6 \times 10^3$ s^{-1}.[47] With the knowledge of these rate constants we can stipulate that NO_2 and N_2O_3 are present in very negligible amount as reactive intermediates. By applying a steady-state approximation eqn (7) can be attained for the formation of L′ (BCM-NO).

$$\frac{d[L']}{dt} = \frac{k_1 k_4 [L]}{2(k_3[H_2O] + k_4[L])} [NO]_t^2 [O_2]_t \tag{7}$$

From the previously illustrated kinetic studies, it was found that the reaction kinetics follows the second and first order dependence with respect to [NO] and [L] ([BCM]) respectively which lead us to make an assumption that $k_3[H_2O] \gg k_4[L]$. Now eqn (7) reduces to eqn (8).

$$\frac{d[L']}{dt} = \frac{k_1 k_4 [L]}{2k_3[H_2O]} [NO]_t^2 [O_2]_t \tag{8}$$

As the kinetics was performed maintaining the pseudo-first-order conditions, taking L (BCM) as a minor component (the dissolved $[O_2]_t = 2.5$ mM at 25 °C) eqn (8) reduces to eqn (9), where $k_{obs} = \{d[L']/dt\}/[L]$

$$k_{obs} = k'[NO]_t^2 \tag{9}$$

taking,

$$k' = \frac{k_1 k_4}{2k_3[H_2O]} [O_2]_t \tag{10}$$

The value of k_4 is evaluated by utilizing the previously observed values of k_1 and $k_3[H_2O]$ mentioned above along with $k' = 8.60 \times 10^6$ M^{-2} s^{-1}, achieved from the linear plot of k_{obs} vs.

$[NO]^2$ at 15 °C. From all of these data the value of k_4 was estimated to be 17.3×10^5 M^{-2} s^{-1} and found to be very much similar in order to some analogous reactions of N_2O_3 as follows: HSA (0.3×10^5 M^{-1} s^{-1}), N-acetyl cysteine (1.5×10^5 M^{-1} s^{-1}), GSH (2.9×10^5 M^{-1} s^{-1}), Cys (2.6×10^5 M^{-1} s^{-1}), and BSA (0.06×10^5 M^{-1} s^{-1}). Interestingly, this result is also in accord with our reported works.[34,48]

Limit of detection

We have also performed a study to evaluate the detection limit of NO by BCM which is revealed to be very low ~16 nM (Fig. S15†) making the probe very sensitive towards NO in macrophase cultures,[49] where nitric oxide is present in the micromolar to nanomolar range. So the concerned NO probe (BCM) is highly applicable for monitoring NO quantitatively in these cell types.

pH stability

To be an efficient fluorescent probe, it should show pH tolerance in the physiological range of pH so that it is easily applicable in bio-organisms. For this purpose we have assessed the pH effect on the photophysical behavior of BCM in the absence and presence of excess NO. Fig. 3 shows a very high fluorescence intensity of the probe and its NO treated product in a low pH range (2–3). Probably the PET based probe BCM, due to the presence of an electron donor group (–NH-NH$_2$) is converted to its protonated form which would block the PET process generating the fluorescence intensity at a lower pH range. In the pH range 4–8 the probe shows very weak fluorescence, however on treatment with NO it displays a drastic enhancement in fluorescence intensity due to the oxatriazole formation. Moreover, at alkaline pH (>8) the fluorescence intensity of the NO treated product is inhibited likely due to the rapid decomposition of N_2O_3 (eqn (4)), formed in the reaction of NO_2 and NO (eqn (3)) causing the availability of smaller and smaller amounts of reactive species (N_2O_3) towards the probe BCM (eqn (5)). Overall the pH study displays the well applicability of the probe at biological pH for tracing nitric oxide.

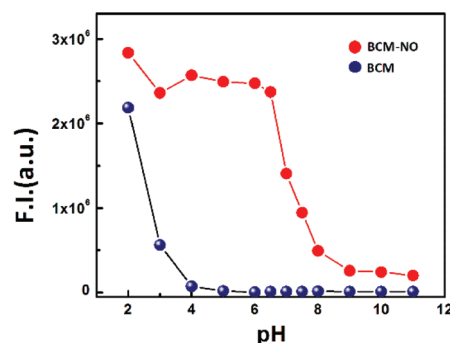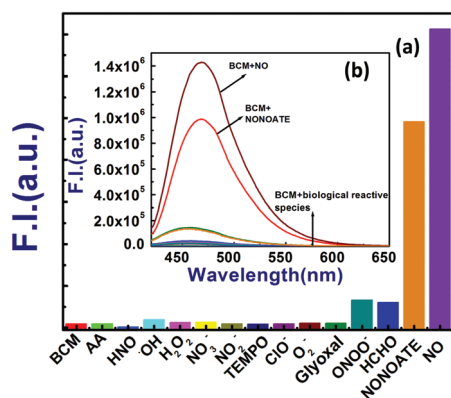**Fig. 3** pH dependent NO detection by BCM at 470 nm $\lambda_{ex} = 410$ nm at 25 °C in 10 mM HEPES buffer.

Fig. 4 (a) Bar plot presents the fluorescence responses of BCM at 470 nm (λ_{ex} = 410 nm) towards various biologically reactive species in HEPES buffer at pH 7.0, BCM = 20 μM, X^{n-} = 50 μM at 25 °C; (b) corresponding spectral responses.

Analyte selectivity experiment

The selectivity of a fluorescent probe towards a particular analyte is ensured by providing an appropriate binding site and some special chemical properties. Herein, the reactivity assay of probe BCM towards NO was conducted by using a broad array of putative interfering species like reactive species, important metal ions, and anions in 10 mM HEPES buffer, at 25 °C at pH 7.0. Fig. S16–S19† clearly show that BCM is silent in fluorescence response towards essential metal ions and anions. Likewise, the selectivity of BCM towards NO was ensured by reacting BCM with relevant biologically reactive species like H_2O_2, ClO^-, KO_2, $\cdot OH$, NO, NO_2^-, NO_3^-, TEMPO, glyoxal, $ONOO^-$, HNO, AA (ascorbic acid), and HCHO which revealed that none of these potential analytes triggered a fluorescence enhancement, except for NO (Fig. 4). To our delight, important cellular metabolites like AA, glyoxal, and HCHO interact hardly with the concerning probe. So, this high selectivity is very much advantageous for precise detection of NO in biological milieu.

Geometry optimization with an electronic structure

To get a theoretical overview on the interaction between BCM and NO we have conducted the DFT and TDDFT calculations of the probe (BCM) and its NO mediated product (BCM-NO). Fig. 5 presents the optimized geometry of both the compounds having the C1 point group. The structural compositions of these compounds have been established using mass spectroscopy which indicates the formation of oxatriazole from car-
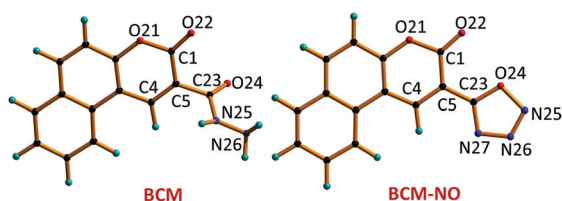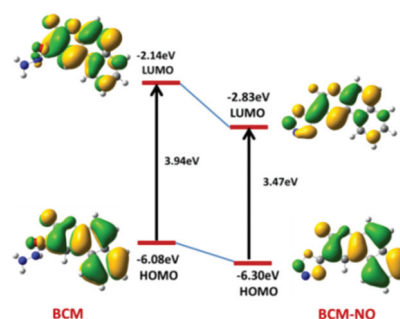

Fig. 6 Frontier molecular orbitals of probe BCM and BCM-NO.

bohydrazide in the presence of NO. All the important geometrical parameters of the probe BCM and BCM-NO are tabulated in Tables S1 and S2.† For the BCM-NO product the N–O bond distance is 1.43 Å, whereas the C–O bond distances lie in the range of 1.2–1.4 Å.

In the ground state the density of electron clouds mainly prevails on the HOMO and LUMO of the 3-oxo-3H-benzo[f]chromene-2-carbaldehyde and 3-oxo-3H-benzo[f]-chromene-2-carboxylic acid amide moiety respectively in the probe BCM. In the case of BCM-NO, the electron clouds mainly reside on the HOMO and LUMO of the benzo[f]chromen-3-one and 3-[1,2,3,4]oxatriazol-5-yl-chromen-2-one moiety respectively (Fig. S20†). These compositions are important to know the behaviour of the transition as well as the absorption spectra of both BCM and BCM-NO. The calculated HOMO–LUMO energy gap associated with BCM and BCM-NO is 3.94 eV and 3.47 eV respectively (Fig. 6). By exploiting the TDDFT method, the UV-Vis absorption spectra of BCM and BCM-NO were obtained at room temperature in aqueous medium (Fig. S21†). The absorption band of BCM at 374 nm in pure aqueous medium corresponds to the peak at 354 nm (Fig. S20†) obtained from the TDDFT calculation which is assigned to the $S_0 \rightarrow S_1$ electronic transitions with significant oscillator strength (Tables S3 and S4†), whereas for BCM-NO the theoretically evaluated absorption band at 407 nm is ascribed to the peak at 386 nm also associated with the $S_0 \rightarrow S_1$ electronic transitions (Fig. S20†). So, from this information it can be speculated that the experimental results have good agreement with the theoretical results.

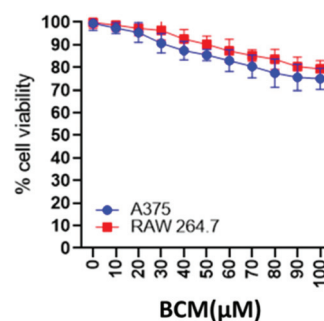
Fig. 5 Optimized geometry of BCM and BCM-NO.

Fig. 7 Graphical picture of the cell viability study of BCM.

8454 | *Org. Biomol. Chem.*, 2020, **18**, 8450–8458

This journal is © The Royal Society of Chemistry 2020

NO detection in live cells

Fluorescence imaging studies were executed to explore the detecting capability of BCM as a NO sensor in living cells. The probe's cytotoxicity has been assessed in A375 and Raw 264.7 cells (Fig. 7).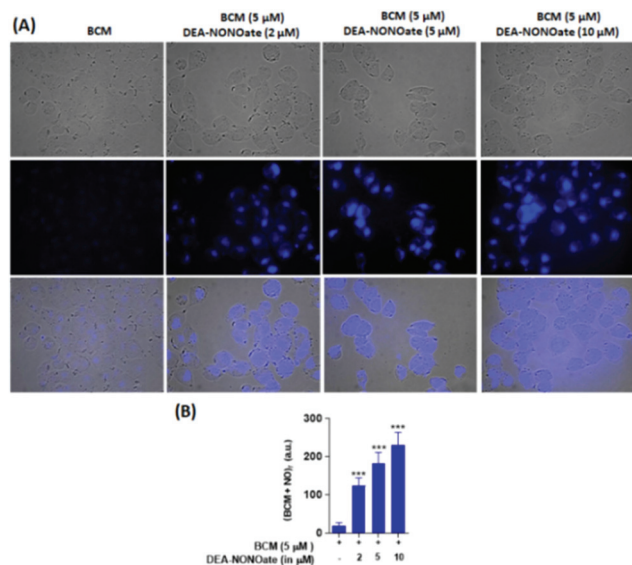 The cell lines showed the evidence of well admis-sibility of BCM (more than 80% of the cell is viable up to 60 μM of BCM), indicating its effectiveness as a NO sensor in live cells also. Exogenously stimulated NO sensing practicabil-ity of BCM was measured in A375 cells. The live cells were treated with the NO donor DEA-NONOate followed by incu-bation with the probe. BCM-NO showed intracellular fluo-rescence compared to the BCM probe only (Fig. 8). Likewise, endogenously stimulated NO sensing of the BCM probe has been estimated in Raw 264.7 cells where the cells were treated with LPS (1.0 mg mL^{-1}) and IFN-γ (1000 U mL^{-1}) for 6 h and then treated with probe BCM (Fig. 9). Very obviously, in the presence of the NO stimulator the cells exhibited high fluo-rescence compared to the non-stimulated and PTIO (NO sca-venger) treated ones.

Additionally, flow cytometric studies were performed in Raw 264.7 cells for the evaluation of NO, showing a positive shift in the fluorescence peak for LPS + IFN-γ stimulated cells in contrast to the non-stimulated cells and PTIO (200 mM) (Fig. 9C). So finally it can be concluded that BCM showed an excellent nontoxic fluorescence response towards NO for the purpose of cell imaging exogenously and endogenously.
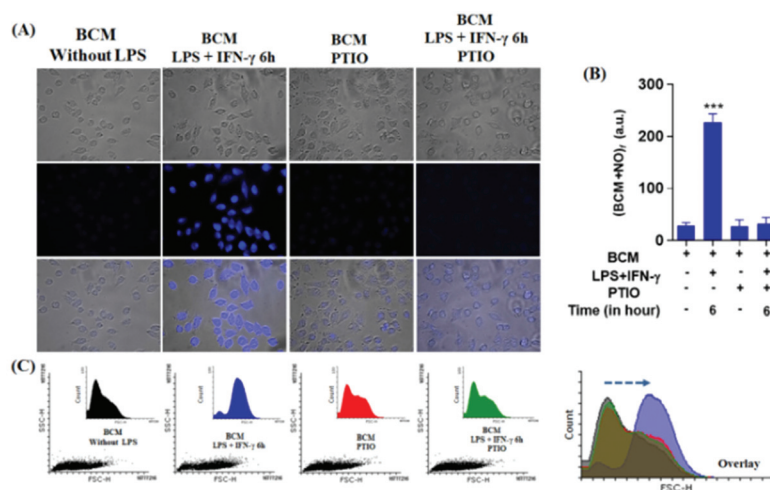

Fig. 8 (A) Images of A375 cells incubated with 5 μM BCM for 30 min and then incubated with DEA-NONOate (2, 5 and 10 μM) for 30 min. The blue fluorescence was observed owing to the reaction of NO with BCM. Images were captured at 63× objective. (B) Quantification of fluor-escence intensity in response to the intracellular NO interaction with BCM.

Experimental section

Materials

The reagents like 2-hydroxy-1-naphthaldehyde, diethyl-malo-nate, piperidine, glacial acetic acid, hydrazine hydrate are of reagent grade and purchased from Sigma Aldrich. The sodium salts of anions, the salts of metal ions (Pb^{2+}, Mn^{2+}, Co^{2+}, Ni^{2+},

Fig. 9 Endogenous recognition of NO with flow cytometry assay: (A) fluorescence images of Raw 264.7 macrophage cells incubated with BCM in the absence of LPS and stimulated with LPS + IFN-γ for 6 h followed by the addition of PTIO, a NO scavenger. The corresponding images were cap-tured at 63× objective. (B) The characteristic bar plots display the changes in the fluorescence intensity of BCM upon interaction with LPS + IFN-γ, PTIO and LPS + IFN-γ + PTIO, respectively. The experiments were performed thrice and related data are presented as mean ± SD. For statistical importance the estimated results were verified with the student's t test. P values ≤0.05 were statistically significant. (C) Flow cytometry experiment of NO with BCM by using Flowing Software version 2.5.1. The representative dot plot of forward (FSC-H) versus side (SSC-H) scatter and the corres-ponding histogram plot displaying a positive response for gated Raw 264.7 macrophage cells towards NO. The overlap histogram plot indicates a positive shift in the fluorescence intensity peak of LPS + IFN-γ stimulated NO taken by BCM compared to without LPS + IFN-γ and PTIO.

This journal is © The Royal Society of Chemistry 2020

Org. Biomol. Chem., 2020, 18, 8450–8458 | 8455

Zn^{2+}, Cu^{2+}, Al^{3+}, Hg^{2+}, Mg^{2+}, Fe^{3+}, La^{3+}, Cr^{3+} and Cd^{2+}) and biologically reactive species (H$_2$O$_2$, O^{2-}, TEMPO radical, NO$_3^-$, NO$_2^-$, ClO$^-$, AA, NO$^+$, DEA-NONOate (sodium salt) were obtained either from Sigma-Aldrich or from other commercial suppliers and used without further purification. Solvents like DMF, MeCN, *etc.*, (Merck, India) were of reagent grade and dried using standard methods.

Synthesis of ligand

The ligand 3-oxo-3*H*-benzo[*f*]chromene-2-carboxylic acid hydrazide (designated as BCM) was synthesized by two step easy procedures.

Step-1: synthesis of 3-oxo-3*H*-benzo[*f*]chromene-2-carboxylic acid ethyl ester (L^1). 2-Hydroxy-1-naphthaldehyde (10 mmol, 1.72 g) and di-ethyl malonate (20 mmol, 3.2 g) are mixed in a round bottom flask in 20 ml ethanol under heating and stirring conditions in the presence of 1 ml piperidine and 2 drops of glacial acetic acid. This reflux was continued for 6 h. After cooling at room temperature, the precipitate was filtered. After washing it with the mix solvent (hexane and ethyl acetate) a light yellow colour solid was obtained and characterized by ^{1}H NMR (Fig. S1†) and ^{13}C NMR (Fig. S2†).^{1}H NMR (in DMSO-d$_6$) (δ, ppm): 9.24 (d, 1H, −CH), 8.50–8.47 (m, 1H, −ArH), 8.26–8.23 (1H, m, −ArH), 8.02 (1H, d, −ArH), 7.75–7.72 (1H, m, −ArH), 7.63–7.60 (1H, m, −ArH), 7.53–7.50 (1H, m, −ArH), 4.34 (q, 2H, −CH$_2$), 1.37 (t, 3H, −CH$_3$). ^{13}C NMR (in DMSO-d$_6$) (δ, ppm): 162.8, 155.9, 155.0, 143.7, 135.9, 129.6, 128.9, 126.3, 122.0, 116.4, 111.7, 61.2, 14.0.

Step-2: synthesis of 3-oxo-3*H*-benzo[*f*]chromene-2-carboxylic acid hydrazide (BCM). The compound obtained from step-1 was dissolved in 20 ml of ethanol (5 mmol, 1.34 g) and hydrazine hydrate was added in an equimolar ratio (5 mmol) under refluxing conditions for 6 h. A yellow solid was formed during the reaction. The product BCM was collected and analyzed by ^{1}H NMR (Fig. S3†), ^{13}C NMR (Fig. S4†) and mass spectroscopy (Fig. S5†). ESI-MS$^+$ (*m/z*): 277 (BCM + Na$^+$), ^{1}H NMR (in DMSO-d$_6$) (δ, ppm): 9.68 (1H, S, −CH), 9.39 (1H, S, −NH), 8.58 (1H, d, −ArH), 8.31 (1H, d, −ArH), 8.09 (1H, d, −ArH), 7.79 (1H, t, −ArH), 7.69–7.63 (2H, m, −ArH), 4.79 (2H, m, −NH$_2$). ^{13}C NMR (in DMSO-d$_6$) (δ, ppm): 160.2, 159.7, 154.0, 141.7, 135.4, 129.9, 128.9, 128.8, 126.5, 122.2, 117.5, 116.3, 112.6.

Physical instrumentation and experimental methods

The descriptions of instruments used in the experiment, the preparation of solution, and the experimental methods to carry out this work are supplied in the ESI.†

Conclusion

In brief, we are reporting herewith a smart fluoregenic probe BCM on the benzocoumarin platform which selectively recognises NO under physiological conditions. From the linear F.I. *vs.* [NO] plot obtained from the fluorescence titration experiment yields K_f = (4.33 ± 0.48) × 10^4 M^{-1}. Here, the acid-hydra-zide moiety of probe BCM reacts with NO/O$_2$ to form the electron deficient 1,2,3,4-oxatrizole moiety which is solely responsible for fluorescence enhancement through the PET blocking mechanism. The outstanding sensing performance of BCM towards NO is also illustrated by its very low detection limit (16 nM), and specific response to NO with desirable selectivity and sensitivity in the presence of other biologically reactive species which makes the probe highly potent for NO detection in the biological environment. The reaction mechanism of BCM and NO was confirmed by kinetic studies which reveals the 1st order dependence on BCM and the 2nd order dependence on NO. The pH variation study for NO detection also supports BCM as an efficient NO sensor in a wide range of pH. Beside these, the bio-imaging implication of this probe is also appreciable owing to its least cytotoxicity and biocompatibility for *in vitro* NO detection. The application of BCM can also be extended to flow cytometric analysis of exogeneous and endogeneous NO in living cells. So, all the above-mentioned experiments and information confirm BCM as a very appropriate probe for the tracking of NO.

Conflicts of interest

There are no conflict of interest to declare.

Acknowledgements

References

1 (*a*) P. F. Bove and A. D. V. Vliet, *Free Radical Biol. Med.*, 2006, **41**, 515–527; (*b*) A. H. Ashoka, F. Ali, R. Tiwari, R. Kumari, S. K. Pramanik and A. Das, *ACS Omega*, 2020, **5**, 1730–1742.

2 D. J. Stuehr, J. Santolini, Z. Q. Wang, C. C. Wei and S. Adak, *J. Biol. Chem.*, 2004, **279**, 36167–36170.

3 (*a*) P. Pacher, J. S. Beckman and L. Liaudet, *Physiol. Rev.*, 2007, **87**, 315–424; (*b*) Y. Liu, H. Fan, Y. Wen, T. Jia, Q. Su and F. Lia, *Dyes Pigm.*, 2019, **166**, 211–216.

4 A. De Mel, F. Murad and A. M. Seifalian, *Chem. Rev.*, 2011, **111**, 5742–5767.

5 Y. Iwakiri and M. Y. Kim, *Trends Pharmacol. Sci.*, 2015, **36**, 524–536.

6 S. P. Hussain, L. J. Hofseth and C. C. Harris, *Nat. Rev. Cancer*, 2003, **3**, 276–285.

7 B. V. Khan, D. G. Harrison, M. T. Olbrych, R. W. Alexander and R. M. Medford, *Proc. Natl. Acad. Sci. U. S. A.*, 1996, **93**, 9114–9119.

8 K. Pantopoulos and M. W. Hentze, *Proc. Natl. Acad. Sci. U. S. A.*, 1995, **92**, 1267–1271.

8456 | *Org. Biomol. Chem.*, 2020, **18**, 8450–8458

This journal is © The Royal Society of Chemistry 2020

9 (a) B. J. Privett, J. H. Shin and M. H. Schoenfisch, *Chem. Soc. Rev.*, 2010, **39**, 1925–1935; (b) S. Biswas, Y. Rajesh, S. Barman, M. Bera, A. Paul, M. Mandal and N. D. P. Singh, *Chem. Commun.*, 2018, **54**, 7940–7943.

10 S. R-Nuévalos, M. Parra, S. Ceballos, S. Gil and A. M. Costero, *J. Photochem. Photobiol., A*, 2020, **388**, 112132.

11 (a) E. Sasaki, H. Kojima, H. Nishimatsu, Y. Urano, K. Kikuchi, Y. Hirata and T. Nagano, *J. Am. Chem. Soc.*, 2005, **127**, 3684–3685; (b) Z. Yu, J. Zhou, X. Dong, W. Zhao and Z. Chen, *Anal. Chim. Acta*, 2019, **1067**, 88–97.

12 Y. Yang, S. K. Seidlits, M. M. Adams, V. M. Lynch, C. E. Schmidt, E. V. Anslyn and J. B. Shear, *J. Am. Chem. Soc.*, 2010, **132**, 13114–14116.

13 L. E. McQuade and S. J. Lippard, *Inorg. Chem.*, 2010, **49**, 7464–7471.

14 M. H. Lim and S. J. Lippard, *Inorg. Chem.*, 2004, **43**, 6366–6370.

15 L. Y. Niu, Y. Z. Chen, H. R. Zheng, L. Z. Wu, C. H. Tung and Q. Z. Yang, *Chem. Soc. Rev.*, 2015, **44**, 6143–6160.

16 M. Gao, F. Yu, C. Lv, J. Choo and L. Chen, *Chem. Soc. Rev.*, 2017, **46**, 2237–2271.

17 N. Zhang, Y. Si, Z. Sun, L. Chen, R. Li, Y. Qiao and H. Wang, *Anal. Chem.*, 2014, **86**, 11714–11721.

18 F. Yu, P. Li, G. Zhao, T. Chu and K. Han, *J. Am. Chem. Soc.*, 2011, **133**, 11030–11033.

19 G. Chen, Q. Fu, F. Yu, R. Ren, Y. Liu, Z. Cao, G. Li, X. Zhao, L. Chen, H. Wang and J. You, *Anal. Chem.*, 2017, **89**, 8509–8516.

20 (a) W. Hu, D. Boateng, J. Kong and X. Zhang, *Austin J. Biosens. Bioelectron.*, 2015, **1**, 1–9; (b) T. Zhou, J. Wang, J. Xu, C. Zheng, Y. Niu, C. Wang, F. Xu, L. Yuan, X. Zhoa, L. Liang and P. Xu, *Anal. Chem.*, 2020, **92**, 5064–5072.

21 (a) C. J. Reinhardt, E. Y. Zhou, M. D. Jorgensen, G. Partipilo and J. Chan, *J. Am. Chem. Soc.*, 2018, **140**, 1011–1018; (b) Y. Huo, J. Miao, J. Fang, H. Shi, J. Wang and W. Guo, *Chem. Sci.*, 2019, **10**, 145–152.

22 (a) C. Xu, C. Xin, C. Yu, M. Wu, J. Xu, W. Qin, Y. Ding, X. Wang, L. Li and W. Huang, *Chem. Commun.*, 2018, **54**, 13491–13494; (b) X. Lv, Y. Wang, S. Zhang, Y. Liu, J. Zhang and W. Guo, *Chem. Commun.*, 2014, **50**, 7499–7502.

23 M. H. Lim and S. J. Lippard, *J. Am. Chem. Soc.*, 2005, **127**, 12170–12171.

24 D. A. Jose, N. Sharma, R. Sakla, R. Kaushik and S. Gadiyaram, *Methods*, 2019, **168**, 62–75.

25 A. S. M. Islam, M. Sasmal, D. Maiti, A. Dutta, S. Ganguly, A. Katarkar, S. Gangopadhyay and M. Ali, *ACS Appl. Bio Mater.*, 2019, **2**, 1944–1955.

26 D. Maiti, A. S. M. Islam, M. Sasmal, C. Prodhan and M. Ali, *Photochem. Photobiol. Sci.*, 2018, **17**, 1213–1221.

27 (a) A. Dutta, A. S. M. Islam, D. Maiti, M. Sasmal, C. Prodhan and M. Ali, *Org. Biomol. Chem.*, 2019, **17**, 2492–2501; (b) P. Srivastava, M. Verma, S. Sivakumar and A. K. Patra, *Sens. Actuators, B*, 2019, **291**, 478–484.

28 X. Zhang, B. Wang, Y. Xiao, C. Wang and L. He, *Analyst*, 2018, **143**, 4180–4188.

29 X.-X. Chen, L.-Y. Niu, N. Shao and Q.-Z. Yang, *Anal. Chem.*, 2019, **91**, 4301–4306.

30 A. Beltrán, M. I. Burguete, D. R. Abánades, S. D. Pérez-Sala, V. Luis and F. Galindo, *Chem. Commun.*, 2014, **50**, 3579–3581.

31 Q. Wang, X. Jiao, C. Liu, S. He, L. Zhaoab and X. Zeng, *J. Mater. Chem. B*, 2018, **6**, 4096–4103.

32 S.-J. Li, D.-Y. Zhou, Y. Li, H.-W. Liu, P. Wu, J. Ou-Yang, W.-L. Jiang and C.-Y. Li, *ACS Sens.*, 2018, **3**, 2311–2319.

33 (a) C. Sun, W. Shi, Y. Song, W. Chen and H. Ma, *Chem. Commun.*, 2011, **47**, 8638–8640; (b) A. V. Latha, M. Ayyappan, A. R. Kallar, R. V. Kakkadavath, S. P. Victor and S. Selvam, *Mater. Sci. Eng., C*, 2020, **108**, 110463.

34 (a) A. S. M. Islam, R. Bhowmick, B. C. Garain, A. Katarkar and M. Ali, *J. Org. Chem.*, 2018, **83**, 13287–13295; (b) C. M. Wu, Y. H. Chen, K. Dayananda, T. W. Shiue, C. H. Hung, W. F. Liaw, P. Y. Chen and Y. M. Wang, *Anal. Chim. Acta*, 2011, **708**, 141–148; (c) M. E. Azab, H. M. F. Madkour and M. A. E. Ibraheem, *Phosphorus, Sulfur Silicon Relat. Elem.*, 2006, **181**, 1299–1313; (d) M. K. Ibrahim, K. El-Adl, M. F. Zayed and H. A. Mahdy, *Med. Chem. Res.*, 2015, **24**, 99–114.

35 (a) H. Ammar, S. Fery-Forgues and R. El. Gharbi, *Dyes Pigm.*, 2003, **57**, 259; (b) S. Sastry, *Biophys. Chem.*, 2001, **91**, 191; (c) M. Chiyomi, M. Toshinobu, K. Yasuko, T. Kenichiro, Y. Hideyuki, N. Hitoshi, Y. Masatoshi and T. Akira, *Chem. Pharm. Bull.*, 2005, **53**, 750.

36 (a) M. A. Saleh, A. Kamel, A. El-Demerdash and J. Jones, *Chemosphere*, 1998, **36**, 1543–1552; (b) H. Yu, H. Mizufune, K. Uenaka, T. Moritoki and H. Koshima, *Tetrahedron Lett.*, 2005, **61**, 8932–8938; (c) S. Xiao, T. Yi, F. Li and C. Huang, *Tetrahedron Lett.*, 2005, **46**, 9009–9012.

37 M. Walshe, J. Howarth, M. T. Kelly, R. O'Kennedy and M. R. Smyth, *J. Pharm. Biomed. Anal.*, 1997, **16**, 319–325.

38 (a) B. Kovac and I. Novak, *Spectrochim. Acta, Part A*, 2002, **58**, 1483; (b) B. A. Elsayeda, I. A. Ibrahema, M. S. Attia, S. M. Shaabana and M. M. Elsenety, *Sens. Actuators, B*, 2016, **232**, 642–652.

39 (a) R. Zhang, H. Zheng and J. Shen, *Synth. Met.*, 1999, **106**, 157–160; (b) N. Mishra, V. Patil, A. Asrondkar, A. S. Bobade and A. S. Chowdhary, *World J. Pharm. Res.*, 2015, **4**, 627–636.

40 (a) J. Preat, D. Jacquemin and E. A. Perpète, *Chem. Phys. Lett.*, 2005, **415**, 20–24; (b) Rajesha, H. S. B. Naik, H. N. H. Kumar, K. M. Hosamani and K. M. Mahadevan, *ARKIVOC*, 2009, **2**, 11–19; (c) R. M. Zaki, Y. A. Elossaily and A. M. Kamal El-Dean, *Russ. J. Bioorg. Chem.*, 2012, **38**, 639–646.

41 A. S. M. Islam, R. Alam, A. Katarkar, K. Chaudhuri and M. Ali, *Analyst*, 2015, **140**, 2979–2983.

42 H. Kojima, N. Nakatsubo, K. Kikuchi, S. Kawahara, Y. Kirino, H. Nagoshi, Y. Hirata and T. Nagano, *Anal. Chem.*, 1998, **70**, 2446–2453.

This journal is © The Royal Society of Chemistry 2020

Org. Biomol. Chem., 2020, **18**, 8450–8458 | **8457**

43 H. Kojima, M. Hirotani, N. Nakatsubo, K. Kikuchi, Y. Urano, T. Higuchi, Y. Hirata and T. Nagano, *Anal. Chem.*, 2001, **73**, 1967–1973.

44 E. Sasaki, H. Kojima, H. Nishimatsu, Y. Urano, K. Kikuchi, Y. Hirata and T. Nagano, *J. Am. Chem. Soc.*, 2005, **127**, 3684–3685.

45 V. G. Kharitonov, A. R. Sundquist and V. S. Sharma, *J. Biol. Chem.*, 1994, **269**, 5881–5883.

46 M. Grätzel, S. Taniguchi and A. Henglein, *Ber. Bunsen-Ges. Phys. Chem.*, 1970, **74**, 488–492.

47 W. R. Licht, S. R. Tannenbaum and W. M. Deen, *Carcinogenesis*, 1988, **9**, 365–372.

48 A. S. M. Islam, R. Bhowmick, K. Pal, A. Katarkar, K. Chaudhuri and M. Ali, *Inorg. Chem.*, 2017, **56**, 4324–4331.

49 T. Chen, R. Zamora, B. Zuckerbraun and T. R. Billiar, *Curr. Mol. Med.*, 2003, **3**, 519–526.

Dansyl-appended Cu[II]-complex-based nitroxyl (HNO) sensing with living cell imaging application and DFT studies†

Debjani Maiti,[a] Abu Saleh Musha Islam, [ID][a] Ananya Dutta,[a] Mihir Sasmal,[a] Chandraday Prodhan[b] and Mahammad Ali [ID] *[a,c]

We introduce herein, a novel copper complex-based fluorescent probe **[Cu[II](DQ$_{468}$)Cl]$^+$** that exhibits a significant fluorescence turn-on response towards nitroxyl (HNO) with high selectivity over other biological reactive oxygen, nitrogen and sulfur species, including nitric oxide (NO). A smart strategy, involving HNO-induced reduction of paramagnetic **[Cu[II](DQ$_{468}$)Cl]$^+$** to diamagnetic **[Cu[I](DQ$_{468}$)]$^+$** with concomitant fluorescence enhancement *via* a PET mechanism is focused here. This reduction-based strategy was also supported by X-band EPR response and mass spectroscopy. The metal free probe (**DQ$_{468}$**) showed high affinity towards Cu^{2+} to form **[Cu[II](DQ$_{468}$)Cl]$^+$** with a 0.091 μM detection limit, which subsequently enabled the detection of HNO in an organo-aqueous medium at biological pH (7.4) in the green wavelength region (λ_{em} = 543 nm) with a LOD of 0.41 μM. The ground-state geometries of **DQ$_{468}$**, **[Cu[II](DQ$_{468}$) Cl]$^+$** and **[Cu[I](DQ$_{468}$)]$^+$** were optimized by DFT calculations, which revealed that the central metal ion in **[Cu[II](DQ$_{468}$)Cl]$^+$** is in a distorted tetrahedral geometry with the *C*1 point group. Additionally, the negligible cytotoxicity and good biocompatibility make the developed probe useful for the *in vitro* detection of HNO.

Introduction

Over the past few decades, the development of a fluorescent probe for the detection of metal ions[1] has attracted a great deal of attention from chemists and biologists due to the key role these ions play in chemistry and biology and due to their effects on the environment.[2] For instance, cupric ion (Cu^{2+}) is an environmental pollutant at high concentration[3] and one of the most abundant essential trace metal ions[4] in the human body, with the highest concentration found in the liver. The dysregulation of copper homeostasis causes various diseases, like Menkes,[5] amyotrophic lateral sclerosis[6] and Alzheimer's disease.[7] The EPA (U.S. Environmental Protection Agency) has set the maximum level of copper in drinking water at 1.3 ppm (~20 μM). So, the sensitive detection of copper levels in biological systems and in the environment is highly necessary.

Very recently, copper-bound fluorescent probes have been developed for the detection of some biological reactive nitrogen species, like nitric oxide (NO) and nitroxyl (HNO).[8–12] Nitric oxide(NO) is a very reactive gaseous free-radical, responsible for both the physiological and pathological activities of various biological organisms[13–19] and being present in the nervous,[20] immune[21] and cardiovascular[22] systems. Another species of concern is the nitroxyl (HNO) biomolecule, which is the protonated and one-electron reduced analogue of NO. Though HNO and NO are very closely related species, they have distinct chemical and biochemical properties.[23] So, the development of chemical tools that can distinguish HNO over NO is very necessary. From recent advances in the medical activities of HNO, it has also been reported that HNO confers vasoprotective effects,[24] enhances heart muscle contractility[25] and inhibits platelet aggregation.[26] Significantly, HNO regulates cardiovascular functions and also acts as an important tool for the treatment of heart failure.[25,27] In spite of the aforementioned progress made around HNO, still the roles of it in biology are largely unknown. So, some probe that could monitor HNO sensitively and selectively over other interfering reactive species is highly desired for the further analysis of HNO. Frequently, some difficulties are encountered in the sensing of HNO, such as:[28–30] (i) the detection of HNO may be interfered with by some biologically reducing agents; (ii) the

[a]Department of Chemistry Jadavpur University, Kolkata 700 032, India. E-mail: m_ali2062@yahoo.com, mali@chemistry.jdvu.ac.in; Fax: +91-33-2414-6223
[b]Molecular & Human Genetics Division, CSIR-Indian Institute of Chemical Biology, 4 Raja S.C. Mallick Road, Kolkata-700032, India
[c]Vice-Chancellor, Aliah University, ll-A/27, Action Area II, Newtown, Kolkata, West Bengal 700160, India. E-mail: vc_au@aliah.ac.in
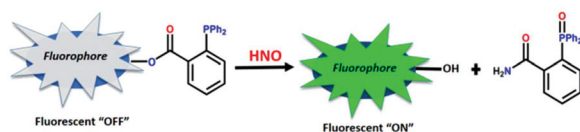†Electronic supplementary information (ESI) available. See DOI: 10.1039/ c8dt04564j

very low concentration of HNO in biological systems may not be sufficient to produce a visible response towards a probe; and (iii) the pH-dependent response of HNO towards a probe.
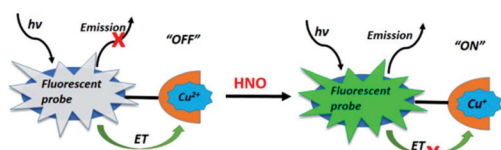
There are many varieties of techniques for HNO detection, *i.e.* chromatography, electrochemical analysis,[31] high performance liquid chromatography (HPLC),[32] chemiluminescence,[33] *etc*. Although these methods are sensitive, they are associated with sophisticated instrumentation, complicated sample preparation and can cause the destruction of tissues or cells. So, they are not suitable for living cell applications. Very recently, the technique associated with fluorescence spectroscopy is considered the gold standard due to its direct and precise measurement and also due to its sensitivity and well-defined spatiotemporal resolution.[34] Using the fluorescence method, an HNO-detecting probe should have some properties, *e.g.* high affinity for HNO without any interference from other biological reactive species, work downstream the NO oxidation products, water solubility and membrane permeability.

To date, a number of fluorescent sensors that can track HNO in live cells have been developed. One of the common types is Staudinger ligation-based HNO sensing (Scheme 1(i)). Here, a chemo-specific reaction occurs with a triphenyl phosphine moiety to form an aza-ylide intermediate, which in turn reacts with an adjacent ester moiety, leading to the removal of alcohol and an enhancement of the fluorescence intensity.[35–39] Another common design of HNO probe involves the HNO-induced reduction of Cu(II) to Cu(I) (Scheme 1(ii)).[40–42] Here, the fluorescence of the photo-emissive ligand is quenched due to binding with the paramagnetic cupric ion, and the regeneration of fluorescence intensity occurs upon HNO treatment due to the conversion of Cu(II) to diamagnetic Cu(I). The unpaired electron in the d orbital of the Cu(II) centre can reliably achieve this quenching by either electron or energy transfer (Scheme 1). Exploiting this strategy, Lippard and Rosenthal pioneered the building of a BODIPY-based nitroxyl
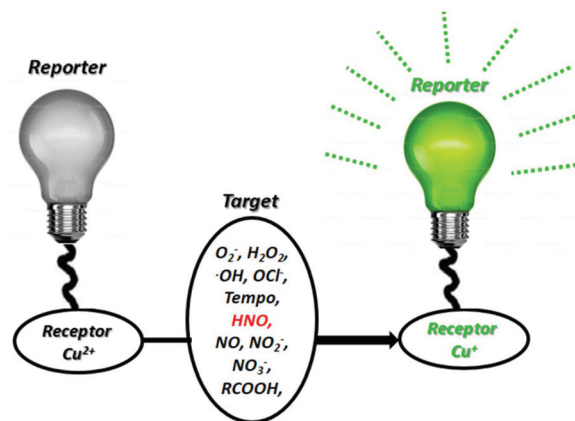

Scheme 2 Schematic representation of the copper-complex-based sensor for the detection of HNO. Here, the copper complex shows a weak fluorescence (light bulb off); and the only target HNO reduces the PET effect and enhances the fluorescence intensity (light bulb on).

sensor.[40] Yao *et al.* also reported a similar type of Cu^{2+}-chelating system using coumarin fluorophore.[42] Besides, a number of related Cu-complex-based nitroxyl probes have been developed so far using this redox-based strategy, but most of them are prone to being sensitive towards other biological reductive species, like cysteine(CYS), homocysteine(HCY), glutathione (GSH), ascorbate, H_2S, *etc.*, along with HNO present in the living matrices.[29,30]

To overcome the lack of selectivity of the so-called Cu^{II}-complex-based HNO probe, we synthesized [Cu^{II}-DQ_{468}] as an HNO probe upon a dansyl-quinoline platform, which is highly sensitive and selective towards HNO but remains almost indifferent towards other biologically abundant reducing agents. DQ_{468} shows typical dansyl green emission, which is better for living samples. Moreover, Cu^{II}-DQ_{468} detects HNO effectively in the biological pH range and it is water friendly, low cytotoxicity and cell permeable, thus offering better detection of HNO in living cells. Dansyl is a classical fluorophore, and is used widely for its solvatochromism and high emission quantum yields.[43–45] Additionally, we employed 8-amino-quinoline as an excellent receptor for coordination to Cu(II) ions[41,46] and methyl pyridine as an auxiliary group for strong coordination with Cu(II). This new probe displayed excellent sensitivity and selectivity towards HNO over other biologically reactive species (Scheme 2) and it was successfully applied to intracellular HNO detection. The coordination mode of the metal-free probe towards Cu^{2+} was established by ground-state DFT calculations on both the ligand and copper complexes.

Experimental section

Physical measurements

To record the IR spectra, an IR 750 series-II FTIR (Nickolet Magna) spectrophotometer was used in the range 400–4000 cm^{-1} on KBr pellets. An Agilent 8453 Diode-array UV-Vis spectrophotometer was used for recording the elec-

Scheme 1 General mechanism of sensing HNO using: (i) Staudinger ligation-based mechanism involving the release of a fluorophore; (ii) HNO-induced reduction of Cu^{II} complex. The electron transfer (ET) from the fluorophore (photoexcited state) to the metal centre (paramagnetic Cu^{2+}) makes the probe nonfluorescent (OFF state). The selective reduction of Cu(II) to Cu(I) by HNO stops the ET, thereby restoring the emission of the fluorophore (ON state).

tronic spectra using 8 : 2 MeCN and HEPES buffer (10 mM) as the solvent in a 1 cm quartz cuvette in the range 200–900 nm. Fluorescence studies were carried out in a PTI (model QM-40) spectrofluorometer. ESI-MS$^+$ (m/z) spectra were recorded using a high-resolution mass spectrometer (Model: QTOF Micro YA263). ^{1}H NMR spectra were recorded in DMSO-d_6 with a Bruker 300 MHz instrument using trimethylsilane ($\delta = 0$) as an internal standard. The X-band EPR spectral studies were performed on an EPR-Spectrometer (Model: JEOL, JES-FA 200). The interaction of the copper complex towards HNO at different pH values was investigated. The pH of these solutions were recorded on a digital pH meter (Model: Systronics 335, India) in the pH range 2–11, which was previously calibrated using buffers of pH 4, 7 and 10. For the cell imaging study, a fluorescence microscope (Leica DM3000, Germany) was used.

Materials and methods

8-Aminoquinoline, 2-chloromethyl pyridine hydrochloride, dansyl chloride and potassium carbonate were used to prepare the ligand. These reagents were purchased from Sigma-Aldrich. Biological reactive species (H_2O_2, O^{2-}, TEMPO radical, NO_3^-, NO_2^-, ClO^-, AA), metal ions (Co^{2+}, Mn^{2+}, Na^+, Ni^{2+}, Zn^{2+}, Cu^{2+}, Al^{3+}, Hg^{2+}, Pb^{2+}, Sm^{3+}, Mg^{2+}, K^+, Fe^{3+}, Cr^{3+} and Cd^{2+}) and all the tested amino acids were obtained either from Sigma-Aldrich or from other commercial suppliers and used without further purification. Solvents like MeOH, MeCN, THF, *etc.*, (Merck, India) were of reagent grade and dried before use.

Synthesis of the ligand

The ligand 5-dimethylamino-naphthalene-1-sulfonic acid pyridin-2-ylmethyl-quinolin-8-yl-amide (designated as **DQ$_{468}$**) was synthesized by a facile two-step procedure.

Step 1: Synthesis of pyridin-2-ylmethyl-quinolin-8-yl-amine, L^1

Excess potassium carbonate (30 mmol) was added to the solution of 8-aminoquinoline (1 g, 6.93 mmol) in 20 ml dry acetonitrile with stirring for 1 h at room temperature. Then, a solution of 2-chloromethyl pyridine hydrochloride (1.13 g, 6.93 mmol) in acetonitrile was added to the reaction mixture drop-wise under refluxing conditions at 120 °C. The reaction was continued for 8 h. After completion, the solvent was evaporated and the residual part was purified through column chromatography using ethyl-acetate and hexane (v/v = 3 : 7) as the eluent to obtain a pure yellow oily product, which was characterized and analyzed by ^{1}H NMR (Fig. S1†), ^{13}CNMR (Fig. S2†) and HRMS (Fig. S3†). ESI-MS$^+$ (m/z): 236.1119 (**L^1** + **H$^+$**), ^{1}H NMR (in DMSO-d_6) (δ, ppm): 8.76 (s, 1H, –NH), 8.57 (d, 1H, –ArH), 8.20 (1H, t, –ArH), 7.71 (1H, d, –ArH), 7.49 (1H, m, –ArH), 7.39 (2H, d, –ArH), 7.26 (2H, m, –ArH), 7.04 (d, 1H, –ArH), 6.56 (d, 1H, –ArH), 4.58 (d, 2H, –CH$_2$).

Step 2: Synthesis of 5-dimethylamino-naphthalene-1-sulfonic acid pyridin-2-ylmethyl-quinolin-8-yl-amide, DQ$_{468}$

The compound obtained from step 1 (3 mmol) was further treated with excess potassium carbonate (15 mmol) in dry acetonitrile for 1 h under stirring. Dansyl chloride (3 mmol) was added to it in a cold condition under a nitrogen atmosphere. The reaction was allowed to continue overnight at room temperature. Then, the solvent was evaporated and purified by column chromatography using ethyl-acetate and hexane (v/v = 3 : 7) as the eluent to obtain a pure solid product (**DQ$_{468}$**), which was characterized and analyzed by ^{1}H NMR (Fig. S4†), ^{13}C NMR (Fig. S5†), HRMS (Fig. S6†) and FTIR (Fig. S7†). ESI-MS$^+$ (m/z): 469.2234 (**DQ$_{468}$** + **H$^+$**), ^{1}H NMR (in DMSO-d_6) (δ, ppm): 8.38 (d, 1H, –ArH), 8.31 (s, 1H, –ArH), 8.18–8.21 (3H, t, –ArH), 7.90 (1H, d, –ArH), 7.76 (3H, t, –ArH), 7.53 (3H, m, –ArH), 7.26 (1H, t, –ArH), 7.17 (1H, d, –ArH), 7.02 (d, 2H, –ArH), 5.28 (s, 2H, –CH$_2$), 2.77 (d, 6H, –CH$_3$).

Solution preparation for the UV-Vis absorption and fluorescence studies

A 10 mL 1.0×10^{-3} M stock solution of the ligand **DQ$_{468}$** was prepared in acetonitrile for the spectral studies. A stock solution of 1.0×10^{-2} M CuCl$_2$·2H$_2$O and Angeli's salt[9] in water were prepared in deoxygenated, deionized water separately under a N$_2$ atmosphere. A nitric oxide solution was prepared by purging nitric oxide gas for 15 min in a sealed vial with a syringe in deoxygenated water to give a resultant concentration of 1.74×10^{-3} M.[47,48] ONOO$^-$ and ·OH solutions were prepared using a reported methods.[49] A 100 mL, 10.0 mM (4-(2-hydroxyethyl)-1-piperazineethanesulfonic acid) (HEPES) buffer solution was prepared with adjusting its pH to 7.0 using HCl and NaOH and the ionic strength of this solution was maintained at 0.10 M (NaCl) throughout the measurements. In this work, 20 μM **DQ$_{468}$** solution was taken in a cuvette containing 2.5 ml solution of MeCN–HEPES buffer (v/v = 8 : 2 ratio) and titrations were carried out with Cu^{2+} solution for maximum fluorescence quenching and with the subsequent incremental addition of HNO in regular time intervals for fluorescence regeneration at $\lambda_{ex} = 390$ nm and with 5 nm × 3 nm slits.

Calculation of the LOD

To determine the analytical limit of detection (LOD) of the ligand **DQ$_{468}$** and [Cu^{II}(DQ$_{468}$)Cl]$^+$, we have followed the 3σ method.

$$\text{LOD} = 3 \times S_d/S$$

where, S_d is the standard deviation taken from the intercept of the plot of F.I. *vs.* [**DQ$_{468}$**] and [**Cu^{II}(DQ$_{468}$)Cl**]$^+$ and S is the slope obtained from the linear part of the titration plot of FI *vs.* [Cu^{2+}], [HNO].

Calculation of the quantum yield

For the determination of fluorescence quantum yields (Φ), we used the following equation

$$\Phi_{sample} = (\text{OD}_{std} \times A_{sample})/(\text{OD}_{sample} \times A_{std}) \times \Phi_{std}$$

where, A_{sample} and A_{std} represent the areas under the fluorescence spectral curves of the sample and standard, respectively. The optical densities of the sample and standard are designated as OD$_{sample}$ and OD$_{std}$, respectively, at the exci-

tation wavelength. Here, quinine sulfate was taken as the standard (Φ_{std} = 0.54) for the quantum yield calculation of the ligand DQ_{468} and $[Cu(DQ_{468})Cl]^+$.

Job's plot

We determined the composition of the complex by the help of Job's method. In this method, we performed fluorescence intensity measurements of a series of solutions with the sum of DQ_{468} and $CuCl_2$ constant in a fixed volume, but changing the individual molar concentration and then plotted the results against the mole fraction of Cu^{2+}. A breaking point was found at 0.5 mole fraction value, corresponding to the (1:1) complex formation of DQ_{468} with respect to Cu^{2+}.

Cell culture

Human hepatocellular liver carcinoma (HepG2) cell line (NCCS, Pune, India) was grown in DMEM supplemented with 10% FBS and antibiotics (penicillin, 100 μg ml^{-1}; streptomycin, 50 μg ml^{-1}). Cells were cultured at 37 °C in a 95% air, 5% CO_2 incubator.

Cell cytotoxicity assay

The cytotoxicity for ligand DQ_{468} was assessed by the 3-(4,5-dimethylthiazol-2-yl)-2,5-diphenyltetrazolium bromide (MTT) cell viability assay. HepG2 cells (1×10^5 cells per well) were cultured in a 96-well plate incubated at 37 °C, and were exposed to varying concentrations of DQ_{468} (5, 10, 20, 30, 40, 50, 60, 70, 80, 90 and 100 μM) for 24 h. After the incubation, 10 μL of MTT solution [5 mg ml^{-1}, dissolved in 1× phosphate-buffered saline (PBS)] was added to each well of the 96-well culture plate, and then incubated at 37 °C for 4 h. The media were decanted from the wells and 100 μL of 0.04 N acidic isopropyl alcohol was added into each well to solubilize the intracellular formazan crystals (blue-violet) formed. Absorbance of the solutions was measured at 595 nm (EMax Precision MicroPlate Reader, Molecular Devices, USA). Values were calculated as the mean ± standard errors of three independent experiments. The cell viability was expressed as the optical density ratio of the treatment to control.

Cell imaging study

HepG2 cells were cultured in a 35 × 10 mm culture dish on a cover-slip for 24 h at 37 °C. The cells were treated with 5 μM and 10 μM solutions of DQ_{468}, prepared by dissolving it in a mixed solvent of DMSO : water = 1 : 9 (v/v) and incubated for 1 h at 37 °C. For the complex formation study with Cu^{2+} ions, HepG2 cells were preincubated with 10 μM of DQ_{468} for 60 min at 37 °C, followed by washing three times with 1× PBS and subsequent incubation with 10 μM of Cu^{2+} for 60 min at 37 °C. To study the nitroxyl (HNO) sensing property of the ligand, HepG2 cells were preincubated with 10 μM of DQ_{468} for 60 min at 37 °C, followed by washing three times with 1× PBS and subsequent incubation with 10 μM of Cu^{2+} for 60 min at 37 °C again, followed by washing three times with 1× PBS and subsequent incubation with 10 μM of Angeli's salt [$Na_2N_2O_3$], for 60 min at 37 °C. Fluorescence images of HepG2

cells were taken by a fluorescence microscope (Leica DM3000, Germany) with an objective lens of 40× magnification.

Computational details

Ground-state electronic structures of the ligand and complexes were calculated in acetonitrile solution using the DFT method[50] associated with the conductor-like polarizable continuum model (CPCM).[51] Becke's hybrid function[52] with the Lee–Yang–Parr (LYP) correlation function[53] were utilized throughout the study. The fully optimized geometries of the ligand and complexes were determined without any symmetry restrictions. The nature of all the stationary points for both the metal-free ligand DQ_{468} and its Cu^{2+} complex were recognized by using normal mode analysis. The UV-Vis absorption spectral properties of DQ_{468} and the complexes $[Cu^{II}(DQ_{468})Cl]^+$ and $[Cu^{I}(DQ_{468})]^+$ in acetonitrile were estimated on the basis of their optimized ground-state geometries, by time-dependent density functional theory (TDDFT)[54] related to the conductor-like polarizable continuum model (CPCM).[51] We computed the lowest 40 singlet–singlet transitions and the electronic excitation energies were obtained accurately due to the presence of electronic correlation in the TDDFT (B3LYP) method.[55] For ground-state optimization, we used the 6-31G(d) basis set. Gauss View 5.1 software was used for the calculation of the electron density plots in the frontier molecular orbital. All the calculations were obtained using Gaussian 09W software package.[56] We also used the Gauss Sum 2.1 programe[57] for the calculation of the molecular orbital contributions from atoms or groups.

Results and discussion

Synthesis and photophysical properties

Scheme 3 displays the synthetic pathway of our present probe DQ_{468}. It consists of two steps of easy nucleophilic substitution
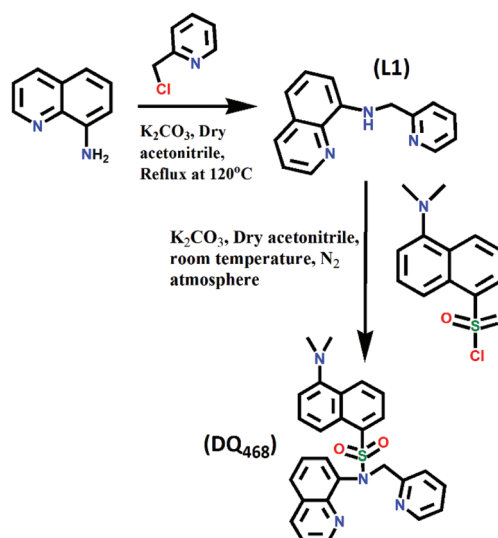
Scheme 3 Synthetic route of probe DQ_{468}.

reactions. First, 8-aminoquinoline was allowed to react with 2-(chloromethyl) pyridine (a commercially accessible pyridine derivative) in the presence of K_2CO_3 in MeCN in a 1 : 1 mole ratio under refluxing conditions for 24 h to obtain one of the substrates (pyridin-2-ylmethyl-quinolin-8-yl-amine) of our probe. Then, this compound was treated immediately with dansyl chloride, a fluorophoric moiety, in a 1 : 1 mole ratio under a N_2 atmosphere in a cold condition and allowed to proceed overnight under stirring. The intermediate and target compound were thoroughly characterized by different spectroscopic techniques. The complex $\mathbf{Cu^{II}\text{-}DQ_{468}}$ was prepared by the stoichiometric reaction of $CuCl_2 \cdot 2H_2O$ and $\mathbf{DQ_{468}}$ in MeCN and characterized by mass and EPR analysis. These studies are in good agreement with the chemical formula of the complex. Before going for more detailed experiments, we checked the fluorescence responses of $\mathbf{DQ_{468}}$ against Cu^{II} in various solvents, like THF, MeOH and MeCN. It was observed that the complex formation of $\mathbf{DQ_{468}}$ with Cu(II) occurred in MeCN efficiently, while in THF and MeOH, a large excess of Cu^{2+} was needed to quench the fluorescence intensity (Fig. S8†). So we selected MeCN as an organic solvent for the more detailed studies. There is also a previous report where MeCN was used as a solvent for the reduction of Cu(II) to Cu(I).[58]

UV-Vis study

The spectrophotometric titration of the probe was performed with the gradual addition of Cu^{2+} in an aqueous–organic medium (10 mM HEPES buffer : acetonitrile = 2 : 8 solution, v/v) at pH 7.0. This study clearly demonstrated that the absorption of $\mathbf{DQ_{468}}$ at 337 nm vanishes gradually, with the concomitant development of a peak at 370 nm upon the incremental addition of Cu^{2+} (Fig. 1). This occurrence is expected due to the coordination of $\mathbf{DQ_{468}}$ towards Cu^{2+}. The data obtained from the UV-Vis titration was solved easily using the Benesi–

Hildebrand equation, where A_0 and A_{max} are the absorbances of the ligand in the absence and in the presence of excess Cu^{2+}.

By considering eqn (1), a linear fit was obtained from the plot of $(A_{max} - A_0)/(A - A_0)$ vs. $1/[M]$, which clearly manifested the 1 : 1 complex formation ($n = 1$) and provided an apparent formation constant K_f of $(1.74 \pm 0.17) \times 10^4 \ M^{-1}$ (Fig. 1).

$$\frac{(A_{max} - A_0)}{(A - A_0)} = 1 + \frac{1}{K[M]^n} \qquad (1)$$

Fluorescence quenching studies

The emission spectral pattern of the probe $\mathbf{DQ_{468}}$ exhibited a typical dansyl green fluorescence at $\lambda_{em} = 543$ nm with excitation at 390 nm. The fluorescence titration of $\mathbf{DQ_{468}}$ with Cu^{2+} was performed taking a fixed concentration of $\mathbf{DQ_{468}}$ (20 μM) in aqueous–acetonitrile medium (10 mM HEPES buffer : acetonitrile = 2 : 8 solution, v/v) at pH 7.0 and $\mu = 0.10$ M NaCl. Then, freshly prepared Cu^{2+} solution was added progressively, which led to the gradual decrease in the fluorescence intensity of $\mathbf{DQ_{468}}$. The complete complex formation occurred upon the addition of ~5 equivalent of Cu^{2+}, yielding almost a 7-fold decrease in fluorescence intensity, which was sufficient to detect Cu^{2+} (Fig. 2) with a limit of detection of 0.091 μM (Fig. S9†). The degree of fluorescence quenching was evaluated by obtaining a linears Stern–Volmer plot between the ratio of the relative fluorescence intensities, (F_{max}/F) and Cu^{2+} ion concentration,[59] where F_{max} and F are the steady state fluorescence intensities in the absence and presence of the quencher (Cu^{2+}), respectively, at the wavelength maximum, and $[Q]$ is the quencher concentration. The estimated (K_{SV}, quenching constant Stern–Volmer constant) was found to be $K_{SV} = (7.32 \pm 0.08) \times 10^4 \ M^{-1}$ (Fig. 2(b))

$$\frac{F_{max}}{F} = 1 + K_{SV}[Q] \qquad (2)$$

From the literature reports,[60,61] we could presume that a strong interaction had been taken place between $\mathbf{DQ_{468}}$ and
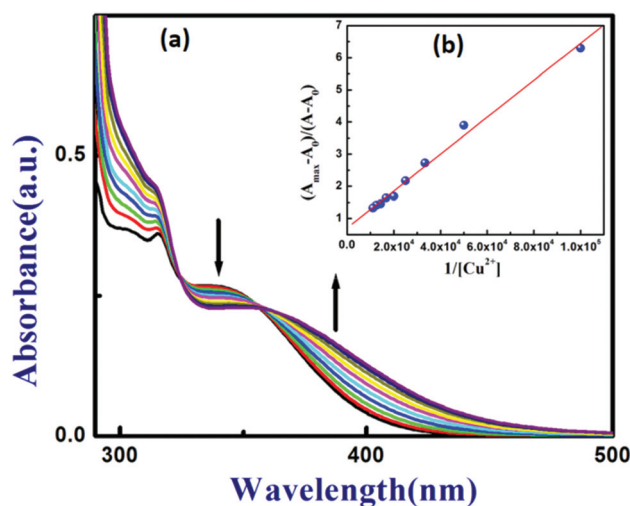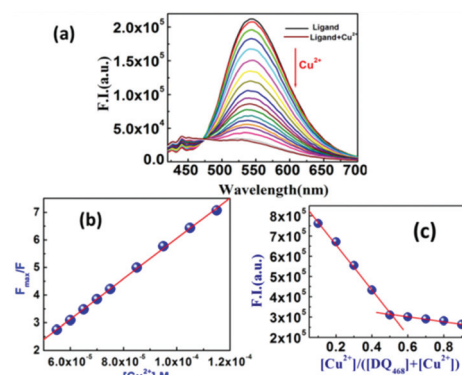

Fig. 1 (a) Absorption titration of $\mathbf{DQ_{468}}$ with the gradual addition of Cu^{2+} in MeCN : HEPES buffer medium (v : v = 8 : 2) at pH 7.0 at 25 °C; (b) Benesi–Hildebrand plot.

Fig. 2 (a) Fluorescence titration of $\mathbf{DQ_{468}}$ (20 μM) at 25 °C by the incremental addition of Cu^{2+} (0–100 μM) in HEPES buffer (10 mmol) : acetonitrile medium (2 : 8) at pH 7.0 with $\lambda_{ex} = 390$ nm and $\lambda_{em} = 543$ nm. (b) Linear Stern–Volmer plot, (c) Job's plot.

doubly charged copper ion, resulting in the effective quenching of the fluorescence intensity of **DQ₄₆₈**, which could be ascribed to the photoinduced electron transfer (PET) mechanism from the dansyl fluorophore to the chelated Cu^{2+}. A Job's plot was constructed to determine the nature of the complex $[Cu(DQ_{468})Cl]^+$ by following the change in fluorescence intensity at 543 nm (Fig. 2(c)). The Job's plot clearly exhibited the 1 : 1 complex formation by a break at 0.5. This was further supported by the mass spectrum of this species with m/z = 566.168, which corresponds to that of $[Cu(DQ_{468})Cl]^+$ (Fig. S10†). We also calculated the quantum yield of the metal free **DQ₄₆₈** and $[Cu(DQ_{468})Cl]^+$, which were found to be 0.135 and 0.026, respectively.

Analyte selectivity studies of $[Cu(DQ_{468})Cl]^+$ and HNO-induced reduction of Cu^{2+}

The ability of a fluorescent probe to sense a particular analyte depends on the specificity of its chemical reactions and chemical properties. We checked the reactivity of the probe (**DQ₄₆₈**) towards some commonly known metal ions. This study exhibited a high affinity of the probe only towards Cu^{2+} (Fig. S11†) without any interference of other metal ions, except Fe^{3+}, which showed a slight quenching of FI of **DQ₄₆₈**, but it was interesting to see that the further addition of HNO produced no influence on its FI. Thus, the recognition of HNO is highly selective towards the $[Cu(DQ_{468})Cl]^+$ complex. This Cu^{II}-complex is also inert towards other commonly known biological reactive oxygen, nitrogen and sulfur species (ROS, RNS, RSS) present in live cells. The selectivity tests were performed in aqueous–acetonitrile (v/v = 2 : 8) medium at pH 7.0 and μ = 0.10 M NaCl, taking a fixed concentration of **DQ₄₆₈** (20 μM). We screened a wide array of reactive oxygen, nitrogen and sulfur species, like NO, H_2O_2, NO_3^-, NO_2^-, AA, ClO^-, O_2^-, $^\bullet OH$, TEMPO, $ONOO^-$, HS^-, S^{2-} in excess (10 equivalence). But none other than HNO could induce an enhancement of the fluorescence intensity of our Cu-complex. After treatment with Angeli's salt (HNO donor), the fluorescence intensity was restored up to 90% (6-fold). In aqueous solution (pH 7,) Angeli's salt ($Na_2N_2O_3$) undergoes dissociation to form HNO as well as $NaNO_2$[62] which may be the reason behind the reduction of metal ions. To verify that HNO was solely responsible for the regeneration of fluorescence through reduction, the reactivity of $[Cu(DQ_{468})Cl]^+$ towards $NaNO_2$ was checked. But here, no detectable fluorescence enhancement was observed (Fig. 3) leading to the conclusion that the fluorescence enhancement occurred only due to HNO, not by the side product (NO_2^-).

Interestingly, the probe $[Cu(DQ_{468})Cl]^+$ showed no significant change in fluorescence intensity upon the addition of saturated NO solution even though HNO and NO are very closely related biological species. So, the difference in the interaction of $[Cu(DQ_{468})Cl]^+$ towards NO and HNO magnifies the beauty of our system towards HNO detection over NO in biology. Our probe also showed inertness towards biologically abundant reactive sulfur species, like L-(+)-cysteine, GSH and HCY (Fig. 4), and also towards important amino acids. All
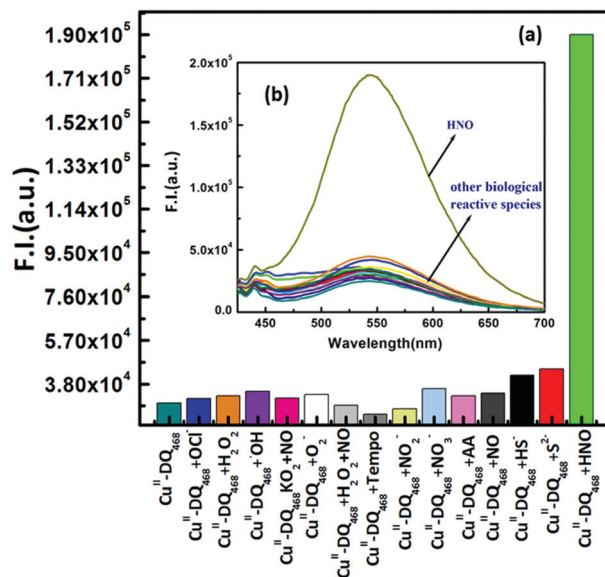

Fig. 3 (a) Bar plot representing the fluorescence responses of $[Cu^{II}(DQ_{468})Cl]^+$ at 543 nm (λ_{ex} = 390 nm) towards various biological reactive species in MeCN : HEPES buffer (8 : 2, v/v) at room temperature at pH 7.0, **DQ₄₆₈** = 20 μM, X^n = 200 μM. (b) Corresponding spectral responses of **DQ₄₆₈**.
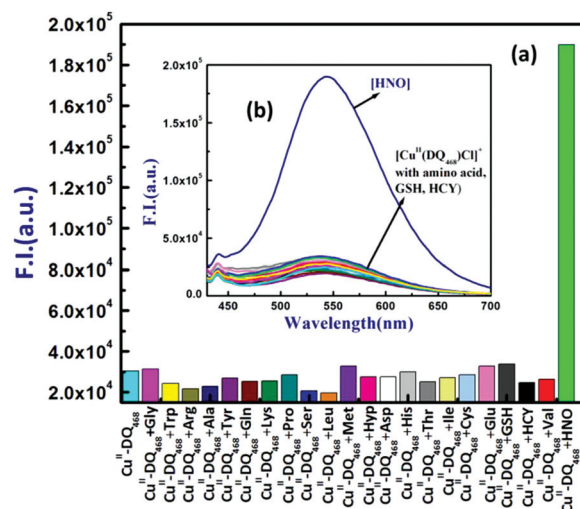
Fig. 4 (a) Bar plot representing the fluorescence responses of $[Cu^{II}(DQ_{468})Cl]^+$ at 543 nm (λ_{ex} = 390 nm) towards various amino acids with the conditions: (8 : 2, v/v) MeCN/HEPES buffer; 25 °C, pH 7.0 $[Cu^{II}(DQ_{468})Cl]^+$ = 20 μM, amino acid = 200 μM. (b) Corresponding spectral responses of $[Cu^{II}(DQ_{468})Cl]^+$ towards different amino acids.

these experiments showed that our Cu-complex-based HNO probe was highly specific towards HNO over other reactive species present in the biological milieu.

Fluorescence studies on HNO-induced reduction of $[Cu(DQ_{468})Cl]^+$

HNO is a sufficiently strong reducing reagent for the quantitative reduction of Cu(II) to Cu(I). So in our present work, there

was an adequate possibility for the formation of diamagnetic Cu^I from paramagnetic Cu^{II} with the concomitant regeneration of the fluorescence intensity under the influence of HNO. This redox-based HNO sensing strategy is a useful pathway for the detection of HNO in living cells also. We found there was a marked increase in fluorescence response (30-fold) of **[Cu(DQ₄₆₈)Cl]⁺** upon the incremental addition of HNO in pure MeCN, but when the same experiment was performed in MeCN–HEPES buffer (9 : 1 v/v) at pH 7.0, the fluorescence enhancement was observed to be an 8-fold and 6-fold enhancement in 8 : 2 (v/v) MeCN–H₂O (Fig. S12†). We used MeCN–H₂O (8 : 2 v/v) throughout the experiments as the extent of fluorescence regeneration in this solvent mixture was sufficient to detect HNO intracellularly in living cells. It was noteworthy that the fluorescence intensity of **DQ₄₆₈** dramatically reduced (almost 7-fold) in 8 : 2 MeCN-HEPES buffer at pH 7.0 upon the addition of ~5 equivalent of Cu^{2+} and upon exposure to HNO, whereby the Cu(II)-complex gets reduced to Cu(I), rendering the complex diamagnetic and restoring its fluorescence intensity up to 90% to that of **DQ₄₆₈**, with a detection limit of 0.41 µM (Fig. S13†). The formation constant of **[CuI(DQ₄₆₈)]⁺** with HNO was determined by the Benesi–Hildebrand equation, and was found to be $(3.096 \pm 0.08) \times 10^3$ M⁻¹ (Fig. 5).
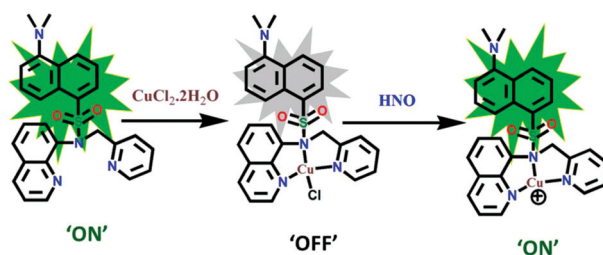
Mechanistic view of HNO sensing

To date, in the case of previously reported Cu^{2+}-ion-assisted HNO probes, the regeneration of the fluorescence intensity occurred in one of three ways (Scheme 4):[10,40–42,46] (a) turn-on sensing by the reduction of the metal center with a simultaneous displacement of the probe; in this process a N-nitrosation reaction occurs on the secondary nitrogen atom with the concomitant removal of Cu(I); in this case, the fluorescence emission property of the probe may be changed; (b) turn-on sensing due to the reduction of Cu^{2+} without removal of the fluorophore; in this mechanism, 100% recovery of the
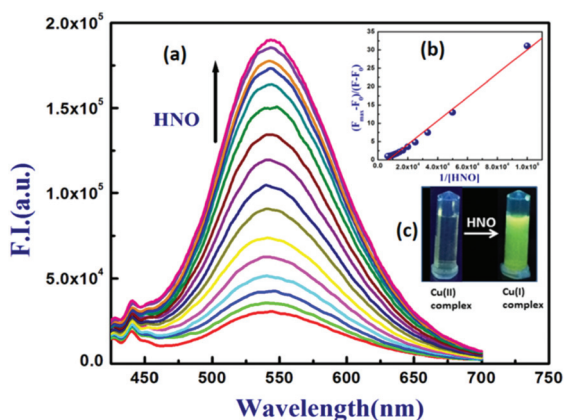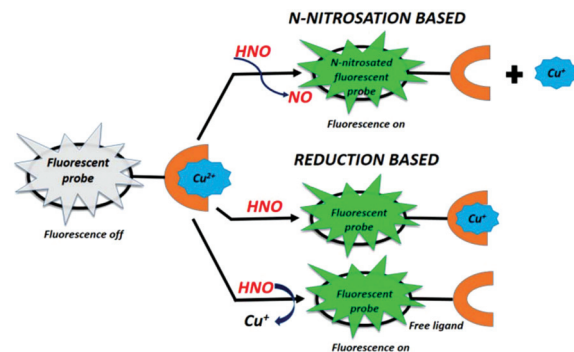
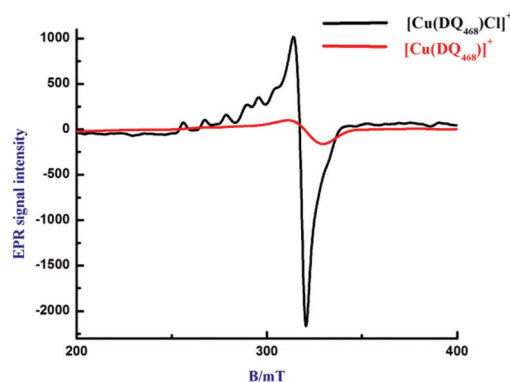

Scheme 4 Established mechanisms for HNO detection.

Scheme 5 Operative mechanism in present HNO detection.

fluorescence intensity of the probe may not occur because the PET from the fluorophore to the Cu⁺ is not fully blocked, leading to lowering of the electron density on the probe; and (c) turn-on sensing caused by the formation of diamagnetic Cu⁺ species from Cu^{2+} with subsequent removal of the probe; this mechanism results in ~100% recovery of the fluorescent intensity. Among the above-said probable mechanisms, particularly (b) is operative in our present investigation; (Scheme 5). Here, **DQ₄₆₈** forms a Cu^{II}-complex leading to fluorescence quenching (PET ON), and subsequent regeneration of fluorescence is achieved by the nitroxyl (HNO), transforming Cu(II) to Cu(I) (PET OFF).[40,42,63,64] This phenomenon was evidenced by the EPR spectroscopy (Fig. 6) and mass spec-

Fig. 5 (a) Fluorescence titration of **[CuII(DQ₄₆₈)Cl]⁺** at 25 °C by the incremental addition of HNO in acetonitrile : HEPES buffer (8 : 2) (10 mmol) at pH = 7.0 with λ_{ex} = 390 nm and λ_{em} = 543 nm; (b) Benesi–Hildebrand plot. (c) UV exposed emission image of **[CuII(DQ₄₆₈)Cl]⁺** and **Cu(I)-DQ₄₆₈**.

Fig. 6 EPR spectrum of **[CuII(DQ₄₆₈)Cl]⁺** (20 µM) and **[CuI(DQ₄₆₈)]⁺** (*in situ* reduction with excess Na₂N₂O₃) at 77 K.

troscopy (Fig. S14†) analyses. The EPR spectrum of [Cu(DQ$_{468}$)Cl]$^+$ is a typically axial type with $g_\perp$ = 2.051 and $g_\parallel$ = 2.321, indicating the presence of a paramagnetic Cu^{2+} ion. Then upon treatment with Na$_2$N$_2$O$_3$ in MeCN, the spectrum clearly showed that the previous characteristic signals of Cu^{2+} vanished to base-line, i.e. the newly formed product was EPR silent, indicating the presence of the metal ion in its reduced form (Cu^I). Here, as the metal is still co-ordinated with the probe as Cu$^+$, PET is not blocked fully, resulting in a lowering of the fluorescence intensity with respect to metal-free DQ$_{468}$. We also checked the fluorescence response of DQ$_{468}$ towards CuCl salt. The corresponding spectrum was very much similar to that of the HNO-treated spectrum of Cu^{II}-DQ$_{468}$ (Fig. S15†). This HNO-induced reduction was further supported by the mass spectroscopy, with the ESI-MS$^+$ of [Cu(DQ$_{468}$)Cl]$^+$ corresponding to (m/z): 566.1152 (Fig. S10†) and ESI-MS$^+$ of [Cu(DQ$_{468}$)]$^+$ corresponding to (m/z): 531.1822 (Fig. S14†).

pH effect on [Cu^{II}(DQ$_{468}$)Cl]$^+$ and [Cu^I(DQ$_{468}$)]$^+$

For the proper biological application of any fluorescent sensor, the sensing should occur in a wide array of pH because different cells, or different compartments of a same cell, may have different pH values. However, in the presence of copper (II) chloride, the fluorescence of DQ$_{468}$ was of low intensity and exhibited almost an invariant emission profile over a pH range from 2 to 8 (Fig. 7). Then upon treatment with HNO, the Cu(II)-complex-based probe exhibited a drastic enhancement in fluorescence intensity in a wide scale of pH (4–10). This large increase in fluorescence intensity in a wide range of pH suggests our Cu-complex-based probe [Cu(DQ$_{468}$)Cl]$^+$ could safely be used in HNO detection in living cells at different pH.

Theoretical studies

Geometry optimization and electronic structure. To get some idea about the interaction of Cu^{2+} complex and HNO, we carried out DFT and TDDFT calculations of DQ$_{468}$, [Cu^{II}(DQ$_{468}$)Cl]$^+$ and [Cu^I(DQ$_{468}$)]$^+$.[65,66] Fig. 8 shows the opti-

mized geometries of DQ$_{468}$, [Cu^{II}(DQ$_{468}$)Cl]$^+$ and [Cu^I(DQ$_{468}$)]$^+$ with the C1 point group. The nature of all the stationary points for both the free ligand DQ$_{468}$ and its Cu-complexes were recognized by using normal mode analysis. The global minima of DQ$_{468}$, [Cu^{II}(DQ$_{468}$)Cl]$^+$ and [Cu^I(DQ$_{468}$)]$^+$ were confirmed by the positive values of all the frequencies. The compositions of the Cu-complexes were determined by mass spectroscopy as [Cu^{II}(DQ$_{468}$)Cl]$^+$ and [Cu^I(DQ$_{468}$)]$^+$, which displayed the presence of one chlorine in the molecular fragment of Cu^{2+} complex and the absence of the same in its reduced product. The central metal ion Cu^{2+} was in the distorted tetrahedral arrangement, while the metal ion was coordinated through naphthalene-1-sulfonic acid methylamide-N1, 2-methyl-pyridine-N44 and quinoline-N60 along with one chlorine atom (Cl34). All the calculated important geometrical parameters of the free ligand DQ$_{468}$, [Cu^{II}(DQ$_{468}$)Cl]$^+$ and [Cu^I(DQ$_{468}$)]$^+$ are listed in Table S1, S2 and S3.† The calculated Cu–N bond distances fell in the range 1.94–2.81 Å in the Cu^{2+} complex. The Cu33–N1 bond length was slightly larger than other Cu–N bond lengths, which may be due to weak coordination of the through N1, as it is directly attached to the highly electron withdrawing –SO$_2$R group. After complex formation, there are changes in some C–S, S–N and N–C bond lengths with respect to the free ligand. In the ground state of DQ$_{468}$, the electron density resides mainly on the HOMO, LUMO and LUMO+1 molecular orbitals of the dansyl, quinoline and naphthalene fragments of the ligand, respectively (Fig. S16†). For the [Cu^{II}(DQ$_{468}$)Cl]$^+$ complex, the electron density was mainly localized on the HOMO and HOMO−5 molecular orbitals of the dimethyl-naphthalen-1-yl-amine fragment and for LUMO, it resided on the quinoline-8yl-amine moiety. HOMO−5 molecular orbital mainly originate from ligand π and π* orbital contributions, while the HOMO and LUMO orbitals originate from the metal d orbital along with ligand π orbital contributions (Fig. S17†). For the reduced species [Cu^I(DQ$_{468}$)]$^+$, the electron cloud resides mainly on HOMO, HOMO−3, HOMO−2 and HOMO−4 molecular orbitals of the dimethyl-naphthalen-1-yl-
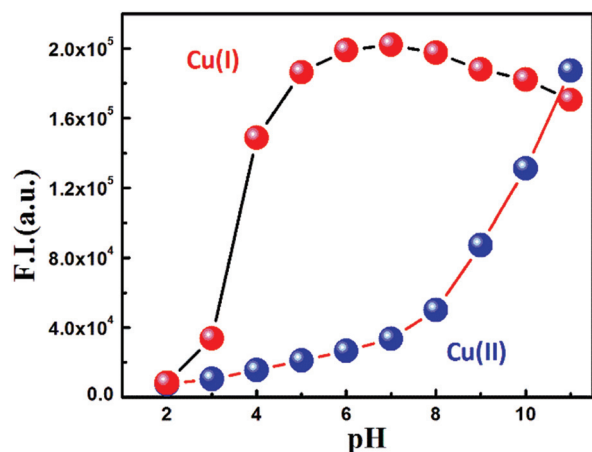

Fig. 7 pH-Dependent fluorescence responses of [Cu^{II}(DQ$_{468}$)Cl]$^+$ and [Cu^I(DQ$_{468}$)]$^+$ in 8 : 2 (v/v) MeCN/HEPES buffer medium.
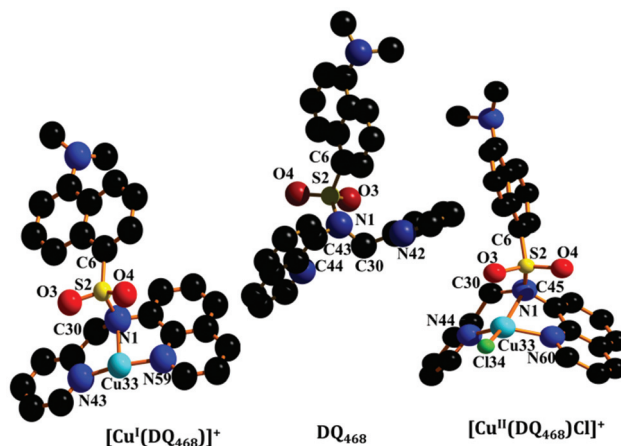

Fig. 8 Optimized geometry of ligand and Cu-complexes.

amine moiety with Cu atom. Also, the HOMO−1, LUMO, LUMO+2, LUMO+1 and LUMO+6 molecular orbitals originate from the Cu^{2+} coordination sphere, quinoline moiety, 5-di-methylamino-naphthalene-1-sulfonic acid (pyridin-2-ylmethyl)-amide fragment and naphthalene moiety, respectively (Fig. S18–S20†). These compositions are useful in understanding the nature of transition as well as the absorption spectra of both the free ligand and its Cu-complexes. From Fig. 9, the HOMO–LUMO energy gaps of $[Cu^{II}(DQ_{468})Cl]^{+}$, $[Cu^{I}(DQ_{468})]^{+}$ and DQ_{468} were 2.51 eV, 2.92 and 3.91 eV, respectively. The ligand DQ_{468} showed an absorption band at 337 nm in acetonitrile–water (8 : 2) at room temperature, which corresponds to the absorption band at 354.85 obtained from TDDFT calculations, and as given in Table S4.† This band was assigned to $S_0 \rightarrow S_1$ electronic transitions (Fig. S16†). The absorption energy along with their oscillator strengths are given in Table S4.† The complex $[Cu^{II}(DQ_{468})Cl]^{+}$ showed an absorption band at 370 nm (Fig. S17†) in acetonitrile–water (8 : 2) at room temperature and the corresponding calculated absorption band was located at 375.33 (Table S5†), ascribed to the electronic transition $S_0 \rightarrow S_{20}$. The reduced complex $[Cu^{I}(DQ_{468})]^{+}$ displayed an absorption band at 340 nm, which is ascribed to the transitions $S_0 \rightarrow S_{13}$, $S_0 \rightarrow S_7$ and $S_0 \rightarrow S_8$ (Fig. S18–S20†) in the range of 335 nm to 391 nm, with a significant oscillator strength, which were in agreement with our experimental results (Table S6†).

Cytotoxicity studies and cell imaging

Considering the fluorescence emitting property of DQ_{468} in the absence of Cu^{2+} ions, it was further checked for its sensing ability in living cells. To determine whether DQ_{468} has cytotoxic effects, a cell viability assay using MTT was performed with calculating the % cell viability on HepG2 cells (Fig. 10). There was no significant reduction in the tetrazolium salt
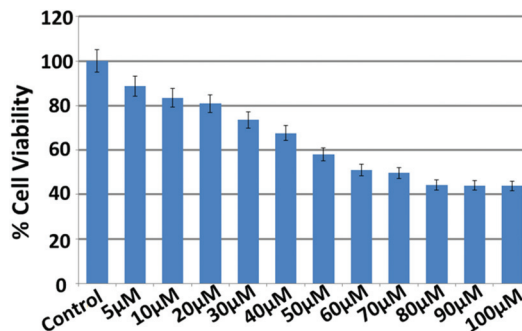

Fig. 10 Percent (%) cell viability of HepG2 cells treated with different concentrations (1–100 μM) of DQ_{468} for 24 h, as determined by MTT assay.

(reflected by a decrease in formazan production) for DQ_{468} up to 20 μM, thus suggesting that bellow 20 μM ligand concentration, DQ_{468} would be much more effective for the analysis of its fluorescence emissions *in vitro*. More than 80% cell viability was observed for DQ_{468} at 5 μM and 10 μM, after which the viability of the HepG2 cells decreased. Hence, further experiments were carried out with 5 μM and 10 μM of DQ_{468} for treatment. The ligand DQ_{468} exhibited prominent intracellular green fluorescence in HepG2 cells treated with 5 μM of the ligand and incubated for 1 h; which was found to be increased when the HepG2 cells were incubated with 10 μM of DQ_{468} for 60 min at 37 °C (Fig. 11). However, the fluorescence emission was significantly quenched in the presence of 10 μM Cu^{2+} ions. Upon the further addition of Angeli's salt (10 μM) at 37 °C, the green fluorescence emission was recovered due to the reduction of Cu^{2+} ions to Cu^{+} ions. So, our present ligand
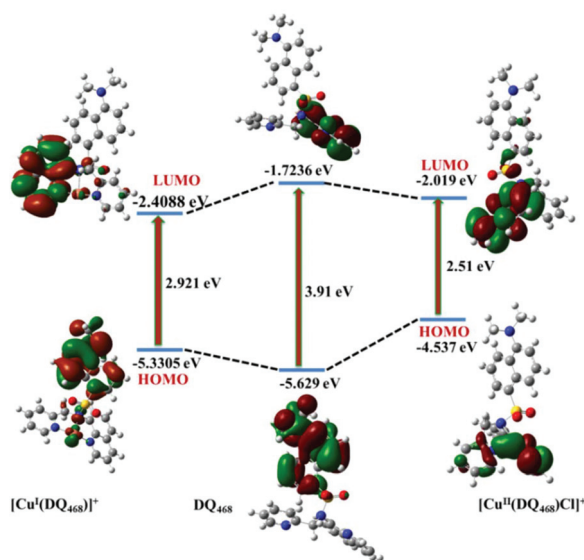
Fig. 9 Frontier molecular orbitals of DQ_{468}, $[Cu^{II}(DQ_{468})Cl]^{+}$ and $[Cu^{I}(DQ_{468})]^{+}$ complex.

Fig. 11 The fluorescence images of HepG2 cells were captured (40×) after incubation with 5 and 10 μM of DQ_{468} for 60 min at 37 °C, which showed green fluorescence emission. The emission quenches in the presence of Cu^{2+} ions, as the HepG2 cells were treated with 10 μM of Cu^{2+} ions, followed by washing three times with 1× PBS, and incubation with 10 μM of DQ_{468} for 60 min at 37 °C. The fluorescence emission reappeared in the presence of 10 μM of $Na_2N_2O_3$ for 60 min at 37 °C, which reduces the Cu^{2+} ions concentration by converting them to Cu^{+} ions.

DQ₄₆₈ was able to detect Cu^{2+} and HNO sequentially in biological samples with low cytotoxicity.

Conclusion

In summary, we synthesized a fluorogenic probe **DQ₄₆₈** in a facile manner on a dansyl-quinoline platform. Here, first the metal-free probe **DQ₄₆₈** showed high fluorescence intensity, which gets quenched by the coordination with paramagnetic Cu^{2+} (7-fold) with $K_{SV} = (7.32 \pm 0.08) \times 10^4$ M^{-1}. The binding ratio of **DQ₄₆₈** towards Cu^{2+} was obtained by Job's method and by mass spectroscopy showing 1 : 1 complex formation with a limit of detection of 0.091 μM. This Cu^{II} complex-based system was allowed to react with Angeli's salt (HNO donor), an ample reducing agent. Very obviously, the Cu^{II} was converted to the diamagnetic Cu^{I} and fluorescence intensity was regenerated. This reduction based turn-on sensing was well established by mass spectroscopy as well as EPR spectroscopy, which showed that the previously observed peak for Cu^{II} gets dropped to the base line in the presence of HNO, indicating the reduction of the metal centre. This Cu^{II}-complex-based probe also showed high affinity only towards HNO, being inert towards other commonly known RNS, ROS and RSS, and even towards NO abundant in biological milieu, thus signifying it's efficiency as a good nitroxyl sensor in a wide range of physiological pH. In view of its proper biological activity, our present system also qualified under the eligibility criteria due to its negligible cytotoxicity and biocompatibility with an *in vitro* sensing ability in living cells. So, all these above experiments and discussions certify our probe as a good candidate for nitroxyl sensing.

Conflicts of interest

There are no conflicts to declare.

Acknowledgements

References

1 (*a*) A. P. D. Silva, H. Q. N. Gunaratne, T. Gunnlaugsson, A. J. M. Huxley, C. P. McCoy, J. T. Rademacher and T. E. Rice, *Chem. Rev.*, 1997, **97**, 1515; (*b*) T. Gunnlaugsson, J. P. Leonard and J. N. S. Murray, *Org. Lett.*, 2004, **6**, 1557; (*c*) C. Yu, J. Zhang, J. Li, P. Liu, P. Wei and L. Chen, *Microchim. Acta*, 2011, **174**, 247.

2 J. S. Kim and D. T. Quang, *Chem. Rev.*, 2007, **107**, 3780.

3 (*a*) B. High, D. Bruce and M. M. Richter, *Anal. Chim. Acta*, 2001, **449**, 17; (*b*) L. Tapia, M. Suazo, C. Hödar, V. Cambiazo and M. González, *BioMetals*, 2003, **16**, 169.

4 (*a*) M. C. Linder and M. Hazegh-Azam, *Am. J. Clin. Nutr.*, 1996, **63**, 797S; (*b*) R. Uauy, M. Olivares and M. Gonzalez, *Am. J. Clin. Nutr.*, 1998, **167**, 952S.

5 (*a*) Z. Xu, S. J. Han, C. Lee, J. Yoon and D. R. Spring, *Chem. Commun.*, 2010, **46**, 1679; (*b*) X. Cao, W. Lin and W. Wan, *Chem. Commun.*, 2012, **48**, 6247; (*c*) C. S. Lim, J. H. Han, C. W. Kim, M. Y. Kang, D. W. Kang and B. R. Cho, *Chem. Commun.*, 2011, **47**, 7146; (*d*) Y. Zhao, X. B. Zhang, Z. X. Han, L. Qiao, C. Y. Li, L. X. Jian, G. L. Shen and R. Q. Yu, *Anal. Chem.*, 2009, **81**, 7022.

6 (*a*) T. P. Thomas, M. T. Myaing, J. Y. Ye, K. Candido, A. Kotlyar, J. Beals, P. Cao, B. Keszler, A. K. Patri, T. B. Norris and J. R. Baker, *Biophys. J.*, 2004, **86**, 3959; (*b*) Y. Liu, X. H. Dong, J. Sun, C. Zhong, B. Li, X. You, B. Liu and Z. Liu, *Analyst*, 2012, **137**, 1837.

7 (*a*) D. W. Domaille, L. Zeng and C. J. Chang, *J. Am. Chem. Soc.*, 2010, **132**, 1194; (*b*) Q. Qu, A. Zhu, X. Shao, G. Shi and Y. Tian, *Chem. Commun.*, 2012, **48**, 5473.

8 (*a*) M. H. Lim, D. Xu and S. J. Lippard, *Nat. Chem. Biol.*, 2006, **2**, 375; (*b*) S. Kim, M. A. Minier, A. Loas, S. Becker, F. Wang and S. J. Lippard, *J. Am. Chem. Soc.*, 2016, **138**, 1804; (*c*) M. D. Pluth, M. R. Chan, L. E. McQuade and S. J. Lippard, *Inorg. Chem.*, 2011, **50**, 9385.

9 A. T. Wrobel, T. C. Johnstone, A. D. Liang, S. J. Lippard and P. Rivera-Fuentes, *J. Am. Chem. Soc.*, 2014, **136**, 4697.

10 X. Sun, G. Kim, Y. Xu, J. Yoon and T. D. James, *ChemPlusChem*, 2016, **81**, 30.

11 (*a*) A. Dutta, R. Alam, A. S. M. Islam, A. Dutta and M. Ali, *Dalton Trans.*, 2018, **47**, 11563; (*b*) T. Anand, G. Sivaraman and D. Chellappa, *J. Photochem. Photobiol., A*, 2014, **2**, 47.

12 (*a*) A. Kalita, P. Kumar, R. C. Deka and B. Mondal, *Inorg. Chem.*, 2011, **50**, 11868; (*b*) P. Kumar, A. Kalita and B. Mondal, *Dalton Trans.*, 2012, **41**, 10543.

13 D. D. Thomas, L. A. Ridnour, J. S. Isenberg, W. Flores-Santana, C. H. Switzer, S. Donzelli, P. Hussain, C. Vecoli, N. Paolocci, S. Ambs, C. A. Colton, C. C. Harris, D. D. Roberts and D. A. Wink, *Free Radicals Biol. Med.*, 2008, **45**, 18.

14 G. A. Blaise, D. Gauvin, M. Gangal and S. Authier, *Toxicology*, 2005, **208**, 177.

15 C. Q. Li and G. N. Wogan, *Cancer Lett.*, 2005, **226**, 1.

16 V. Calabrese, C. Mancuso, M. Calvani, E. Rizzarelli, D. A. Butterfield and A. M. G. Stella, *Nat. Rev. Neurosci.*, 2007, **8**, 766.

17 A. S. Vidwans, S. Kim, D. O. Coffin, D. A. Wink and S. J. Hewett, *J. Neurochem.*, 1999, **72**, 1843.

18 L. A. Ridnour, D. D. Thomas, C. Switzer, W. Flores-Santana, J. S. Isenberg, S. Ambs, D. D. Roberts and D. A. Wink, *Nitric Oxide*, 2008, **19**, 73.

19 M. B. Grisham, D. Jourd'Heuil and D. A. Wink, *Am. J. Physiol.: Gastrointest. Liver Physiol.*, 1999, **276**, G315.

20 D. S. Bredt, P. M. Hwang and S. H. Snyder, *Nature*, 1990, **347**, 768.

21 C. Bogdan, *Nat. Immunol.*, 2001, **2**, 907.

22 R. O. Cannon, *Clin. Chem.*, 1998, **44**, 1809.

23 J. M. Fukuto, C. J. Cisneros and R. L. Kinkade, *J. Inorg. Biochem.*, 2013, **118**, 201.

24 M. L. Bullen, A. A. Miller, K. L. Andrews, J. C. Irvine, R. H. Ritchie, C. G. Sobey and B. K. Kemp-Harper, *Antioxid. Redox Signaling*, 2011, **14**, 1675.

25 N. Paolocci, W. F. Saavedra, K. M. Miranda, C. Martignani, T. Isoda, J. M. Hare, M. G. Espey, J. M. Fukuto, M. Feelisch, D. A. Wink and D. A. Kass, *Proc. Natl. Acad. Sci. U. S. A.*, 2001, **98**, 10463.

26 R. F. Dautov, D. T. M. Ngo, G. Licari, S. Liu, A. L. Sverdlov, R. H. Ritchie, B. K. Kemp-Harper, J. D. Horowitz and Y. Y. Chirkov, *Nitric Oxide*, 2013, **35**, 72.

27 C. H. Switzer, W. Flores-Santana, D. Mancardi, S. Donzelli, D. Basudhar, L. A. Ridnour, K. M. Miranda, J. M. Fukuto, N. Paolocci and D. A. Wink, *Biochim. Biophys. Acta*, 2009, **1787**, 835.

28 C. Liu, Z. Cao, Z. Wang, P. Jia, J. Liu, Z. Wang, B. Han, X. Huang, X. Li, B. Zhu and X. Zhang, *Sens. Actuators, B*, 2015, **220**, 727.

29 Y. Zhou, Y. W. Yao, J. Y. Li, C. Yao and B. P. Lin, *Sens. Actuators, B*, 2012, **174**, 414.

30 M. Royzen, J. J. Wilson and S. J. Lippard, *J. Inorg. Biochem.*, 2013, **118**, 162.

31 (*a*) S. A. Suárez, D. E. Bikiel, D. E. Wetzler, M. A. Martí and F. Doctorovich, *Anal. Chem.*, 2013, **85**, 10262; (*b*) V. K. Gupta, M. R. Ganjali, P. Norouzi, H. Khani, A. Nayak and S. Agarwal, *Crit. Rev. Anal. Chem.*, 2011, **41**, 282.

32 J. A. Reisz, C. N. Zink and S. B. King, *J. Am. Chem. Soc.*, 2011, **133**, 11675.

33 (*a*) T. Malinski and Z. Taha, *Nature*, 1992, **358**, 676; (*b*) L. A. Ridnour, J. E. Sim, M. A. Hayward, D. A. Wink, S. M. Martin, G. R. Buettner and D. R. Spitz, *Anal. Biochem.*, 2000, **281**, 223; (*c*) T. Nagano and T. Yoshimura, *Chem. Rev.*, 2002, **102**, 1235; (*d*) E. M. Hetrick and M. H. Schoenfisch, *Annu. Rev. Anal. Chem.*, 2009, **2**, 409.

34 (*a*) J. R. Lakowicz, *Principles of Fluorescence Spectroscopy*, Springer-Verlag, Berlin, 3rd edn, 2006; (*b*) X. Li, X. Gao, W. Shi and H. Ma, *Chem. Rev.*, 2014, **114**, 590; (*c*) L. Yuan, W. Lin, K. Zheng and S. Zhu, *Acc. Chem. Res.*, 2013, **46**, 1462.

35 H. Zhang, R. Liu, Y. Tan, W. H. Xie, H. Lei, H. Cheung and H. Sun, *ACS Appl. Mater. Interfaces*, 2015, **7**, 5438.

36 K. Zheng, H. Chen, S. Fang and Y. Wang, *Sens. Actuators, B*, 2016, **233**, 193.

37 K. Kawai, N. Ieda, K. Aizawa, T. Suzuki, N. Miyata and H. Nakagawa, *J. Am. Chem. Soc.*, 2013, **135**, 12690.

38 B. Dong, K. Zheng, Y. Tang and W. Lin, *J. Mater. Chem. B*, 2016, **4**, 1263.

39 (*a*) P. Liu, X. Han, F. Yu and L. Chen, *Chin. J. Anal. Chem.*, 2015, **43**, 1829; (*b*) P. Liu, X. Jing, F. Yu, C. Lv and L. Chen, *Analyst*, 2015, **140**, 4576; (*c*) X. Jing, F. Yu and L. Chen, *Chem. Commun.*, 2014, **50**, 14253.

40 J. Rosenthal and S. J. Lippard, *J. Am. Chem. Soc.*, 2010, **132**, 5536.

41 U. P. Apfel, D. Buccella, J. J. Wilson and S. J. Lippard, *Inorg. Chem.*, 2013, **52**, 3285.

42 Y. Zhou, K. Liu, J.-Y. Li, Y. Fang, T.-C. Zhao and C. Yao, *Org. Lett.*, 2011, **13**(6), 1290.

43 A. Dhir, V. Bhalla and M. Kumar, *Org. Lett.*, 2008, **10**, 4891.

44 Y. Hu, B. Wang and Z. Su, *Polym. Int.*, 2008, **57**, 1343.

45 M. H. Lee, H. J. Kim, S. Yoon, N. Park and J. S. Kim, *Org. Lett.*, 2008, **10**, 213.

46 M. H. Lim, B. A. Wong, W. H. Pitcock, D. Mokshagundam, M. H. Baik and S. J. Lippard, *J. Am. Chem. Soc.*, 2006, **128**, 14364.

47 D. Maiti, A. S. M. Islam, M. Sasmal, C. Prodhan and M. Ali, *Photochem. Photobiol. Sci.*, 2018, **17**, 1213.

48 A. S. M. Islam, M. Sasmal, D. Maiti, A. Dutta, B. Show and M. Ali, *ACS Omega*, 2018, **3**, 10306.

49 S. Miyamoto, G. R. Martinez, A. P. B. Martins, M. H. G. Medeiros and P. DiMascio, *J. Am. Chem. Soc.*, 2003, **125**, 4510.

50 R. G. Parr and W. Yang, *Density Functional Theory of Atoms and Molecules*, Oxford University Press, Oxford, 1989.

51 (*a*) V. Barone and M. Cossi, *J. Phys. Chem. A*, 1998, **102**, 1995; (*b*) M. Cossi and V. Barone, *J. Chem. Phys.*, 2001, **115**, 4708; (*c*) M. Cossi, N. Rega, G. Scalmani and V. Barone, *J. Comput. Chem.*, 2003, **24**, 669.

52 A. D. Becke, *J. Chem. Phys.*, 1993, **98**, 5648.

53 C. Lee, W. Yang and R. G. Parr, *Phys. Rev. B: Condens. Matter Mater. Phys.*, 1998, **37**, 785.

54 (*a*) M. E. Casida, C. Jamoroski, K. C. Casida and D. R. Salahub, *J. Chem. Phys.*, 1998, **108**, 4439; (*b*) R. E. Stratmann, G. E. Scuseria and M. J. Frisch, *J. Chem. Phys.*, 1998, **109**, 8218; (*c*) R. Bauernschmitt and R. Ahlrichs, *Chem. Phys. Lett.*, 1996, **256**, 454.

55 (*a*) T. Liu, H. X. Zhang and B. H. Xia, *J. Phys. Chem. A*, 2007, **111**, 8724; (*b*) X. Zhou, H. X. Zhang, Q. J. Pan, B. H. Xia and A. C. Tang, *J. Phys. Chem. A*, 2005, **109**, 8809; (*c*) X. Zhou, A. M. Ren and J. K. Feng, *J. Organomet. Chem.*, 2005, **690**, 338; (*d*) A. Albertino, C. Garino, S. Ghiani, R. Gobetto, C. Nervi, L. Salassa, E. Rosenverg, A. Sharmin, G. Viscardi, R. Buscaino, G. Cross and M. Milanesio, *J. Organomet. Chem.*, 2007, **692**, 1377.

56 M. J. Frisch, G. W. Trucks, H. B. Schlegel, G. E. Scuseria, M. A. Robb, J. R. Cheeseman, G. Scalmani, V. Barone, B. Mennucci, G. A. Petersson, H. Nakatsuji, M. Caricato, X. Li, H. P. Hratchian, A. F. Izmaylov, J. Bloino, G. Zheng, J. L. Sonnenberg, M. Hada, M. Ehara, K. Toyota, R. Fukuda, J. Hasegawa, M. Ishida, T. Nakajima, Y. Honda, O. Kitao, H. Nakai, T. Vreven, J. A. Montgomery Jr., J. E. Peralta, F. Ogliaro, M. Bearpark, J. J. Heyd, E. Brothers, K. N. Kudin, V. N. Staroverov, R. Kobayashi, J. Normand, K. Raghavachari, A. Rendell, J. C. Burant, S. S. Iyengar, J. Tomasi, M. Cossi, N. Rega, J. M. Millam, M. Klene, J. E. Knox, J. B. Cross, V. Bakken, C. Adamo, J. Jaramillo, R. Gomperts, R. E. Stratmann, O. Yazyev, A. J. Austin, R. Cammi, C. Pomelli, J. W. Ochterski, R. L. Martin, K. Morokuma,

V. G. Zakrzewski, G. A. Voth, P. Salvador, J. J. Dannenberg, S. Dapprich, A. D. Daniels, Ö. Farkas, J. B. Foresman, J. V. Ortiz, J. Cioslowski and D. J. Fox, *Gaussian 09, (Revision A.1)*, Gaussian, Inc., Wallingford, CT, 2009.

57 N. M. O'Boyle, A. L. Tenderholt and K. M. Langner, *J. Comput. Chem.*, 2008, **29**, 839.

58 M. Sarma, A. Kalita, P. Kumar, A. Singh and B. Mondal, *J. Am. Chem. Soc.*, 2010, **132**, 7846.

59 Y. Liu, K. Ai, X. Cheng, L. Huo and L. Lu, *Adv. Funct. Mater.*, 2010, **20**, 951.

60 (*a*) X. Chen, S. W. Nam, G. H. Kim, N. Song, Y. Jeong, I. Shin, S. K. Kim, J. Kim, S. Park and J. Yoon, *Chem. Commun.*, 2010, **46**, 8953; (*b*) M. Royzen, Z. Dai and J. W. Canary, *J. Am. Chem. Soc.*, 2005, **127**, 1612.

61 Y. Q. Wang, H.-M. Zhang, G.-C. Zhang, W.-H. Tao, Z.-H. Fei and Z.-T. Liu, *J. Pharm. Biomed. Anal.*, 2007, **43**, 1869.

62 M. E. Murphy and H. Sies, *Proc. Natl. Acad. Sci. U. S. A.*, 1991, **88**, 10860.

63 R. Alam, T. Mistri, P. Mondal, D. Das, S. K. Mandal, A. R. Khuda Bukhsh and M. Ali, *Dalton Trans.*, 2014, **43**, 2566.

64 B. Dong, X. Kong and W. Lin, *ACS Chem. Biol.*, 2018, **13**, 1714.

65 M. A. Michael, G. Pizzella, L. Yang, Y. Shi, T. Evangelou, D. T. Burke and Y. Zhang, *J. Phys. Chem. Lett.*, 2014, **5**, 1022.

66 W. Yang, X. Chen, H. Su, W. Fanga and Y. Zhang, *Chem. Commun.*, 2015, **51**, 9616.